



# University of HUDDERSFIELD

## University of Huddersfield Repository

Charles, Christopher Jon

The Biodegradation of Isosaccharine Acids under Hyperalkaline Conditions

### Original Citation

Charles, Christopher Jon (2017) The Biodegradation of Isosaccharine Acids under Hyperalkaline Conditions. Doctoral thesis, University of Huddersfield.

This version is available at <http://eprints.hud.ac.uk/id/eprint/32619/>

The University Repository is a digital collection of the research output of the University, available on Open Access. Copyright and Moral Rights for the items on this site are retained by the individual author and/or other copyright owners. Users may access full items free of charge; copies of full text items generally can be reproduced, displayed or performed and given to third parties in any format or medium for personal research or study, educational or not-for-profit purposes without prior permission or charge, provided:

- The authors, title and full bibliographic details is credited in any copy;
- A hyperlink and/or URL is included for the original metadata page; and
- The content is not changed in any way.

For more information, including our policy and submission procedure, please contact the Repository Team at: [E.mailbox@hud.ac.uk](mailto:E.mailbox@hud.ac.uk).

<http://eprints.hud.ac.uk/>

# The Biodegradation of Isosaccharinic Acids Under Hyperalkaline Conditions

---

Christopher Jon Charles, BSc (Hons), MRes



*A thesis submitted to the University of Huddersfield in partial fulfilment of the requirements for the degree of Doctor of Philosophy*

**Department of Biological Sciences**  
**February 2017**

*This work was partially funded by Radioactive Waste Management limited.*



## **Copyright Statement**

- i. The author of this thesis (including any appendices and/or schedules to this thesis) owns any copyright in it (the “Copyright”) and s/he has given The University of Huddersfield the right to use such Copyright for any administrative, promotional, educational and/or teaching purposes.
- ii. Copies of this thesis, either in full or in extracts, may be made only in accordance with the regulations of the University Library. Details of these regulations may be obtained from the Librarian. This page must form part of any such copies made.
- iii. The ownership of any patents, designs, trade marks and any and all other intellectual property rights except for the Copyright (the “Intellectual Property Rights”) and any reproductions of copyright works, for example graphs and tables (“Reproductions”), which may be described in this thesis, may not be owned by the author and may be owned by third parties. Such Intellectual Property Rights and Reproductions cannot and must not be made available for use without the prior written permission of the owner(s) of the relevant Intellectual Property Rights and/or Reproductions.

## **Acknowledgements**

I would like to thank Prof. Paul Humphreys for his tutelage and support throughout not just my PhD experience but also my undergraduate days. His patience and professional approach has helped towards moulding me into not just a scientist but also a better person. Dr. Simon Rout deserves particular acknowledgement for his seemingly limitless resourcefulness at repairing machines and finding 'lost' laboratory equipment as well as becoming a good friend. I would like to extend thanks to Prof. Alan McCarthy and his team at the Institute of Integrative Biology at the University of Liverpool for assisting in some very tedious molecular biology training and work. I would also like to thank the Unisense team in Aarhus, Denmark for their memorable training sessions and seminars.

Thanks are extended to my placement students Eva Garrett, Kim Patel and Emily Woodhead who kept the laboratory work entertaining and Richard Wormald for his enjoyable companionship on numerous site visits. Finally I would like to thank my future wife Sarah Abigail Dix for her support throughout this period and my family and friends who managed to make me go out and socialise rather than become a permanent feature within the laboratory.

## Abstract

One of the current proposed strategies for the disposal of intermediate level radioactive waste (ILW) is that of an underground facility termed a geological disposal facility (GDF). Under the anoxic alkaline conditions ( $10.5 < \text{pH} < 13$ ) expected to develop within an ILW-GDF cellulose will undergo chemical degradation to a range of cellulose degradation products (CDP). The major components of which will be the isosaccharinic acids (ISA). ISA is of particular interest with regards to the long term performance of a GDF due to its ability to complex radionuclides altering their solubility and thus the long term retention of such radionuclides. The removal of these complexants by microbial action could therefore have an impact upon the long term performance of an ILW-GDF.

The biofilm mode of existence is able to increase the resistance of microbes to environmental stresses and could be a mechanism for microbial survival under ILW-GDF conditions. Recent research has shown the ability of microbes from an ILW-GDF anthropogenic analogue site to degrade ISA under hyperalkaline conditions, however, no studies have yet looked at the ability of alkaliphilic biofilms to survive under these conditions whilst using ISA as a carbon source. The aim of this work was to ascertain the ability of alkaliphilic biofilm consortia to survive and degrade ISA under near field conditions and to further investigate the mechanisms of this survival.

Using cotton bait, biofilm was able to be grown in-situ at an analogue site located at Harpur Hill, Buxton, UK. Enrichment of this biofilm using CDP driven microcosms under both sulphate reducing and methanogenic conditions at pH 11 showed the degradation of the  $\alpha$ -ISA,  $\beta$ -ISA and xylo ISA types through a fermentation pathway to acetate and hydrogen. Investigation into the morphology of these microcosms revealed the microbes to exist within flocs or aggregates of EPS which had a complex EPS composition. Microelectrode profiling of these flocs revealed areas of lower pH than the external pH to be present within the interior of these flocs, a finding which was attributed to microbial survival under the alkaline conditions.

Floc cultures were able to form thick dense biofilm within sand columns which enhanced the rate of ISA degradation and facilitated the production of methane and sulphide under relevant conditions. Micro-electrode pH profiling again demonstrated low pH areas within the biofilm which contributed towards biofilm survival and ISA degradation up to pH 13. Biofilms were able to impact ILW-GDF relevant surfaces with evidence of carbonation and EPS substances found upon NRVB, steel and graphite surfaces.

The ability of biofilms to form under ILW-GDF conditions could facilitate microbial survival under ILW-GDF conditions and have an impact upon the long term performance of an ILW-GDF. This could be through the carbonation of NRVB surfaces, the blocking of pore throats, gas production, microbial induced corrosion related to sulphide production and through the removal of radionuclide complexants.

## Contents

1. Nuclear waste disposal concept and the generation of isosaccharinic acids .....	21
1.1 Overview .....	22
1.2 Nuclear waste legacy.....	22
1.2.1 Low level wastes.....	22
1.2.2 Intermediate level waste .....	23
1.2.3 High level waste.....	23
1.3 Geological disposal of nuclear wastes .....	24
1.4 Alkaline cellulose degradation under ILW-GDF conditions .....	29
1.4.1 Cellulosic materials.....	29
1.4.2 Anaerobic, alkaline degradation of cellulose.....	29
1.4.3 Significance of ISA within ILW-GDF concept .....	31
1.5 Summary of chapter .....	32
2. Microbial processes under ILW-GDF conditions.....	34
2.1 Overview .....	35
2.2 Microbial survival under ILW-GDF conditions.....	35
2.2.1 Natural analogue sites .....	36
2.2.2 Anthropogenic analogue sites .....	37
2.3 Biofilm formation.....	39
2.4 Biofilms with relevance to an ILW-GDF concept .....	44
2.4.1 Microbial processes under ILW-GDF conditions.....	45
2.4.2 Fermentation .....	45
2.4.3 Methanogenesis.....	46
2.4.4 Sulphate reduction .....	47
2.5 Microbial degradation of ISA .....	50
2.6 Summary of chapter .....	52
3. Methods for the analysis of environmental microbiology .....	53

3.1	Overview .....	54
3.2	Culturing techniques .....	54
3.3	Microscopy studies.....	55
3.4	Viability studies.....	56
3.5	Nucleic acid approaches.....	57
3.5.1	Nucleic acid extraction .....	57
3.5.2	Polymerase chain reaction methodologies.....	57
3.5.3	Cloning of PCR products .....	58
3.5.4	Next generation techniques.....	59
3.5.5	Microbial 16S community analysis .....	59
3.6	Summary .....	64
4.	Aims and objectives.....	65
5.	Experimental methodologies .....	67
5.1	General reagents.....	68
5.2	Media.....	68
5.2.1	Mineral media .....	68
5.2.2	Generation of cellulose degradation products (CDP) .....	69
5.3	Sample preparation.....	69
5.4	Analytical methodologies.....	69
5.4.1	High performance anion exchange chromatography with pulsed amperometric detection (HPAEC-PAD).....	69
5.4.2	Gas chromatography .....	70
5.4.3	BacVis gas detection system.....	71
5.4.4	Determination of total carbon, organic and inorganic carbon .....	71
5.4.5	Ion chromatography .....	71
5.4.6	Determination of iron (II) and (III) content .....	72
5.4.7	Dry weight, volatile solids and inorganic ash content .....	72

5.4.8	Measuring ATP content of biofilm samples .....	72
5.4.9	Extraction and composition of exopolymeric substances (EPS) .....	73
5.4.10	EPS calcium binding assay .....	75
5.4.11	Floc size distribution.....	76
5.4.12	Floc quantification via flow cytometry.....	76
5.4.13	Measurement of floc zeta potential at different pH values .....	76
5.5	Aqueous sulphide determination.....	77
5.5.1	pH and redox determination.....	77
5.5.2	Extraction of ISA from environmental samples .....	77
5.5.3	Extraction of VFA from environmental samples.....	77
5.6	Microscopy techniques.....	78
5.6.1	Sample preparation .....	78
5.6.2	Fluorescence microscopy.....	78
5.6.3	Confocal scanning laser microscopy .....	79
5.6.4	Scanning electron microscopy and elemental analysis.....	80
5.7	Molecular biology .....	81
5.7.1	Extraction and purification of nucleic acids .....	81
5.7.2	Polymerase chain reaction (PCR) .....	83
5.7.3	cDNA synthesis .....	85
5.7.4	qPCR of <i>dsrA</i> gene.....	85
5.7.5	Cloning of 16S rRNA gene.....	86
5.7.6	Analysis of 16S rRNA clone library sequences.....	87
5.7.7	16S rRNA gene clone library nucleotide accession numbers.....	88
5.7.8	Microbial community analysis via MiSeq platform .....	88
5.7.9	Microbial community BioProject accession numbers .....	90
5.8	Analogue sites .....	90
5.8.1	Cotton preparation .....	90

5.8.2	Analogue site investigation.....	91
5.8.3	Work flow for analogue sites investigation .....	94
5.8.4	Genetic analysis of cotton samples .....	95
5.9	Microcosm investigations .....	95
5.9.1	Liquid batch fed microcosms.....	95
5.9.2	pH survival subcultures.....	97
5.9.3	Biofilm formation upon stainless steel under alkaline sulphate reducing conditions.....	98
5.9.4	Free drift sulphate reducing investigation.....	98
5.9.5	Recirculation biofilm system .....	99
5.9.6	Single pass NRVB column biofilm system .....	102
5.9.7	Preparation of NRVB.....	105
5.9.8	Calculating rate constants .....	105
5.10	Micro pH and redox electrode profiling .....	105
5.10.1	pH floc profile.....	105
5.10.2	Biofilm pH and redox profile.....	106
6.	Harpur Hill, Buxton analogue site investigation and microcosm experiments .....	107
6.1	Rationale.....	108
6.2	Results and discussion.....	108
6.2.1	Analogue site investigation and analysis of colonised cotton .....	108
6.2.2	Microcosm studies .....	113
6.2.3	Properties of polymicrobial flocs.....	118
6.2.4	Survival of microorganisms within polymicrobial flocs. ....	127
6.3	Conclusion.....	133
6.4	Key findings .....	134
7.	Biofilm based systems .....	135
7.1	Rationale.....	136

7.2	Results and discussion.....	136
7.2.1	Formation of biofilm and the associated degradation of ISA under ILW-GDF conditions.....	136
7.2.2	The degradation of ISA by biofilms at hyperalkaline pH values.....	145
7.2.3	Biofilms formation in the near field upon ILW-GDF relevant surfaces.....	163
7.3	Conclusion.....	189
7.4	Key findings .....	190
8.	ISA degradation under sulphate reducing conditions .....	191
8.1	Rationale.....	192
8.2	Results and discussion .....	192
8.2.1	Liquid microcosm investigation under ILW-GDF conditions.....	192
8.2.2	Free drift study.....	199
8.2.3	Steel surface biofilm investigation under ILW-GDF conditions.....	209
8.3	Conclusion.....	223
8.4	Key findings .....	223
9.	Analogue site investigations .....	225
9.1	Rationale.....	226
9.2	Results and discussion.....	227
9.2.1	Chemical analysis of analogue sites .....	227
9.2.2	Analysis of colonised cotton at different analogue sites.....	233
9.3	Conclusion.....	250
9.4	Key findings .....	251
10.	Concluding remarks .....	252
11.	References.....	256
	Associated data .....	279

Word count excluding appendices and references – 54,728

## List of Figures

Figure 1.1: Artists impression of a geological disposal facility.....	24
Figure 1.2: The multi-barrier system for ILW disposal.....	25
Figure 1.3: Details and example cutaways of ILW waste canisters. ....	26
Figure 1.4: pH evolution of the near field GDF.....	27
Figure 1.5: Overview of the evolution of an ILW-GDF.....	28
Figure 1.6: Structure of cellulose and cellobiose.....	29
Figure 1.7: The peeling reaction of cellulose under anaerobic alkaline conditions.....	31
Figure 1.8: The diastereomers of isosaccharinic acid. ....	31
Figure 2.1: The microbial biofilm structure and the interactions between EPS components. ....	42
Figure 2.2: Syntrophic interactions in biofilm. ....	43
Figure 2.3: Fermentation end products of different bacterial genera.....	46
Figure 2.4: Overview of the dissimilatory sulphate reduction pathway. ....	48
Figure 5.1: Borehole location plan of Buxton site.....	92
Figure 5.2: Borehole location plan of Horton quarry site. ....	92
Figure 5.3: Borehole location plan of Tarmac quarry site. ....	93
Figure 5.4: Workflow for cotton harvested from analogue sites. ....	94
Figure 5.5: Overview of microcosm formation and maintenance. ....	97
Figure 6.1: Microscopy investigation of the cotton. ....	110
Figure 6.2: Elemental composition of biofilm formed upon colonised cotton. ....	111
Figure 6.3: 16S rRNA gene clone libraries of the colonised cotton. ....	113
Figure 6.4: Chemistry of the CDP driven pH 11 microcosm. ....	114
Figure 6.5: 16S rRNA gene microbial community analysis of pH 11 microcosm. ....	116
Figure 6.6: Rarefaction and Rank abundance curves for pH 11 microcosm via MiSeq approach.....	118
Figure 6.7: Microscopy investigation into the morphology of the pH 11 microcosm.....	119
Figure 6.8: Size distribution of polymicrobial flocs within pH 11 microcosm. ....	120
Figure 6.9: CLSM investigation of polymicrobial floc from pH 11 microcosm.....	121
Figure 6.10: Archaeal and bacterial FISH investigation of flocs.....	122
Figure 6.11: FISH investigation showing spatial distribution of <i>Alishewanella</i> , <i>Dietzia</i> and <i>Clostridia</i> within polymicrobial flocs. ....	123
Figure 6.12: Composition of extracted polymicrobial floc EPS.....	124
Figure 6.13: FTIR of polymicrobial floc EPS. ....	125

Figure 6.14: Elemental composition of EPS based crystalline precipitate. ....	126
Figure 6.15: Polymicrobial floc EPS calcium binding curve. ....	127
Figure 6.16: pH survival curves of polymicrobial flocs. ....	128
Figure 6.17: pH profiles through polymicrobial flocs. ....	129
Figure 6.18: Zeta potential measurements of polymicrobial flocs at different pH values....	129
Figure 6.19: Live/dead images of polymicrobial flocs after pH survival testing period. ....	130
Figure 6.20: Isoelectric focussing gel of extracted protein from polymicrobial floc EPS. ..	132
Figure 7.1: Time lapse pictures showing formation of biofilm in sand column at pH 11. ....	137
Figure 7.2: SEM investigation into biofilm formed in sand column using recirculation system at pH 11. ....	138
Figure 7.3: CLSM images of biofilm formed in pH 11 sand column. ....	139
Figure 7.4: Chemistry of pH 11 recirculation biofilm based system. ....	141
Figure 7.5: Chemistry of biofilm only component of pH 11 recirculation system. ....	143
Figure 7.6: Chemistry of the liquid only component of the pH 11 recirculation system. ....	143
Figure 7.7: CLSM investigation of EPS aggregates originating from biofilm. ....	144
Figure 7.8: ISA degradation by sand column biofilms at different pH values. ....	147
Figure 7.9: VFA production from single pass biofilm systems. ....	148
Figure 7.10: Gas production from biofilms under hyperalkaline pH range. ....	148
Figure 7.11: pH measurements of single pass system under hyperalkaline range. ....	149
Figure 7.12: Microelectrode pH profiles through sand column biofilm under hyperalkaline conditions. ....	150
Figure 7.13: FTIR analysis of biofilm EPS under different hyperalkaline pH values. ....	153
Figure 7.14: EDS analysis of sand columns with and without biofilms under different hyperalkaline pH values. ....	154
Figure 7.15: CLSM imaging of sand column biofilms under different hyperalkaline pH values. ....	156
Figure 7.16: 16S rRNA gene microbial community of sand column biofilms under different hyperalkaline pH values. ....	159
Figure 7.17: Rarefaction and rank abundance curves for biofilm communities under different hyperalkaline pH values. ....	160
Figure 7.18: SEM images of sand column biofilms under different hyperalkaline pH values. .....	162
Figure 7.19: Redox measurements in sand column biofilms under different pH values. ....	163

Figure 7.20: Live/dead imaging of flocs leaving sand column biofilms at different hyperalkaline values.....	164
Figure 7.21: pH measurements of NRVB column outlet.....	165
Figure 7.22: Carbonation surface testing of NRVB columns. ....	166
Figure 7.23: SEM images of NRVB surfaces exposed at different hyperalkaline values under both abiotic and biotic conditions. ....	168
Figure 7.24: Elemental composition of NRVB surfaces at different hyperalkaline pH values exposed to both biofilm and abiotic systems. ....	169
Figure 7.25: CLSM imagery of NRVB surfaces under different hyperalkaline values exposed to biotic conditions.....	171
Figure 7.26: Comparison of total ISA removed by passage through NRVB column at different hyperalkaline pH values. ....	174
Figure 7.27: TOC and IC measurements of biofilm and control systems at different hyperalkaline pH values.....	177
Figure 7.28: SEM imaging of graphite discs under biofilm and control systems at various hyperalkaline pH values.....	179
Figure 7.29: EDS investigation into the elemental surface composition of graphite surfaces at different hyperalkaline pH values. ....	180
Figure 7.30: CLSM imaging of biotic exposed graphite discs at different hyperalkaline pH values. ....	181
Figure 7.31: SEM images of steel disc surfaces under different hyperalkaline values. ....	183
Figure 7.32: Elemental composition of steel disc surfaces at different hyperalkaline pH values. ....	185
Figure 7.33: CLSM investigation of steel surfaces exposed to biotic conditions under different hyperalkaline pH values. ....	187
Figure 7.34: SEM investigation of biofilm formed upon steel disc surfaces at different hyperalkaline pH values.....	188
Figure 8.1: Chemistry of pH 11 sulphate reducing liquid microcosm.....	193
Figure 8.2: Microscopy investigation into the morphology of sulphate reducing microcosm. ....	195
Figure 8.3: Elemental composition of pH 11 sulphate reducing system flocs.....	195
Figure 8.4: pH profile through sulphate reducing floc at pH 11.....	196
Figure 8.5: Extraction of EPS components from flocs under hyperalkaline sulphate reducing conditions.....	198

Figure 8.6: FTIR of EPS extracted from flocs under hyperalkaline sulphate reducing conditions.....	198
Figure 8.7: ISA degradation within free drift systems.....	201
Figure 8.8: Chemistry of free drift systems. ....	202
Figure 8.9: Morphology of the free drift subcultures. ....	203
Figure 8.10: Comparison of theoretical and system acetate and sulphide within sulphate reducing free drift system. ....	204
Figure 8.11: qPCR analysis of the <i>dsrA</i> gene and its transcripts within the free drift sulphate reducing subculture.....	205
Figure 8.12: Community composition of free drift subcultures. ....	207
Figure 8.13: Rarefaction and rank abundance curves of different free drift subculture systems.....	209
Figure 8.14: Chemistry of hyperalkaline steel disc microcosm under sulphate reducing conditions.....	211
Figure 8.15: CLSM imaging of biofilms formed upon steel discs under ILW-GDF conditions.....	213
Figure 8.16 : Rarefaction and rank abundance curves of steel disc biofilms grown under hyperalkaline conditions.....	215
Figure 8.17: 16S rRNA gene community analysis of biofilms formed upon steel discs under hyperalkaline conditions. ....	217
Figure 8.18: SEM imaging of biofilm coated steel discs before and after biofilm removal.	219
Figure 8.19: Elemental composition of steel discs coated by biofilm and controls. ....	221
Figure 9.1: Photographs of hyperalkaline areas tested at different analogue sites. ....	229
Figure 9.2: CLSM imaging of biofilm formed upon cotton after 3 month incubation period at different potential analogue sites. ....	235
Figure 9.3: SEM imaging of biofilm formed upon cotton after a 3 month incubation period at different potential analogue sites. ....	236
Figure 9.4: EDS investigation into the composition of biofilms from upon cotton from different potential analogue sites. ....	237
Figure 9.5: Archaeal 16S rRNA community analysis of different potential analogue sites.	242
Figure 9.6 : Bacterial 16S rRNA community analysis of different potential analogue sites. ....	244
Figure 9.7: Rarefaction and rank abundance curves of biofilms formed in-situ at different potential analogue sites.....	246

Figure 9.8: Distribution of the shared OTU's and sequence reads across biofilms from different potential analogue sites. ....	247
Figure 9.9: Heat map at the genus level of shared OTU's between biofilms at different potential analogue sites. ....	249

## List of Tables

Table 2.1: Biofilm properties of EPS components. ....	40
Table 2.2: Sulphate reduction and methanogenesis processes.....	47
Table 5.1: Composition of mineral media per 1 litre.....	68
Table 5.2: Composition of trace elements solution per 1 litre.....	68
Table 5.3: 5 colour CLSM stain properties.....	80
Table 5.4: Oligonucleotide FISH probes.....	80
Table 5.5: 16S rRNA gene PCR primer used for the formation of clone libraries.....	84
Table 5.6: 16S rRNA primers used for microbial community analysis.....	85
Table 5.7: Ligation reaction conditions for pGEM T easy cloning kit.....	87
Table 5.8: Details of microbial community analysis investigations.....	88
Table 5.9: Bioproject and Biosample accession details.....	90
Table 5.10: NRVB composition. ....	105
Table 6.1: Analysis of porewater, sediment and cotton retrieved from the Buxton analogue site.....	108
Table 6.2: ISA degradation rate constants of pH 11 methanogenic microcosm.....	114
Table 6.3: Cell concentration and associated biomass over two week period.....	115
Table 6.4: Alpha diversity statistics of pH 11 microcosm.....	117
Table 6.5: Carbon distribution of pH 11 microcosm.....	120
Table 6.6: Dry weight, volatile solids and ash content of polymicrobial flocs.....	125
Table 6.7: Monomer composition of polymicrobial floc EPS.....	132
Table 7.1: First order rate constants for the pH 11 biofilm based system.....	142
Table 7.2 : pH of recirculation biofilm based systems.....	142
Table 7.3: First order rate constants for ISA degradation in biofilm at different pH values.....	148
Table 7.4: EPS extraction of sand column biofilms under hyperalkaline conditions.....	152
Table 7.5: EPS percentage composition of sand columns biofilms under hyperalkaline condition.....	152

Table 7.6: Dry weight, inorganic content and volatile solids of sand columns biofilms under hyperalkaline conditions. ....	153
Table 7.7: Monomer analysis of the polysaccharide component of sand column biofilms under different hyperalkaline pH values. ....	157
Table 7.8: Statistical comparison of sand column biofilm communities under hyperalkaline pH values. ....	157
Table 7.9: Alpha diversity statistics for sand column biofilm communities at different hyperalkaline pH values. ....	160
Table 7.10 : Viable cell measurements and related cell dry weight of sand column biofilms at different hyperalkaline pH values. ....	162
Table 7.11: Cell density and dry weight measurements of flocs leaving sand column biofilms at different hyperalkaline values. ....	164
Table 7.12: Amount of ISA removed due to passage through NRVB column at different hyperalkaline pH values under both abiotic and biotic systems. ....	175
Table 8.1: First order rate constants for ISA degradation under sulphate reducing conditions. ....	193
Table 8.2: pH measurements of pH 11 sulphate reducing microcosm. ....	194
Table 8.3: Sulphate and sulphide measurements of pH 11 sulphate reducing microcosm. ...	194
Table 8.4 : Dry weight, volatile solids and inorganic matter of sulphate reducing system flocs. ....	196
Table 8.5: Monomer analysis of polysaccharide component extracted from floc EPS under sulphate reducing hyperalkaline conditions. ....	199
Table 8.6: P value distribution for the comparison between different free drift subcultures.	208
Table 8.7: Alpha diversity statistics of different free drift systems. ....	208
Table 8.8: First order rate constants for ISA degradation within steel disc system. ....	210
Table 8.9: pH values of sulphate reducing disc reactor under hyperalkaline conditions. ....	212
Table 8.10: Alpha diversity statistics for biofilms grown on steel discs under hyperalkaline conditions. ....	214
Table 9.1: Chemical analysis of different potential ILW analogue sites. ....	230
Table 9.2: Chemical analysis after 3 month cotton incubation period at different potential analogue sites. ....	232
Table 9.3: Alpha diversity statistics for biofilms formed at different potential analogue sites. ....	246

Table 9.4: Probability testing for the comparison of biofilm communities at different potential analogue sites. ....	246
Table 9.5: Shared OTU's between biofilms from different potential analogue sites. ....	248

## List of Diagrams

Diagram 5.1: Standard microcosm vessel.....	95
Diagram 5.2: Small Biocell diagram. ....	99
Diagram 5.3: Recirculation based biofilm system. ....	100
Diagram 5.4: Liquid only component of recirculation system. ....	101
Diagram 5.5: Single pass system for testing biofilm activity .....	102
Diagram 5.6: Single pass system with NRVB column. ....	103
Diagram 5.7: Large Biocell with NRVB column. ....	104

## List of Equations

Equation 1.1: Thorium, calcium, ISA complexation. ....	32
Equation 2.1: Anaerobic oxidation of methane. ....	43
Equation 3.1: Chao1 species richness estimator. ....	61
Equation 3.2: Abundance based coverage estimator. ....	61
Equation 3.3: Shannon diversity index. ....	62
Equation 3.4: Simpson diversity index. ....	62
Equation 3.5: Goods coverage estimator. ....	62
Equation 3.6: Libshuff method. ....	63
Equation 5.1: The ideal gas law.....	71
Equation 5.2: Gene copy number in a known amount of DNA.....	86
Equation 5.3: Cloning vector inset DNA calculation. ....	86
Equation 5.4: Significance test for two different microbial communities. ....	90
Equation 5.5: Theoretical ISA driven sulphate reduction.....	96
Equation 5.6: Exponential growth / decay equation. ....	105
Equation 7.1: The fermentation of ISA to acetate. ....	144

## List of Abbreviations

ACE – Abundance coverage based estimator

AGR – Advanced gas-cooled reactor

APS – Adenosine phosphosulfate

ATP – Adenosine triphosphate

BLAST – Basic local alignment search tool

DsrAB-C – Dissimilatory sulphite reductase complex

*dsrA* - Dissimilatory sulphite reductase subunit A

cDNA – Complementary deoxyribose nucleic acid

CDP - Cellulose degradation products

ConA - Concanavalin A, tetramethylrhodamine conjugate

CLSM – Confocal scanning electron microscopy

CTAB - Cetyl-trimethylammonium bromide

DNA – Deoxyribose nucleic acid

DNase – Deoxyribonuclease

dNTPs - Nucleoside triphosphates

DW – Dry weight

EDS - Electron dispersive X-ray spectroscopy

EDTA - Ethylenediaminetetraacetic acid

EPS - Exopolymeric substances

FISH - Fluorescence in-situ hybridisation

FITc - Fluorescein isothiocyanate

GDF – Geological disposal facility

GC – Gas chromatography

HLW – High level waste

HPAEC-PAD - High performance anion exchange chromatography with pulsed amperometric detection

IC – Ion chromatography

ILW – Intermediate level waste

ILW-GDF - Intermediate level waste geological disposal facility

ISA - Isosaccharinic acid

LLW – Low level waste

LLWR – Low level waste repository

MPN – Most probable number

MSA – Metasaccharinic acid

NDA – Nuclear Decommissioning Authority

NCBI – National Centre for Biotechnology Information

NRVB – Nirex reference vault backfill

OTU – Operational taxonomic unit

PAPs - 3'-phosphoadenosine-5'-phosphosulfate

PBS - Phosphate buffered saline

PCR – Polymerase chain reaction

PLFA - Phospholipid-derived fatty acids

qPCR – Quantitative polymerase chain reaction

RDP – Ribosomal database project

RNA – Ribose nucleic acid

RNase – Ribonuclease

rRNA – Ribosomal RNA

SAOB - Sulphide anti-oxidant buffer

SDS-PAGE - Sodium dodecyl sulfate polyacrylamide gel electrophoresis

SEM - Scanning electron microscopy

SRB – Sulphate reducing bacteria

SRR – Sulphate reduction rate

TAEB - Tris-acetate EDTA buffer

TC - Total carbon

TCA - Trichloroacetic acid

TEA – Terminal electron acceptor

TEM – Transmission electron microscopy

TFA - Trifluoroacetic acid

TIC – Total inorganic carbon

TOC – Total organic carbon

Tris-HCl - Trizma<sup>®</sup> hydrochloride

UK – United Kingdom

VFA – Volatile fatty acid

VS – Volatile solids

XISA – Xylo isosaccharinic acid

# **1. Nuclear waste disposal concept and the generation of isosaccharinic acids**

## **1.1 Overview**

One of the current proposed strategies for the disposal of radioactive waste is that of an underground facility termed a geological disposal facility (GDF). This chapter will discuss the details of such a facility with regard to the current nuclear waste inventory destined for disposal within the United Kingdom (UK). Although both intermediate and high level wastes are destined for disposal via a GDF only the intermediate fraction contains a range of cellulose bearing materials. Under the anoxic alkaline conditions expected to develop within a GDF, cellulose will undergo chemical degradation to a range of cellulose degradation products (CDP). The major components of which will be the isosaccharinic acids (ISA). ISA is of particular interest with regards to the long term performance of a GDF due to its ability to complex radionuclides altering their solubility and thus the long term retention of such radionuclides.

## **1.2 Nuclear waste legacy**

The generation of radioactive wastes within the UK results from electricity generation from nuclear power stations, the associated production and processing of the nuclear fuel, the use of radioactive materials in industry, medicine and research and from military nuclear programmes. The production of radioactive waste within the UK began in 1947 with the construction of the first nuclear reactor by the Atomic Energy Research Establishment (AERE) Harwell, which aimed to demonstrate the viability of commercial reactors (1). This was followed by the establishment of the first nuclear power station Calder Hall 1 at Sellafield in 1956. The UK nuclear industry rapidly expanded from that point with the construction of 11 Magnox power stations coming into operation between 1956 and 1971 and 7 advanced gas cooled reactors (AGR) coming into operation between 1976 and 1989 (1). The wastes generated by the operation of these facilities and their associated decommissioning is categorised based on its thermal and radioactive output. As of 2013 the UK radioactive waste inventory of 4.5 million cubic meters was composed of high level waste (0.02 %), intermediate level waste (6.4 %) and low level waste (93.6 %) (2). These types of wastes are discussed briefly below.

### **1.2.1 Low level wastes**

Low level wastes (LLW) generated within the UK are currently disposed of via a low level waste repository (LLWR) at Drigg, Cumbria which has been in operation for over 50 years. The waste to be disposed of generally consists of paper, cardboard, plastic, protective clothing, soil, rubble and metal (3), which has a radioactive content not exceeding 4 GBq

(gigabecquerels) per tonne of alpha, or 12 GBq per tonne of beta/gamma activity (1). LLW waste which is not suitable for incineration or recycling is compacted into steel containers which are then filled with cement and placed into concrete-lined vaults. LLW has radioactive emissions which fall below the limit for emplacement within a GDF and as such the disposal strategy does not rely on saturated alkaline conditions (2). In this case the cellulose portion of the waste undergoes anaerobic microbial based degradation rather than alkaline chemical hydrolysis (4).

### **1.2.2 Intermediate level waste**

Intermediate level waste (ILW) exceeds the upper boundaries for LLW classification but does not require cooling to be taken into account during storage. The UK inventory as of 2013 contained 290 000 m<sup>3</sup> of ILW designated waste which contained approximately 2000 tonnes of cellulosic materials such as wood, cloth and paper (2). This ILW waste also contains a range of other organic and inorganic matter resulting from the operation and decommissioning of facilities (5, 6) including:

- Wide range of forms of steel, including cladding, reactor components, site equipment and plant items.
- Graphite mainly in the form of moderator blocks from final stage reactor dismantling at Magnox and AGR power stations.
- Concrete and rubble generated from the dismantling and decommissioning of facilities.
- Sludges, spent ion-exchange resins and flocs: resulting from the treatment of liquid effluents and from the corrosion of fuel-related waste stored under water.

### **1.2.3 High level waste**

Although only a small portion of the total UK radioactive waste inventory by volume, the high level waste (HLW) inventory is expected to account for over 95% of its total radioactivity by 2040 (7). HLW is categorised as waste which requires cooling due to its radioactivity and is produced initially as a nitric acid solution that is a by-product from the reprocessing of spent nuclear fuel. This waste is converted into a solid glass prior to disposal using vitrification and requires long time frames for the radioactivity to reduce through natural decay processes (8). There is no cellulose material associated with this waste form and it is to be stored separately from both ILW and LLW (9).

### 1.3 Geological disposal of nuclear wastes

Current UK government policies for the long term disposal of long lived radioactive wastes such as HLW and ILW is that of GDF. Waste is to be permanently stored in a facility up to 1000 m below ground (Figure 1.1) with siting of any such site within the UK based on the volunteerism of the local community. At the time of writing the location of such a facility is undecided (5, 9). A strategy employing a cementitious based buffer and backfill is considered within this thesis, however, other options including clay based buffers and backfill, magnesium oxide and crushed host rock can be employed (7).

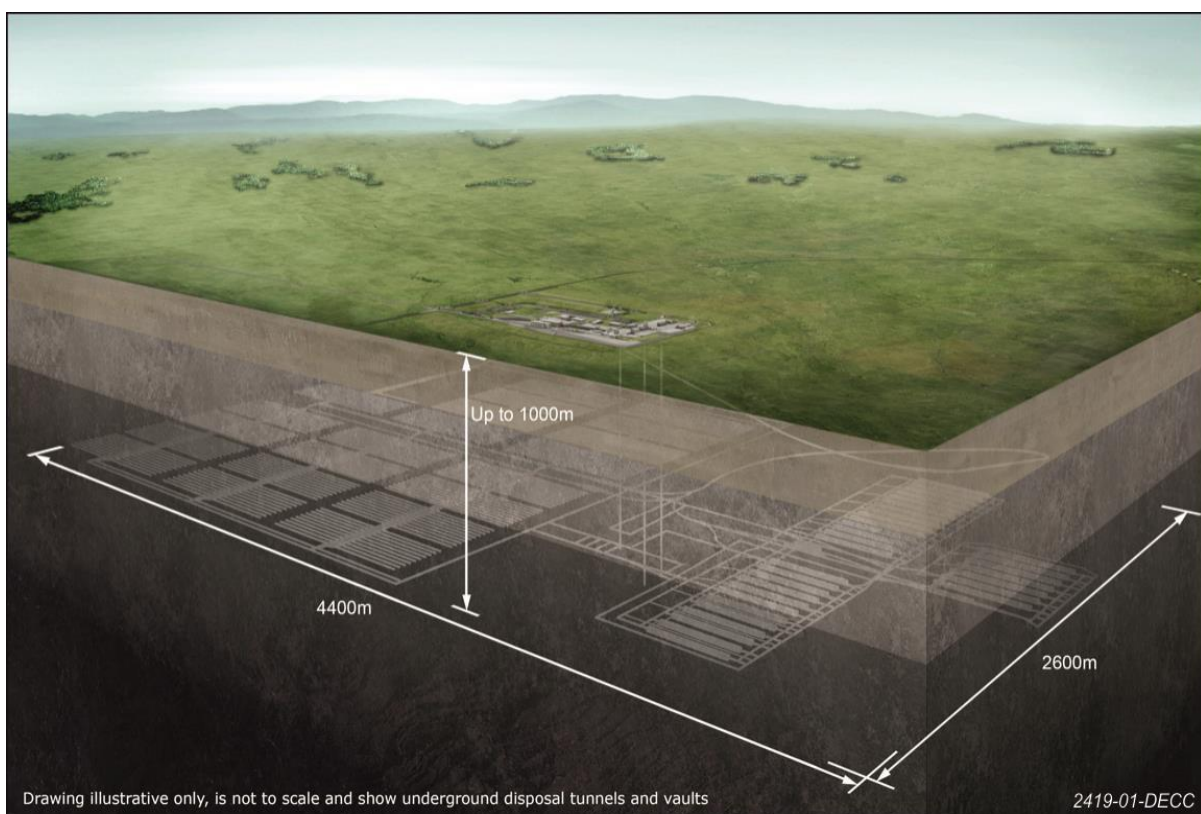


**Figure 1.1: Artists impression of a geological disposal facility.** Figure is taken from D.E.C.C. 2014 white paper on the implementation of a UK based GDF (9).

A GDF facility will consist of both a surface facility and an underground facility. The surface facility will receive waste and then transport it to the underground facility. The underground facility will then indefinitely host the waste utilising a multi-barrier system to isolate it from the biosphere during long term storage (Figure 1.2) (5, 9).

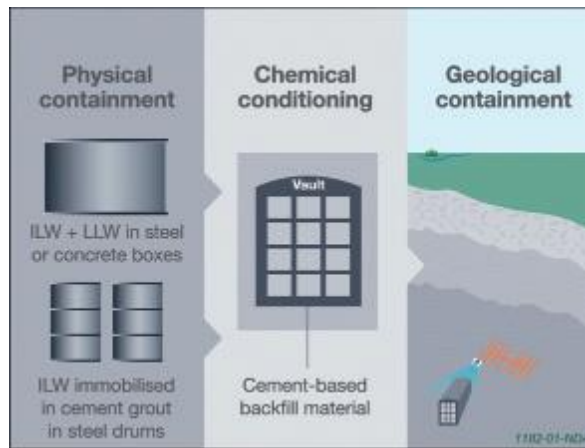
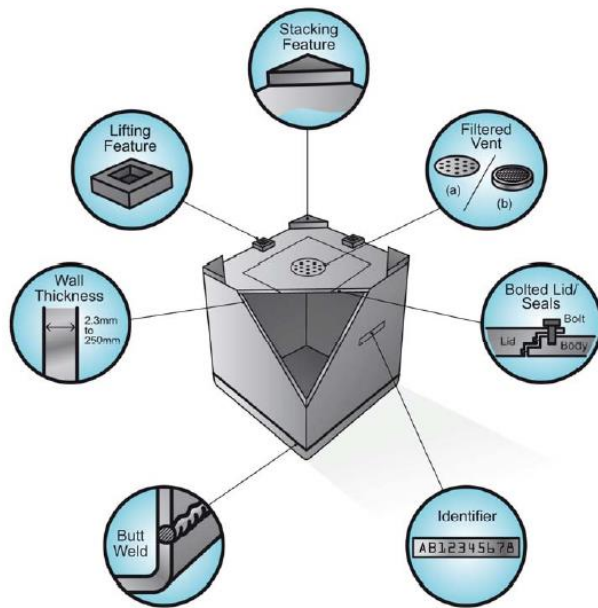


**Figure 1.2: The multi-barrier system for ILW disposal.** Figure is taken from the N.D.A. 2010 report ‘An introduction to the generic disposal system safety case’ (5).

There are three main categories of ILW which include liquids and slurries immobilised in a solid matrix, homogenous sludges and grouted wastes (intimately and annular) (7). The first phase of the multi-barrier system is that of physical containment by the compaction and conditioning of the waste into a 500 L stainless steel canister or 3 cubic meter stainless steel or concrete box within a cement grout matrix. The packages are designed with vents to allow the escape of corrosion gases to prevent over pressurisation and are described further in Figure 1.3 (6, 10).



(a) Container lid with vent holes. (b) Sintered lid



**Figure 1.3: Details and example cutaways of ILW waste canisters.** Figure adapted from N.D.A. reports (6, 10).

A cementitious backfill composed of lime, limestone flour and Ordinary Portland cement known as Nirex reference vault backfill (NRVB) is used to backfill the waste inside a subterranean vault and forms the second stage of the multi-barrier system by employing chemical conditioning to the waste (11). The NRVB is designed to be highly porous and relatively low strength to allow for the formation of homogenous chemical conditions, gas migration and the ability to retrieve waste if needed (12, 13). Upon saturation of the NRVB encapsulated facility by ground water a hyperalkaline environment should form in the near field which is expected to aid radionuclide retention within the GDF through sorption to the backfill and the formation of insoluble carbonates (7). During the evolution of the near field, conditions will initially be made hyperalkaline ( $> \text{pH } 13$ ) by the dissolution of alkali metal hydroxides with a temperature of up to  $80\text{ }^{\circ}\text{C}$  due to the cement curing process (7). During this process the near field conditions are also expected to become anaerobic due to the removal of oxygen through steel based corrosion events (14). As time progresses both the pH and temperature are expected to fall with interactions between the backfill and groundwater maintaining a pH of around 12.5 due to the dissolution of Portlandite and the generation of hydroxyl ions ( $\text{OH}^-$ ). The pH is expected to further reduce as time progresses due to the

dissolution of cement hydration products including calcium silicate hydrate (CSH) gels bringing the pH to a value between pH 10 and pH 12.5 (12). Beyond this the pH is expected to be buffered by the dissolution of low solubility minerals such as calcium carbonate (7, 12). This process is summarised in Figure 1.4.

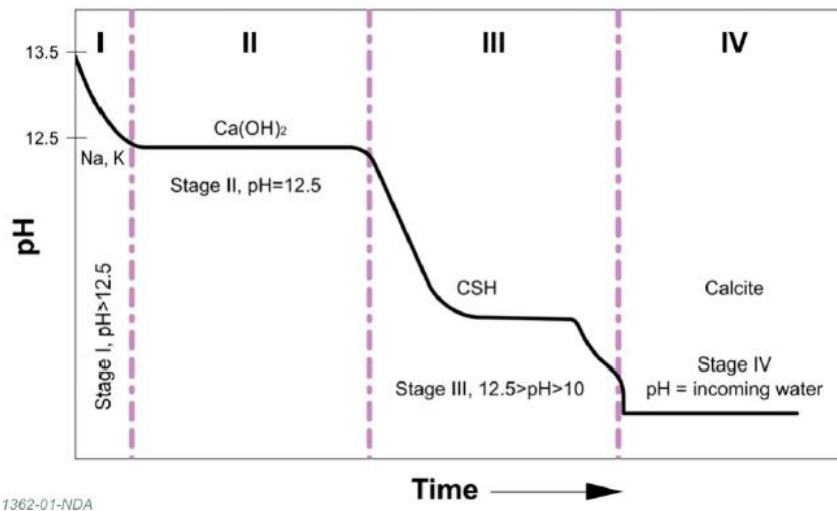


**Figure 1.4: pH evolution of the near field GDF.** Figure taken from N.D.A. ‘Near-field Evolution Status Report’ (7).

The final component to the multi-barrier system is that of the host rock the GDF is to be placed within. The host rock should be able to both conduct heat to prevent large temperature rises within the GDF and disperse gases to prevent mechanical disruption of the facility (13). As well as providing a weak hydrogeological environment which slows the progression of ground water to allow for the evolution of such a facility at a slow rate which can be forecast with confidence (15). The host rock should also provide properties that retard the movement of any radionuclides in groundwater including sorption onto mineral surfaces and properties that promote hydraulic dispersion and dilution of radionuclide concentrations (16). The host rock properties must also show little fluctuation over the time period for which the GDF is to be operational with examples of high strength host rock including crystalline igneous, metamorphic rock or older sedimentary rocks such as granite (15). An overview of the evolution of an ILW-GDF is given in Figure 1.5.

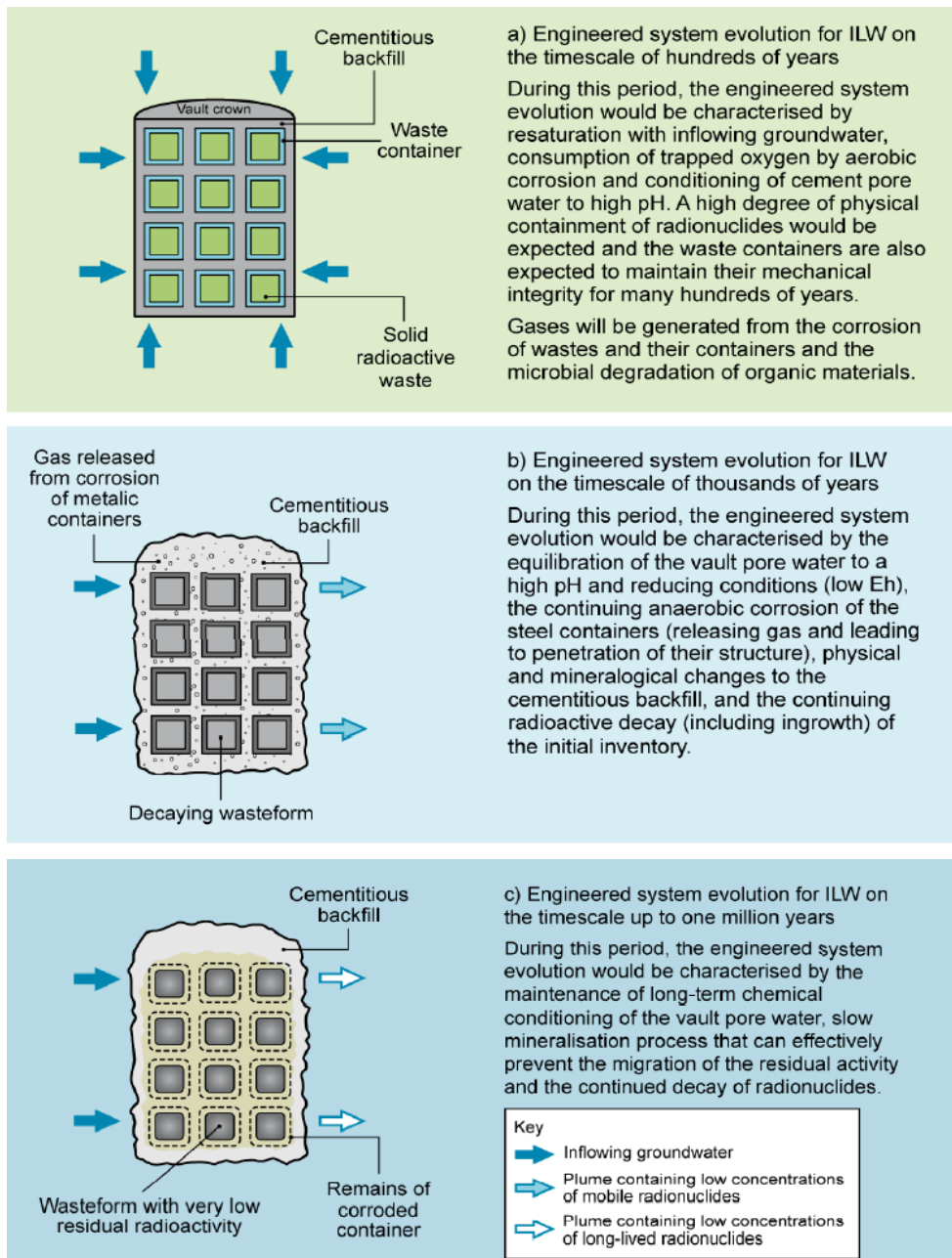


**Figure 1.5: Overview of the evolution of an ILW-GDF.** Figure taken from N.D.A. ‘Near-field Evolution Status Report’ (7).

## 1.4 Alkaline cellulose degradation under ILW-GDF conditions

### 1.4.1 Cellulosic materials

The heterogeneous nature of the ILW to be disposed of within a GDF will result in a range of cellulosic materials being present. Materials such as cotton are primarily composed of cellulose polymers and more complex materials such as woods are composed of multiple polymers including cellulose, hemicellulose and lignin (17). Both cellulose and hemicellulose are susceptible to chemical degradation under alkaline conditions with differences in the solubility of cellulose and hemicellulose leading to different degradation rates under these conditions (18). The structure of cellulose is composed of repeating units of the disaccharide cellobiose through (1,4)- $\beta$ -D-glucose unit linkage where each glucose unit is rotated 180° to its neighbouring unit with intra-molecular hydrogen bonding between the 3-OH and the preceding ring O5 (19, 20) (Figure 1.6). In comparison hemicellulose is composed of a range of monosaccharides which vary depending upon its synthesis sources, but in general contains repeating units of xylans, galactoglucomannans, glucomannans and arabinogalactans (21). Cellulose is synthesised through chain elongation at the reducing end of the polymer with both amorphous and crystalline regions occurring as the chain extends resulting in a biopolymer with a higher degree of polymerisations compared to hemicellulose (20).

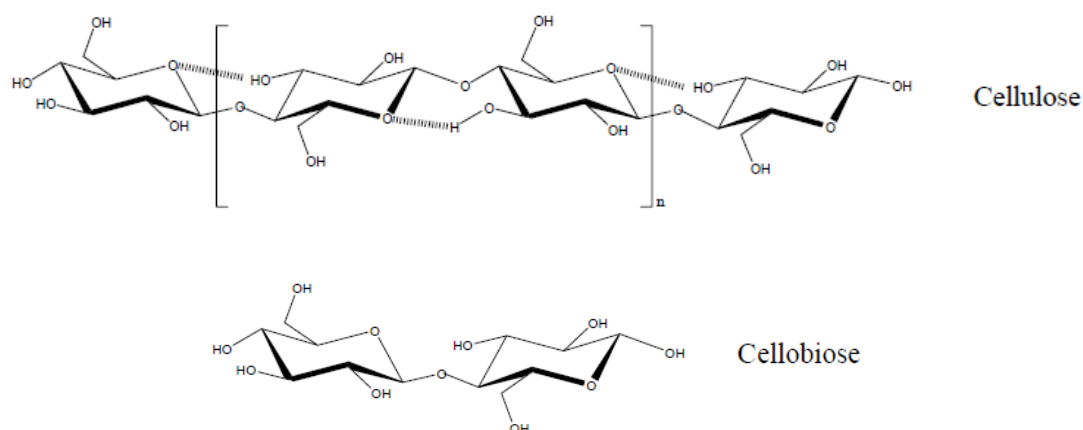


**Figure 1.6: Structure of cellulose and cellobiose**

### 1.4.2 Anaerobic, alkaline degradation of cellulose

Following maturation of the GDF a chemically reducing, anaerobic, high pH environment of around pH 12.5 with temperatures of up to 80 °C are expected (7, 13). Under these conditions cellulose may be degraded via a process known as the ‘peeling reaction’ in which glucose like units are progressively stripped from the ends of the D-anhydroglucopyranose (20, 22, 23) (Figure 1.7). The peeling reaction continues along a cellulose chain until the exposure of

a crystalline region upon which a physical stopping reaction takes place due to a reduced accessibility of reactive end groups (20, 22). Reactions can further occur if an end group becomes soluble or mid chain scission occurs through radiolytic processes yielding new exposed end groups (24, 25). With regards to cellulose degradation within a GDF, chemical degradation of cellulose is expected to constitute the majority of the degradation type in comparison to radiolytic degradation (20). The major products from the alkaline degradation of cellulose under repository conditions are the radionuclide complexants the  $\alpha$  and  $\beta$  diastereomeric forms of 2-C-(hydroxymethyl)-3-deoxy-D-pentonic(isosaccharinic) acid (ISA) (Figure 1.8), alongside a range of other low abundance CDP's. The additional potential CDP's are extensively discussed by Knill and Kennedy (22) who used a variety of cellulose sources under a range of different temperature and alkali values and catalogued the associated CDP's generated. Among the additional CDP's are short chained organic acids including acetic acid, formic acid, propionic acid and lactic acid which can be utilised as carbon sources for microbial metabolism (26). Where ISA is generated from the peeling reaction of the amorphous regions of cellulose,  $\alpha$  and  $\beta$  gluco-metasaccharinic (MSA) are formed in the termination reactions when a crystalline region is reached (20, 24). There is little literature available to suggest a role for MSA in the complexation of radionuclides but it could, however, act as potential carbon source for microbial metabolism. Hemicellulose is likely to be present within an ILW-GDF and as it is soluble under these conditions is likely to be completely hydrolysed (18), with the gluco and galactoglucomannan components of hemicellulose degraded in the same fashion as cellulose. The xylan components, however, are likely to form xylosaccharinic acid (3-deoxy-2-C-(hydroxymethyl)-tetronic acid, (XSA)) (20, 27). XSA can exhibit similar radionuclide complexation behaviour as ISA but will probably not be in a high enough concentration to adversely affect long term repository performance (28).

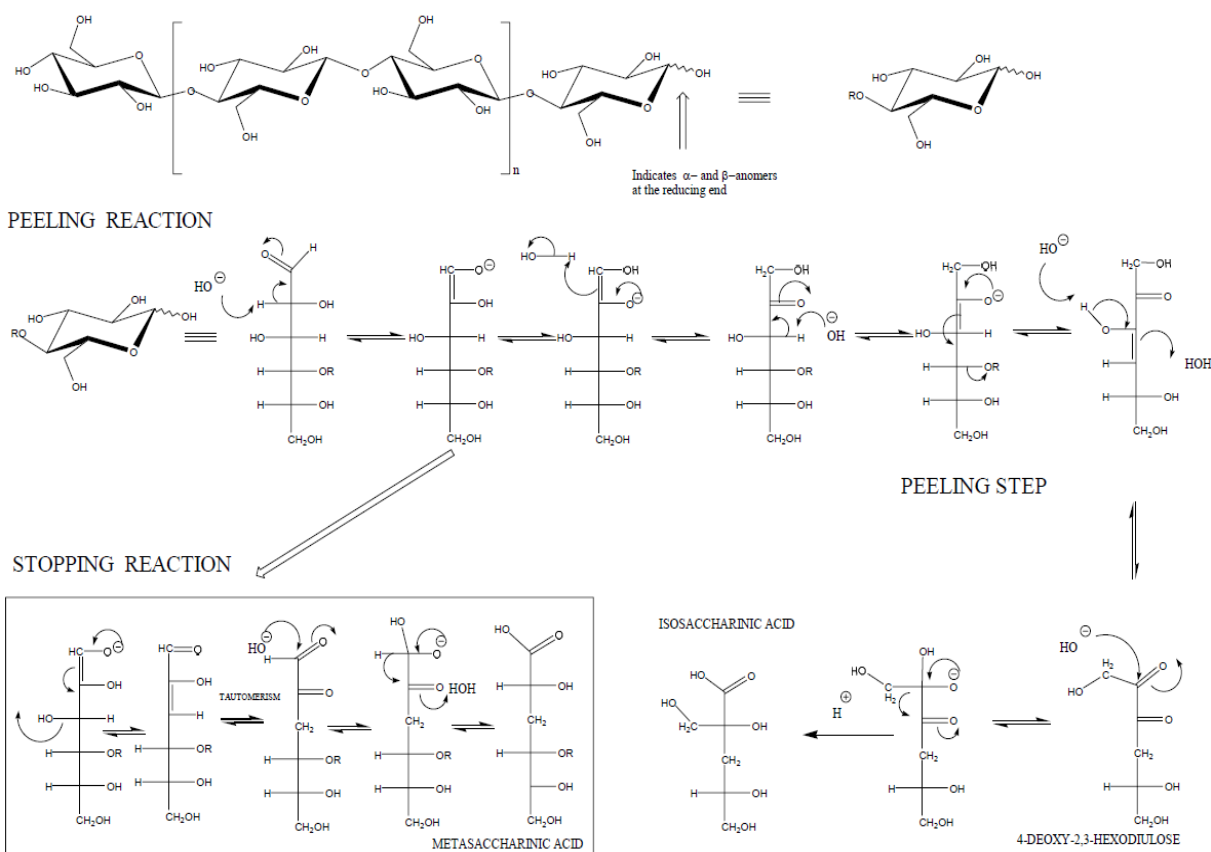


**Figure 1.7: The peeling reaction of cellulose under anaerobic alkaline conditions.**  
Figure taken from (20).

### 1.4.3 Significance of ISA within ILW-GDF concept

The generation of both  $\alpha$ -ISA and  $\beta$ -ISA (Figure 1.8) will comprise up to 80 % of the CDP's generated under ILW-GDF conditions (24, 29). The diastereomers of ISA are of particular importance to the long term performance of an ILW-GDF due to their ability to complex radionuclides leading to changes in their solubility and potentially altering the migration of radionuclides (18).

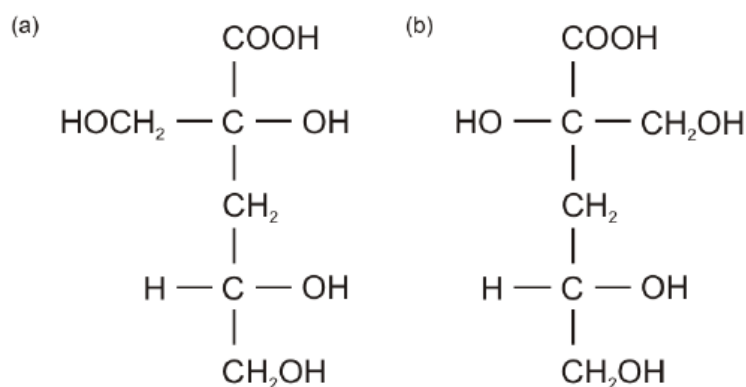
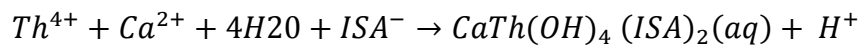


**Figure 1.8: The diastereomers of isosaccharinic acid.**

Under hyperalkaline conditions ISA has been shown to form soluble complexes with a range of radionuclides including plutonium (30, 31), thorium (32), americium (33), europium (32), nickel (34) and uranium (35), with an extensive review provided by Gaona *et al.* (36). ISA within cellulose degradation leachates has been shown to increase the solubility of plutonium above pH 12 at a concentration above  $10^{-5}$  M, with the solubility of plutonium increasing from  $10^{-8}$  to  $10^{-4}$  M given ISA concentration changes from  $10^{-5}$  to  $10^{-3}$  M (31, 36). Investigations using  $\alpha$ -ISA showed its ability to complex uranium at pH 13.5 (35) and nickel under alkaline conditions (34). Investigations using thorium have shown the ability of ISA to increase the solubility of thorium under alkaline conditions up to pH 13.3, with thorium able to form a calcium ISA complex under alkaline conditions between pH 10.7 and pH 13.3 (Equation 1.1) (32).



**Equation 1.1: Thorium, calcium, ISA complexation.**

Considering the cementitious nature of the disposal concept, modification of the interactions between radionuclides and the engineered barriers are an important factor towards long term retention of radionuclides within a GDF. Work by Wieland *et al* (37) showed a reduced ability of hardened cement pastes to uptake thorium at pH 13.3 when  $\alpha$ -ISA concentrations were above  $10^{-4}$  M. Similar results were also seen using NRVB and plutonium, where an  $\alpha$ -ISA concentration of 0.01 M reduced the logarithmic sorption constant of plutonium ( $R_d$ ) from  $5 \text{ dm}^3 \text{ kg}^{-1}$  (without ISA) to  $2 \text{ dm}^3 \text{ kg}^{-1}$  (31). The ability of calcite, an important component in host rock has also been shown to have a reduced ability to sorb europium, americium and thorium at concentration values above  $10^{-5}$  M ISA (33). The ability of microorganisms to degrade ISA could therefore have an impact on the long term performance of an ILW-GDF through the removal of these complexants.

## 1.5 Summary of chapter

The UK has a large nuclear inventory from a long nuclear legacy which can be categorised into high, intermediate and low level waste forms based upon the materials radioactivity and heat generation. A current option for the disposal of the ILW portion of the inventory is via a GDF which will operate via a multi-barrier system to retain the waste. This barrier will consist of physical containment using steel canisters, chemical containment using a cementitious backfill and geological confinement and containment via the host rock the facility is placed in. Upon saturation of an ILW-GDF with groundwater, an anoxic

hyperalkaline environment is expected to form in which the cellulosic portion of the waste is expected to undergo alkaline hydrolysis via the peeling reaction to form a range of cellulose degradation products. The  $\alpha$  and  $\beta$  diastereomeric forms of ISA are expected to be the major components of these CDP and have relevance to the long term performance of an ILW-GDF due to their ability to form soluble complexes with certain radionuclides potentially enhancing their migration into the biosphere.

## **2. Microbial processes under ILW-GDF conditions**

## 2.1 Overview

There is the potential for microbial colonisation of an ILW-GDF during the construction phase and/or from the subterranean biosphere post closure (26). The generation of ISA from the cellulosic component of the ILW could act as a potential carbon source for microbial metabolism through processes such as fermentation and anaerobic respiration linked to terminal electron acceptors (TEA) (20). Inundating ground water is expected to have passed through the microbial thermodynamic ladder whereby higher energy yielding TEA's such as oxygen, nitrate and iron are sequentially utilised as ground water passes through the deep biosphere (38). The waters of the UK are rich in sulphate and coupled with the hydrogen produced through corrosion processes may lead to the generation of methanogenic and sulphate reducing conditions within the near field to the waste. This chapter will address the potential for microbes surviving under the hyperalkaline conditions expected within an ILW-GDF and will discuss related fermentation, sulphate reducing and methanogenic metabolic processes. This chapter will also discuss the impact that biofilm formation may have upon the ability of microbes to survive under ILW-GDF conditions and the relevance biofilm formation may have upon the long term performance of an ILW-GDF.

## 2.2 Microbial survival under ILW-GDF conditions

Conditions within an ILW-GDF are likely to be anaerobic, chemically reducing and highly alkaline with calcium dominated porewaters due to leaching from the cementitious backfill and the corrosion of steel materials (7, 14). Tolerance to alkaline conditions by microorganisms is well documented under a range of laboratory conditions (39, 40) as well in different environments such as soda lakes (41), ophiolites (42) and serpentinite hosted alkaline seeps (43). Microorganisms able to tolerate and grow under alkaline conditions above pH 9.0 are termed alkaliphilic and have unique adaptations to survive the external environmental stress (44). In order for microbes to survive under alkaline conditions the pH of the cytoplasm within the cell must be maintained to allow for the proper function of enzymes and metabolic processes (45). Most non-extremophilic microbes maintain a cytoplasmic pH within the range of pH 7.4 to pH 7.8 (46) where as alkaliphilic bacteria are reported to tolerate much higher values generally >2 pH points below the external pH value (47). For example *B. pseudofirmus* OF4 maintains an approximate cytoplasmic pH value of pH 8.2 when growing on malate at pH 10.5 (48). The ability of alkaliphilic microbes to maintain cytoplasmic pH homeostasis under alkaline conditions relies on transporters and enzymes that promote proton capture and retention such as ATP synthase and Na<sup>+</sup>/H<sup>+</sup>

antiporters (47). The *mrp* antiporter is one such  $\text{Na}^+/\text{H}^+$  linked example which allows *Bacillus* species to tolerate alkaline conditions (49) with complexes of these *mrp* proteins theorised to funnel external protons to the antiporter region (47, 50). The production of metabolic acids through fermentation processes occurs within the cytoplasm and can also contribute to a lowering of the cytoplasmic pH as seen in an antiporter mutant *Bacillus* species (47, 51). Further alkaliphilic adaptations also include the incorporation of larger amounts of teichuronic acids in the cell walls (52) and acidic lipids such as cardiolipin and phosphatidylglycerol within cell membranes of the bacteria (53). Utilising these previously described adaptations alkaliphilic microbes are able to survive and grow under even the most hyperalkaline of conditions with *Bacillus* and *Clostridia* species detected in a steel slag contaminated wetland at pH 13.2 (54) and various microbial species detected in the pH 12.5 groundwater's of the Maqarin area of Jordan (55).

### 2.2.1 Natural analogue sites

The use of analogue sites enables the investigation of both chemical and microbial processes under the conditions expected to form within an ILW-GDF (56). Numerous sites around the world possess hyperalkaline sediments and waters which have formed due to the local geochemistry of the rock formations of the region (42, 43) or through evaporation processes (41, 57). At these sites an array of microbial processes are still able to proceed despite the external alkaline conditions (58-60). A common hyperalkaline formation is that of the soda lake, an area characterised by high salinity and alkaline waters of between pH 8.0 and ~pH 12 (41). At these sites carbonate is the dominant anion within the waters with  $\text{Ca}^{2+}$  cations at low levels and NaCl in varying quantities sometimes reaching hypersaline values (61). Studies of the microbiology of the sediments of these areas, have revealed microbial communities that have members unique to these areas and have most likely evolved separately under the alkaline conditions (41). Studies at Mono Lake, California (~pH 10.0) have revealed a wide range of microbial diversity within the meromictic layers at the site consisting mainly of bacteria from Actinobacteria, *Bacillus*, *Clostridia*,  $\alpha$  and  $\gamma$  Proteobacteria and *Bacteroides* lineages (62). Further studies of other soda lakes have revealed a similar large degree of microbial diversity (61) with processes including sulfate reduction (63), methanogenesis (64) and the anaerobic oxidation of methane (65) all occurring under these conditions.

Ophiolite complexes of mafic and ultramafic rocks generally have hyperalkaline waters associated with them due to serpentinization processes (66). A potential natural analogue site in the Troodos mountains in Cyprus has been investigated for its microbial diversity (67).

The site harbours hyperalkaline springs (pH 10 – 11) which are rich in calcium due to the interaction of  $\text{Mg}(\text{HCO}_3)_2$  type meteoric groundwaters with the ultramafic rocks of the ophiolite (68). Samples taken from a range of hyperalkaline locations at the site showed a wide range of bacterial diversity which included the potential capacity for hydrogen oxidation through *Hydrogenophaga* species, the ability to fix nitrogen via *Paenibacillus* species and iron(III) reduction through microcosm experiments (67). The microbial diversity of other ophiolite based sites has been investigated at range of locations around the globe including the Semail ophiolitic complex in Oman (69), Del Puerto in California (68) and the Leka complex, Norway (42), with each site possessing a wide range of bacteria. The Maqarin site in Jordan possesses hyperalkaline calcium rich waters which are a result of interactions with naturally occurring cement minerals and not due to the alteration of ultramafic minerals (70). Investigations into the microbial diversity at this site have revealed between  $10^3$  and  $10^5$  cells  $\text{mL}^{-1}$  of water with Proteobacteria the dominant phylum and further investigations showing the local consortia at the site capable to respire anaerobically using a range of carbon sources (71).

### **2.2.2 Anthropogenic analogue sites**

Anthropogenic sites are generally formed by contamination from industrial processes such as limestone processing, steelwork slags and bauxite processing which lead to the generation of extreme geochemical environments including the generation of alkaline conditions (54, 56, 72). Sites are often contaminated with bactericidal heavy metals such as arsenic, chromium, copper and zinc (73, 74) and other chemical compounds such as xenobiotics (75). The initial response of the local microbial consortia at these sites is to reduce in population size and diversity; however, as time progresses the local consortia can adapt and evolve to survive (76). Examples of this can be seen in the generation of chromium resistant microorganisms at a site contaminated by tannery waste (77) and the evolution of acidophilic microorganisms in acid mine drainage (78).

A former lime burning waste disposal site near Buxton, UK has previously been investigated as an anthropogenic analogue for some aspects of ILW waste disposal (56, 79). At this site historical lime kiln wastes made up of lime, calcined limestone, coal ash, part burnt coal and clinker were disposed of in the valley adjacent to the works. Percolation of rain water through this waste has led to hyperalkaline calcium hydroxide leachates which upon contact with atmospheric carbon dioxide form a calcium carbonate tufa (56, 79). Investigations of the sediments beneath this tufa surface has revealed an active diverse microbial consortia

composed of previously unidentified bacteria of Comamonadaceae, Bacteroidetes, Firmicutes and Thermotogae species which were capable of both nitrate and iron reduction at ~pH 12.0 (56). At the boundaries between the hyperalkaline calcium rich porewaters and organic materials, both  $\alpha$  and  $\beta$  forms of ISA have been detected in-situ (80), with small scale batch investigations using porewaters and soils from the site also demonstrating ISA generation under lab scale conditions in a temperature dependant manner (80). Further the degradation of ISA has been demonstrated under methanogenic, sulphate reducing, iron reducing and nitrate reducing conditions using sediments from the site to form different types of liquid cultures at a variety of pH values (81-83). Further to the ability of the microorganisms present at the site to degrade ISA, investigations using sediments from the site have also shown evidence of iron, nitrate and sulphate reduction at alkaline pH values using lactate and acetate as electron donors (60). Microbial community analysis of the hyperalkaline sediments at the site via 454 pyrosequencing (83) and MiSeq platforms (84) has revealed a large degree of bacterial diversity despite the hyperalkaline porewaters of up to and above pH 13, with bacteria from the Firmicutes, Proteobacteria and Bacteroidetes Phyla forming the majority of the bacterial components. In addition to the bacterial component, methanogenic archaea were also detected in the sediments at the site but in very low abundance (84).

### **2.3 Biofilm formation**

The bacterial biofilm is argued to be the most successful form of life on earth (85). This is in part due to the large scale distribution of biofilms under most of the planets moderate and hostile environments including animals (86), aquifers (87), deep sea sediments (88), hydrothermal areas (89), permafrost (90) and rock faces (91) to name but a few. Within a bacterial biofilm as little as 10 % of the dry mass can be cells with the rest being made up of extracellular polymeric substances (EPS) (85). EPS is the external gel like matrix in which the cells embed themselves and is formed from a scaffold like structure of extracellular DNA (eDNA), proteins, polysaccharides and lipids (92). Interactions between the different functional groups of these EPS components assist in the stability of the EPS matrix (93) (Figure 2.1). As well as stability these components also assist in providing an array of biochemical and physical properties to the biofilm, with a summary provided in Table 2.1. The production of a biofilm allows cells to adhere to surfaces with cells embedded within the biofilm operating under a different lifestyle than compared to planktonic existence (94). Biofilms also provide a protective barrier from the external environment in which the bacteria can modify the local conditions resulting in increased resistance to a vast array of environmental stresses such as desiccation, solar radiation, pH and temperature shifts and predation (95). This protective environment can be greatly beneficial to bacterial survival and propagation as seen by the increased resistance of biofilms to antibiotics and attack from the immune system in human wounds (96, 97). Modification of the local biofilm environment can come from a range of sources including by-products of microbial metabolism (98) or by EPS components themselves, with bacteria within acid mine drainage biofilms shown to specifically secrete proteins with a high isoelectric point in order to buffer the internal pH of the biofilm (99).

Function	Relevance for biofilm	EPS components involved	Reference
Adhesion	The attachment of planktonic cells to both biotic and abiotic surfaces.	DNA, polysaccharides and protein.	(100, 101)
Aggregation	The ability of cells to form an immobilised population leading to high cell densities in local areas.	DNA, polysaccharides and protein.	(100, 101)
Cohesion	Formation of hydrated polymer network that mediates biofilm stability often through the interaction with multivalent cations.	Neutral and charged polysaccharides, DNA and proteins.	(102, 103)
Enzyme content	The biofilm allows for the binding of enzymes within the matrix acting as a potential external digestive system.	Protein.	(104)
Exchange of genetic information	Facilitates horizontal gene transfer between cells.	DNA.	(105)
Nutrient source	Biofilm components provide a carbon, nitrogen and phosphorus source.	Potentially all EPS components.	(106)
Protective barrier	Confers resistance to environmental stresses (antibiotics, antimicrobials, predation, and oxidation) and host defences.	Polysaccharides and protein.	(95, 96)
Sink for excess energy	Allows for the formation of external carbon stores.	Polysaccharides.	(85)
Sorption of organic compounds	Allows for the accumulation of organic compounds from the environment including xenobiotics.	Charged or hydrophobic polysaccharides and proteins.	(107, 108)
Sorption of inorganic compounds	Allows for the accumulation of metals and promotes mineral formation, ion exchange mechanisms and polysaccharide gel formation.	Charged polysaccharides and proteins.	(108, 109)
Water retention	Maintenance of a highly hydrated local environment leads to resistance against desiccation.	Hydrophilic polysaccharides and lipids.	(85, 110)

**Table 2.1: Biofilm properties of EPS components.**

In order to initiate biofilm formation a free floating cell must adhere to a surface to initiate micro-colony formation through aggregation, a mathematical model of this process is given by Johnson (111). The adherence of a cell to a surface can be separated out into three phases the conditioning of a surface and the primary and secondary forms of adhesion termed ‘docking’ and ‘locking’ by Dunne (112). The conditioning of a surface is the coating of the surface with polymers and molecules present within the surrounding media, an example of such is the ‘acquired pellicle,’ which develops on tooth enamel surfaces in the oral cavity (113). A conditioned surface may then facilitate the primary or docking phase of a cell which may encounter the surface either through random chance propelled via fluidic motion or via chemotaxis or motility (112). This reversible stage of adhesion is generally dictated by the net sum of attractive or repulsive forces between the cell and the surface, with forces including hydrophobic interactions, electrostatic forces and van der Waals forces (114). The condition of a surface can influence this stage by providing additional interactions between the cell and the surface as seen in the adhesion of bacteria to the oral acquired pellicle (115) or *Staphylococcus epidermidis* to polyethylene in the presence of surface-activated platelets (116). The secondary form of adhesion is known as locking whereby the cell becomes

irreversibly bound to the surface through adhesion mediated structures such as pili, fimbriae, and fibrillae (112). EPS produced at this point helps to mediate adhesion between the cell and the surface by interactions between ligand molecules and through the modulation of the physiochemical properties of the localised area (114). During this phase other microbes may also stick to the cells forming aggregates upon the surface with the adhesion of one cell possibly promoting the adhesion of cells from different species (117). Once adhered the cells begin to divide and produce EPS to form biofilm, with the growth of any such biofilm limited by the available nutrients and the perfusion of nutrients through the biofilm materials themselves (112). Eventually during the maturation of a biofilm a stage is reached whereby the biofilm reaches a critical mass and planktonic cells begin to escape the biofilm. This allows the possibility of biofilms to form elsewhere in the surrounding environment and may also occur through sloughing of biofilm material its self, forming small aggregates of EPS and cells (113). The growth and development of cells within a biofilm is closely regulated with cell to cell signalling through quorum sensing via chemical messengers such as acylated homoserine lactones (118). Quorum sensing has been shown to regulate genes involved in development of biofilm and promote the dispersion of cells out of the biofilm (118), with its disruption adversely effecting biofilm formation and development (119). The ability of microbes to immobilise themselves to surfaces allows for microbial populations to exploit nutrient rich areas and provides a greater access to genetic diversity. Although growth rates are slower within a biofilm compared to planktonic cultures the benefits provide a clear selective advantage to survival in harsh or nutrient poor environments.

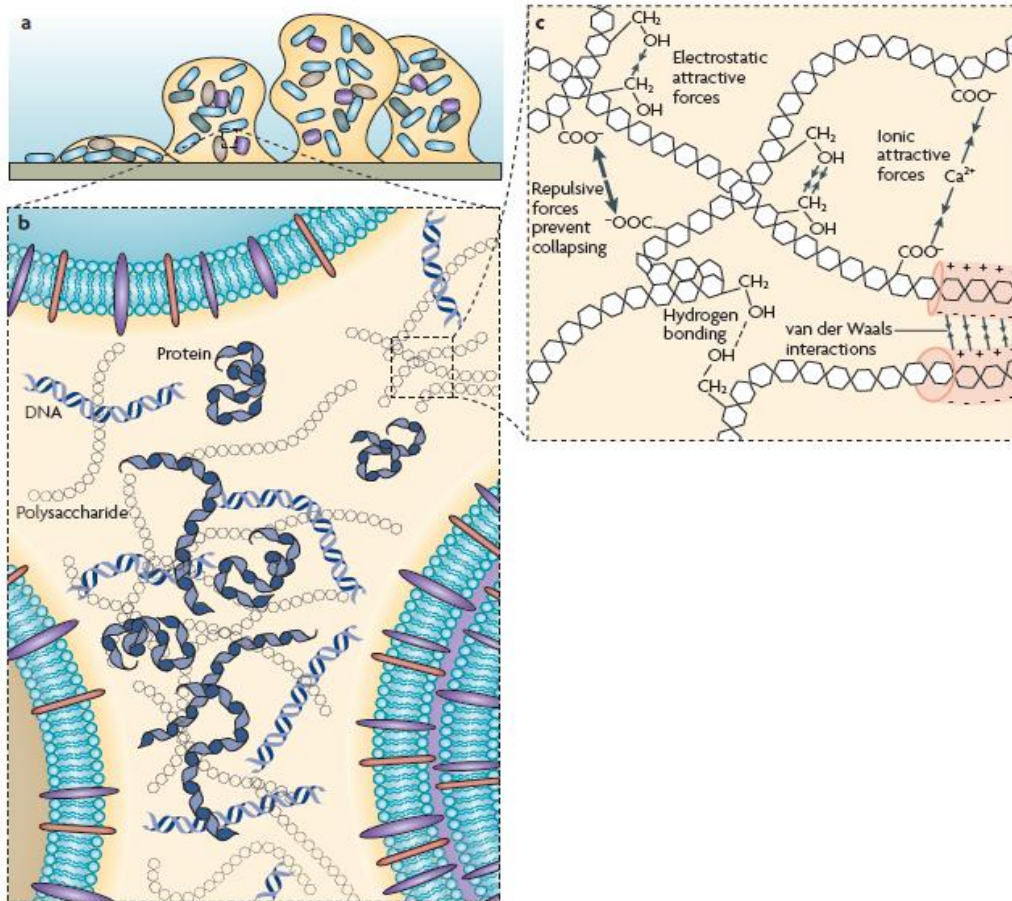
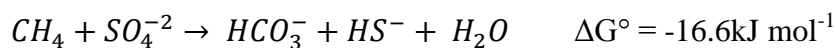


**Figure 2.1: The microbial biofilm structure and the interactions between EPS components.** [A] Diagram showing cell attachment to a surface followed by subsequent aggregation and biofilm development. [B] The major EPS matrix components shown in between cells. [C] Diagram of interactions between EPS components. Figure adapted from (85).

The close proximity of cells to one another within a biofilm allows for syntrophic relationships such as the interspecies hydrogen transfer between fermenters and methanogens to take place (120). The ability of bacteria to form syntrophic relations allows microbial processes to proceed near the thermodynamic limits of life as seen in the process of the anaerobic oxidation of methane where sulphate is used as a TAE (Equation 2.1) (121). The energy generated from this process ( $\Delta G^\circ = -16.6\text{kJ mol}^{-1}$ ) is lower than the required minimum biochemically convertible energy that can be used by a bacterial cell ( $-20\text{kJ mol}^{-1}$ ) hence the process of AOM in theory does not yield enough energy to synthesise ATP (122, 123). Therefore organisms living in syntrophy such as methanogens and sulphate reducing bacteria (SRB) as seen in microbial mats in the black sea which carry out AOM (124) overcome this by the removal of end products by one species which are a result of the utilisation of a substrate by another (123).



**Equation 2.1: Anaerobic oxidation of methane.**

A biofilm is theorised to be a highly competitive environment with only bacteria that can operate synergistically and effectively under the environmental conditions earning and keeping a place within the biofilm (85, 125). Biofilms can come in an array of forms including thin films formed on materials such as steel, thick microbial mats and suspended EPS based aggregates termed ‘flocs’ (95). Floc based systems are seen commonly in wastewater treatment and have a complex but organised structure with bacteria around the outer surfaces of the aggregate feeding metabolic products such as hydrogen and acetate in towards the centre for methanogens to utilise (Figure 2.2) (126, 127). There is evidence to suggest that the architecture of biofilm is complex with aggregates of cells (rather than monolayers of cells) in a heterogeneous microstructure which can possess pores and channels for water flow (128). Further the biofilm structure itself can also change varying upon the environmental conditions (95, 129) with biofilms under high shear stresses as experienced by dental plaques resulting in a biofilm with a compact stratified appearance (130) whereas biofilms in flowing water exhibit a longer flowing streamer like structure (129).

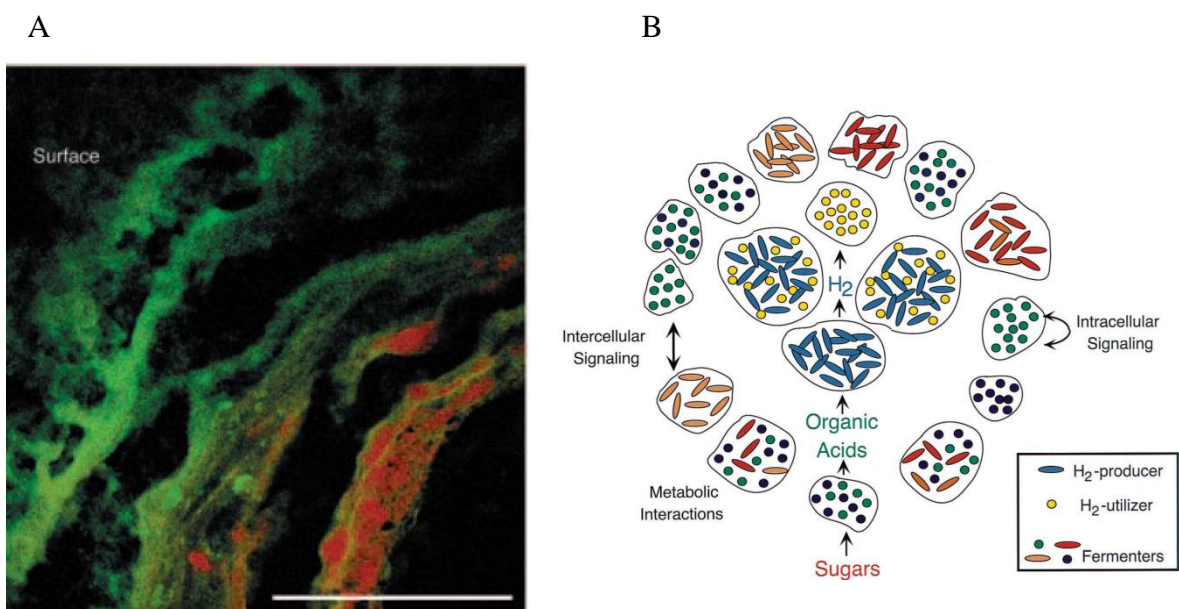


**Figure 2.2: Syntrophic interactions in biofilm.** [A] Distribution of bacteria (green) and archaea (red) through aggregate, archaea are situated towards centre. [B] Diagram showing flow of nutrients and syntrophic interactions in aggregate. Figures taken from (95, 127).

## 2.4 Biofilms with relevance to an ILW-GDF concept

The ability of biofilm to exist in harsh environmental conditions is well documented with biofilms seen in acid mine drainage (131), polar regions (132) and hot springs (133). An ILW-GDF offers an anoxic, hyperalkaline, calcium dominated environment with low nutrients and limited availability of TEA's due the passage of ground waters through the thermodynamic ladder (38). Despite these conditions the biofilm mode of life has been reported at serpentinite-hosted hyperalkaline springs under these conditions (67, 134). The ability for microbes to colonise a GDF throughout its lifespan either through pre-closure contamination or post-closure through groundwater percolation could potentially lead to the formation of biofilm within microsities formed in the near field. These biofilms could affect long term repository performance in a number of ways through biological and chemical processes (26). The ability of microorganisms to form biofilm within the pore throats of porous media can lead to the blockage and lowering of the porosity of this media in what is known as bio-clogging (135). The action of microbial metabolism in biofilms within pore throats could also lead to the formation of mineral precipitates such as calcite as seen in *Sporosarcina pasteurii* biofilms grown on granite in the presence of calcium chloride (136). The clogging of pore throats and the formation of calcium carbonate under these conditions could potentially help to prolong hydraulic retention within a GDF by sealing cracks and fractures as seen in fracture sealing by calcite at the Maquarin site (7). The formation of biofilm, however, could also reduce the ability of host rocks to interact with radionuclides, with experiments by Anderson *et al* (137) showing a reduced ability of granitic host rocks to sorb cobalt, molybdenum, neptunium, americium and thorium when coated in biofilm. The ability of microbes within biofilms to degrade ISA could potentially reduce the migration of radionuclides with associated microbial metabolism producing calcium carbonate precipitates as seen in the lithification processes of microbial mats (138). This formation of carbonate precipitate could have an impact upon radionuclide solubility as radionuclides such as uranium will co-precipitate with calcium carbonate (139). The products of the microbial metabolism could also have an impact upon the surface properties of the engineered barriers through the carbonation of the NRVB surface which could modify its ability to interact with radionuclides (140, 141). Further the production of gas through processes such as methanogenesis could also act as a potential mechanism for the transport of C-14 out of the GDF into the biosphere (142). There is currently a paucity of information regarding the ability of microorganisms to form biofilm under the hyperalkaline conditions expected within an ILW-GDF. Recent studies have shown the ability of biofilms grown in crushed sandstone

columns to survive up to pH 13 (143), whilst causing a level of bio-clogging and interacting with technetium altering its migration through the system (144). These studies, however, employed a media which contained the organic supplement yeast extract which is not expected to be present under ILW-GDF conditions and used lactate and acetate as surrogate for ISA. As such the studies do not shed light on the ability of biofilms to form under ILW-GDF conditions with CDP, specifically the different forms of ISA, as the primary carbon source.

#### **2.4.1 Microbial processes under ILW-GDF conditions**

Due to passage of groundwaters through the thermodynamic ladder of microbial respiration any groundwater saturating an ILW-GDF is expected to be depleted of most potential TEA's (38). As sulphate is abundant in most UK ground waters (145) it possible that it could be present within the near field alongside carbon dioxide as the most probable TEA's to drive microbial processes. Under the conditions expected within the near field and considering the availability of TEA's, fermentation, methanogenesis and potentially sulphate reduction would be expected to be the dominant microbial processes. It should be noted that due to the heterogeneous nature of ILW, TEA's including nitrate, iron and manganese may leach from the waste (7), these TEA's would, however, be in a small amount compared to carbon dioxide and potentially sulphate.

#### **2.4.2 Fermentation**

The process of fermentation occurs when no appropriate TEA is available for higher energy generating processes through oxidative phosphorylation, with energy generation instead driven by substrate level phosphorylation or the use of an endogenous TEA (146, 147). Examples of this can be seen in the generation of ethanol in the absence of oxygen by yeast during the brewing process (148). Hydrolysis of polymers such as polysaccharides, nucleic acids, proteins and lipid generate a range of monomeric units suitable for fermentation processed including sugars (hexoses, pentoses, tetroses), amino acids, polyols, purines and pyrimidines (149). The general products of fermentation vary with bacterial species and carbon source with end products including alcohols, volatile fatty acids (VFA) and gases such as hydrogen and carbon dioxide (149) (Figure 2.3). The process of fermentation is based within the cytoplasm of the cell with products such as acetate and ethanol excreted into the external environment. Under alkaline conditions the end products of fermentation can help to buffer the cytoplasmic pH (47, 51) with hydrogen generation processes through fermentation identified in hyperalkaline springs (>pH 10) of the Samail ophiolite in northern Oman (150).

The ability of microbes to ferment CDP in an ILW-GDF could generate a lower pH niche through the generation of acids as seen in alkaline culture experiments where the pH is not attenuated (151). Also fermentation end products could further fuel other microbial metabolic processes including methanogenesis and sulphate reduction.

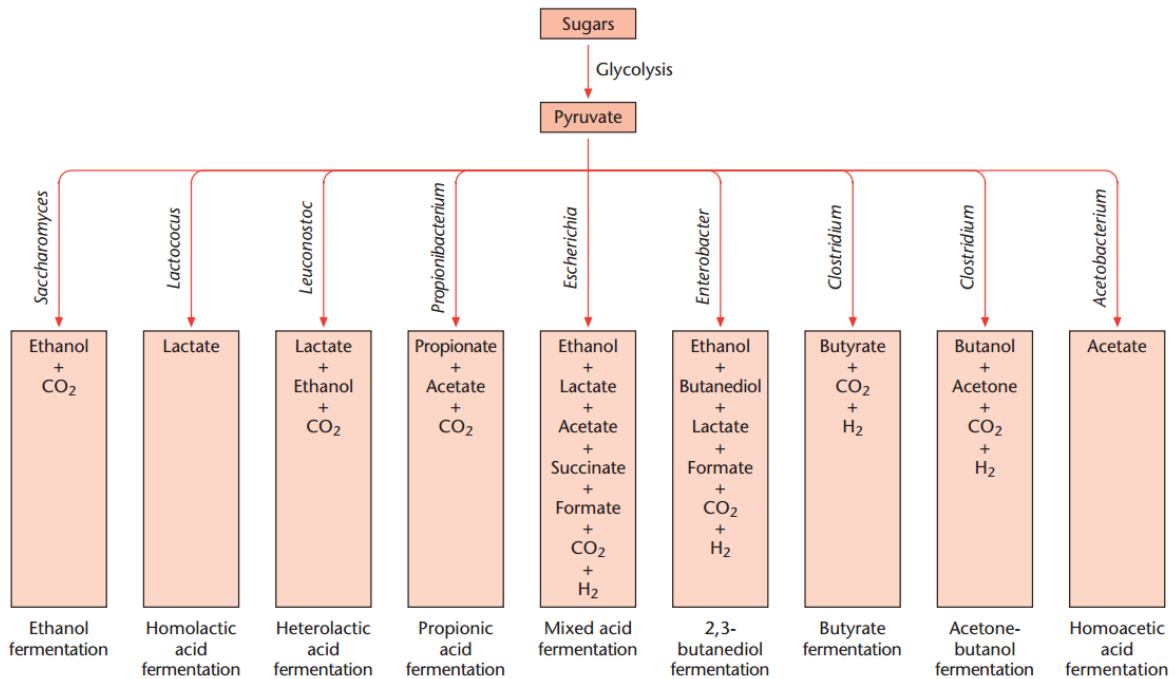


**Figure 2.3: Fermentation end products of different bacterial genera.** Figure taken from (149).

### 2.4.3 Methanogenesis

Methanogenesis is linked to the fermentation processes of anaerobic degradation, with the products of fermentation acting as substrate for methanogenesis. Methanogenesis is carried out solely by archaea, which can be divided in 5 orders: Methanobacteriales, Methanomicrobiales, Methanopyrales, Methanococcales, and Methanosarcinales (152). Methanogenic archaea have been identified and isolated from a range of alkaline environments including soda lakes (64) and low salt alkaline sediments (153). Methanogens can use three different pathways utilising different electron donors to drive their metabolism. These include the CO<sub>2</sub> reduction pathway in which formate or H<sub>2</sub> is oxidised and CO<sub>2</sub> is reduced to CH<sub>4</sub> (154). The acetotrophic pathway in which acetate is converted to CH<sub>4</sub> and CO<sub>2</sub> (155) and finally CH<sub>4</sub> generation through the utilisation of methylotrophic substrates such as, methylamines, methylsulfides and methanol (156). These reactions and their associated Gibbs free energies are shown in Table 2.2. The upper limit for methanogenesis via the CO<sub>2</sub> reduction pathway appears to be dictated by a salt concentration of 90 g L<sup>-1</sup> with

methanogens using the different pathways above this threshold (121). Consequently investigations of methanogenesis at pH 9.7 using slurries from Big Soda Lake, Nevada, USA showed CH<sub>4</sub> production through only the methylotrophic pathway using methanol, trimethylamine and methionine (157). In alkaline areas of lower salinities methanogens capable of autotrophic growth via the CO<sub>2</sub> reduction pathway have been isolated from a range of environments. Worakit *et al* (153) isolated strains of *Methanobacterium alcaliphilum* sp. from the lakes in the Wadi el Natrun of Egypt that were capable of autotrophic growth up to pH 10. From this same area Boone *et al* (158) isolated a further 5 strains of methanogenic bacteria, 4 from low salt areas of a pH between 8.3 – 9.3 which were strictly autotrophic only producing CH<sub>4</sub> through the CO<sub>2</sub> reduction pathway. The last strain was found to be a strict methylotroph which originated from an area with a higher salinity and a pH of 9.7 (158). Reports of acetotrophy by methanogens under alkaline conditions appear to be scarce with one instance reported by Oremland & Miller (159) who used carbon 14 labelled acetate methods to detect acetate utilising methanogens at Soap Lake, Washington, USA.

Reaction	$\Delta G^\circ$ (kJ mol <sup>-1</sup> ) pH 7	Reference
<b>Sulphate reduction</b>		
$4\text{H}_2 + \text{SO}_4^{2-} + \text{H}^+ \rightarrow \text{HS}^- + 4\text{H}_2\text{O}$	-155	(160)
$\text{Acetate}^- + \text{SO}_4^{2-} \rightarrow 2\text{HCO}_3^- + \text{HS}^-$	-47.6	(161)
$\text{Lactate}^- + 0.5\text{SO}_4^{2-} \rightarrow \text{Acetate}^- + \text{HCO}_3^- + 0.5\text{HS}^-$	-80.2	(161)
$\text{Propionate} + 0.75 \text{SO}_4^{2-} \rightarrow \text{Acetate}^- + \text{HCO}_3^- + 0.75\text{HS}^- + 0.25\text{H}^+$	-37.7	(161)
<b>Methanogenic reactions</b>		
$4\text{H}_2 + \text{HCO}_3^- + \text{H}^+ \rightarrow \text{CH}_4 + 3\text{H}_2\text{O}$	-135.6	(162)
$\text{Acetate}^- + \text{H}_2\text{O} \rightarrow \text{CH}_4 + \text{HCO}_3^-$	-31.0	(162)
$\text{Methanol} + \text{H}_2 \rightarrow \text{CH}_4 + \text{H}_2\text{O}$	-112.5	(162)

**Table 2.2: Sulphate reduction and methanogenesis processes.**

#### 2.4.4 Sulphate reduction

The reduction of sulphate can be split into two pathways; the assimilatory pathway and the dissimilatory pathway (163). The assimilatory pathway is utilised to satisfy the nutrition requirement of a cell through the synthesis of sulphur containing components and uses sulphate converted to 3'-phosphoadenosine-5'-phosphosulfate (PAPs) as its substrate (163). The dissimilatory pathway, however, is used by a cell to generate energy by using sulphate as a TAE, with this form of sulphate reduction carried out by microorganisms from the  $\beta$ -Proteobacteria, Clostridia, Nitrospirae, Thermodesulfobiaceae, Thermodesulfobacteria, Crenarchaeota and Euryarchaeota lineages (161). A complete review of the enzymatic

processes of dissimilatory sulphate reduction is given by Bradley *et al* (164). Briefly; sulphate is taken into the cell and converted to adenosine phosphosulfate (APS) via ATP sulphurylase, APS reductase then converts APS to sulphite which is then further reduced to hydrogen sulphide by the dissimilatory sulphite reductase complex DsrAB-C (164) (Figure 2.4).

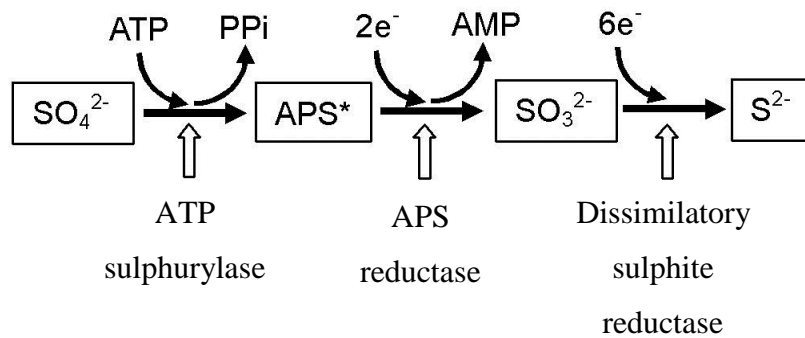


**Figure 2.4: Overview of the dissimilatory sulphate reduction pathway.**

The reduction of sulphate by the sulphate reducing bacteria (SRB) is not limited to a moderate environment (165). The ability of these bacteria to couple the oxidation of a wide range of organic electron donors to sulphate has allowed them to colonise even the most inhospitable regions on earth (161). Of the alkaline environments found on earth, soda lakes are the most extensively researched in terms of alkaliphilic SRB (63). Soda lakes represent a significant challenge to life with environmental conditions consisting of high pH values up to and above pH 11 and salinities up to saturation levels (63, 165). Despite these conditions the SRB thrive in these environments and are considered to be an important component in the associated microbial sulphur cycle at these locations (165). SRB are metabolically diverse and are capable of both autotrophic and heterotrophic growth with the SRB's currently divided into two groups; those which degrade organic compounds incompletely to acetate and those which degrade organic compounds completely to  $\text{CO}_2$  (166). Sulphate reducing reactions form sulphide as an end product and an overview of the main pathways for sulphate reduction and their associated Gibbs free energies are shown in Table 2.2. The energies listed in Table 2.2 show the free energy change under standard conditions at pH 7; however environmental bacteria especially those in high pH environments will have free energy changes which may differ significantly from theoretical values. Oren *et al* (121) calculated that the  $\Delta G_f$  of protons changes from -39.83 kJ per mole at pH 7 to -56.9 kJ per mole at pH 10 as proton releasing reactions become more energetically favourable.

Studies using  $^{35}\text{SO}_4^{2-}$  have allowed for the rates of sulphate reduction in different alkaline environments to be established. The sediments from different soda lakes in the Kulunda Steppe in south eastern Siberia, Russia were shown to have sulphate reduction rates (SRR) of up to  $423 \mu\text{mol dm}^{-3} \text{ day}^{-1}$  (63). With SRR of  $113 \mu\text{mol dm}^{-3} \text{ day}^{-1}$  reported at pH 10.7 from the sediments of lake Tanatar I (east) (63). Further, enrichment of slurries from these sites at pH 10 with either  $\text{H}_2$  or a mixture of volatile fatty acids (lactate and butyrate) were both shown to be able to stimulate sulphate reduction (63). Studies at Lake Mono, California, USA using sediments from an area at pH 9.8 were shown to actively reduce sulphate to sulphide with rate constants between  $7.6 \times 10^{-4}$  to  $3.2 \times 10^{-6} \text{ hr}^{-1}$  and a reduction rate of sulphate of  $27.8 \text{ mmol m}^{-2} \text{ day}^{-1}$  (167). Sulphate reduction with different electron donors was demonstrated using water of Big Soda Lake, Nevada, USA at pH 9.7 (168). Of the organic electron donors used methanol, lactate and acetate at 1 mM gave corresponding SRR's of 0.84, 0.94 and  $1.04 \mu\text{mol L}^{-1} \text{ day}^{-1}$ , respectively.  $\text{H}_2$  gas at a final concentration of 3.2 mM gave a sulphate reduction rate of  $1.62 \mu\text{mol L}^{-1} \text{ day}^{-1}$  (168).

Studies of low saline hyperalkaline areas using the sediments found at anthropogenic analogues sites for an ILW-GDF have been conducted using the previously described site at Buxton, UK (79). Incubation at pH 10, 11 and 12 with acetate, lactate and yeast extract as electron donors have shown little or no sulphate reduction over a ten week period (60). Further studies using the alpha form of calcium ISA as an electron donor also failed to demonstrate evidence of sulphate reduction at pH value 10 and 11 over a 2 week period (83). In contrast to this, SRBs have been shown to survive in biofilm operating at pH 10.2, with sulphide produced within the alkaline waters at a Danish district heating plant leading to corrosion issues of the plant apparatus (169).

High pH environments could favour SRB growth by the fact that sulphide produced as an end product of sulphate reduction would be present in its ionic form  $\text{HS}^-$ .  $\text{HS}^-$  is a less toxic end product compared to  $\text{H}_2\text{S}$  as it cannot freely cross the cell membrane allowing a much greater concentrations of substrates and end products to be tolerated (165). Given that SRB's are metabolically flexible, able to use a range of electron donors and acceptors including radionuclides such as uranium (161) and that they have colonised hyperalkaline areas around the globe (63). It would not unrealistic given the timeframes associated with an ILW-GDF that SRB's could colonise and possibly affect ILW-GDF performance especially if biofilms are able to produce sulphide, which could lead to the microbial induced corrosion of steel materials (170).

## 2.5 Microbial degradation of ISA

A range of studies have concentrated on the degradation of the ISA contained in black liquor which is the waste product from the Kraft process. The Kraft process produces bleached wood pulp from wood chips to form paper and is described further by Courchene (171). The end product is almost entirely cellulose fibres with the high temperature and alkaline treatment of the wood chips producing a range of CDP's including the  $\alpha$  and  $\beta$  forms of ISA and XISA from hemicellulose. Wang *et al* (172) investigated the ability of anaerobic microorganisms to degrade the ISA's present within Kraft black liquor in the presence and absence of chlorinated lignin derivatives. The author found that ISA was able to be degraded with methane as the end product in the presence or absence of chlorinated lignin derivatives. The study which used microbes from a bioreactor treating Kraft waste also compared the microbes ability to degrade glucose as well as ISA and found differences in methane production rates which was theorised to be linked to the formation of two different microbial consortia (172). Investigations by Strand *et al* (173) looked at the ability of microbes to degrade  $\alpha$ -ISA under aerobic conditions. The study included 22 laboratory strains isolated from forest soils and samples taken from in and around a Kraft paper mill. Of the samples tested only samples taken from the paper mill area (bar one) were able to degrade  $\alpha$ -ISA with the author suggesting the degradation of ISA required an unusual or modified enzyme compared to the breakdown of other carbohydrates (173). The ability of microbes isolated from Kraft waste contaminated land to degrade ISA under aerobic conditions has further been demonstrated in the works of Pekarovičová (174) and Bailey (175), where Bailey (174) showed the inability of two ISA degrading isolates to degrade glucose.

In studies aimed at investigating the microbiology of the disposal concept for radioactive wastes, ISA has been shown to be degraded under a range of conditions. Grant *et al* (176) investigated the degradation of carbon 14 labelled ISA using both planktonic and biofilm cultures at pH 10.5 under nitrate reducing conditions. Microbial consortia from hyperalkaline areas and areas contaminated with Kraft waste were able to degrade ISA in both planktonic and biofilm cultures with rates of ISA degradation of 0.2 to 5.6 mol ISA yr<sup>-1</sup> g<sup>-1</sup> biomass and 40 to 350 mol ISA yr<sup>-1</sup> m<sup>-2</sup>, respectively (176). Carbon 14 labelled ISA was found to be degraded to <sup>14</sup>CO<sub>2</sub> where nitrate was used as an electron donor and reduced to nitrite then to nitrogen gas. Studies by Rout *et al* (177) found that microbial communities from neutral areas including canal sediments could degrade the  $\alpha$  and  $\beta$  forms of ISA under methanogenic, sulphate and iron reducing conditions, coupling its degradation to appropriate TEA under far

field conditions. Further work using liquid methanogenic microcosms showed the ability of these microbes to degrade ISA decreased as the pH value rose. At pH 10 and above these natural communities struggled to degrade ISA and instead microcosms became dominated by microbes turning over biomass (81). Similar studies by Rout *et al* (80) using sediments from the previously described Buxton analogue site (79) found the microbial community present to be able to degrade both the  $\alpha$  and  $\beta$  forms of ISA under methanogenic conditions at pH 11. ISA under these conditions was theorised to be degraded through fermentation to acetate, hydrogen and carbon dioxide which then further drove methanogenesis (80). Rout *et al* (80) reported first order rate constants of ISA degradation at pH 11 of  $1.69 \times 10^{-1} \text{ day}^{-1}$  for  $\alpha$ -ISA and  $1.13 \times 10^{-1} \text{ day}^{-1}$  for  $\beta$ -ISA which were greater than those reported for consortia obtained from neutral sediments operating under the same conditions but at pH 10 (177). Investigations by Bassil *et al* (83) used sediments from the previously described Buxton analogue site (79) to degrade calcium  $\alpha$ -ISA under aerobic, iron, nitrate and sulphate reducing conditions. The author also provided microbial community analysis for the related ISA degrading liquid microcosms, however, as only  $\alpha$ -ISA instead of CDP was utilised it may have resulted in a significantly altered result. This is shown in work by Kyeremeh *et al* (84) who examined the microbial community evolution of two Buxton sediment formed microcosms at pH 9 under methanogenic conditions. One microcosm was fed with calcium  $\alpha$ -ISA and one with CDP, with analysis of the communities after a ten week feed/waste period finding a significant difference between the two (84). Investigations using cellulosic materials under hyperalkaline conditions with sediments from the Buxton analogue site have revealed the ability of the microbes present within the site to degrade ISA as it is produced via the alkaline peeling reaction causing a related acidification of the local area (80, 178). Rout *et al* (80) showed a temperature dependant fashion with which the ISA was degraded, favouring 20°C and produced an Arrhenius curve showing a higher rate of the generation of ISA from organic materials at this temperature under ILW-GDF conditions (80). To date no examples of biofilms able to degrade  $\alpha$ -ISA,  $\beta$ -ISA and XISA under methanogenic and sulphate reducing conditions using CDP under hyperalkaline conditions have been published.

## **2.6 Summary of chapter**

A range of hyperalkaline areas have demonstrated the ability of microbes to survive and proliferate under the conditions expected within an ILW-GDF. The ability of microbes to form biofilms could enhance resistance to environmental stresses and could act as a survival mechanism under ILW-GDF conditions. The ability of microbes to degrade ISA has been demonstrated up to pH 11 under methanogenic conditions and at lower pH values under a range of conditions. The ability of microbes to degrade ISA combined with biofilm formation could have an impact upon the long term performance of an ILW GDF through the removal of complexants, blocking of pore throats, changes to the surface chemistry of engineered and natural barriers and through gas production.

### **3. Methods for the analysis of environmental microbiology**

### **3.1 Overview**

The ability to investigate and characterise a system be it natural or laboratory based gives insights into the potential impact the associated microbiology might have on that system. A variety of techniques exist which can be utilised towards this goal, with the focus of the following chapter upon the investigation of microbiological processes relevant to the radioactive waste disposal concept, where possible. The isolation and cultivation of microorganisms and the ability to identify them through molecular techniques is a key component of characterising systems. A range of technologies utilising the conserved 16S rRNA gene have developed towards the purpose of microbial community analysis with the most recent next generation techniques generating large datasets requiring specialised bioinformatic analysis.

### **3.2 Culturing techniques**

Microorganisms can be cultured from an environmental site using either solid or liquid based mediums, whereby the composition of the medium combined with the culture conditions (temperature, O<sub>2</sub> concentrations, pH) will dictate the types of microorganisms isolated (179). Enriching microbes from an environmental sample under conditions similar to the environmental conditions can give insights into the potential metabolic abilities or survival capabilities of a microbial consortia at a given site. Examples of this can be seen in microcosm studies where the different potential metabolic terminal electron accepting processes of microbes from a hyperalkaline sediment were tested at different pH values (60). The operation of a microcosm is flexible with different types of configurations dependent upon the desired output and goals of the studies. Configurations can include single batch fed systems which are sealed to allow geochemical conditions to develop over time or continuously fed systems in which nutrients are delivered slowly via a steady stream through the system. Microcosms can be seeded with pure cultures of microbes or environmental samples containing diverse microbial populations and be liquid based or can contain a solid substrate for microbial colonisation. Polymicrobial microcosms are likely to maintain and highlight syntrophic relationships which can occur under the environmental conditions. Liquid batch fed systems using polymicrobial consortia have been used to investigate the abilities of microorganisms from both pH neutral and hyperalkaline sediments to degrade ISA under a variety of conditions including methanogenic, iron reducing and sulphate reducing (80, 81, 177). Continuous flow systems with a biofilm component have shown the impact of biofilm formed upon crushed sandstone upon the migration of technetium and survival at

high pH (144). Rather than seeding complex mixtures of microorganisms, microcosms can also be run with pure cultures, which can give insights into the rates of specific processes as seen in rate of uranium absorption to microbial biomass by different *Microbacterium* isolates (180). In order to get a pure culture a range of isolation techniques can be used such as streak plating on solid medium or through the use of dilution as seen in the Most Probable Number (MPN) technique. These techniques can be applied directly onto environmental samples with the MPN technique utilised to estimate the number of viable organisms in sites of interest for disposal strategies including bentonite deposits in Japan (181) and from areas around the Yucca Mountain, Nevada (182). It should be noted however, that the majority of microorganism are believed to be unculturable on liquid or solid medium and therefore techniques such as the MPN may not capture the true diversity at a given site (179).

### **3.3 Microscopy studies**

The direct visualisation of microbes can be achieved using a variety of microscopy techniques. Scanning electron microscopy (SEM) and transmission electron microscopy (TEM) approaches can be used to view the morphology of individual bacterial cells and the architecture of biofilms. SEM techniques include the dehydration and coating of a sample with an electron dense metal such as gold, whereas TEM techniques require the sample to be fixed in a solid support matrix such as Spurr's resin and the sample cut into ultrathin sections. Both techniques have numerous advantages and disadvantages with the related techniques for viewing microorganisms reviewed by Kalab *et al* (183). SEM has been used to investigate the different microbial morphologies in boom clay materials (184) and both SEM and TEM can be coupled to energy-dispersive X-ray spectroscopy (EDS) to investigate the elemental composition of microscopic structures. Brown *et al* (185) used a TEM EDS approach to show the formation of mineral precipitates in EPS materials of biofilms growing within fractures of the granitic rock faces of the Underground Research Laboratory at the Canadian Shield (185). With Reith *et al* (186) showing the biomineralisation of gold upon biofilm materials via a SEM EDS method.

Combining microscopy with fluorescence stains can be used to view individual bacteria or their EPS components in environmental samples. Stains which are membrane permeable and intercalate with DNA such as DAPI or acridine orange have been used to count total microbial cells within leachates and ground water at different sites relevant to the disposal concept (71). A combination of stains which take advantage of membrane permeability and impermeable stains can be used to distinguish between alive and dead cells. Chicote *et al*

(187) used a commercial kit which utilised SYTO 9 and propidium iodide to distinguish between alive and dead cells in spent fuel ponds, with propidium iodide only staining cells with compromised cell membranes. As well as cells, stains can also be directed at the different components of the biofilm materials with Chen *et al* (188) showing a 6 colour staining method for the staining of the polysaccharide, protein, extracellular DNA and lipid fraction of EPS based aggregates. Techniques such as confocal scanning laser microscopy (CLSM) can combine the use of fluorescence stains with microscopy to build high resolution images of biofilm structures as well as 3D renders through biofilm materials. Biofilms have been imaged using this technique under a range of conditions and upon different surfaces with CLSM imagery showing micro-colony formation of *Streptococcus mutans* in biofilms (189) and the biofilm architecture of 60 opportunistic pathogens (190).

Fluorochromes can be ligated to oligonucleotide probes which are complementary to specific RNA/DNA sequences within bacterial cells. Using fluorescence in-situ hybridisation (FISH) techniques, bacteria which contain certain genes can be selectively stained and viewed using fluorescence microscopy (191). This technique has been used to view the spatial distribution of bacteria and archaea in biofilm and aggregates through the use of probes aimed at the 16S rRNA gene (127) and can be used to count specific types of bacteria in multiplex assays under environmental conditions (191).

### **3.4 Viability studies**

The ability to detect and quantify microorganisms in-situ can be achieved by using biochemical markers only present in viable microorganism such as adenosine triphosphate (ATP). ATP is the universal energy currency of a cell and is therefore only present in cells which are active and alive (192). The detection of ATP has identified viable microorganisms down to a level of  $2 \times 10^3$  cells ml<sup>-1</sup> within the Fennoscandian Shield groundwaters (193) and has been used to detect viable microorganisms in bentonite from canister retrieval experiments at the Hard Rock Laboratory (194). Another method is to use phospholipid fatty acid (PLFA) analysis which extracts microbial membrane materials using an organic solvent. PLFA analysis can be used to estimate total microbial biomass in samples as well give a representation of the microbial groups presents through the use of group specific biomarkers (195). This method has been used to estimate microbial numbers per gram of dry rock at the proposed nuclear waste repository at Yucca Mountain, Nevada (182) and was used to estimate the number and types of bacteria in a compacted clay based buffer which had been buried for 6.5 years at AECL's Underground Research Laboratory (196).

## 3.5 Nucleic acid approaches

### 3.5.1 Nucleic acid extraction

The extraction of nucleic acids either DNA or RNA is the initial step required for subsequent analysis via different molecular biology techniques. Sequencing of extracted DNA or RNA can be undertaken to determine the genes present and the active genes currently being transcribed in what is termed meta-genomics and meta-transcriptomics, respectively. The extraction of nucleic acids from environmental samples can prove to be a difficult endeavour due a number of factors including pH, humic acids and clay minerals (197, 198). Numerous methods can be employed for the extraction of genomic materials with cells initially lysed via chemical or physical methods with further chemical treatment used to remove cell debris and contaminants of nucleic acid preparations. Griffiths *et al* (198) developed methodologies specifically aimed at the extraction of microbial genomic materials from environmental samples which reduce the contaminants and increase the purity of the extracted nucleic acids. A number of commercial kits are now available for the extraction of nucleic acids which aim to simplify and speed up the process of extracting nucleic acids and a range of these kits have been compared and reviewed by Ariefdjohan *et al* (199).

### 3.5.2 Polymerase chain reaction methodologies

Polymerase chain reaction (PCR) is a technique used to amplify a specific region of DNA and utilises DNA polymerase isolated from *Thermus aquaticus* (200) and oligonucleotide primers which are generally ~ 25 base pairs in length. The primers are complimentary to the 3' ends of the sense and antisense DNA strands of the target area and combined with cycles of heating and cooling with deoxynucleoside triphosphates (dNTPs), amplify the region of interest in an exponential manner (201). Utilising this method combined with nested PCR, specific microbial lineages were identified within microcosms degrading ISA by Rout *et al* (177). This technique although capable of identifying specific regions of interest does suffer from some drawbacks associated with the binding of the primer to some sequences more strongly than others. This primer bias as shown by the experiments of Suzuki *et al* (202) leads to a disproportionate amplification of the more strongly binding regions and can thus skew results when multiple species of a gene of interest are present.

The amplification of a gene through PCR can be quantified using fluorescent markers that only fluoresce upon the formation of a PCR product. Using this quantitative PCR (qPCR) approach the abundance of certain genes in environmental samples can be quantified when compared against a standard curve. The presence of *Rhodanobacter* and the associated

abundance of nitrate reductase genes were determined in the contaminated subsurface of the nuclear legacy site at Oakridge facility using this approach (203). Lear *et al* (204), similarly used a qPCR technique to track bacteria from the *Geobacteriaceae* family in flow through columns which were investigating the effects of microbial iron reduction upon technetium solubility. The generation of cDNA from mRNA can be used as a template for amplification via qPCR and can give an insight into the transcription rates of specific genes and therefore the rates of specific metabolic processes. Chin *et al* (205) showed expression of the genes *rdA* and *omcB* to correlate with rates of fumarate and iron reduction, respectively using this approach. This may not, however, be the case in all scenarios with the transcription of the *drsA* gene found not to correlate well with rates of sulphate reduction under certain circumstances (206). Work by Strattan (207) addressed this issue by normalising the expression of *dsr* mRNA transcripts against the genes found in the genomic DNA of sulphate reducing bacteria in order to ascertain a rate of sulphate reduction on a per cell basis. With this approach potentially offering a true measure of sulphate reduction in both lab based cultures and in-situ at environmental sites.

### **3.5.3 Cloning of PCR products**

The prokaryotic 16S rRNA gene is highly conserved between bacterial species and is subject to a slow evolution rate. Because of this facet phylogenetic relationships can be constructed through the sequencing and comparison of the 16S rRNA sequences of other known bacterial species (208, 209). The extracted genomic DNA of an environmental sample is likely to contain numerous different 16S rRNA gene copies due to the diversity of microbial community present. The process of cloning these 16S rRNA genes to get a single gene sequence for DNA sequencing and analysis, first requires amplification by PCR using universal primers (210). The PCR products are then ligated into plasmids and transformed into a competent strain of *E.coli* which is generally only capable of the uptake of a single plasmid copy (211). Through a selection process via insertional inactivation techniques such as blue/white screening, colonies successfully transformed should only contain multiple copies of the same PCR product (212). Extraction of the plasmid followed by sequencing of the PCR fragment then allows phylogenetic assignment of 16S rRNA gene through the use of databases and search tools such as the NCBI Basic Local Alignment Search Tool (BLAST) (208). Through this approach unculturable microbial species from environmental samples can be detected and quantified as a proportion of the community. Rout *et al* (80) used this approach to investigate the microbial community of a pH 11 ISA degrading microcosm under

methanogenic conditions using sediments from a hyperalkaline analogue site and ISA degrading microcosms at pH 7, 9.5 and 10 using circumneutral canal sediment (81). With Pedersen *et al* (213) using cloning and sequencing techniques to characterise the microbial communities of deep crystalline bedrock with relevance to the disposal of nuclear waste.

### **3.5.4 Next generation techniques**

The term next generation refers to high throughput techniques for DNA/RNA sequencing and has led to the ability of microbial communities to be characterised via the sequencing of up to millions of copies of 16S rRNA gene sequences. Through the use of platforms such as Illumina HiSeq or Ion torrent platforms, the ability to sequence whole meta-genomes or meta transcriptomes of environmental samples, microcosms or pure isolates is now possible. These approaches allow for an in-depth analysis of genes which are present or active under environmental conditions and allow for the pathway reconstruction of metabolic processes. Transcriptomic approaches by Urich *et al* (214) have combined the analysis of mRNA and 16S rRNA to simultaneously analyse the active genes and microbial community of an environmental sample, with the use of rRNA-tags able to taxonomically bin genes. The use of cDNA generated from 16S rRNA rather than rDNA has the potential to give insights into the microbes which are active within an environmental sample. This approach has been undertaken by Kambura *et al* (215) who found significant difference between the 16S rRNA and rDNA libraries of microbial communities extracted from hypersaline, hyperalkaline hot springs at Lake Magadi and Little Magadi in Kenya. In environmental samples there may exist a subset of dead cells which could skew rDNA results, however, in reactors which are subject to a waste/feed regime to impose growth rates upon the microorganisms, only those actively respiring and growing will remain within the reactor. Therefore a more labour intensive approach such as the generation of cDNA and analysis of the 16S rRNA community may not yield any additional valuable information in these instances.

### **3.5.5 Microbial 16S community analysis**

#### ***3.5.5.1 Assignment of phylogeny***

Next generation approaches for microbial community analysis via the 16S rRNA gene can generate a large amount of data (up to millions of individual sequences). The assignment of phylogeny and the subsequent statistical analysis can require large processing power and specialised computing skills and software. Sequencing companies can offer in house bioinformatic analysis of samples and provide specialist software to analyse and browse the data as seen in provision of CLcommunity by Chunlab (South Korea). The assignment of

phylogeny to these sequences is conducted against databases such as the EzTaxon database (216) or the Ribosomal Database Project database (217). Sequences are initially aligned against a reference such as the Silva reference alignment (218) then compared against a database using search tools such as the BLAST algorithm (208). Sequence similarity to known previously sequenced microbes can then be investigated using different confidence intervals and taxonomic levels (217). Sequences can be further analysed for chimeric sequences using algorithms such as UCHIME in software suites such as Mothur or QIIME (219-221).

Sequences from a sample can be grouped into Operational Taxonomic Units (OTU) whereby they are clustered based on their sequence similarity using a similar confidence interval set by the researcher. Kyeremeh *et al* (84) used a 95% confidence interval to group microbial communities capable of ISA degradation at pH 9.0. Different clustering methodologies can be utilised with methods such as the CD-HIT method which significantly reduces clustering time and improves on issues with OTU over estimation by employing unique algorithms (222). Sequences grouped into OTU's can then be further analysed for alpha and beta diversity statistics.

#### **3.5.5.2 *Alpha diversity statistics***

The alpha diversity statistics analyse the properties of a single sample whereas the beta diversity statistics compare all samples within the project. Measuring the alpha diversity of individual samples can give statistics for the comparison of the microbial diversity between the site of interest and other sites. One such example of this would be comparing if the availability of more nutrients has changed the microbial diversity at a site (223). Statistics such as the qualitative Chao1 (Equation 3.1) (224) and Abundance-based Coverage Estimator (ACE) (Equation 3.2) (225) can be used to estimate species richness of a sample with the generation of rarefaction curves showing if the sampling depth was sufficient. The rarefaction curve is a plot of the number of species found as a function of the number of sequence reads, with the curve plateauing as the number of species left to find through sampling reduces. Rank abundance curves represent another way of investigating how well the microbial communities have been sampled (226). Species are ordered along the x-axis from most to least abundant with the y-axis showing the abundance of each individual species. In microbial ecology diverse environments are characterised by an initial sharp peak which trails off due to a few species in the sample being relatively abundant with a larger degree of rare lower abundance species (226). Further details regarding the aforementioned statistics and their

application in microbial ecology studies can be found in a review by Hughes *et al* (226). Quantitative measures such as the Shannon diversity index (Equation 3.3) (227) which accounts for both abundance and evenness of the species present or the Simpson diversity index (Equation 3.4) (227) which calculates the probability that two organisms sampled from a community will belong to different species are commonly used to report the diversity of microbial populations. Additional information regarding different diversity indices can be found in the work by Boyle *et al* (228) who investigated the sensitivity of 9 different diversity indices in response to perturbations in community structure. Using a coverage statistic such as the Goods' coverage estimator (Equation 3.5) the percentage of the total species which is represented in a sample can be quantified (229). By using a combination of the aforementioned statistics the effectiveness of the sampling undertaken on a given population can be analysed and evaluated, with this approach used to evaluate the effect of antimicrobials on communities in a distal colon model (229).

$$S_1 = S_{obs} + \frac{F_1^2}{2F_2}$$

**Equation 3.1: Chao1 species richness estimator.** Where  $S_{obs}$  is the number of species in the sample,  $F_1$  is the number of singletons (the number of species with only a single occurrence in the sample) and  $F_2$  is the number of doubletons (the number of species with exactly two occurrences in the sample).

$$S_{ace} = S_{common} + \frac{S_{rare}}{C_{ace}} + \frac{F_1}{C_{ace}} \gamma_{ace}^2$$

**Equation 3.2: Abundance based coverage estimator.** Where  $S_{common}$  are the species that occur more than 10 times in the sampling,  $S_{rare}$  are those species which occur 10 times or less,  $C_{ace}$  is the sample abundance coverage estimator, and finally  $\gamma_{ace}$  is the estimated coefficient of variation for  $F_1$  for rare species.

$$H' = - \sum_{i=1}^R p_i \ln p_i$$

**Equation 3.3: Shannon diversity index.** Where  $P_i$  is the proportion of individuals belonging to the  $i^{\text{th}}$  species in the dataset of interest and  $R$  is the species richness or number of species present within the data set.

$$l = \frac{\sum_{i=1}^R n_i(n_i - 1)}{N(N - 1)}$$

**Equation 3.4: Simpson diversity index.** Where  $n_i$  is the total number of individuals in a given species and  $N$  is the total number of species.

$$Goods = 1 - \left( \frac{\text{number of individuals in species}}{\text{total number of individuals}} \right)$$

**Equation 3.5: Goods coverage estimator.**

### 3.5.5.3 *Beta diversity*

Beta diversity was conceived by Whittaker (230) in 1960 to explain changes in diversity along transects or across environmental gradients. The application of beta diversity approaches in general look to compare and contrast two or more microbial communities with measures used to compare the diversity of certain environments or investigate how communities are impacted by environmental factors such as pollutants (223). Using this approach the Human Microbiome Project Consortium (231) analysed 4,788 samples taken from different areas of 242 phenotyped adults and compared the microbial communities based on a wide range of factors. Similar multivariate analysis approaches have been applied to investigate the microbial communities in modified atmosphere packed salmon and coalfish (232) and to investigate the impact land management has upon microbial communities inhabiting grasslands (233). These aforementioned examples used a variety of approaches for the analysis of beta diversity including ordination based methods with additional beta diversity approaches such as UniFrac which uses a phylogenetic tree and accounts for the history of shared ancestry between communities further explained in work by Lozupone and Knight (223). For smaller sampling approaches ordination based methods for analysis may not prove to be effective as other methods for analysis such as the Libshuff method. The Libshuff method was one of the first beta diversity statistics developed and uses nucleotide distances to determine whether two communities are significantly different (Equation 3.6) (234). Test statistics  $C_x$  and  $C_{xy}$  are developed from the two microbial communities and curves are generated for each. A Cramer Von Mises test statistic is then used to compare the distance between the curves with Monte Carlo simulation used to generate a P value to test for a significant difference between the two microbial populations (234). The RDP (217) now offers a web based service in which statistical testing of two microbial communities can be undertaken at different taxonomic level negating the need for large amounts of processing power and computer literacy often associated with the above approaches (217).

$$\Delta C_{XY} = \sum_{D=0.0}^{0.5} (C_X - C_{XY})^2$$

**Equation 3.6: Libshuff method.** The generation of the Cramer Von Mises test statistic where  $C_x$  is the homologous coverage of library 1 and  $C_{xy}$  is the heterologous coverage of library 1 given gene library 2 and  $D$  is evolutionary distance.

### **3.6 Summary**

The generation of microcosms from environmental samples offer the opportunity to investigate microbial processes occurring under the conditions expected within an ILW-GDF. The application of methods to isolate microorganisms combined with pure culture studies which can be pivotal in identifying biochemical pathways such as those responsible for the degradation of ISA under ILW-GDF conditions. Microscopy studies can be applied to the detection of microbes and their viability under harsh conditions in-situ. Techniques such as FISH can used to further identify the presence or absence of microorganisms in systems, with fluorescent stains combined with techniques such as CLSM revealing not just biofilm presence but also its composition and architecture. Nucleic acid based approaches can reveal the unculturable microbes at environmental sites and reveal the complex community structures with next generation technologies increasing the resolution of this approach. Bioinformatic analysis of microbial communities allows the diversity to quantified and compared against other datasets offering insights into the evolution and distribution of microbes in harsh environments.

## **4. Aims and objectives**

The ability of microorganisms to survive the conditions expected within the near field of an ILW-GDF coupled with the biodegradation of the different forms of ISA have implications for the long term performance of an ILW repository. Previous research has found that microorganisms from both circumneutral and hyperalkaline sediments possess the capability to degrade both  $\alpha$ -ISA and  $\beta$ -ISA under a range of conditions and pH values. Currently there are no published instances for the degradation of XISA. These previous investigations have primarily focussed on liquid based cultures and have not featured a biofilm component. Biofilms are known to be the dominant survival strategy for microbial growth and increase the ability of the microbes to survive environmental extremes. Currently however, there is an absence of data regarding the ability of microbes to form biofilm under ILW-GDF conditions when using the different forms of ISA, including XISA, as a carbon source. This work will ascertain the ability of microbes to form biofilm and degrade the different forms of ISA under ILW-GDF conditions, both in-situ at analogue sites and also under a range of laboratory conditions.

The objectives towards achieving the overall aim of this work are summarised below:

- Using cotton ‘baits’ biofilm will be cultured in-situ at different potential anthropogenic analogue sites for an ILW-GDF. The microbial communities and biofilm composition formed in-situ shall be analysed and compared.
- Colonised cotton from the Harpur Hill, Buxton analogue site will be used to form liquid and biofilm microcosms for the analysis of ISA degradation capabilities.
- Biofilm formation, composition, microbial survival and ISA degradation shall be assessed under hyperalkaline conditions expected within the near field.
- The impact of biofilm formation and microbial metabolism upon surfaces relevant to an ILW-GDF concept shall be assessed. These surfaces will include sand, graphite, NRVB and steel
- The ability of ISA degradation to drive further metabolism such as methanogenesis and sulphate reduction shall be assessed. With the impact of sulphate reducing biofilms upon steel surfaces under hyperalkaline conditions investigated.
- By comparing microbial communities an insight into the common core components of microbes surviving under ILW-GDF conditions is expected to be gained.

## **5. Experimental methodologies**

## 5.1 General reagents

All general reagents described throughout the following experimental methodology sections were purchased from either: Fisher Scientific UK (Loughborough, Leicestershire, UK), LabM Limited (Haywood, Lancashire, UK) or Sigma-Aldrich Co. Ltd (Gillingham, Dorset, UK) unless otherwise stated.

## 5.2 Media

### 5.2.1 Mineral media

Mineral media was prepared in accordance to BS ISO 14853:2005 (235). Briefly the reagents listed in Table 5.1 were added to a 1 L Schott bottle and brought up to volume with ultrapure water. The volume was then nitrogen purged for approximately 20 minutes before being autoclaved. The media was then further nitrogen purged and reduced with sodium dithionate until the resazurin indicator within the media turned clear. The media was adjusted to the desired pH value using 2 M sodium hydroxide and 2 M hydrochloric acid.

Reagent	Chemical formula	Concentration (g L <sup>-1</sup> )
Potassium dihydrogen phosphate	KH <sub>2</sub> PO <sub>4</sub>	0.270
Disodium hydrogen phosphate dodecahydrate	Na <sub>2</sub> HPO <sub>4</sub> .12H <sub>2</sub> O	1.120
Ammonium chloride	NH <sub>4</sub> Cl	0.530
Calcium chloride dihydrate	CaCl <sub>2</sub> .2H <sub>2</sub> O	0.075
Magnesium chloride hexahydrate	MgCl <sub>2</sub> .6H <sub>2</sub> O	0.100
Iron(II) chloride tetrahydrate	FeCl <sub>2</sub> .4H <sub>2</sub> O	0.020
Resazurin (oxygen indicator)		0.001
Disodium sulphide nonahydrate	Na <sub>2</sub> S.9H <sub>2</sub> O	0.100
10ml Trace elements solution	See Table 5.2	See Table 5.2

**Table 5.1: Composition of mineral media per 1 litre**

Reagent	Chemical formula	Concentration (g L <sup>-1</sup> )
Manganese chloride tetrahydrate	MnCl <sub>2</sub> .4H <sub>2</sub> O	0.050
Boric acid	H <sub>3</sub> BO <sub>3</sub>	0.005
Zinc chloride	ZnCl <sub>2</sub>	0.005
Copper chloride	CuCl <sub>2</sub>	0.003
Disodium molybdate dihydrate	Na <sub>2</sub> MoO <sub>4</sub> .2H <sub>2</sub> O	0.001
Cobalt chloride hexahydrate	CoCl <sub>2</sub> .6H <sub>2</sub> O	0.100
Nickel chloride hexahydrate	NiCl <sub>2</sub> .6H <sub>2</sub> O	0.010
Disodium selenite	Na <sub>2</sub> SeO <sub>3</sub>	0.005
Disodium tungstate	Na <sub>2</sub> WO <sub>4</sub> .2H <sub>2</sub> O	0.002

**Table 5.2: Composition of trace elements solution per 1 litre**

### **5.2.2 Generation of cellulose degradation products (CDP)**

Cellulose degradation products (CDP) were generated using methods previously described by Rout *et al.* (177). Briefly, 200g laboratory tissue (Pristine Paper Hygiene, UK) was added to 1.8 L of 0.1 M sodium hydroxide and 10 g L<sup>-1</sup> calcium hydroxide in nitrogen purged ultrapure water in a pressure vessel. The vessel was sealed and the headspace flushed for 30 minutes with nitrogen to remove oxygen. The vessel was then incubated at 80 °C for 30 days after which the resultant liquid was filtered through a 0.22 µm filter unit (Millipore, UK) within a nitrogen atmosphere glovebox. The filtered CDP was stored in the dark using sterile 1 L Schott bottles with a nitrogen headspace under ambient conditions.

### **5.3 Sample preparation**

Liquid removed from microcosms or systems for analysis was transferred to sterile tubes (1.5 mL or 50 mL in volume) and centrifuged at 5,000 x g for 10 minutes to pellet any biological matter and solids. The resulting supernatant was then passed through a 0.45 µm syringe filter (Millipore, UK) into sterile tubes and stored at -20 °C if long term storage was required before analysis. The term ‘sample’ in the following experimental sections refers to fluid collected from experimental systems and treated and stored as per the above description.

### **5.4 Analytical methodologies**

#### **5.4.1 High performance anion exchange chromatography with pulsed amperometric detection (HPAEC-PAD)**

##### **5.4.1.1 *Isosaccharinic acid detection and quantification***

The alpha, beta and xylo forms of isosaccharinic acid (ISA) were detected and quantified using a Dionex 3000 or 5000 ion chromatography system employing HPAEC-PAD. The system used for this purpose comprised of an auto-sampler (AS50), gradient pump (GS50) and electrochemical detector (ED50). The detector used a gold working electrode and Ag/AgCl reference electrode in amperometric detection mode which employed a pre-programmed quadrupole wave form. Using an isocratic mobile phase of NaOH (50mM) with a flow rate of 0.5 mL min<sup>-1</sup>, a 10 µL injection of analyte was separated using a Dionex CarboPac PA20 column (250 mm length, 3 mm internal diameter, 6 µm particle size with a 10 Å pore size). With the system also featuring a CarboPac PA20 guard column (3 x 150 mm) which analytes passed through before reaching the main PA20 column. After the analysis of each individual sample the column was regenerated by eluting with 200 mM NaOH for a 20 minute period. All samples were amended with 40 ppm D-ribonic acid prior

to analysis as an internal standard. Pure alpha, beta and xylo forms of isosaccharinic acid were prepared as per methods outlined in Almond *et al* (27) and Shaw *et al* (29) and used to generate standard curves for the quantification of ISA. The Chromeleon 7.0 software package was used to integrate and process chromatograms.

#### **5.4.1.2 Neutral sugars and uronic acid detection and quantification**

Using the Dionex 3000 chromatography system employing HPAEC-PAD and the same system outlined previously for the detection of ISA, neutral sugars and uronic acids were detected and quantified. For the detection of these compounds however, a different methodology was employed with analytes eluted in aqueous 10 mM NaOH for 20 minutes followed by a blend of 83 % 10 mM NaOH : 17 % 150 mM NaOH : 1 M sodium acetate for 25 minutes. This allowed for the simultaneous determination of neutral sugars and uronic acids. Analytes were quantified against appropriate standards made up in ultrapure water.

### **5.4.2 Gas chromatography**

#### **5.4.2.1 Detection and quantification of volatile fatty acids**

Volatile fatty acids (VFA) composition and concentration of samples was determined using a HP GC6890 (Hewlett Packard, UK) gas chromatograph fitted with an auto-sampler. Before analysis, samples (1.5 mL) were acidified by the addition of 85 % phosphoric acid (100  $\mu$ L) with a 1  $\mu$ L volume of acidified sample injected into the system. Samples were passed through a HPFFAP column (30 m x 0.535 mm x 1.00  $\mu$ m; Agilent Technologies, UK) using helium as a carrier gas. VFA's were detected using a flame ionization detector using a hydrogen/air gas blend with the system running under the following conditions: initial temperature of 95  $^{\circ}$ C for 2 minutes, followed by an increase to 140  $^{\circ}$ C at a ramp rate of 10  $^{\circ}$ C  $\text{min}^{-1}$  with no hold, followed by a second ramp to 200  $^{\circ}$ C at a ramp rate of 40  $^{\circ}$ C  $\text{min}^{-1}$  with a hold of 10 minutes, falling to a post run temperature of 50  $^{\circ}$ C. VFA's were identified and quantified against a standard mix of VFA's (Supelco analytical, US) with chromatograms processed using the Chemstation software package (Agilent Technologies, UK).

#### **5.4.2.2 Gas composition**

The composition of microcosm headspace gas was measured using an Agilent GC6850 equipped with HP-PLOT/Q column with particle traps (35 m x 0.32 mm x 20  $\mu$ m, Agilent Technologies, UK). 25  $\mu$ L of headspace gas was removed using a lockable syringe and injected into the column using nitrogen as a carrier gas. A thermal conductivity detector was used to detect different gas species with the system operating under the following conditions:

initial temperature of 60 °C for 2 minutes, followed by an increase to 120 °C at a ramp rate of 30 °C min<sup>-1</sup> with a detector temperature of 250 °C. Gas headspace pressure was measured using a digital manometer (TPI, UK) before gas sample periods. Quantification of different gas species was determined by using standards of a known composition and the ideal gas equation shown below in Equation 5.1.

$$PV = nRT$$

**Equation 5.1: The ideal gas law.** Where: P = Pressure (bar), V = Volume (L), n = Moles of gas (mol), R = Universal gas constant (8.314 L bar K<sup>-1</sup> mol<sup>-1</sup>), T = temperature of gas (K)

### 5.4.3 BacVis gas detection system

Microcosm gas composition and pressure was measured using sensors for methane (BCP-CH<sub>4</sub>), carbon dioxide (BCP-CO<sub>2</sub>) and hydrogen (BCP-H<sub>2</sub>) connected to BACCom12 multiplexer operating BacVis software (BlueSens gas sensor GmbH, Germany).

### 5.4.4 Determination of total carbon, organic and inorganic carbon

Samples were diluted 10 fold in ultrapure water with total carbon (TC) and total inorganic carbon (TIC) determined with a Shimadzu TOC5000A (Shimadzu, Japan) using a nitrogen carrier gas at 150 mL min<sup>-1</sup>. Total organic carbon (TOC) was then calculated as the difference between the measured IC and TC components. TC was quantified against a standard curve produced using potassium hydrogen phthalate in ultrapure water with the IC component quantified against standards produced using a combination of sodium hydrogen carbonate and sodium carbonate.

### 5.4.5 Ion chromatography

#### 5.4.5.1 Sulphate and nitrate quantification

Sulphate and nitrate were detected and quantified using a Metrohm 850 Professional IC (Metrohm, UK) with pulsed amperometric detection, employing a Metrohm Metrosep A Supp 5 column (4 x 150 mm, 5 µm particle size), eluting with an isocratic mobile phase of 3.2 mM sodium carbonate and 1.0 mM sodium hydrogen carbonate. The system used a suppressor with a reagent solution consisting of 0.1 M H<sub>2</sub>SO<sub>4</sub> and 0.1 M oxalic acid in a 9:1 v/v ultrapure water and acetone mix. Samples were diluted 50-fold in ultrapure water before analysis. Sulphate and nitrate were quantified against calibration curves (0 – 50 ppm) made using sodium sulphate and magnesium nitrate standards made up in ultrapure water.

#### **5.4.5.2 Determination of calcium concentration**

Calcium was detected and quantified using a Metrohm 850 Professional IC (Metrohm, UK) using a conductivity detector, employing a Metrohm C4 Column (4.6 x 250 mm, 5 µm particle size) eluting with a mobile phase of 4.6 mM phosphoric acid. Calcium was quantified against a calibration curve (0 – 50 ppm) using calcium chloride in ultrapure with samples diluted 50-fold in ultrapure water before analysis.

#### **5.4.6 Determination of iron (II) and (III) content**

Aqueous iron (II) and (III) concentration within environmental samples was determined using the methods of Viollier *et al* (236). Briefly, to a 1 mL water sample (which had been centrifuged at 10,000 x g for 1 minute to remove large particulate matter) 100 µL of 0.01 M ferrozine reagent prepared in 0.1 M ammonium acetate was added. The absorbance was then measured at 562 nm, with this stage of the procedure quantifying the iron (II) within the water sample. The remaining iron (III) within the water sample was reduced by the addition of 150 µL 1.4 M hydroxylamine hydrochloride (prepared in 2 M HCl) to 800 µL of the water sample. This was then mixed via gentle pipetting and left for 10 minutes at room temperature. After this incubation period 50 µL of 10 M ammonium acetate (adjusted to pH 9.5 with ammonium hydroxide) was added and the absorbance measured at 562 nm. A range of standards were made using iron (II) chloride tetrahydrate and iron (III) chloride hexahydrate to generate a calibration curve.

#### **5.4.7 Dry weight, volatile solids and inorganic ash content**

The dry weight (DW), volatile solid (VS) and inorganic ash content of biofilm materials was determined as per BS ISO 6496:1999 (237). Briefly, dry weight was determined gravimetrically by drying samples overnight at 105°C and the inorganic ash content determined gravimetrically after combustion of samples in a muffle furnace (Carbolite, UK) at 500 °C for 2 hours. The volatile solids were then determined by the difference between the dry weight and ash weight.

#### **5.4.8 Measuring ATP content of biofilm samples**

ATP/biomass detection was undertaken using a 3M Clean-Trace Biomass Detection Kit and Luminometer employing a modified method (3M, UK). The sample (biofilm or cell pellet) was washed once with pH 4 PBS and then reconstituted in pH 7 PBS to remove interference from excess alkalinity and salts. The samples were then processed as per the normal instructions provided with the kit. Following analysis ATP concentrations were quantified against a standard curve of known *Escherichia coli* K12 cell concentrations ( $10^2$  to  $10^8$  CFU

mL<sup>-1</sup>) to give cell number in *E.coli* equivalents. Cell concentration was given as *E.coli* equivalents with 350 fg carbon per cell and an empirical biomass of C<sub>5</sub>H<sub>7</sub>O<sub>2</sub>N (238).

#### **5.4.9 Extraction and composition of exopolymeric substances (EPS)**

##### **5.4.9.1 Extraction of crude EPS**

Crude EPS was extracted from biofilm materials using a multiple extraction method outlined by Ras *et al* (239), which extracts different components of EPS based upon the disruption of different chemical bonds. Samples were collected by centrifugation (10,000 x g for 5 minutes) with the supernatant drawn off and the samples resuspended in phosphate buffered saline (PBS) (pH 9) by vortexing. Samples were then sonicated at a power density of 0.75 W mL<sup>-1</sup> for a 3 x 2 minutes period with a vortexing step in-between each sonication period. Samples were then amended with ice cold ethanol to a final concentration of 40 % (v/v) and left for 2 hour at 4 °C. After the incubation period samples were centrifuged for 10 minutes at 10,000 x g with the supernatant drawn off, syringe filtered and stored at -20 °C for further analysis. The remaining pellet was then treated with 2 % (w/v) ethylenediaminetetraacetic acid (EDTA) in 0.3 M Tris-HCl buffer at pH 8 for 1 hour at room temperature and centrifuged for 10 minutes at 10,000 x g with the supernatant drawn off, syringe filtered and stored at -20 °C for further analysis. Ethanol and EDTA crude EPS extracts were not combined due to the insolubility of EDTA in ethanol. After each step the ATP concentration of the crude EPS extracts and cell pellets (method described in section 5.4.8.) were measured to determine the amount of contamination via cell lysis.

##### **5.4.9.2 Measuring EPS protein content**

The protein content of the crude EPS extract was measured using the Bradford assay method (240). The Bradford reagent was prepared by adding 12.5 mg of Coomassie blue G250 to 7.5 mL 95 % ethanol (v/v) and 30 mL 85 % (v/v) phosphoric acid with the solution brought up to a final volume of 125 mL by the addition of ultrapure water. 50 µL of crude EPS extract was then added to 1.5 mL of Bradford reagent and left for 20 minutes at room temperature. 1 mL of the mixture was then transferred to a cuvette and the absorbance read at 595 nm. Protein content was quantified against a standard curve using bovine serum albumin as the protein source.

##### **5.4.9.3 Measuring EPS carbohydrate content**

The carbohydrate content of the crude EPS extract was measured using the phenol sulfuric acid method as described by Dubios *et al* (241). 100 µL of crude EPS sample was added to

50  $\mu$ L 80 % (w/v) phenol and 2 mL concentrated H<sub>2</sub>SO<sub>4</sub> with the mixture then vortexed and incubated at room temperature for ten minutes. 1 mL of the solution was then transferred to a cuvette and the absorbance read at 490 nm. Carbohydrate content was quantified against a standard curve using glucose as the carbohydrate source.

#### **5.4.9.4 Measuring EPS lipid content**

The lipid content of the crude EPS extract was measured using the methods of Bligh and Dyer (242). To 1 mL crude EPS extract a 3.75 mL mixture of a 2:1 methanol:chloroform reagent was added and the sample mixed. To the mixture a further 1.25 mL of chloroform was added and mixed well. Finally 1.8 mL ultrapure water was added to the sample and mixed then centrifuged for 5 minutes at 1000 RPM and the lower aqueous layer transferred to a porcelain weighing boat. The mixture was allowed to dry overnight with the lipid content determined gravimetrically. A control using 1 mL of ultrapure water was run alongside each crude EPS sample.

#### **5.4.9.5 Measuring EPS DNA amount**

The DNA content of the crude EPS extract was measured using Jenway Genova nano spectrophotometer (Jenway, Bibby Scientific, UK ) with either PBS with 40 % (w/v) ethanol or 2 % EDTA in 0.3 M Tris-HCl buffer at pH 8 as a blank depending on the crude extract analysed.

#### **5.4.9.6 Preparation of dialysis tubing**

Cellulose membrane dialysis tubing (14000 typical molecular weight cut-off, 33 mm width) was prepared by washing under flowing tap water for at least 4 hours. Tubing was then washed in 0.3 % (w/v) sodium sulphide solution at 80 °C for 1 minute followed by washing in hot deionized water at 60 °C for 2 minutes, followed by washing in 0.2 % (v/v) sulphuric acid solution for 1 minute and then finally rinsing with hot deionized water at 60 °C for 2 minutes. Finally the dialysis tubing was rinsed with deionized water and stored at 4 °C in a sealed container containing deionized water

#### **5.4.9.7 Purification of protein and carbohydrate EPS fractions**

In order to purify the extracted crude EPS, dialysis was carried out against ultrapure water for 72 hours with the water changed every 24 hours. The protein and carbohydrate fractions were then isolated from the dialysed EPS using the methods outlined by Marshall *et al* (243). Protein was precipitated using trichloroacetic acid (TCA) to a final concentration of 14 % (v/v), with the sample incubated overnight at 4 °C after TCA addition. Protein was then

pelleted by centrifugation at  $10,000 \times g$  for 60 minutes at  $4\text{ }^{\circ}\text{C}$  and the pellet washed twice with cold acetone, with the centrifugation steps repeated after each wash step. The acetone was allowed air dry and the protein sample was stored at  $-80\text{ }^{\circ}\text{C}$  until needed for analysis. The supernatant generated from the initial TCA treatment was then used to extract the carbohydrate fraction of the crude EPS through the addition of an equal volume of ice cold ethanol. The sample was incubated at  $4\text{ }^{\circ}\text{C}$  overnight and the carbohydrate fraction was precipitated via centrifugation as described above. The resulting pellet was re-dissolved in 10 mL ultrapure water with heating at  $45\text{ }^{\circ}\text{C}$  if required, until it had completely dissolved. The resulting solution was dialysed as described above to remove small neutral sugars, after which the sample was freeze dried.

#### **5.4.9.8 Carbohydrate monomer analysis**

Freeze dried carbohydrate fractions (3 mg) were broken down into monomer units using 2 mL 2 M trifluoroacetic acid (TFA) in a sealed pressure tube with the samples heated at  $120\text{ }^{\circ}\text{C}$  for 2 hours. The samples were then dried under nitrogen and reconstituted in 3 mL ultrapure water to give a  $1\text{ mg mL}^{-1}$  final solution of monomer units. The resulting solution was then analysed using HPAEC-PAD using the methods described in section 5.4.1.2.

#### **5.4.9.9 Protein isoelectric point determination**

Dried protein precipitate (50 mg) was sent to the York University Proteomics and Analytical Biochemistry Laboratory, UK for isoelectric point determination of the proteins extracted from the EPS via 2D sodium dodecyl sulfate polyacrylamide gel electrophoresis (SDS-PAGE). Protein was reconstituted in a load buffer made up of 6 M Urea, 2 M Thiourea and 4 % CHAPS then applied to a 7 cm Bio-Rad pH 3-10 IEF strip. Proteins were then focused over the pH range of the IEF strip before being coated in SDS and separated by size through a 7 cm polyacrylamide gel. The resulting gel was stained with NBS Safe-Blue Coomassie stain before imaging.

#### **5.4.10 EPS calcium binding assay**

Crude EPS was extracted and dialysed by the methods outlined in section 5.4.9 where, after dialysis the fractions were combined and freeze dried to give a representative EPS residue. This EPS was then used to determine the ability of the extracted EPS to bind  $\text{Ca}^{2+}$  ions as per the methods outlined in Braissant *et al* (244). Aqueous suspensions of EPS :  $\text{Ca}^{2+}$  (as calcium chloride) were prepared to concentrations of 0.1, 0.25, 0.5 and  $1.0\text{ g g DW}^{-1}$  and incubated at room temperature for 15 minutes under a nitrogen atmosphere. EPS free controls were run

alongside the samples to determine the amount of calcium lost by interaction with atmospheric CO<sub>2</sub>. Calcium content of the samples was determined via ion chromatography methods outlined in Section 5.4.5.2.

#### **5.4.10.1 Determination of EPS bound calcium**

The calcium content of the EPS used in the calcium binding assay in section 5.4.10 was determined using an using atomic absorbance spectroscopy (Agilent 200 series AA, Agilent, UK) with 1 mg EPS added to a 10 mL mix of 0.1 % (w/v) KCl:1 % (v/v) HNO<sub>3</sub> made up in ultrapure water. The calcium content was quantified against a standard curve using calcium chloride in the previously described solution (0 – 10 mg L<sup>-1</sup>).

#### **5.4.11 Floc size distribution**

Floc size distribution was analysed using a Mastersizer 2000 (Malvern, UK) with a dispersant refractive index of 1.330 and a particle refractive index of 1.572. 25 mL of microcosm fluid was collected with flocs separated via centrifugation. Flocs were then resuspended in 25 mL ultrapure water immediately before analysis.

#### **5.4.12 Floc quantification via flow cytometry**

Floc concentration was determined using a Guava easyCyte™ flow cytometer (Millipore, US) using a 488 nm laser, with unstained flocs and flocs stained using FITc as outlined by Chen *et al* (188). Briefly: 1 mL microcosm fluid was used to collect flocs via centrifugation. Flocs were then washed twice in PBS and reconstituted in 0.1 M sodium bicarbonate. 10 µL of a 10 g L<sup>-1</sup> FITc solution was added to the sample which was then incubated at room temperature for 1 hour. Samples were then washed twice with 0.1 M sodium bicarbonate before being diluted 10 – 100 fold in 0.1 M sodium bicarbonate for analysis. Results were analysed using the GuavaSoft™ suite with green fluorescence events gated against the unstained control, which was washed as per the stained sample.

#### **5.4.13 Measurement of floc zeta potential at different pH values**

In order to investigate floc stability under a range of pH values the zeta potential of the flocs was measured using a Zetasizer nano (Malvern, UK) with a dispersant refractive index of 1.330 and a particle refractive index of 1.572. The zeta potential was calculated using the Smoluchowski's equation. Flocs were isolated by centrifugation and re-suspended in ultrapure water of the desired pH (values between pH 7.0 and pH 12.0) and incubated for 1 hour before analysis.

## **5.5 Aqueous sulphide determination**

Aqueous sulphides were detected using a micro ion electrode (LIS-146AGSCM, Lazar research laboratories Inc, US) and a handheld mV unit. The assay used a sulphide anti-oxidant buffer (SAOB) which was prepared by dissolving 6.7 g of sodium EDTA and 8 g sodium hydroxide in 100 mL nitrogen purged ultrapure water. Once all solids were dissolved 3.5 g of ascorbic acid was added, with the SAOB used within 3 hours of its addition. 1 mL of sample was added to 9 mL SAOB with the mixture vortexed and the probe allowed to stand with the mixture for 2 minutes before a reading was taken. Sulphide was quantified against a standard curve which was generated by using sodium sulphide nonahydrate to generate a range of known sulphide concentrations (0 – 100 mg L<sup>-1</sup>).

### **5.5.1 pH and redox determination**

The pH of liquids including microcosm fluids and hyperalkaline leachates were measured using a handheld portable pH meter with calibrated electrodes (Mettler Toledo, UK). The pH of retrieved soil samples was determined as per BS ISO10390:2005 (245) with in-situ redox values measured using an InLab Redox Micro probe (Mettler Toledo, UK) tested in accordance with BS ISO 11271:2002 (246).

### **5.5.2 Extraction of ISA from environmental samples**

In order to determine extractable ISA from the cotton and sediment samples, 1 g dried material was added to 5 mL 2 M HCl so that the resultant pH was below 4, this was then vortexed and left overnight. The mixture was then centrifuged for 10 minutes at 8000 RPM and the supernatant drawn off and 4 M NaOH added to increase the pH to approximately pH 12. This step was to convert the ISA into the sodium salt. Water was then removed using rotary evaporation at 80 °C and the solids dissolved in ultrapure water to a concentration of 1000 ppm for detection via HPAEC-PAD.

### **5.5.3 Extraction of VFA from environmental samples**

In order to determine extractable VFA from the cotton and sediment samples, 1 g dried material was added to 5 mL 85 % (v/v) H<sub>3</sub>PO<sub>4</sub>, vortexed and left overnight. The mixture was then centrifuged for 10 minutes at 8000 RPM and the supernatant drawn off. The supernatant was diluted tenfold with ultrapure water, with volatile acids detected via gas chromatography.

## 5.6 Microscopy techniques

### 5.6.1 Sample preparation

Biological samples unless otherwise stated were initially fixed in 4 % paraformaldehyde in PBS overnight at 4 °C and washed twice with PBS. Samples were then placed into a storage buffer composed of 140 mL of ultrapure water, 10 mL of 1 M TRIS-HCl (pH7.5) and 250 mL of 96 % (v/v) ethanol and stored at -20 °C before analysis.

### 5.6.2 Fluorescence microscopy

Fluorescence microscopy was carried out using an Olympus BX41 laboratory microscope (Olympus, USA). Live dead staining of both cotton fibres and flocs was carried out using the LIVE/DEAD® *BacLight*<sup>™</sup> kit (Life technologies, UK) under a wet mount using live materials at approximately 500 nm. FITc (Sigma-Aldrich, UK) staining as outlined in Chen *et al* (188) and Section 5.4.12 was used for protein visualization. Individual cells and the associated polysaccharide components were stained using ethidium bromide and calcofluor white, respectively. Flocs were collected via centrifugation and washed with PBS, then heat fixed to a microscope slide. The flocs were stained in-situ with a solution of 1 µM ethidium bromide and 30 mg L<sup>-1</sup> calcofluor white in PBS for 30 minutes. The solution was then removed with ultrapure water and microscope slides air dried before analysis at approximately 400 nm. For all samples autofluorescence controls were performed on materials not exposed to stains.

#### **5.6.2.1 DNase digestion of flocs**

For DNase digestion, microcosm fluid (1 mL) was centrifuged at  $10\,000 \times g$  for 1 min and resuspended in ultrapure water (1 mL). A 10-fold dilution of this was then subjected to digestion by DNase using a DNase 1 kit (Sigma-Aldrich, UK). Flocs were then stained and viewed as per Section 5.6.2.

#### **5.6.3 Confocal scanning laser microscopy**

Confocal laser scanning microscopy (CLSM) of samples was undertaken at the Bio Imaging Centre of Leeds University, UK using a Zeiss LSM880 inverted confocal microscope with image analysis performed using Zen 2.1 (Zeiss Microscopy).

#### **5.6.3.1 5 colour Biofilm EPS imaging**

Staining and visualisation of biofilm EPS components was carried out in line with methods developed for the staining of bio-aggregates (188). Calcofluor white was used for the visualisation of  $\beta$ -1,4 and  $\beta$ -1,3 polysaccharides, Nile red for lipids and hydrophobic sites, Concanavalin A, Tetramethylrhodamine Conjugate (ConA) for  $\alpha$ -Mannopyranosyl,  $\alpha$ -glucopyranosyl sugars, FITc for protein and Syto 63 for total cells and extracellular DNA. The concentration, staining times and the absorbance, emission wavelength for each component can be found in Table 5.3. Samples were kept hydrated throughout the staining procedure with autofluorescence controls performed on materials not exposed to stains.

Stain	Concentration	Time (minute)	Excitation (nm)	Emission (nm)
Calcofluor white	30 mg L <sup>-1</sup>	30	400	410 - 480
Concanavalin A, tetramethylrhodamine conjugate	25 mg L <sup>-1</sup>	30	543	550 - 600
FITc	100 mg L <sup>-1</sup>	60	488	500 - 550
Nile red	0.6 mg L <sup>-1</sup>	10	514	625 - 700
Syto 63	2µM	30	633	650 - 700

**Table 5.3: 5 colour CLSM stain properties**

### 5.6.3.2 FISH probing of flocs

Fluorescence in situ hybridisation (FISH) was carried out as per the methods of Ainsworth *et al* (191). The hybridization was conducted in buffer (0.9 M NaCl, 0.01 % SDS, 0.01 M Tris-HCl, pH 7.2) with 35 % formamide for 1.5 hours at 46 °C with all probes at a concentration of 5 ng µL<sup>-1</sup>. The incubation period was followed by a 10 minute wash in prewarmed buffer (0.08 M NaCl, 0.01 % SDS, 0.01 M Tris-HCl). There was no EDTA in the wash buffer due to its effect on calcium binding and EPS stability. Table 5.4 contains details regarding the probes. All probes were manufactured by MWG Operons and with autofluorescence controls performed on materials not exposed to stains.

Probe	Target	Oligonucleotide sequence	fluorochrome	Excitation (nm)	Emission (nm)	Reference
ARC915	Archaea	5'-GTGCTCCCCGCCAATTCCT-3'	Cy3	548	561	(247)
EUB338	Eubacteria	5'-GCTGCCTCCCGTAGGAGT-3'	FAM	494	519	(247)
GAM42a	Gammaproteobacteria	5'-GCCTTCCCACATCGTTT-3'	Atto425	439	485	(248)
HCG69a	Actinobacteria	5'-TATAGTTACCACCGCCGT-'	Cy3	548	561	(249)
LGC354	Firmicutes	5'-TGGAAGATTCCTACTGC-3'	FITc	494	519	(248)

**Table 5.4: Oligonucleotide FISH probes**

### 5.6.4 Scanning electron microscopy and elemental analysis

Scanning electron microscopy (SEM) was carried out using a Quanta FEG 250 (FEI, USA) or a JSM-6060LV microscope (JEOL, USA) equipped with an electron dispersive X-ray spectroscopy (EDS). Before analysis samples were dehydrated using a serial ethanol dilution of 25, 50, 75 and 100 % (v/v) for 2 minutes per step and then sputter coated via a gold palladium plasma (CA7625 Polaron, Quorum Technologies Ltd, UK).

## 5.7 Molecular biology

### 5.7.1 Extraction and purification of nucleic acids

#### 5.7.1.1 DNA extraction using MO-BIO PowerSoil<sup>®</sup> kit

For the extraction of DNA from the pH 11 fermentative microcosm and from the cotton retrieved from the Buxton site after an in-situ incubation period of 3 months (August, 2014), a PowerSoil<sup>®</sup> DNA extraction kit (MO-BIO, US) was used with the following modifications. For the cotton, approximately 0.25 g was washed with pH 7.0 PBS and loaded into a glass bead tube with 100  $\mu$ L  $\beta$ -mercaptoethanol and the bead beating step extended to 1 hour in order to overcome dampening effects introduced by the material. For the extraction of genomic DNA from the microcosm, 25 mL of microcosm fluid was centrifuged at 5000  $\times g$  for 15 minutes and the pellet resuspended in 25 mL of pH 4.0 PBS. The sample was then centrifuged again at 5000  $\times g$  for 15 minutes and resuspended in 2 mL of pH 7.0 PBS. 1 mL of the concentrated sample was transferred to a 1.5 mL tube and centrifuged again at 10 000  $\times g$  for 1 min, after which the supernatant was removed and the cell pellet resuspended in the reaction fluid provided in the glass bead tubes of the Powersoil kit. The resulting mixture was then transferred back to a glass bead tube and bead beaten with 100  $\mu$ L  $\beta$ -mercaptoethanol for an increased time of 20 minutes to overcome clogging due to the EPS and then run as per the supplier's instruction. These modifications were found to increase the yield and purity of DNA obtained from both samples by removing excess salts, inhibiting nucleases and neutralizing the samples.

#### 5.7.1.2 DNA/RNA co-extraction method for liquid samples

Genomic DNA and RNA was extracted for analysis from samples using a modified version of the Griffiths methods (198). For liquid microcosm samples, 25 mL of microcosm fluid was spun at 5,000  $\times g$  for 10 minutes with the pellet resuspended in 25 mL phosphate buffer as described by Hurt *et al* (197). The sample was then spun again at 5000  $\times g$  for 10 minutes and the pellet re suspended 1 mL in pH 7 ultrapure water. 500  $\mu$ L liquid was then added to a glass bead tube with 0.1 mm diameter glass beads (Cambio, UK). To the bead tube, 450  $\mu$ L of 10 % cetyl-trimethylammonium bromide (CTAB) prepared in 0.7 M sodium chloride and 240 mM phosphate buffer, diluted 50:50 in 240 mM phosphate buffer at pH 8.0 and 450  $\mu$ L phenol chloroform isoamyl alcohol (25:24:1) and 100  $\mu$ L  $\beta$ -mercaptoethanol was added. The bead tube was then beaten at max speed for 10 minutes and centrifuged for 10 minutes at 10,000  $\times g$ . The top layer of the supernatant was removed and mixed with an equal volume

chloroform/isoamyl alcohol (24:1) and spun again for 5 minutes at 10,000  $\times$  g. 450  $\mu$ L of the top layer of the supernatant was then removed. Different precipitation methods and incubation periods were used for the isolation of either just DNA or both DNA and RNA. For just DNA the 450  $\mu$ L supernatant top layer was mixed with 900  $\mu$ L 30 % polyethylene glycol-6000 in 1.6 M sodium chloride and glycogen (Life technologies, UK) and incubated overnight at 4 °C. For DNA/RNA a shorter method was used to reduce the possibility of RNA degradation, with the 450  $\mu$ L top layer mixed with 900  $\mu$ L of ice cold molecular grade ethanol and 1/10<sup>th</sup> the volume of the DNA suspension of 3 M sodium acetate. This was then incubated for a minimum of 1 hour at -20 °C. After incubation both types of samples were then spun at 10,000  $\times$  g for 20 minutes with the pellet resuspended in 200  $\mu$ L ice cold absolute ethanol and spun again for 5 minutes at 10,000  $\times$  g. The ethanol was then removed and the pellet allowed to air dry and after which the pellet was suspended in DNase/RNase free ultrapure water. Reagents not supplied DNase/RNase free were treated with for 2 hours at 37 °C with 0.1 % diethylpyrocarbonate and then autoclaved.

#### **5.7.1.3 DNA/RNA co-extraction method biofilm samples**

The co-extraction of DNA/RNA from biofilm materials upon cotton, sand and steel required a slight modification to the methods described in section 5.6.1.2. Colonised cotton samples were washed with pH 4 and then pH 7 PBS under an inert nitrogen atmosphere to remove any transient microorganisms and to neutralise the cotton samples. Samples were then cut into small sections using sterile scissors and placed in a 15 mL falcon tube with metal beads provided in the RNA PowerSoil<sup>®</sup> kit (Mo-BIO, USA). DNA and RNA was then co-extracted using methods outlined in Section 5.7.1.2. For biofilm formed within a sand column, a sterile spatula was used to remove visible sections of biofilm and place them directly into a PowerSoil<sup>®</sup> glass bead tube which had had the kits suspension buffer removed to be replaced by the reagents used in the modified Griffiths method outlined in Section 5.7.1.2. Biofilm formed upon steel discs was removed by rubbing 0.1 mm diameter glass beads (Cambio, UK) and CTAB buffer on the colonised surface for approximately 1 minute and the resulting suspension collected. The extraction of DNA/RNA was then undertaken as per the methods outlined in Section 5.7.1.2.

#### **5.7.1.4 RNA purification**

From co-extracted DNA/RNA generated via the modified Griffiths method, RNA was isolated by the enzymatic digestion of DNA. This was achieved by using the DNase 1 kit.

Briefly: Extracted RNA was made up to a volume of 8 mL in DNase/RNase free water with 1 mL of a 10X reaction buffer (provided) and 1 mL DNase I (1 unit mL<sup>-1</sup>) added to bring the total volume up to 10 mL. The sample was then gently mixed by inversion and incubated at room temperature for 15 minutes. After incubation the DNase was removed and the RNA purified via the modified Griffiths methods outlined in section 5.7.1.2 and further purified using an RNeasy minielute cleanup kit (Qiagen, UK) to remove excess salts.

#### **5.7.1.5 Quantification of nucleic acids**

Nucleic acid concentration was determined spectrophotometrically using a Jenway Genova nano spectrophotometer (Bibby Scientific, UK) with a sample volume of 1 µL. The samples were analysed using UV light and ratios based on the extinction co-efficient of double stranded DNA and RNA used to determine sample purity.

#### **5.7.1.6 Visualisation of DNA/RNA products**

Genomic DNA/RNA was visualised using gel electrophoresis on 1 % agarose gels prepared in tris-acetate EDTA buffer (TAEB). A 1 % agarose solution was prepared by completely melting the agarose in TAEB by microwaving. To the solution 1 µL of SYBR<sup>®</sup> safe stain (Life Technologies, UK) was added and the solution poured into a gel cast and allowed to set. 5 µL of genomic DNA/RNA was then mixed with 1 µL of 5X loading dye (Bioline, UK) and inserted into each well alongside a 1-10kb ladder (Hyperladder 1kb, Bioline, UK), the gel was then submerged in TAEB buffer and subjected to electrophoresis for 60 minutes at 100 V. Agarose gels were visualised under UV light and an image recorded using the BioDoc-It<sup>®</sup> 210 imaging system (UVP LLC, US).

### **5.7.2 Polymerase chain reaction (PCR)**

#### **5.7.2.1 16S rRNA PCR gene amplification for clone libraries**

From DNA extracted via the PowerSoil<sup>®</sup> DNA extraction kit (MO-BIO, US) the 16S rRNA gene was amplified for Eubacteria and Archaea using the primers listed in Table 5.5. Direct PCR was carried out using the Biomix<sup>™</sup> Red kit (Bioline, UK) which was a mix of reaction buffer, dNTPs, *Taq* polymerase BIOTAQ<sup>™</sup> and magnesium (5 mM). A typical PCR reaction contained 25 µL of Biomix<sup>™</sup> Red, 17 µL of DNase/RNase free water, 3 µL of a 50 : 50 mix of forward and reverse primers at a concentration of 10 pmol and 5 µL of template DNA at a concentration of 5-10 ng µL<sup>-1</sup>. Thermocycler conditions for the samples were as follows; initial denaturation at 94 °C for 5 minutes, followed by 35 cycles of denaturing (94 °C, 1 minute), annealing (60 °C, 1 minute), primer extension (72 °C, 1 minute 30 seconds). This

was followed by a final extension step of 72°C for 5 minutes. Samples were cooled and stored to 4 °C before further analysis. Genomic DNA extracted from *Escherichia coli K-12* and *Methanobacterium bryantii* (DSMZ 863) were used as positive controls for PCR reactions, with negative controls run without genomic DNA. PCR products were visualised on 1 % agarose gels as outlined in section 5.7.1.6.

Target organism	Primer	Sequence	Reference
Eubacteria	pA	5'-AGAGTTTGATCCTGGCTCAG-3'	(250)
	pH	5'-AAGGAGGTGATCCAGCCGCA-3'	(250)
Archaea	304f	5'- CCCTAYGGGGYGCASCAG-3'	(251)
	1000r	5'-GGCCATGCACYWCYTCTC-3'	(251)

**Table 5.5: 16S rRNA gene PCR primer used for the formation of clone libraries.**

#### 5.7.2.2 Hot start PCR for 16S rRNA gene amplification for high-throughput microbial community analysis

For the generation of PCR products for analysis via a MiSeq nano platform (Illumina, USA) the MyTaq<sup>TM</sup> HS red mix (Bioline, UK) was used as it was found to significantly reduce thermocycler reaction time and improve PCR product yield. The mix used an antibody mediated hot-start which reduces non-specific amplification due to a lack of polymerase activity during the reaction set-up. Further the mix contained reaction buffer, dNTPs, Taq polymerase and magnesium. A typical PCR reaction was comprised of 25 µL MyTaq<sup>TM</sup> HS red mix (Bioline, UK), 10 ng of genomic DNA or cDNA with 2 µL 20 uM forward and reverse primer mix (primers used are listed in Table 5.6) with a final reaction volume of 50 µL made up with DNase/RNase free water. The thermocycler run was as follows: initial denaturation 95 °C (1 minute), followed by 30 cycles of denaturation (95 °C, 15 seconds), annealing (60 °C, 30 seconds), extension (72 °C, 15 seconds) with a final extension of 2 minutes at 72 °C. Samples were cooled and stored to 4 °C before further analysis. Genomic DNA extracted from *Escherichia coli K-12* and *Methanobacterium bryantii* (DSMZ 863) were used as positive control for PCR reactions with negative controls run without genomic DNA. PCR products were visualised on 2 % agarose gels at 100 V with a run time of 25 minutes.

Target organism	Primer	Sequence	Overhang	16S region	Sequencing company	Ref.
Eubacteria & Archaea	519f	5'-CAGCMGCCGCGGTAA-3'	5' TCGTCGGCAGCGTCAGAT GTGTATAAGAGACAG-3'	V4	Chunlab	(252)
	785r	5'-TACNVGGGTATCTAATCC-3'	5' GTCTCGTGGGCTCGGAGA TGTGTATAAGAGACAG-3'	V4	Chunlab	(253)
	515f	5'-GTGCCAGCMGCCGCGGTAA-3'	5'- TCGTCGGCAGCGTCAGAT GTGTATAAGAGACAG-3'	V4	Microsynth	(254)
	806r	5'-GGACTACHVGGGTWTCTAAT-3'	5'- GTCTCGTGGGCTCGGAGA TGTGTATAAGAGACAG-3'	V4	Microsynth	(254)

**Table 5.6: 16S rRNA primers used for microbial community analysis**

### 5.7.2.3 Purification of PCR products

PCR products were purified for downstream applications using the Qiaquick PCR purification kit (Qiagen, UK) as per the manufacturer's instructions. Briefly: the PCR product was converted to a salt by the addition of 5 volumes of supplied buffer and 10  $\mu\text{L}$  3 M sodium acetate. The PCR product was then bound to a silica column by centrifugation at 10,000 RPM and cleaned of impurities (primers, dNTPs, polymerases) via washing with an ethanol based buffer. The PCR product was then eluted from the column using DNase/RNase grade water and centrifugation.

### 5.7.2.4 Oligonucleotide primer synthesis

All oligonucleotide primers used in the study were commercially synthesised HPSF (High purity salt free), by MWG Operons and prepared using instructions provided on the synthesis report to make 100 pmol  $\mu\text{L}^{-1}$  stocks.

### 5.7.3 cDNA synthesis

From total RNA extracted from biological samples described previously (Section 5.7.1.4) cDNA was generated using the Tetro cDNA Synthesis Kit (Bioline, UK). Briefly: approximately 10-100 ng RNA was added to 1  $\mu\text{L}$  random hexamer mix, 1  $\mu\text{L}$  10 mM dNTPs mix, 4  $\mu\text{L}$  5x RT buffer, 1  $\mu\text{L}$  RiboSafe RNase inhibitor, 1  $\mu\text{L}$  Tetro reverse transcriptase (200 U  $\mu\text{L}^{-1}$ ) and made up to a final volume of 200  $\mu\text{L}$  using DNase/RNase free water. Samples were then placed in a thermocycler and incubated at 25 °C for 10 minutes followed by heating to 45 °C for 30 minutes. The reaction was terminated by incubating at 85 °C for 5 min. Samples were then chilled on ice and stored at -20 °C for long term storage.

### 5.7.4 qPCR of *dsrA* gene

In order to investigate sulphate reduction under a range of pH values, the primers DSR-1F+ (5'-ACSCACTGGAAGCACGCCGG-3') and DSR-R (5'-GTGGMRCCGTGCAKRTTGG-3') which target the alpha sub unit of the dissimilatory sulphite reductase gene (*dsrA*) (255)

were used with the SensiFAST SYBR® No-ROX Kit (Bioline, UK) which uses an antibody-mediated hot-start DNA polymerase system to reduce the chances of primer/dimers formation. Briefly: 10 ng genomic DNA or 100 ng cDNA was added to 10 µL 2x SensiFAST SYBR® No-ROX Mix along with 1.6 µL of forward and reverse primer at a final concentration of 400 nM with the volume made up to 20 µL using DNase / RNase free water. Samples were then run on a Biorad CFX96 real-time PCR detection system (Biorad, USA) using a blue light channel and measuring an emission wavelength at 520 nm. The thermocycler run was as follows: 2 minutes for cDNA or 3 minutes for genomic DNA at 95 °C for denaturation and polymerase activation, then 40 cycles of 95 °C for 5 seconds (denaturation), 60 °C for 10 seconds (annealing) and 72 °C for 10 seconds (extension). Samples were analysed using the CFX Manager software package to determine threshold cycle (ct value) (Biorad, USA). Control samples consisting of primer with no DNA, DNA with no primer and genomic material treated with DNase before the cDNA synthesis step, were run alongside triplicate samples for each pH value. After amplification samples were visualised using gel electrophoresis in 2 % agar at 100 V for 20 minutes.

A standard curve to calculate gene copy number was generated using known genomic DNA amounts from *Desulfococcus multivorans* (DSMZ 2059) with gene copy number calculated using Equation 5.2 (256).

$$gene\ copies = (DNA\ concentration\ [ng/\mu L]) \left( \frac{1g}{1000^3 ng} \right) \left( \frac{1\ mol\ bp\ DNA}{660\ g\ DNA} \right) \times \left( \frac{6.023 \times 10^{23}\ bp}{mol\ bp} \right) \left( \frac{1\ copy}{genome\ size\ [bp]} \right)$$

**Equation 5.2: Gene copy number in a known amount of DNA.**

**5.7.5 Cloning of 16S rRNA gene**

16S rRNA gene PCR products were ligated into the standard PGEM-T easy cloning vector (Promega, US) as per the manufacturer's instructions with the amount of insert DNA calculated using Equation 5.3.

$$ng\ of\ insert = insert:vector\ molar\ ratio \times \frac{ng\ of\ vector \times kb\ size\ of\ insert}{kb\ size\ of\ vector}$$

**Equation 5.3: Cloning vector inset DNA calculation.** Where An insert : vector molar ratio of 1 : 1 was chosen for all reactions and 50 ng of the 3.0 kb p-GEM vector was used per reaction.

Ligation reactions were prepared in accordance to Table 5.7, with ligation reactions carried out overnight at 4 °C rather than 1 hour. To 50 µL of competent cells, 2 µL of ligation

reaction was added then incubated on ice for 20 minutes. The cells were then heat shocked at 42 °C for 45 seconds before being returned to ice for 2 minutes. SOC medium (Section 5.7.5.1) was added to each reaction to bring the total volume to 1 mL prior to a further incubation step at 37 °C with shaking (150 RPM) for 90 minutes. 250 µL aliquots of transformed cells were then grown on Luria Bertani (LB) agar containing 100 µg mL<sup>-1</sup> ampicillin overlaid with 40 µL of 100 mM IPTG and 40 µL of 40 mg mL<sup>-1</sup> X-GAL (5-bromo-4-chloro-3-indolyl-β-D-galactopyranoside) in N,N dimethylformamide. Plates were left to dry and were then incubated at 37 °C for 24 hours before being transferred to 4 °C to allow for residual colour development. White colonies were then selected for subculturing into 96-well stab plates containing LB agar with 150 µg ml<sup>-1</sup> ampicillin and sequenced using Sanger sequencing technology using the T7 forward primer (GATC Biotech, Germany).

Reagent	Standard reaction	Positive control	Background control
2X Rapid ligation buffer, T4 DNA ligase	5	5	5
pGEM®-T Easy vector (50ng)	1	1	1
PCR product	X	-	-
Control insert DNA	-	2	-
T4 DNA ligase (3 Weiss units/L)	1	1	1
De-ionised water to a final volume of:	10	10	10

**Table 5.7: Ligation reaction conditions for pGEM T easy cloning kit**

#### 5.7.5.1 Preparation of SOC medium

0.5 g of yeast extract powder (MC001) and 2 g of tryptone (MC005) were added to 97.5 mL of de-ionised water and sterilised by autoclaving at 121 °C. After cooling in a class II safety cabinet, 1 mL of 2 M glucose, 0.5 mL of 2 M NaCl, 1 mL of 1 M MgCl and 0.25 mL of 1 M KCl were added. All the solutions were prepared in de-ionised water and filter sterilised using a 0.45 µm syringe filter unit.

#### 5.7.6 Analysis of 16S rRNA clone library sequences

Gene sequences were combined into a single FASTA format file and checked for chimeras using UCHIME algorithm within the Mothur software suite (219, 220) with *Escherichia coli* (Genbank accession number J01695) and *Methanocaldococcus jannaschii* DSM 2661 (accession number L77117) used as relevant references. Sequences were trimmed of primer artefact using the MEGA 6 software package (257) and low quality reads were removed before submission to Genbank. Sequences were then analysed against the NCBI database using Basic Local Alignment Search Tool (MegaBLAST) against the 16S ribosomal RNA

sequences for Bacteria and Archaea database (208). Phylogeny was then assigned to each individual sequence based on the closet sequence match produced from the MegaBLAST output.

### 5.7.7 16S rRNA gene clone library nucleotide accession numbers

The 16S rRNA sequence data from the colonised cotton has been submitted to GenBank under accession numbers KP263977 - KP264111 and the pH 11 microcosm sequences under the numbers KP728118 - KP728176.

### 5.7.8 Microbial community analysis via MiSeq platform

Genomic DNA or PCR amplicons were sent to either Chunlab (South Korea) or Microsynth (Switzerland) for sequencing via a MiSeq nano platform (Illumina, USA) (sample details in Table 5.8). The general pipeline for sequencing included the generation of PCR amplicons from genomic DNA which were then barcoded using an index PCR technique. These PCR amplicons were then purified, quantified and run on the MiSeq nano platform at 250bp paired end. Paired ends were merged using PandaSeq (258) and chimeric sequences identified and removed using the UCHIME algorithm (220). Sequence phylogeny was assigned using the EzTaxon database (216) for the Chunlab samples and the RDP database for the Microsynth samples (217) with OTU clustering performed using CD-HIT-EST at a 95 % confidence interval (222) with alpha diversity statistics assigned using the CLcommunity software suite (Chunlab, South Korea) for the Chunlab samples and the Mothur software suite (219) for the Microsynth samples.

Sample	Genomic DNA / Amplicon	Sequencing company
Buxton site biofilm (Site-B)	Amplicon	Chunlab
Horton site biofilm (Site-H)	Amplicon	Chunlab
Tarmac site biofilm (Site-T)	Amplicon	Chunlab
pH 11 fermentative microcosm	Genomic DNA	Chunlab
pH 11 biofilm	Genomic DNA	Microsynth
pH 12 biofilm	Genomic DNA	Microsynth
pH 13 biofilm	Genomic DNA	Microsynth
pH 11 sulphate reducing microcosm	Genomic DNA	Chunlab
pH 9.5 sulphate reducing microcosm	Genomic DNA	Chunlab
pH 7.5 sulphate reducing microcosm	Genomic DNA	Chunlab
Mb treated sulphate reducing microcosm	Genomic DNA	Chunlab
Grade 304 steel biofilm	Genomic DNA	Chunlab
Grade 316 steel biofilm	Genomic DNA	Chunlab

**Table 5.8: Details of microbial community analysis investigations.**

#### **5.7.8.1 Further microbial community bioinformatic analysis**

Biofilm communities generated in-situ upon cotton in different analogue sites were compared using Taxon XOR analysis in the CLcommunity software suite (Chunlab, South Korea) and related Venn diagrams were produced using EulerAPE (259). Samples were compared against each other for significance testing at a 95 % confidence interval and at family level using the RDP library compare tool, which estimates the probability of observing the difference in a given taxon using the statistical test given in Equation 5.4.

$$p(y|x) = \frac{\binom{N_2}{N_1}^y}{x! y! \left(1 + \frac{N_2}{N_1}\right)^{(x+y+1)}}$$

**Equation 5.4: Significance test for two different microbial communities.** Where  $N_1$  and  $N_2$  are the total number of sequences for library 1 and 2 respectively, and  $x$  and  $y$  are the number of sequences assigned to Taxon T from library 1 and 2 respectively.

### 5.7.9 Microbial community BioProject accession numbers

Sequence libraries were uploaded to Genbank with the BioProject and BioSample accession values detailed in Table 5.9.

Sample	BioProject accession	BioSample accession
Buxton site biofilm (Site-B)	PRJNA314676	SAMN04539308
Horton site biofilm (Site-H)		SAMN04539309
Tarmac site biofilm (Site-T)		SAMN04539318
pH 11 fermentative/methanogenic microcosm	PRJNA314684	SAMN04539439
pH 11 biofilm	PRJNA339714	SAMN05603705
pH 12 biofilm		SAMN05603706
pH 13 biofilm		SAMN05603707
pH 11 sulphate reducing microcosm	PRJNA339716	SAMN05603714
pH 9.5 sulphate reducing microcosm		SAMN05603715
pH 7.0 sulphate reducing microcosm		SAMN05603716
Mo treated sulphate reducing microcosm		SAMN05603731
Grade 304 steel biofilm	PRJNA339724	SAMN05603774
Grade 316 steel biofilm		SAMN05603773

**Table 5.9: Bioproject and Biosample accession details.**

## 5.8 Analogue sites

### 5.8.1 Cotton preparation

In order to prepare the cellulose cotton for incubation, raw woven cotton fabric (Greige) was treated with NaOH to saponify the natural waxes along with an alkali stable phosphate ester detergent to emulsify the suspended impurities. Further treatment with NaOH and phosphonate stabilised  $H_2O_2$  was carried out to bleach the fabric. The cotton was then rinsed, neutralised under acetic acid before finally being rinsed, dried and autoclaved at 121 °C prior to use.

### 5.8.2 Analogue site investigation

2.2 cm Ø boreholes were hand drilled to an approximate depth of 0.5 m into areas inundated with alkaline leachate at analogue sites. A total of 4 boreholes were placed into the Buxton site (Site-B) (Figure 5.1), 6 boreholes were placed into Horton quarry site (Site-H) (Figure 5.2) and 5 boreholes placed into Tarmac quarry site (Site-T) (Figure 5.3). Into each borehole an inert plastic liner with a perforated lower section was placed, a nylon mesh bag containing approximately 1 g of sterile, de-waxed, cotton was then placed at the bottom of each borehole for approximately 3 months. The pH of the porewater was recorded in-situ before emplacement via a handheld portable pH meter with calibrated electrodes (Mettler Toledo, UK). Porewater collected before emplacement was analysed using a range of previously described methods to determine ISA and VFA species content as well as sulphate, nitrate, iron(II) and iron (II), calcium and sodium concentration.

After a period of 3 months, the cotton was recovered along with sediment and porewater samples from the immediate vicinity of the cotton. In-situ pH and redox were recorded prior to sample recovery using a handheld portable pH meter. All recovered materials were sealed in airtight containers along with anaerobic gas packs (Anaerogen, UK) for transport. Sediment and porewater samples were stored at -20 °C until analysis and cotton not used for immediate analysis was stored at -20 °C in a solution of 140 mL of ultrapure water, 10 mL of 1M TRIS-HCl (pH7.5) and 250 mL of 96 % (v/v) ethanol after an overnight fixation step in 4% paraformaldehyde in PBS. The pH and redox of the collected sediment was determined as per methods outlined in Section 5.5.1. For porewater samples ISA and VFA species content as well as sulphate, nitrate, iron (II) and iron (III) concentrations were determined as previously described. Extractable ISA from recovered cotton samples and related sediments was undertaken as per methods outlined in Section 5.5.2.

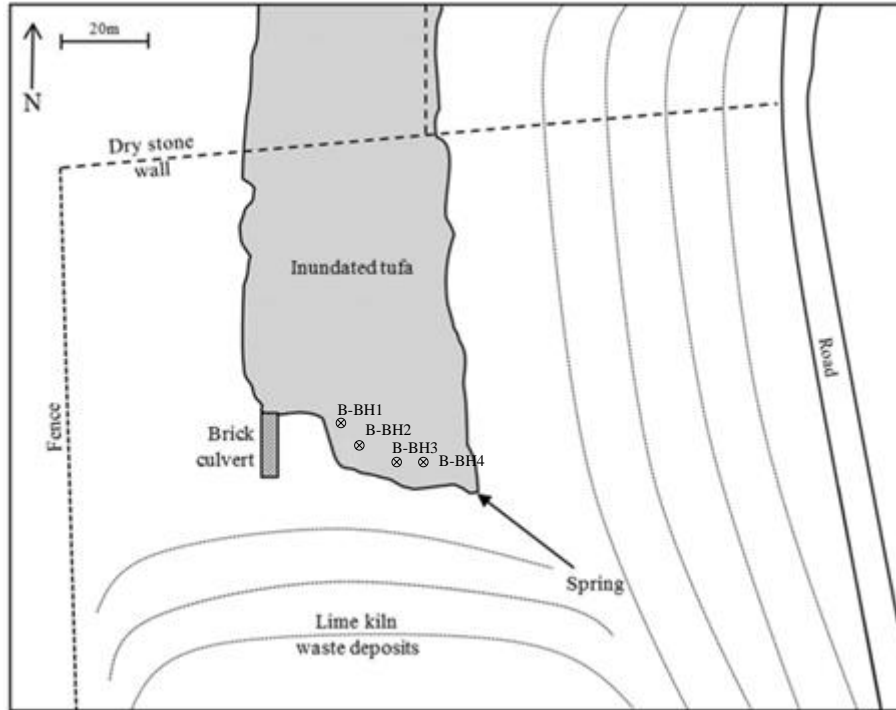


**Figure 5.1: Borehole location plan of Buxton site.** Located at Hapur Hill, UK (53.14 N 1.55 W) an old lime kiln waste disposal site (ca. 140 y).

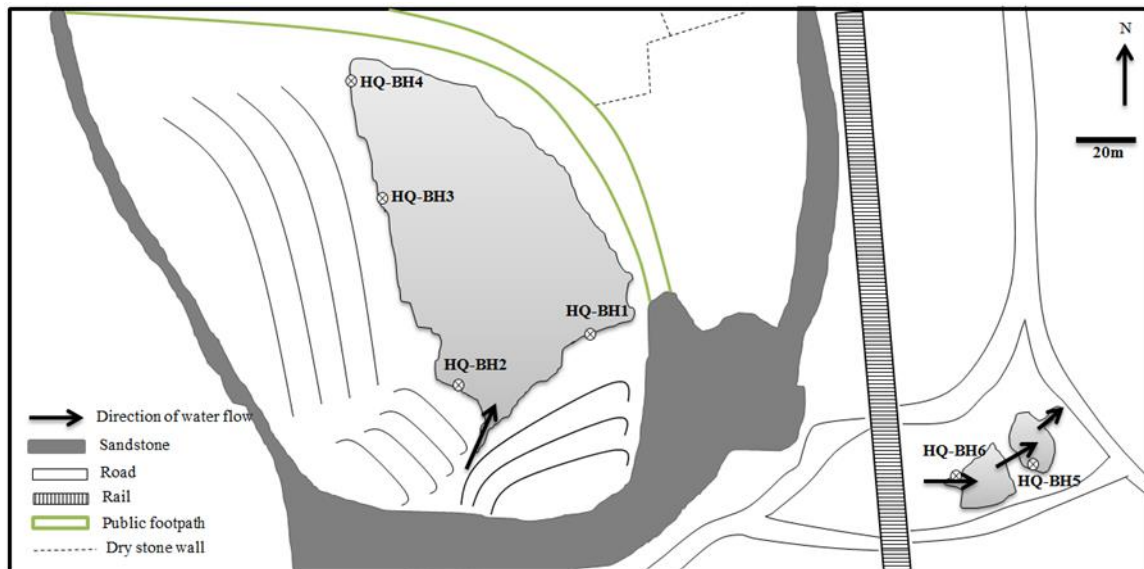


**Figure 5.2: Borehole location plan of Horton quarry site.** Located at Horton-in-Ribblesdale, UK (54.15 N 2.30 W) the site possesses a hyperalkaline lagoon from lime kiln wastes and was formed in the 1940's.

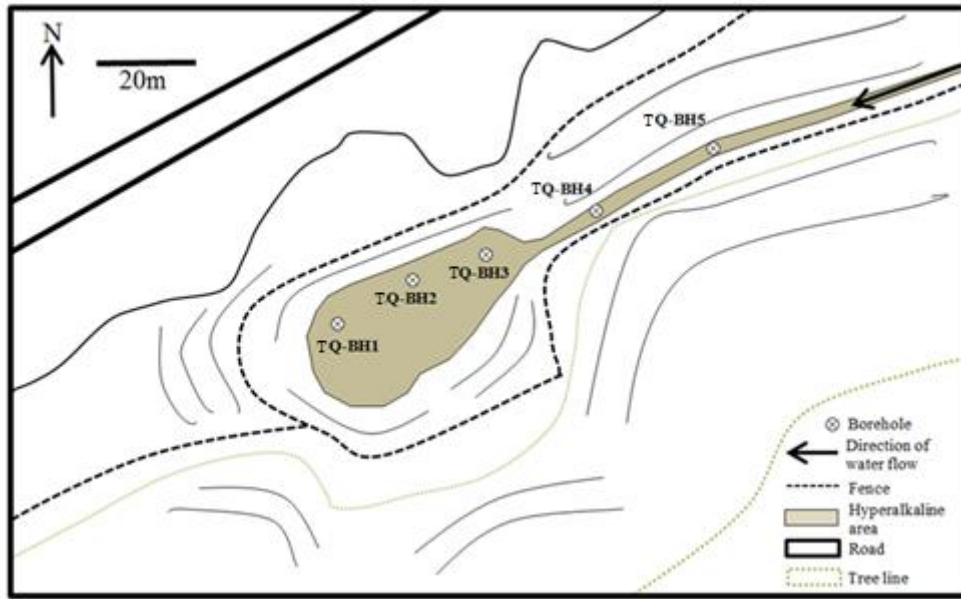


**Figure 5.3: Borehole location plan of Tarmac quarry site.** Located near Grassington, UK (54.05 N 2.03W) the limestone quarry site possess a hyperalkaline engineered basin into which rain water percolates through historic deposits and was formed an estimated 10 years ago.

### 5.8.3 Work flow for analogue sites investigation

The Buxton site (Site-B) was initially used to generate colonised cotton during 2014, with cotton (5 g total) from borehole 2 (B-BH2) used to further form microcosms for the enrichment of ISA degrading microorganisms and to investigate biofilm community composition via cloning and sequencing techniques. During 2015 cotton harvested from boreholes at the Buxton, Horton and Tarmac sites were used to investigate the active biofilm 16S rRNA gene community composition through microbial analysis of cDNA generated from extracted RNA using a MiSeq platform. The related morphology of biofilms was also investigated through the use of CLSM techniques. The work flow for these investigations is summarised in Figure 5.4.

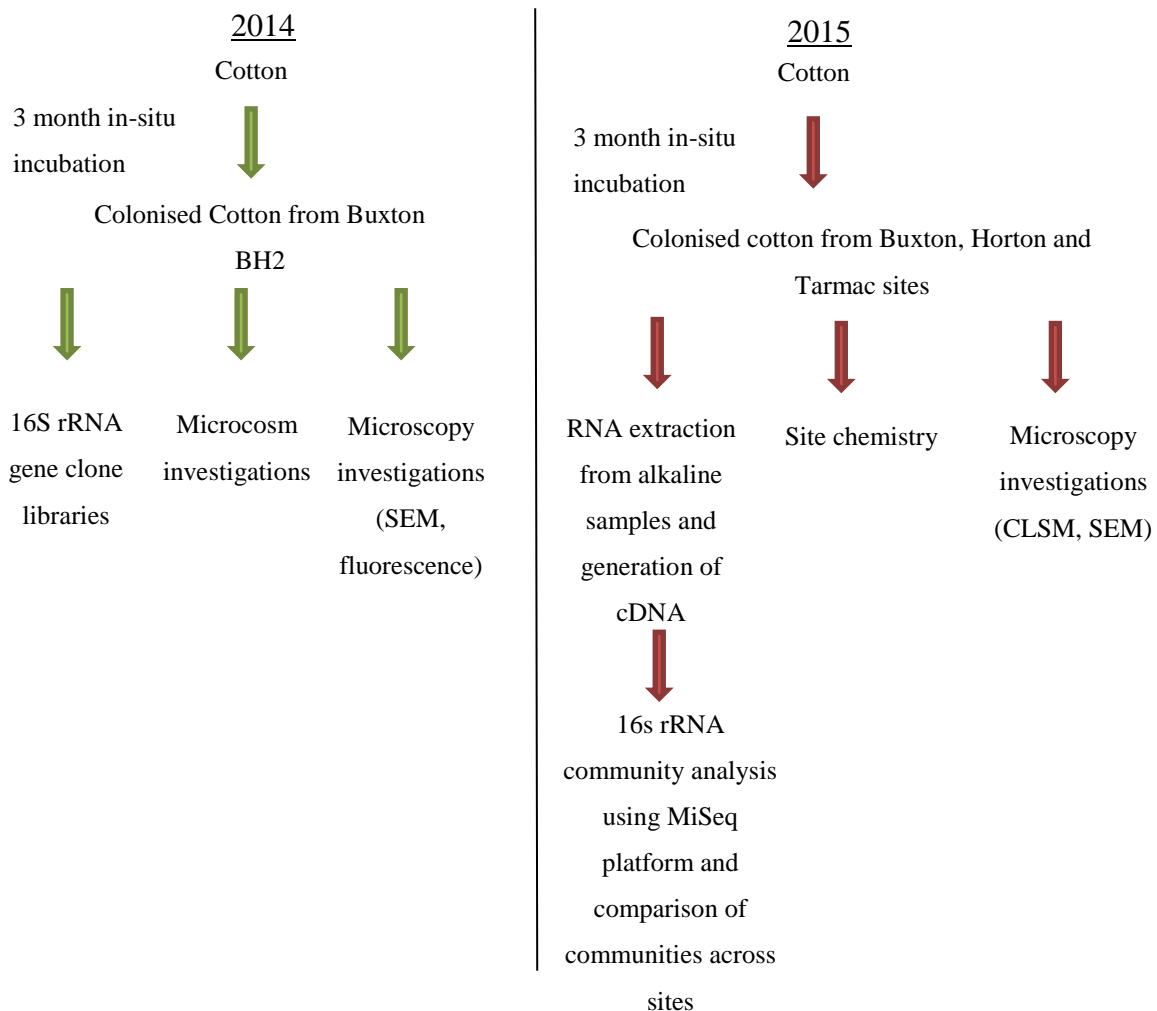


**Figure 5.4: Workflow for cotton harvested from analogue sites.**

#### 5.8.4 Genetic analysis of cotton samples

Cotton from borehole 2 collected during August 2014 was used to generate related clone libraries. Cotton samples collected during August 2015 were used to generate cDNA libraries for community analysis via a MiSeq platform. In order to generate enough RNA for cDNA synthesis samples from each individual sites hyperalkaline boreholes were pooled after extraction.

### 5.9 Microcosm investigations

#### 5.9.1 Liquid batch fed microcosms

In order to investigate ISA degradation under both methanogenic/fermentative and sulphate reducing conditions microcosms were established using approximately 1 g of colonised cotton from Site-B (harvested in August 2014) per microcosm. The cotton was washed with 10 mL N<sub>2</sub> purged sterile PBS under an inert environment to remove any transient microorganisms and added to continuously stirred microcosms containing 175 mL of pre-reduced 10 % CDP and 90 % mineral media at pH 11 and 20°C. A standard microcosm vessel is described in Diagram 5.1.

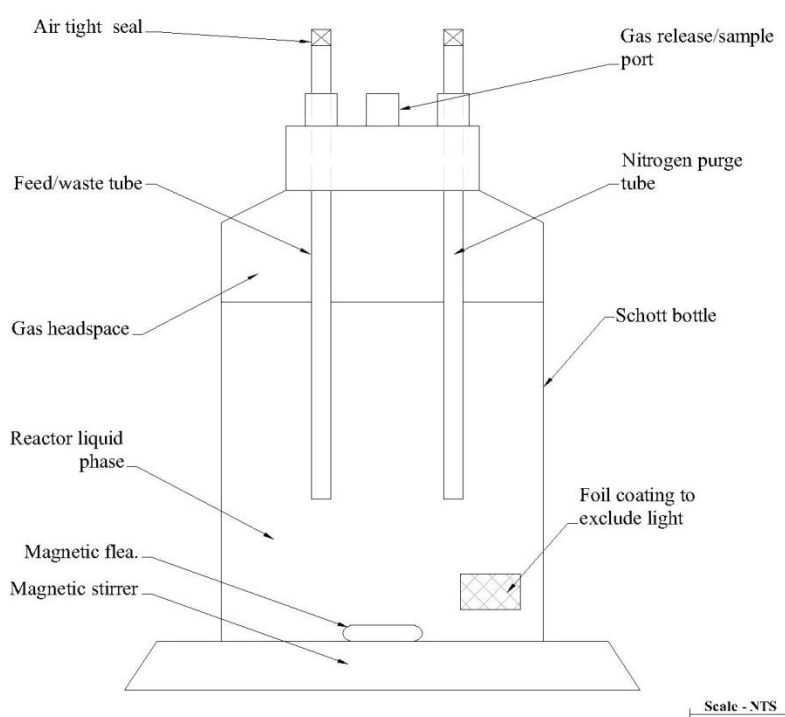
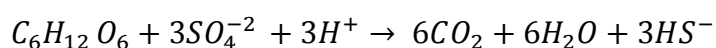


**Diagram 5.1: Standard microcosm vessel.**

The microcosms were brought up to a final volume of 250 mL by feeding 25 mL of CDP every 2 weeks with the pH adjusted using 4 M NaOH every 7 days. During each feeding period the microcosm was purged with nitrogen, with microcosms maintaining a nitrogen headspace to ensure anoxic conditions. For the microcosm under sulphate reducing conditions, sulphate was added with each feed at a concentration of 6.5 mM based on equation 5.5.



**Equation 5.5: Theoretical ISA driven sulphate reduction.**

After reaching the final volume of 250 mL the cotton was removed and the microcosms switched to a 10 % waste/feed cycle with CDP every 2 weeks, with supplementation of mineral media only after the complete replacement of the microcosm volume. The application of the waste/feed cycle was to impose a growth rate upon the microorganisms ensuring only the enrichment of growing microorganisms. The microcosms were maintained with a nitrogen atmosphere and all reagents were reduced prior to use and stored under nitrogen. Resazurin redox indicator present within the mineral media provided an indication of anaerobic conditions within the microcosms and all manipulations of the microcosms were carried out under a stream of nitrogen to maintain anoxic conditions. pH was adjusted after every feed waste cycle using 4 M NaOH. Sufficient time (50 weeks) was allowed for the microcosm chemistry to stabilise and also to allow for the washout of any transient microorganisms. At this time the microcosms were sampled every 2 days over 2 feed/waste cycles to determine the microcosm chemistry and gas headspace content. The process of microcosm establishment and maintenance is summarised in Figure 5.5.

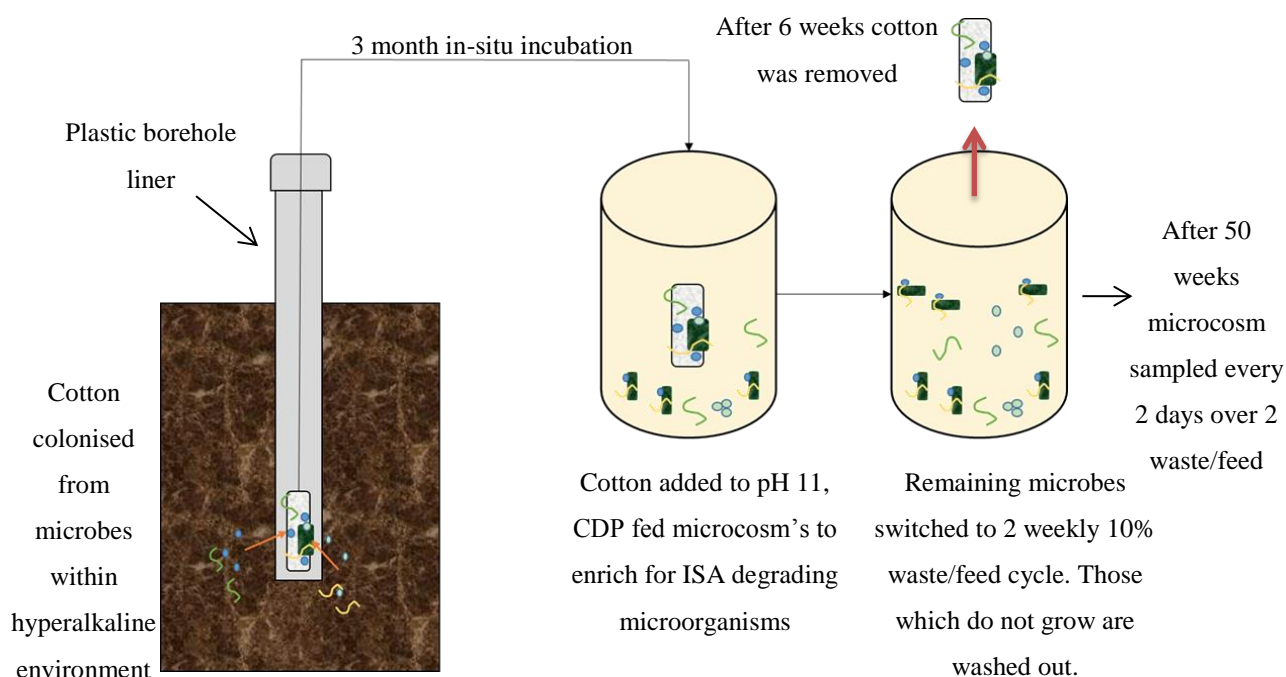


**Figure 5.5: Overview of microcosm formation and maintenance.**

### 5.9.1.1 Control microcosms

Controls amended with  $50 \mu\text{g mL}^{-1}$  chloramphenicol were formed to the same proportions as the test microcosms. The controls were prepared under nitrogen in 100 mL Wheaton bottles in duplicate and had a final volume of 50 mL and were sampled and analysed as per the test microcosms. The controls also contained waste from the main microcosms and served as an abiotic comparison for the elimination of sorption and precipitation events.

### 5.9.2 pH survival subcultures

In order to investigate the ability of the floc communities to survive prolonged exposure to hyperalkaline conditions small scale microcosms of approximately  $10^4 \text{ cells mL}^{-1}$  were formed using 100 mL Wheaton bottles at pH values 11.0, 11.5, 12.0 and 13.0 in duplicate. The microcosms were composed of mineral media and CDP to match the composition of the original microcosm. pH was measured on a weekly basis using a portable handheld probe and meter (Mettler Toledo, UK), with pH adjusted accordingly using 4 M NaOH or 2 M HCl. The head space of the microcosms was kept under nitrogen to ensure anaerobic conditions. The microcosms were sampled on a weekly basis for three weeks with the removal of 1 mL microcosm fluid each week for ATP quantification to determine cell number. Abiotic controls were established for each pH value within the pH range and were sampled as per the above

### **5.9.3 Biofilm formation upon stainless steel under alkaline sulphate reducing conditions**

25 mL waste from the pH 11 microcosm with sulphate (after 2 years under a 2 weekly feed/waste cycle) was added to 475 mL 10% CDP mineral media mix with 4mM sulphate in a 1 L Schott bottle with a 3 port lid (GL45, Schott, UK). To the media 7 x grade 304L austenitic stainless steel discs, 7 x grade 316L austenitic stainless steel discs (2 cm diameter, 1.2 mm thickness, 2B Mill finish) (Syspal, UK) fixed in a mesh bag were added. Discs were autoclaved before use. The subculture microcosm was continuously stirred at 20 °C and waste/fed as per the microcosm described in Section 5.9.1. pH was monitored on a weekly basis and adjusted up to pH 11 with 4 M NaOH if needed. After a 3 month period the microcosm was sampled every 2 days over 2 feed/waste cycles, after which the discs were removed for analysis. Controls were made up in duplicate as per the main sample but without microorganisms. Each control had with 2 x 304L and 316L steel discs in a 50 mL Schott bottle and was sampled as per the main disc reactor.

### **5.9.4 Free drift sulphate reducing investigation**

Three 250 mL subcultures at pH 11 with a 10 % CDP mineral media mix with 3 mM sulphate were formed using 75 mL of microcosm fluid from the pH 11 microcosm under sulphate reducing conditions (after a 2 weekly waste/feed cycle duration of 2 years) described in Section 5.9.1. The pH 11 microcosm fluid was centrifuged at 5,000  $x$  g for 10 minutes and cells resuspended in fresh media 10 % CDP mineral media mix with 3 mM sulphate and distributed evenly between the three vessels for subculture. The subculture vessels were then left for 26 days under a nitrogen headspace with continuous stirring at 20 °C. The vessels were sampled every 2 days to determine reactor chemistry with the headspace flushed with nitrogen to allow for the recording of a pH value during these sampling periods. Sulfide concentration and cells were harvested at pH values 11.0, 10.5, 10.0, 9.5, 9.0, 8.0, 7.0 ( $\pm$  0.25). Controls were established as per the three initial subcultures with one set of subcultures treated with 5 mM molybdate (260) to inhibit sulphate uptake and one set treated with chloramphenicol (5  $\mu$ g mL<sup>-1</sup>) for an abiotic comparison. The control subcultures were sampled as per the main subcultures.

### 5.9.5 Recirculation biofilm system

Biofilm was grown using Ottawa sand as a substrate for adhesion within the recess of a Bio-cell unit (Diagram 5.2).

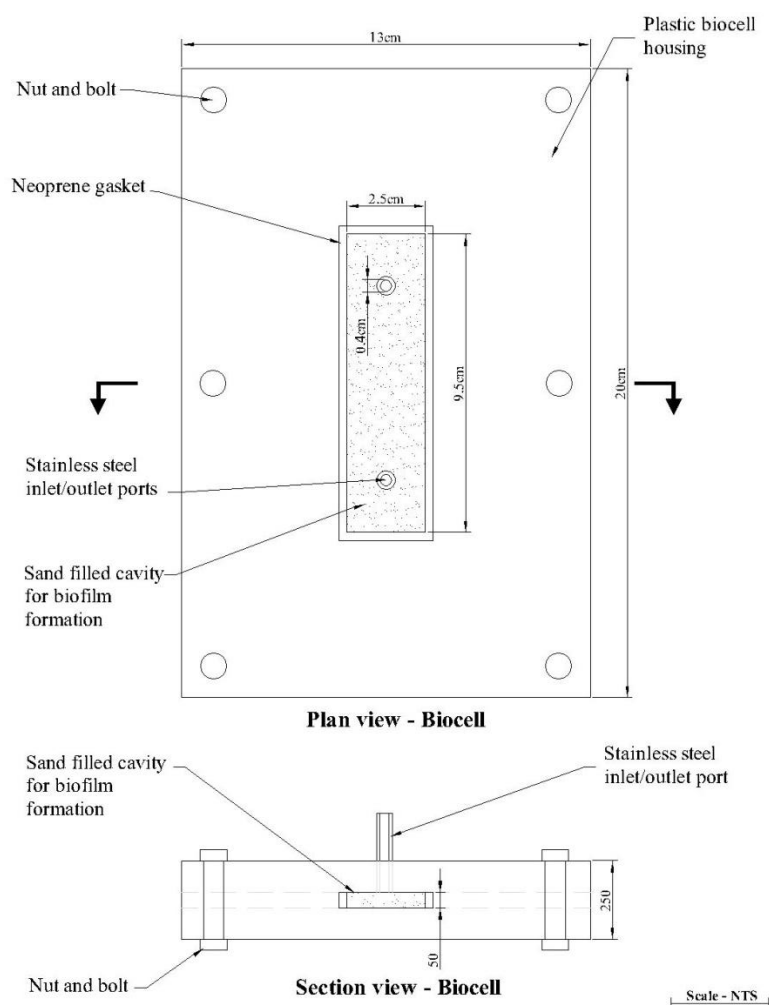


**Diagram 5.2: Small Biocell diagram.**

Each Bio-cell unit held approximately 24 g of sand which was acid washed before use. A larger liquid subculture which was formed from the pH 11 fermentative/methanogenic microcosm described in Section 5.9.1 was used to form biofilm within the sand columns. 25 mL waste from the pH 11 microcosm (taken after 1.5 year duration 2 weekly feed/waste cycle) was added to a 10 % mix of CDP and mineral media to a final volume of 500 mL in a custom 1.5 L reaction vessel. The vessel was equipped with fittings for BacVis headspace gas analysis pods and a 3 port lid (GL45, Schott UK) which included an inlet, outlet and septum sample ports. The subculture microcosm was continuously stirred at 20 °C. Using a peristaltic pump and 0.31 mm internal diameter norprene tubing (Masterflex, Cole-Palmer, UK) fluid was pumped through a Biocell plastic biofilm unit at a rate of 0.35 mL min<sup>-1</sup>, designed to

give the passage of the entire volume of the subculture microcosm per day (Diagram 5.3). The subculture microcosm was run on a 2 weekly 10 % waste feed cycle for 25 weeks (until the chemistry stabilised) and the biofilm reached a visible steady state (loss = growth). The system was then sampled every 2 days over two feed/waste cycle. The Biocell unit and sand column were sterilized before use by the passage of a chlorine solution for 2 hours and washing with sterile ultrapure water for 1 hour. An abiotic control system was set up alongside and run as per the biotic system and differed only by the omission of microorganisms.

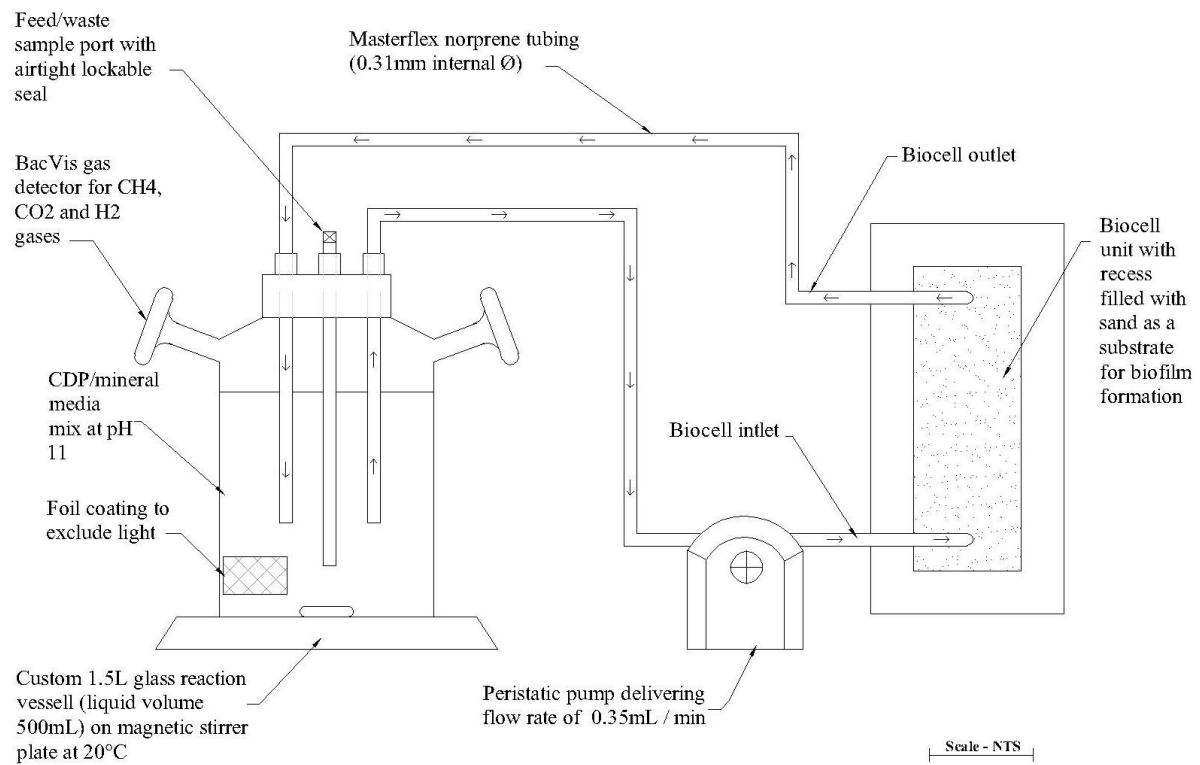


**Diagram 5.3: Recirculation based biofilm system.**

### 5.9.5.1 Testing individual components of recirculation system

In order to determine the distribution of microbial activity within the recirculation system both the liquid and the biofilm components were tested separately for ISA degradation. In order to test the liquid component the main vessel was removed from the biofilm component as shown in Diagram 5.4 and sampled every 2 days over 2 feed/waste cycles. The biofilm component was tested using a single pass system detailed in Diagram 5.5, where a 10 % CDP mineral media mix was passed through a fully developed Biocell unit at a rate of  $0.05 \text{ mL min}^{-1}$ . The outlet from the Biocell then flowed into a vessel fitted with BacVis pods for gas detection and was sampled via a three way lockable valve positioned before the final vessel.

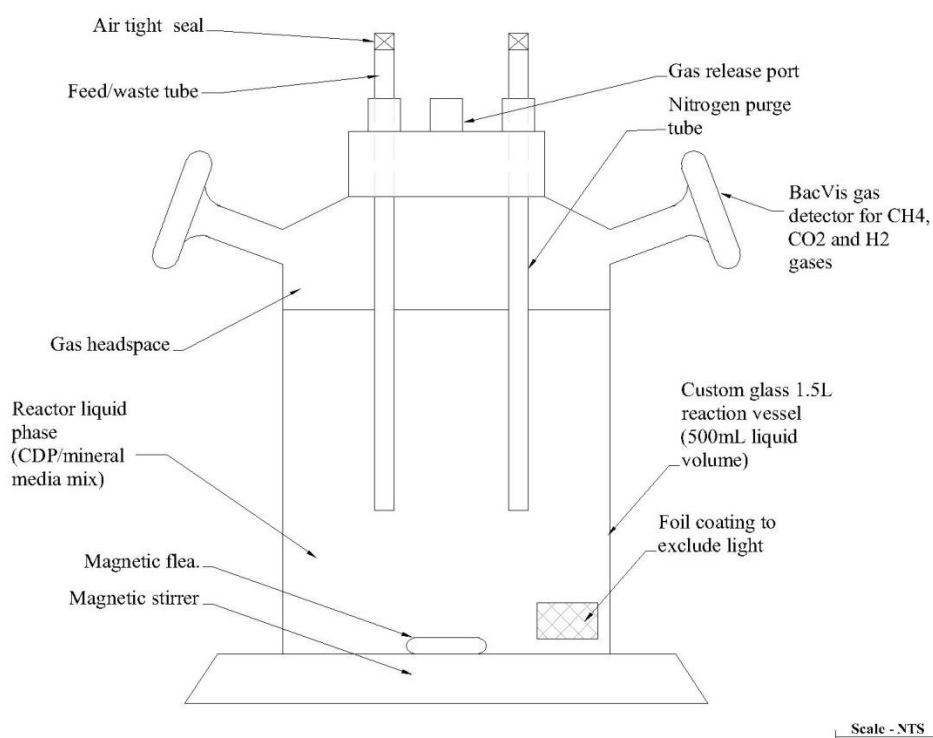


**Diagram 5.4: Liquid only component of recirculation system.**

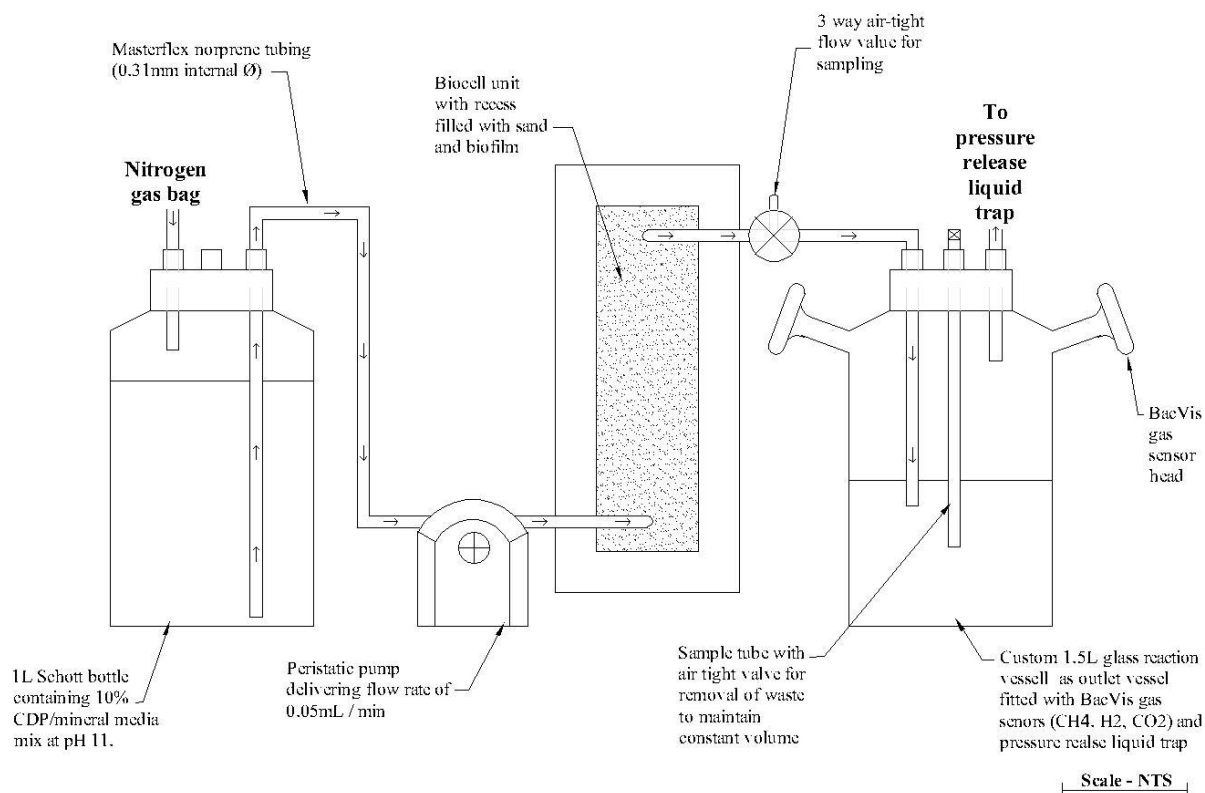


**Diagram 5.5: Single pass system for testing biofilm activity**

### 5.9.6 Single pass NRVB column biofilm system

Sterile Biocell units were placed downstream from a developed biofilm community within the recirculation system described in Section 5.9.5. Units were left to develop a visible steady state biofilm over a 10 week period at pH 11. Once developed a Biocell unit was placed into the system described in Diagram 5.6, which consisted of a single pass system described in Diagram 5.5, with the outlet of this system connected to a large Biocell unit (Diagram 5.7). The recess of Biocell had NRVB cast into it along with 2 x grade 304L austenitic stainless steel discs, 2 x grade 316L austenitic stainless steel discs (2 cm diameter, 1.2 mm thickness) and a 1 cm (approx.) diameter graphite disc. The outlet of the NRVB column passed to into a vessel fitted with BacVis pods for gas detection. The system was sampled via three way lockable valves positioned after the Biocell unit and after the NRVB column. Through the system a 10 % CDP, mineral media mix at pH 11, 12 and 13 was passed at rate of 0.05 mL min<sup>-1</sup> with the system run in duplicate and sampled every 2 days for a 14 day period. Flow rate was constrained to deliver 1 L total volume over a 14 day period. Controls were run in duplicate using the same system and sampling period using a sterile sand column.



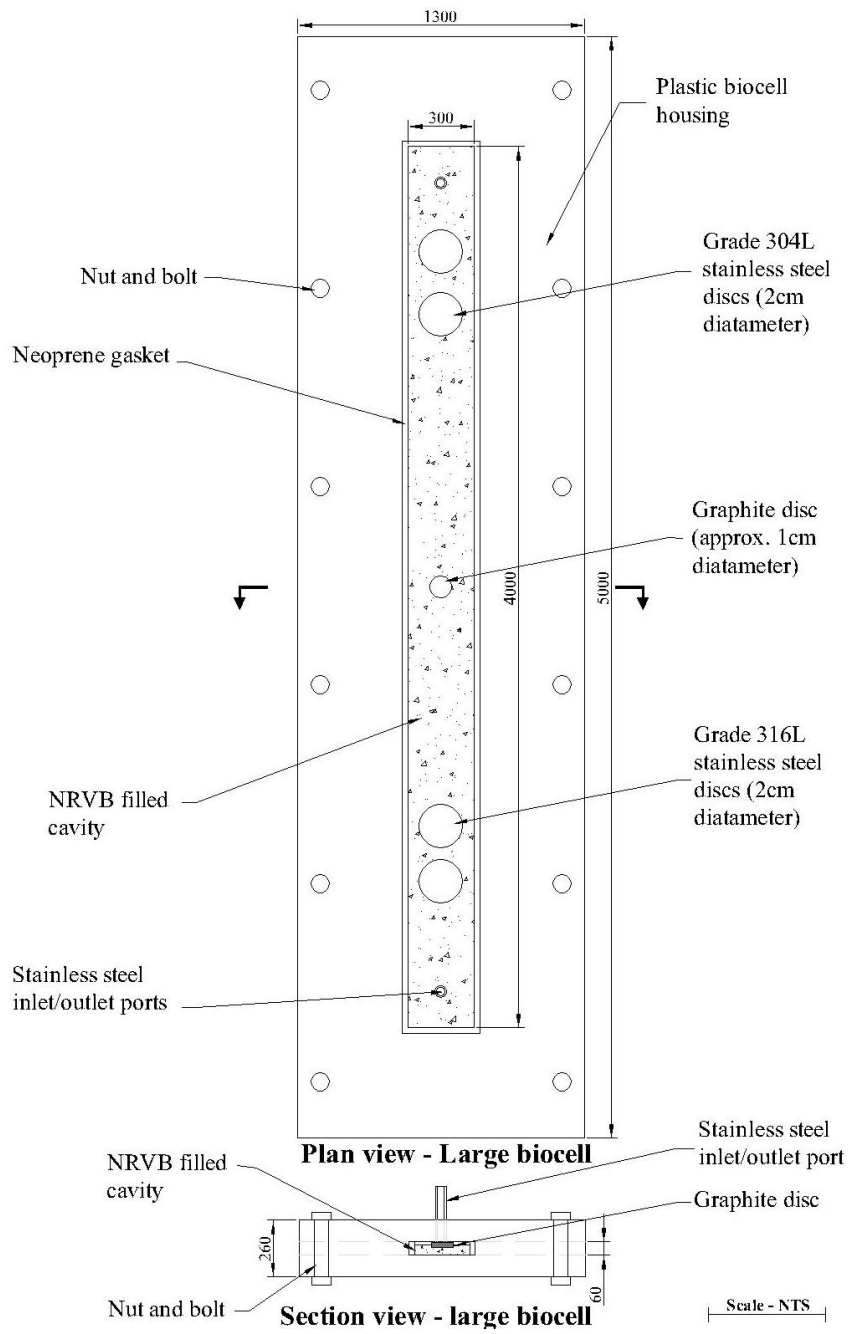


**Diagram 5.7: Large Biocell with NRVB column.**

### 5.9.7 Preparation of NRVB

Nirex reference vault backfill (NRVB) was prepared using methods outlined in Butcher *et al* (12) with the composition of the mix shown in Table 5.10. NRVB was cast into plastic Biocells outlined in Diagram 5.7 to give an approximate final dried weight of 103 g per Biocell. After casting NRVB was allowed to harden overnight at room temperature then in a sealed Biocell cured for 28 days using a saturated Ca(OH)<sub>2</sub> solution.

Component	Mass (g)
Lime	300
Limestone flour	990
Portland cement	900
Water	1230

**Table 5.10: NRVB composition.**

#### 5.9.7.1 Carbonation testing of NRVB

The surface of NRVB was tested for evidence of carbonation by using 1 % (w/v) phenolphthalein ethanol solution (261). The solution was added directly onto the NRVB surface with alkaline areas showing a purple, red colour and carbonated areas becoming colourless.

### 5.9.8 Calculating rate constants

First order rate constants for ISA degradation were calculated according to equation 5.6.

$$C_x = C_0 e^{-kt}$$

**Equation 5.6: Exponential growth / decay equation.** Where  $C_x$  = final concentration,  $C_0$  = start concentration,  $k$  = first order rate constant and  $t$  = time.

## 5.10 Micro pH and redox electrode profiling

### 5.10.1 pH floc profile

pH 11 microcosms under fermentative/methanogenic and sulphate reducing conditions previously described in Section 5.9.1 were used as the inoculation source for all experiments. pH profiles of the flocs were undertaken with a micromanipulator and stand (Unisense, Denmark) using a 10 µm diameter pH electrode with an external reference (Unisense, Denmark) connected to a single channel pH/redox meter supplied by the probe manufacturer (Unisense, Denmark). The probe was calibrated against pH 4, pH 7 and pH 10 standards and tested against pH 11 and pH 12 solutions made using NaOH. Profiles were taken through the flocs at pH 11.0, 11.5 and 12.0. In order to generate the pH profile of the flocs, flocs were

incubated for 1 hour in microcosm fluid at the desired pH and were then injected into agar cubes of the same pH to provide support for the profiling. Control profiles were conducted through plain agar at pH 11.0, 11.5 and 12.0. Data was recorded using the SensorTrace suite (Unisense, Denmark).

#### **5.10.2 Biofilm pH and redox profile**

Profiles were taken through biofilm using a 200  $\mu\text{m}$  diameter micro pH electrode (Unisense, Denmark) with internal reference and a 100  $\mu\text{m}$  redox microelectrode with an external reference (Unisense, Denmark) under a nitrogen atmosphere. Electrodes were connected to a single channel pH/redox meter supplied by the probe manufacturer (Unisense, Denmark). The pH probe was calibrated as per Section 5.10.1 and the redox probe tested as per the manufactures instructions using pH buffer solutions saturated with quinhydrone. pH profiles were undertaken with a micromanipulator and stand supplied by the manufacturer (Unisense, Denmark). Control profiles were taken through pH buffer or pH buffer amended with quinhydrone for the redox probe. Data was recorded using the SensorTrace suite (Unisense, Denmark).

## **6. Harpur Hill, Buxton analogue site investigation and microcosm experiments**

## 6.1 Rationale

The aim of this first section of work was to recover microbial biofilm communities from the Buxton analogue site using in-situ cotton bait. The Buxton analogue site at Harpur Hill was chosen due to the large amount of previous research associated with the site (See Section 2.2.2). Further work would then investigate the ability of the recovered microbial communities to degrade ISA ( $\alpha$ -ISA,  $\beta$ -ISA and XISA) under methanogenic conditions in liquid culture at pH 11. These conditions were chosen due to the likely absence of large amounts of higher energy TEA's within the near field of an ILW-GDF.

## 6.2 Results and discussion

### 6.2.1 Analogue site investigation and analysis of colonised cotton

Chemical analysis of the hyperalkaline areas of the Buxton site have been previously described (56, 80) and Table 6.1 shows the results of the analysis of the porewater, sediment and cotton after a 3 month incubation period. The pH within the vicinity of the cotton samples was between pH 11.5 and pH 12 and redox measurements were found to be negative in both the associated sediment and porewaters. Both the alpha and beta forms of ISA were extracted from the cotton ( $>0.5$  mg g DW<sup>-1</sup>), the sediment ( $>0.5$  mg g DW<sup>-1</sup>) and porewater (7.64 mg L<sup>-1</sup> alpha, 6.82 mg L<sup>-1</sup> beta) indicating in-situ alkaline cellulose hydrolysis (22). The generation of CDPs from the site's soil organic matter has been previously demonstrated (80) and in this study the addition of cotton cellulose resulted in its partial alkaline hydrolysis to CDPs with the concentration of  $\alpha$ -ISA and  $\beta$ -ISA in the porewater and sediments being higher than those measured by Rout *et al* (80). This supports the concept that the hyper-alkaline conditions created at this site are capable of generating CDP. The presence of acetate, a common end product of ISA fermentation (81, 83, 177), in the porewater, sediment and cotton indicates an active anaerobic microbial community in the immediate proximity of the cotton even though the ambient pH was greater than pH 11.0.

Source	pH	eH	Acetate	$\alpha$ -ISA	$\beta$ -ISA
Porewater (mg L <sup>-1</sup> )	11.92	-66	208.9	7.64	6.82
Sediment (mg g DW <sup>-1</sup> )	11.5	-77	127.24	1.01	0.54
Cotton (mg g dry DW <sup>-1</sup> )	N/S	N/S	141.16	2.34	0.85

**Table 6.1: Analysis of porewater, sediment and cotton retrieved from the Buxton analogue site.**

Microscopy analysis of the cotton after retrieval showed areas of EPS indicative of biofilm formation and surface associated mineral precipitates (Figure 6.1 and Figure 6.2) with

individual viable bacterial cells being visible on some fibres (Figure 6.1). This is a marked contrast to the colonisation of cotton incubated in a landfill site under neutral anaerobic conditions reported by McDonald *et al* (262) where fibres were heavily colonised with cells and exhibited the characteristic pits and grooves associated with microbial cellulose hydrolysis. The reduced colonisation of the cotton under the hyperalkaline conditions present at the site are further illustrated by the live/dead staining of the cotton (Figure 6.1D) which revealed a low density of live cells on the individual cotton fibres and within the surrounding biofilm material. This could be attributed to the external environmental stresses forcing microbes to expend additional energy to maintain cytoplasmic homeostasis (45). The formation of biofilm under these conditions could be a survival mechanism whereby a niche site is formed in which EPS acts as a barrier to external environmental stresses (95). Previous work by Grant *et al* (176) has demonstrated the ability of microorganisms under alkaline conditions to form a biofilm upon the surface of the cementitious materials with work by Smith *et al* (143) showing the ability of microbes within biofilms to survive in sandstone columns up to pH 13.

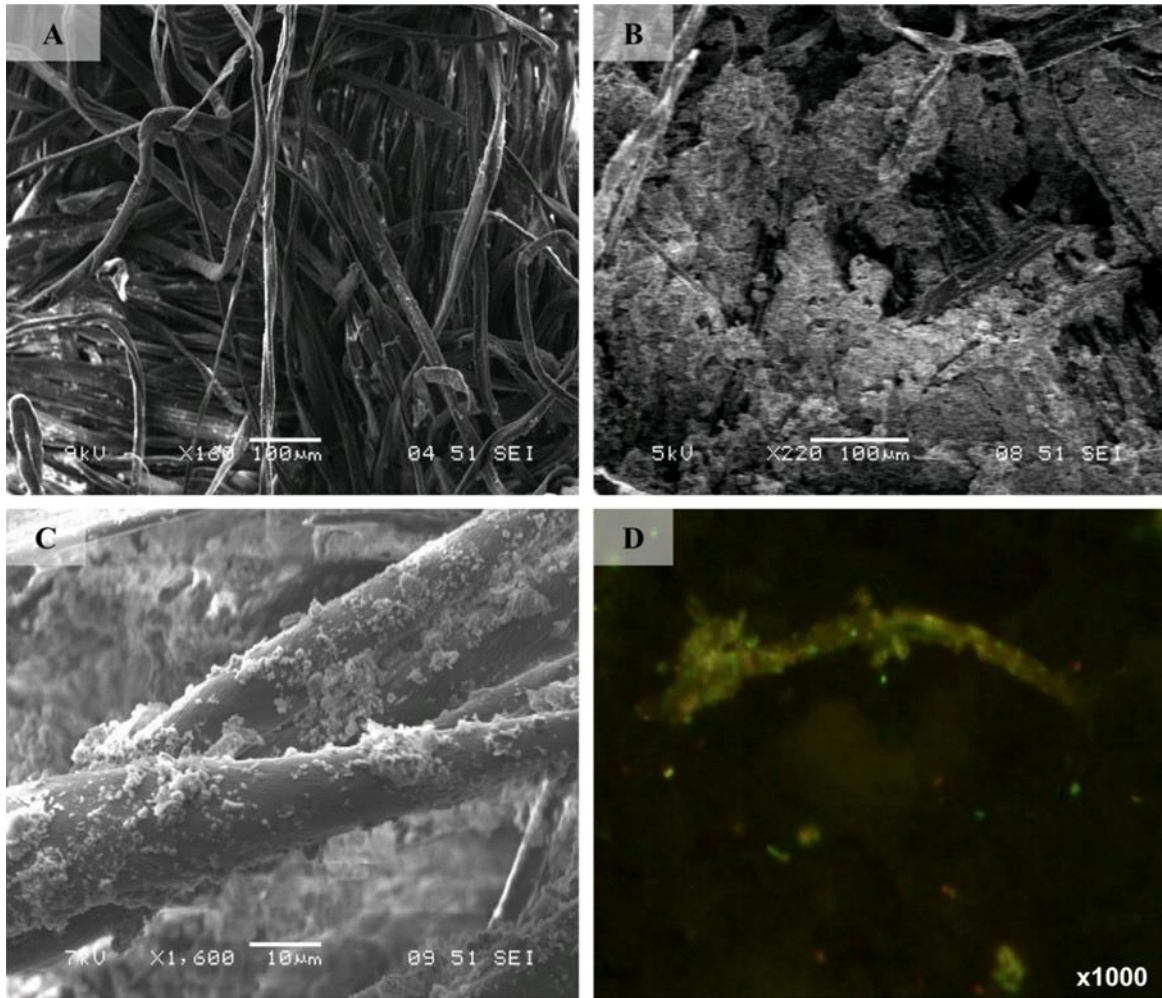
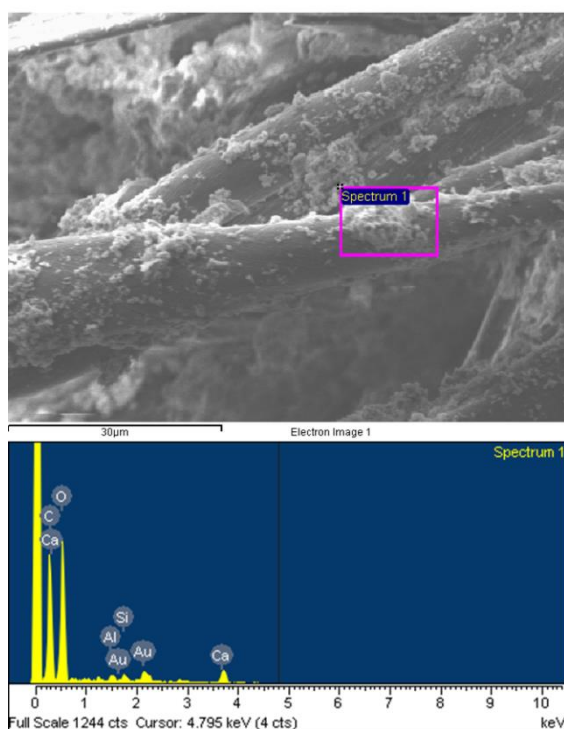


**Figure 6.1: Microscopy investigation of the cotton.** [A] Sterile cotton. [B] Cellulose cotton from the borehole showing biofilm formation. [C] Close up of individual fibre showing individual cells, EPS aggregates and mineral precipitate. [D] Live/dead image of individual cotton fibre (live cells = green, dead cells = red).



Element	Weight (%)
O	46.7
C	29.6
Ca	20.3
Si	2.0
Al	1.4

**Figure 6.2: Elemental composition of biofilm formed upon colonised cotton.** The biofilm possessed areas rich in carbon, oxygen and calcium possibly indicating calcium carbonate formation.

The cotton's Eubacterial clone library was dominated by the Order Clostridiales which represented 58% of the clones obtained (n=67) (Figure 6.3A). Of these Clostridia, 33 sequences most closely matched organisms from the family Clostridiaceae 2, where 13 sequences most closely matched *Clostridium formicaceticum* strain DSM 92 and a further 10 to *Anaerovirgula multivorans* strain SCA. The remaining 9 clones most closely matched sequences belonging to the genus *Alkaliphilus*, of which 8 were closely related to *Alkaliphilus oremlandii* strain OhILAs and 1 related to *Alkaliphilus transvaalensis* strain SAGM1. The remaining clones of the Clostridia were represented by sequences most closely related to organisms from the families Clostridium insertae sedis XI (3 sequences) and Clostridium insertae sedis XIV (2 sequences). The remainder of the clone library was made up of a diverse range of taxonomic families including: representatives from Brucellaceae, primarily related to *Ochrobactrum anthropi* strain ATCC 49188; Corynebacteriaceae, dominated by *Corynebacterium marinum* strain D7015; and the Bacillaceae 1, dominated by *Bacillus pseudofirmus* strain OF4.

The incubation of the cotton cellulose within the hyperalkaline sediment selected for organisms from the Clostridia lineage which contrasts with previous investigations of the background sediments where a larger degree of taxonomic diversity was observed (82, 84, 178) presumably due to greater diversity of energy sources and colonisation from surrounding pasture land. Of the Clostridiaceae 2 species identified, *Clostridium formicaceticum* has broad spectrum carbohydrate fermentation capabilities (263), but has not previously been associated with alkaline conditions. This contrasts with species from the genera *Anaerovirgula* and *Alkaliphilus* which have all been previously associated with alkaline sites (40, 264, 265).

The Archaeal clone library (Figure 6.3B) was dominated (93%) by sequences most closely matching *Methanobacterium alcaliphilum* strain NBRC 105226 (n=68). The remaining sequences were most closely related to *Methanomassiliicoccus luminyensis* strain B10 and *Methanosarcina mazei* Go1. The Archaeal population associated with the cotton was dominated by hydrogenotrophic, alkaliphilic *Methanobacterium*. Although these organisms are able to utilise acetate as a growth factor (266, 267), they are incapable of acetoclastic methanogenesis which could account for the accumulation of acetic acid in extracts from the cotton and surrounding sediment and porewaters. Organisms showing sequence similarity to *Methanobacterium alcaliphilum* were observed, where this organism has been isolated from alkaline sediments (153), whilst *Methanomassiliicoccus luminyensis* has only previously been isolated from human faeces (268). In addition to these hydrogenotrophic methanogens, *Methanosarcina mazei* (269) a halotolerant methanogen able to utilise both hydrogen and acetic acid was also present.

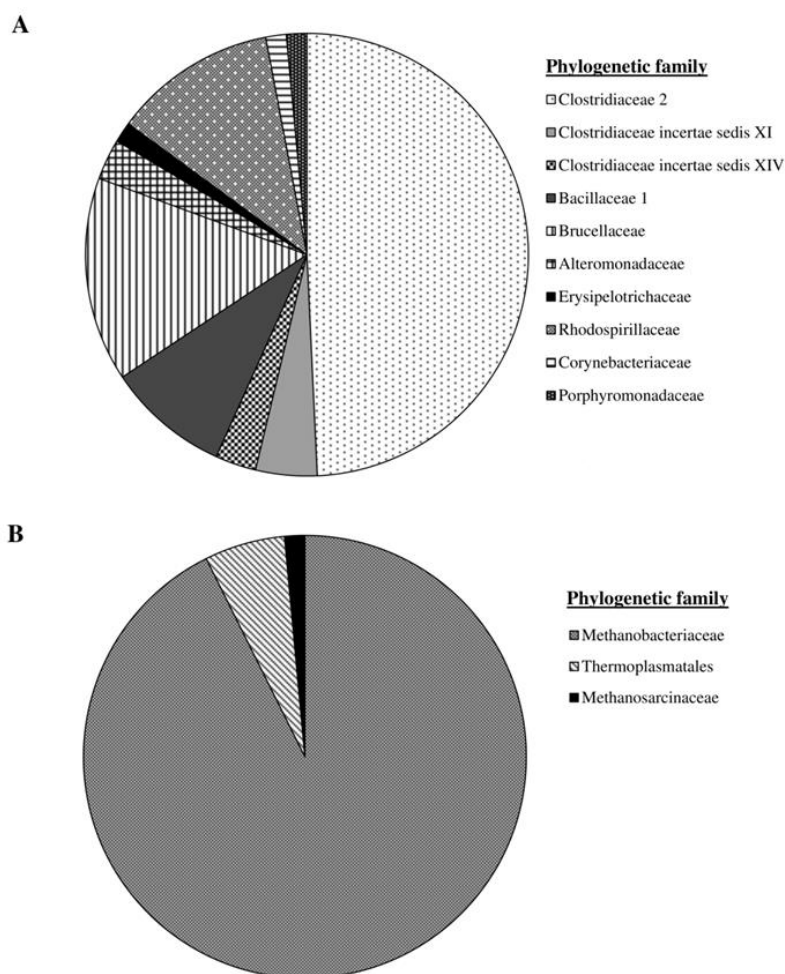


**Figure 6.3: 16S rRNA gene clone libraries of the colonised cotton.**[A] Eubacterial (n = 67). (B) Archaeal (n = 68). Phylogenetic families were assigned to clones through a MegaBLAST database search.

### 6.2.2 Microcosm studies

The fermentative/methanogenic microcosm demonstrated significant degradation of ISA at pH 11.0 over the course of a feed cycle (Figure 6.4) with first order degradation rates shown in Table 6.2. Comparison of the rate constants to those generated in a pH 11 sediment based CDP driven microcosm as reported by Rout et al (80) show similar  $\beta$ -ISA degradation rates but reduced  $\alpha$ -ISA rates. This study is the first to demonstrate the biodegradation XISA with the provision of a related rate constant. The rate of degradation of XISA was higher than  $\alpha$ -ISA and similar to  $\beta$ -ISA and could be a reflection of the different solubilities of the different forms of ISA (20, 270). Acetate was the only VFA detected and gradually accumulated in the system reaching a peak of  $499.8 \text{ mg L}^{-1}$  (SE  $\pm$  49.8), similarly hydrogen gas accumulated in the headspace over the course of the feed cycle reaching 1.00 mmoles (SE  $\pm$  0.04) (Figure 6.4). Neither carbon dioxide nor methane was detected in the headspace of the microcosm,

however, soluble inorganic carbon increased within the system (Figure 6.4) with the pH after each cycle reordered at an average of 10.80 (SE  $\pm$  0.4). The production of acetate and hydrogen as the products of ISA degradation suggest degradation via fermentation processes with similar results produced by Rout *et al* (80, 81) under methanogenic conditions. The chloramphenicol control showed no significant degradation of ISA or acetate or hydrogen production, indicating that ISA degradation was biological not chemical (Figure 6.4).

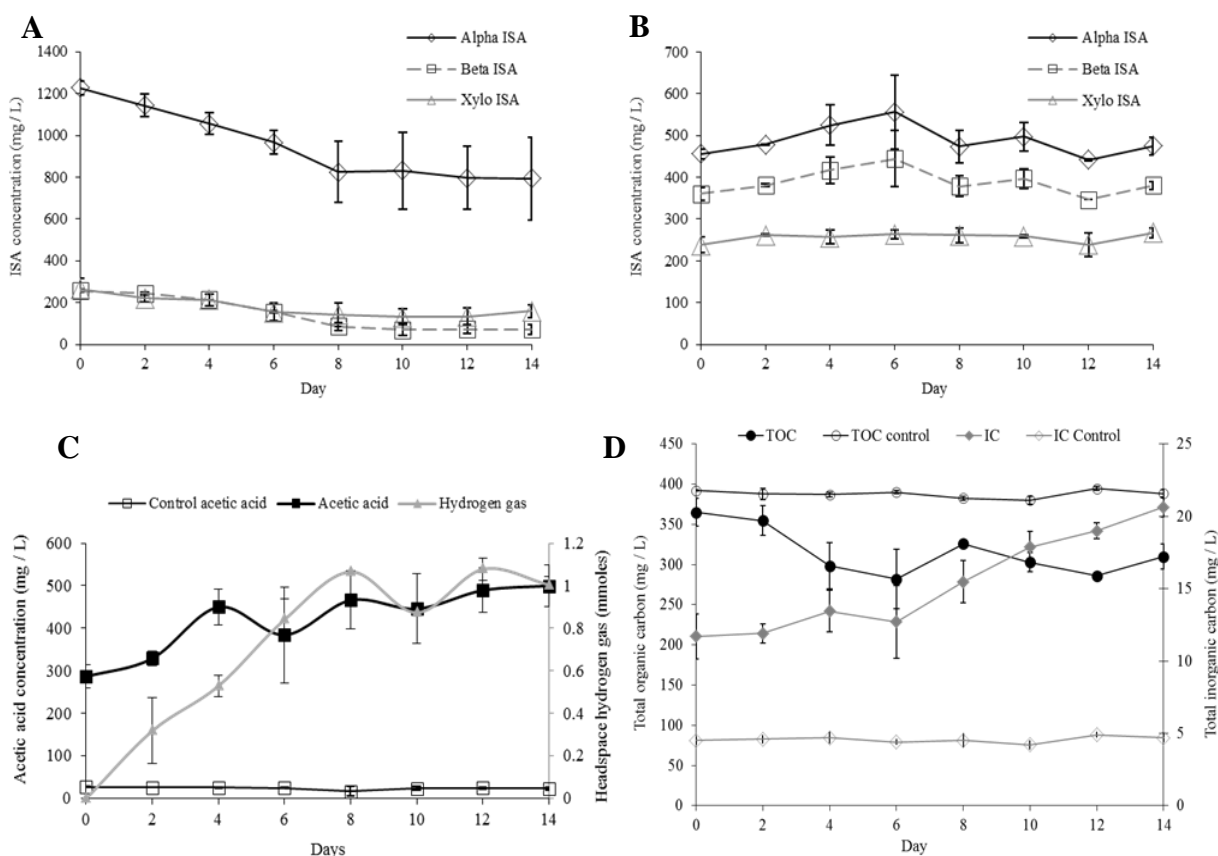


**Figure 6.4: Chemistry of the CDP driven pH 11 microcosm.** [A] All three forms of ISA were able to be degraded by the microcosm. [B] The pH 11 control showed no evidence of ISA degradation. [C] The degradation of ISA resulted in the production of both acetate and hydrogen gas as fermentation end products. The control showed no evidence of acetate generation. [D] TOC decreased as ISA was degraded and IC measurements increased. The control showed no change in both TOC and IC.

	Rate (day <sup>-1</sup> )	SE
$\alpha$ -ISA	$3.33 \times 10^{-2}$	$2.01 \times 10^{-2}$
$\beta$ -ISA	$9.36 \times 10^{-2}$	$2.20 \times 10^{-2}$
XISA	$6.78 \times 10^{-2}$	$2.85 \times 10^{-2}$

**Table 6.2: ISA degradation rate constants of pH 11 methanogenic microcosm.** The rate constants show that both the rate of XISA and  $\beta$ -ISA degradation was faster than  $\alpha$ -ISA degradation.

Measurements of ATP content of the microcosm over two consecutive waste/feed periods showed an increase in cell concentration over the two week period (Table 6.3) and reinforces the biological degradation of ISA as a carbon source.

Day	CFU mL <sup>-1</sup>	SE	Biomass (mg DW)	SE	Biomass (mg C)	SE
0	9.50 x 10 <sup>6</sup>	1.23 x 10 <sup>6</sup>	1.69	0.22	0.83	0.11
7	1.30 x 10 <sup>7</sup>	3.18 x 10 <sup>5</sup>	2.40	0.56	1.18	0.03
14	1.46 x 10 <sup>7</sup>	6.61 x 10 <sup>5</sup>	2.59	0.12	1.28	0.06

**Table 6.3: Cell concentration and associated biomass over two week period.** Cell concentration is given as *E.coli* equivalents with 350 fg carbon per cell and an empirical biomass of C<sub>5</sub>H<sub>7</sub>O<sub>2</sub>N (238).

Analysis of the microbial community of the pH 11 microcosm was undertaken using both a cloning sequencing technique and a MiSeq based platform (Figure 6.5). The cloning and sequencing technique returned a library made up of 59 eubacterial sequence reads and no archaeal reads. In contrast to this a MiSeq platform approach returned 18,854 number of sequence reads which included both bacterial and archaeal sequences. The cloning and sequencing library was dominated by clones of *Alishewanella jeotgali* strain MS1 from the family Alteromonadaceae with a similar but smaller component seen in the MiSeq library. The remainder of the library produced by cloning and sequencing included representatives of the family Bacillaceae, most closely matching *Bacillus pseudofirmus* strain OF4 and *Alkaliphilus crotonatoxidans* strain B11-2 of the family Clostridiaceae 2. In comparison to this the remainder of the library produced by the MiSeq approach contained a much broader range of microbes with 1430 OTU's. The differences observed between the two approaches could be attributed to numerous factors including differences between the extraction techniques used for the genomic DNA, 16S primer type, sequencing depth and procedure bias. From the results obtained it would appear that the MiSeq approach with its higher number of sequence reads offers a higher 16S microbial community resolution as can be seen by the increased Shannon diversity index values (Table 6.4).

The MiSeq approach revealed the microcosm community was dominated by sequence reads associated with the phyla Proteobacteria (39.5%), Actinobacteria (32.9%), Firmicutes (24.9%) and Bacteroidetes (2.3%) making up 99.6% of the library (Figure 6.5). The Proteobacteria and Actinobacteria were each dominated by sequence reads associated with the *Alishewanella* (31.8%) and *Dietzia* (26.7%) genera respectively. Reads associated with *Hydrogenophaga* and *Silanimonas* genera were also detected within the Proteobacteria group, where *Leucobacter* and *Corynebacterium* represented >1% of the total reads within the

Actinobacteria. The Firmicutes detected were not dominated by a particular species per se, where *Anaerobranca* (4.6%), *GQ356941\_g* (4.5%), *Tissierella* (2.7%), *Natronobacillus* (2.6%), *Bacillus* (2.0%) and *Bacillus\_g26* (1.7%) were all represented within the sequence reads. The Bacteroidetes were almost entirely composed of the sequence reads associated with the genus *Aquiflexum* (2.2% of the total reads). The archaeal component of the library made up small fraction of the community (0.01%) and was entirely dominated by a methanogen from the genus *Methanosaeta*. The relatively small composition of the methanogens is likely reflected in the absence of detectable levels of methane in the microcosm.

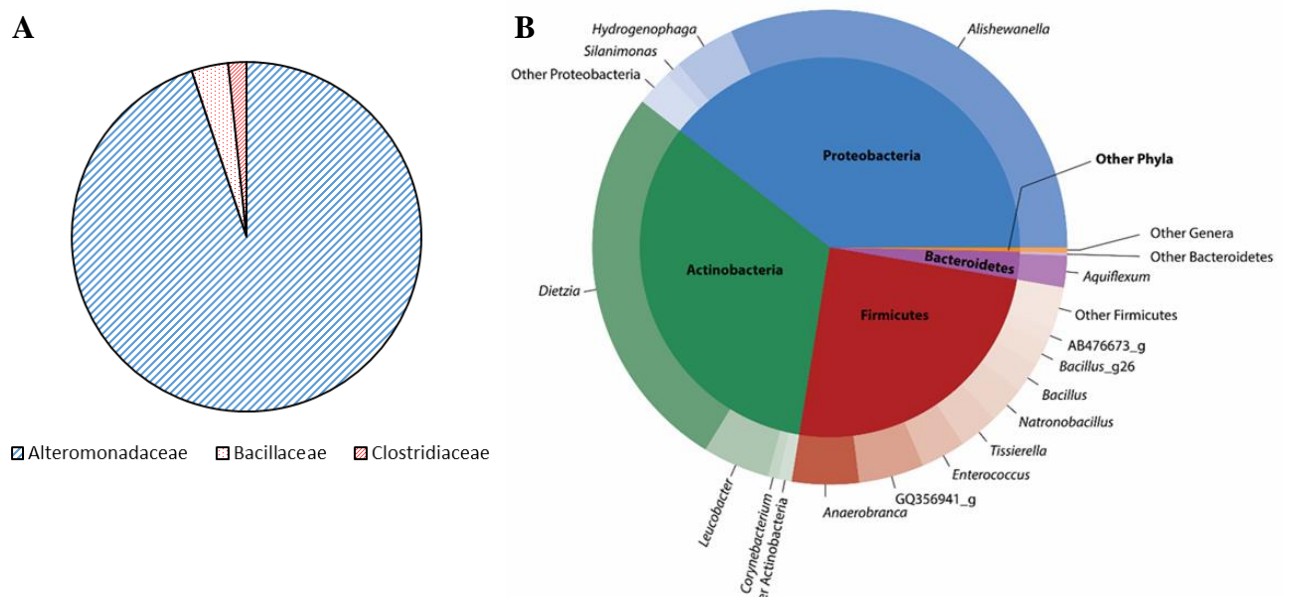


**Figure 6.5: 16S rRNA gene microbial community analysis of pH 11 microcosm.** The MiSeq approach identified a greater number of bacterial lineages offering a greater resolution into the microbial community. The MiSeq approach showed the flocs to be dominated by Actinobacteria, Firmicutes and Proteobacteria. [A] Cloning and sequencing library. [B] MiSeq library.

The microbial community contained a large component of microbes related to bacteria which have previously been associated with alkaline conditions. *Alishewanella* formed a large component of the population. This facultative anaerobic genus is most commonly associated with fermented seafood (271), but has also been isolated from landfill soils (272). Its ability to grow in alkaline conditions up to pH 12 has also been reported (272). Similarly *Dietzia* have been reported in a range of hyperalkaline areas and possess the ability to degrade a range of carbohydrates and pollutants (273, 274). As per the microbial community of the colonised cotton (used as an inoculation source for the microcosm), the microcosm contained a large component of bacteria from the Firmicutes. A number of the Firmicutes detected here have been previously associated with alkaline conditions (40, 264, 265) with ISA degrading

microcosms operating at pH 9.5 and pH 11 as reported by Kyeremeh *et al* (84) and Rout *et al* (80) to also contain similar large Firmicute based components. The diverse metabolic range of the identified bacteria specifically the ability to utilise a range of carbon sources appears to have enhanced the ability of the bacteria to thrive within the CDP driven microcosm.

The rarefaction curve (Figure 6.6A) showed that the MiSeq sampling depth was not sufficient to capture all known species; however the high Goods Coverage showed 95 % of species were identified through the sampling. Combining the Goods Coverage with the rank abundance curve (Figure 6.6B) which shows a classic diverse microbial community distribution as described by Hughes *et al* (226) indicates that the dominant species within the community were identified and only rare low abundance species were left to find. The Chao1 and ACE values reflect this suggesting the last 5% of species to be found would be very low abundance to attain the values reported. The Shannon diversity index demonstrated a surprising degree of diversity despite the harsh conditions within the microcosm with index values higher than those associated with human skin flora (275) and similar to biofilms developed formed from circumneutral floodplains and stream communities under laminar and turbulent flows (276). Although diverse the Shannon index values reported here are lower than those reported by Niederdorfer *et al* (276) for aggregate based communities under circumneutral conditions.

Technique	Valid reads	OTUs	Ace	Chao1	Shannon	Goods Lib. Coverage
Cloning and sequencing	59	9	49.46	14.00	1.44	0.92
MiSeq platform	18854	1430	8521.47	6058.86	4.18	0.95

**Table 6.4: Alpha diversity statistics of pH 11 microcosm.** The MiSeq approach with a greater number of valid reads showed a higher resolution into the microbial community with larger numbers of OTU's detected and higher Shannon index values.

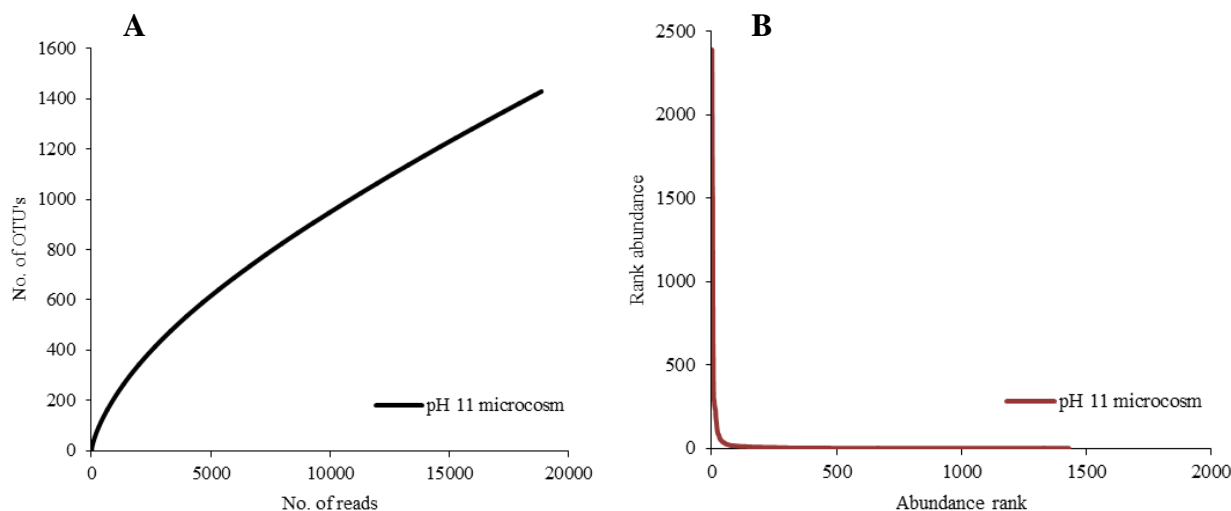


**Figure 6.6: Rarefaction and Rank abundance curves for pH 11 microcosm via MiSeq approach.** [A] The rarefaction curve showed sampling did not reach saturation with regard to OTU detection. [B] Rank abundance curves reflected a diverse microbial community.

### 6.2.3 Properties of polymicrobial flocs

Microscopy based investigations (Figure 6.7) into the morphology of the microbes within the pH 11 microcosm revealed the cells to be existing as aggregate based or ‘floc’ cultures. The microbial flocs were composed of an EPS containing polysaccharides and eDNA. Polysaccharides are a common component of EPS and moderate a range of bacterial biofilm properties including adhesion, cell aggregation, cohesive nature, protection as well as the sorption of organic compounds and inorganic ions (85). Imaging of the polysaccharide component revealed its distribution throughout the floc with large globular like structures (Figure 6.7). DNase treatment caused the loss of these structures resulting in a less compact structure of cells associated with polysaccharide, indicating a relationship between the eDNA and the distribution of the polysaccharide components (Figure 6.7A & B). The role of eDNA within biofilms appears to serve a number of functions (277), in this case it is likely to aid the structure and function of the floc community (278). The presence of eDNA within the floc structure is also likely to act as a phosphate store for the constituent microbial consortia (279). Calcium ions are abundant at the site and within the microcosm, as such the interaction between eDNA and these ions is likely to promote cell aggregation and biofilm formation (102). This is illustrated by the fact that treatment of the flocculates with DNase resulted in the loss of floc stability (Figure 6.7). Further investigations using SEM showed individual flocs to be clusters of cells, polymeric substance and crystalline precipitates (Figure 6.7D).

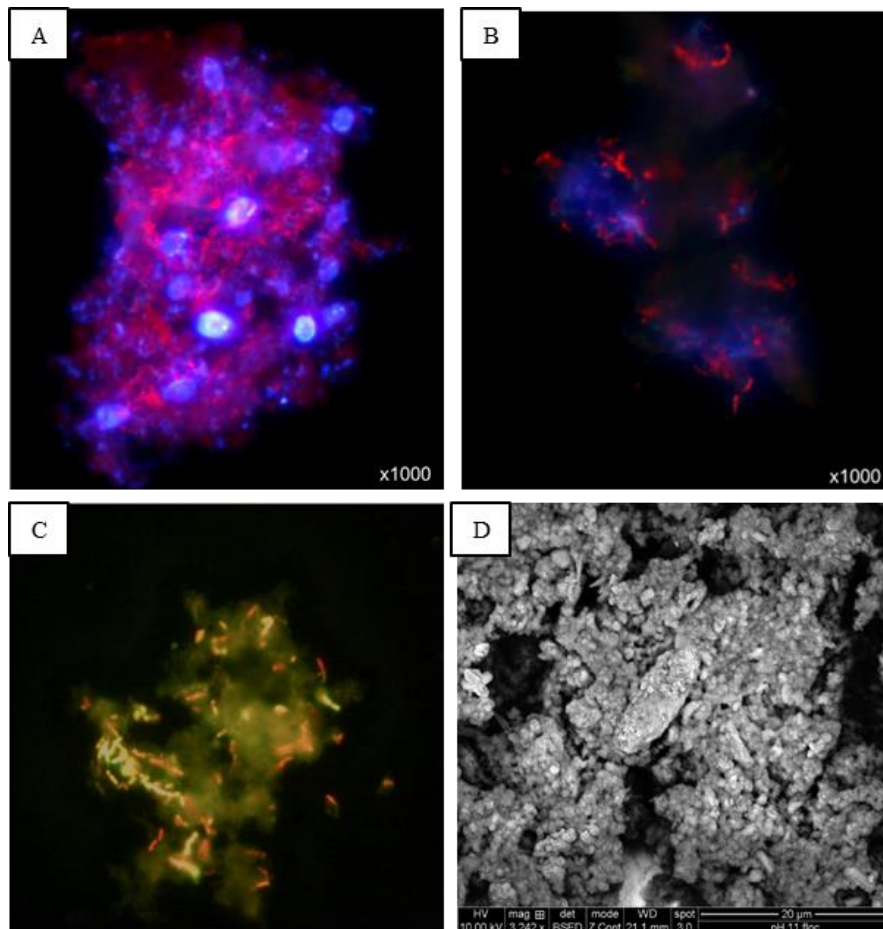


**Figure 6.7: Microscopy investigation into the morphology of the pH 11 microcosm.** [A] Ethidium bromide and Calcofluor white stain of bacterial floc showing individual cells and eDNA (red) and extracellular polysaccharides (blue). [B] DNase digestion of flocs caused them to lose structural integrity. [C] Live/dead image of bacterial flocculate (green = alive cells, red = dead cells). [D] SEM image of flocs shows areas of possible mineral precipitate.

Investigations into the microcosm carbon flow (Table 6.5) highlighted the importance of EPS generation within the system by the fact that >60 % of the available carbon was diverted to EPS formation, a finding similar to the carbon distribution in biofilm systems reported by Jahn and Nielsen (280). The concentration of the polymicrobial flocs was determined via flowcytometric methods as  $1.71 \times 10^6 \pm 8.73 \times 10^4$  per mL of microcosm fluid with 54.4 % of the flocs being >10  $\mu\text{m}$  in diameter reaching a maximum size of 240  $\mu\text{m}$  (Figure 6.8).

Component	mg C	(% ISA C)
ISA degraded	84.00	100.00
VFA produced	19.92	23.71
Associated carbonate	10.13	12.06
Biomass change	0.44	0.53
Remaining (EPS)	53.51	63.70

**Table 6.5: Carbon distribution of pH 11 microcosm.** A large portion of available carbon was diverted towards EPS production indicating its importance towards microbial survival.

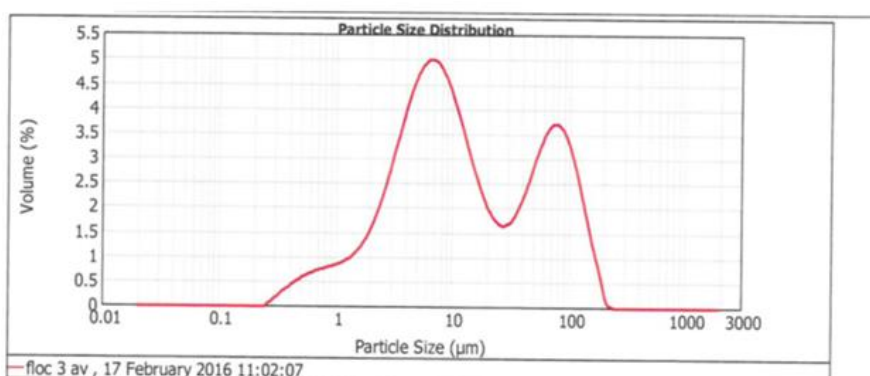


**Figure 6.8: Size distribution of polymicrobial flocs within pH 11 microcosm.** The size distribution curves shows two major peaks one most likely associated with debris, dead cells and smaller aggregates and a second which is associated with the flocs, as seen via microscopy investigations.

CLSM investigations improved upon fluorescence work and revealed the flocs to be composed of a complex mixture of proteins, carbohydrates, lipids, eDNA and cells (Figure 6.9). Imaging of the protein component of the flocs showed large concentrated areas of protein within the flocs (Figure 6.7). Protein serves a wide range of functions within biofilms including the protection from environmental conditions, enzymatic reactions and sorption of organic compounds and inorganic ions (92). The most basal layer of the floc was composed primarily of lipids and  $\beta$ -1,4 and  $\beta$ -1,3 polysaccharides, where the most outer layers of the floc were composed of concentrated areas of proteins, these regions were surrounded by  $\alpha$ -mannopyranosyl and  $\alpha$ -glucopyranosyl sugars which were also closely associated with eDNA. These regions of pyranosyl sugars and eDNA surrounded the crystalline precipitates observed under SEM (Figure 6.7), with similar findings in the EPS of *Aeromonas hydrophila* (281).

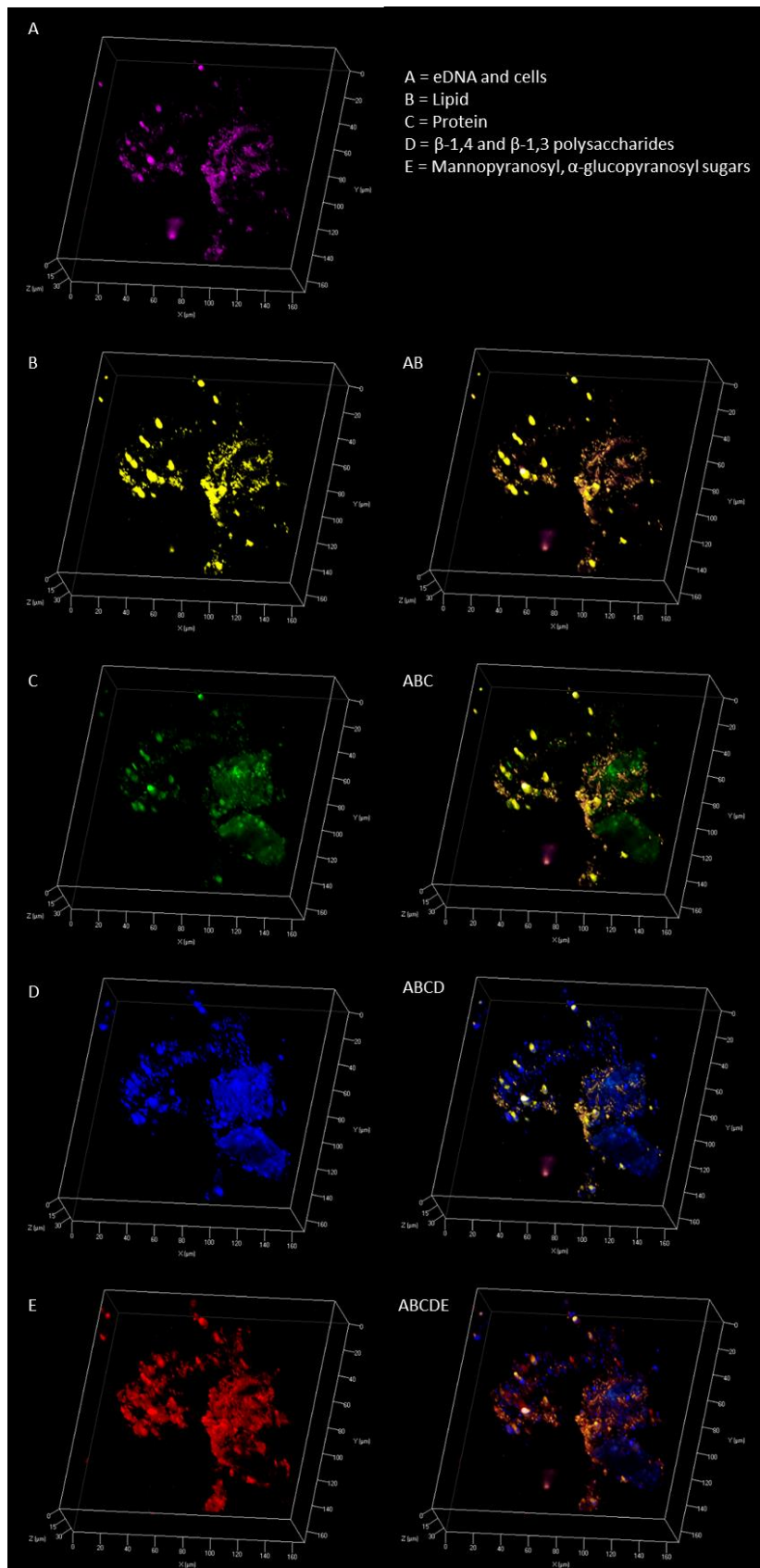


**Figure 6.9: CLSM investigation of polymicrobial floc from pH 11 microcosm.** The EPS had a complex composition of all components tested for with large areas of protein and polysaccharides.

Localisation of bacteria and archaea within the flocs via FISH revealed most cells to be located within the centre of the flocs with larger numbers of bacteria compared to archaea (Figure 6.10). Bacteria rather than archaea populated the areas towards the floc surface, similar to the distributions seen in granular sludge (127). The numbers of bacteria decreased with distance from the central core which could indicate the presence of a niche microsite within the central core where conditions may be more favourable for growth.

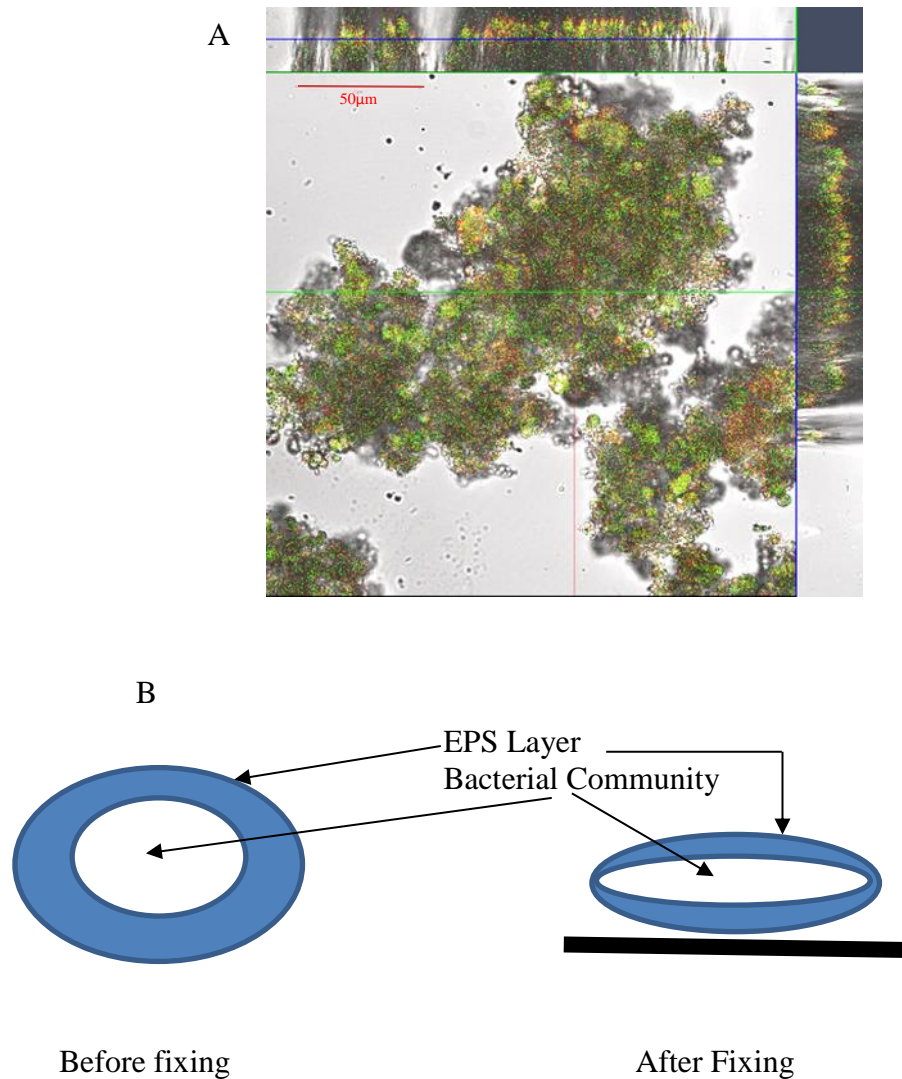


**Figure 6.10: Archaeal and bacterial FISH investigation of flocs.** [A] Bacteria (green) and archaea (red) distribution given with sections through the x and y plane. Both bacteria and archaea appear to be clustered towards the centre of the floc. [B] Fixing of the flocs causes compression of both the EPS layer and bacterial community deforming the image.

From the microbial community analysis of the flocs (Figure 6.5) the three most dominant components *Alishewanella*, *Dietzia* and Clostridia were investigated via FISH to view their spatial distribution within the flocs (Figure 6.11). *Alishewanella* and *Dietzia* were found to occur together within the EPS possibly indicating a synergistic relationship with both capable of biofilm formation (271, 282). The Clostridia were shown to be wide spread throughout the EPS and is most likely a reflection of the phyla not being dominated by one individual species as per the Actinobacteria and Proteobacteria.

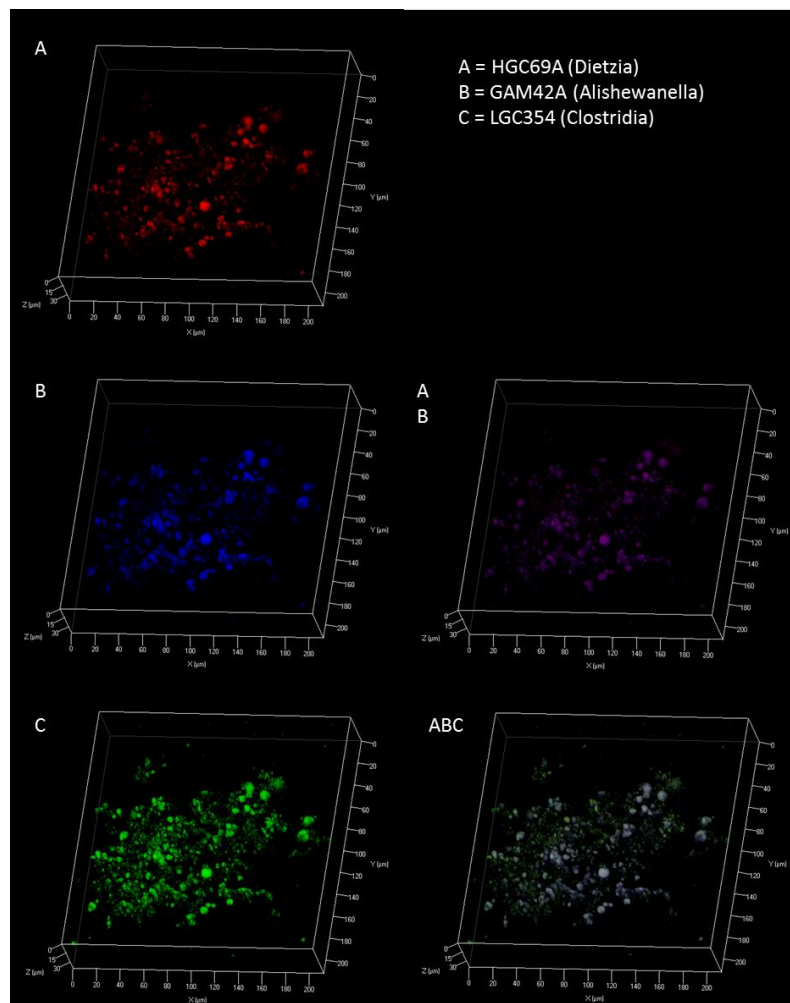


**Figure 6.11: FISH investigation showing spatial distribution of *Alishewanella*, *Dietzia* and Clostridia within polymicrobial flocs. *Alishewanella* and *Dietzia* appeared to co-exist together indicating a possible syntrophic relationship whereas the Clostridia were widely distributed.**

The EPS extracted from the flocs was composed mainly of carbohydrates with smaller fractions of lipids, eDNA and protein (Figure 6.12). The treatment of the flocs with EDTA which acts to chelate metal ions liberated significantly more EPS than sonication and ethanol treatment further indicating a role of calcium in floc formation and stability. Further analysis

of the EPS via FTIR (Figure 6.13) corroborated these findings of a complex EPS composition. A large peak indicative of carbonyl groups was reported between  $1800\text{ cm}^{-1}$  to  $1660\text{ cm}^{-1}$  and a broad peak across the  $3400\text{ cm}^{-1}$  to  $2400\text{ cm}^{-1}$  region showed the presence of carboxylic acids, lipids and amide groups (281, 283). A large absorption peak at  $1392\text{ cm}^{-1}$  further corresponded to the symmetric stretching vibrations of the  $\text{COO}^-$  group in carboxylate anions (281). Spectral regions of  $1,650\text{ cm}^{-1}$  and  $1,540\text{ cm}^{-1}$  showed the presence of protein secondary structure (284) with peaks around  $1323\text{ cm}^{-1}$  showing the C–N stretching vibration of proteins. A large peak at  $1057\text{ cm}^{-1}$  could be attributed to C–O stretching vibration modes of alcohols (281) with peaks between  $1300\text{ cm}^{-1}$  and  $900\text{ cm}^{-1}$  attributed to C—O—C, ring-stretching vibrations and the P=O stretch of phosphodiester (285). Below  $900\text{ cm}^{-1}$  P-O-C, P-O-P stretching and C-O-C, P-O-C bonding gave a variety of peaks relating to phospholipids, ribose-phosphate chain pyrophosphate and aromatics (286). The analysis of the EPS via FTIR revealed a wide variety of functional groups including carboxyl, amine and phosphoric groups which under the alkaline pH could contribute a negative charge to the EPS due to the deprotonation of these groups (287). This negative charge could favourably bind cation species such as calcium to the EPS assisting in the formation and stability of the flocs (288) and could explain the high inorganic ash content of the flocs (Table 6.6).

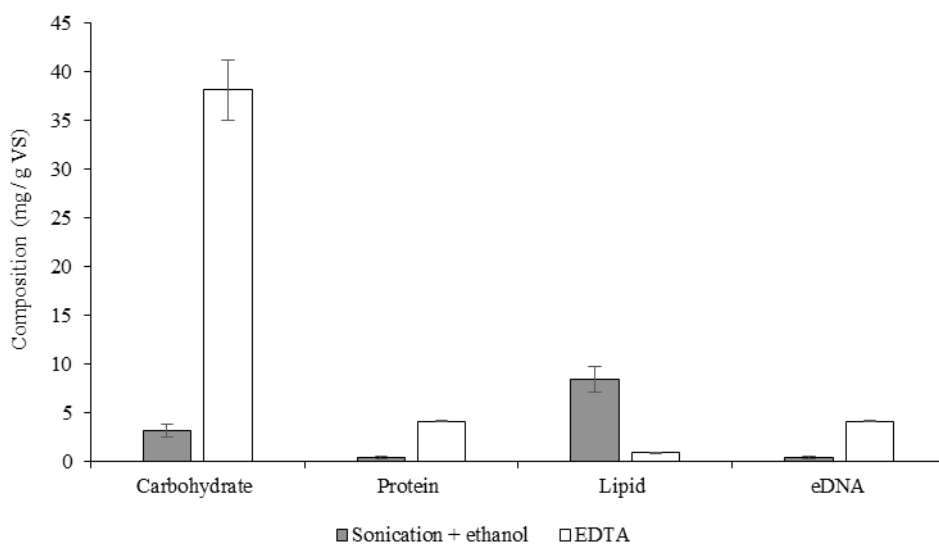


**Figure 6.12: Composition of extracted polymicrobial floc EPS.** Treatment with EDTA yielded the greatest amounts of carbohydrate, eDNA and protein compared to the ethanol treatment indicating ionic interactions between the EPS components possibly related to  $\text{Ca}^{2+}$ . More lipid was extracted by the ethanol treatment due to disruption of hydrophobic interactions.

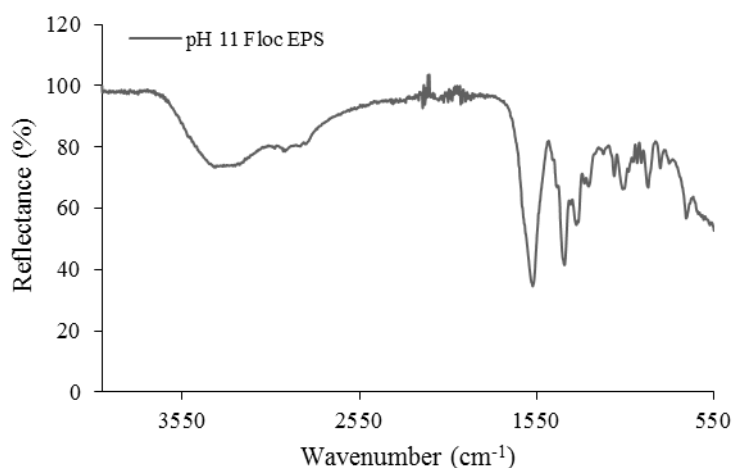
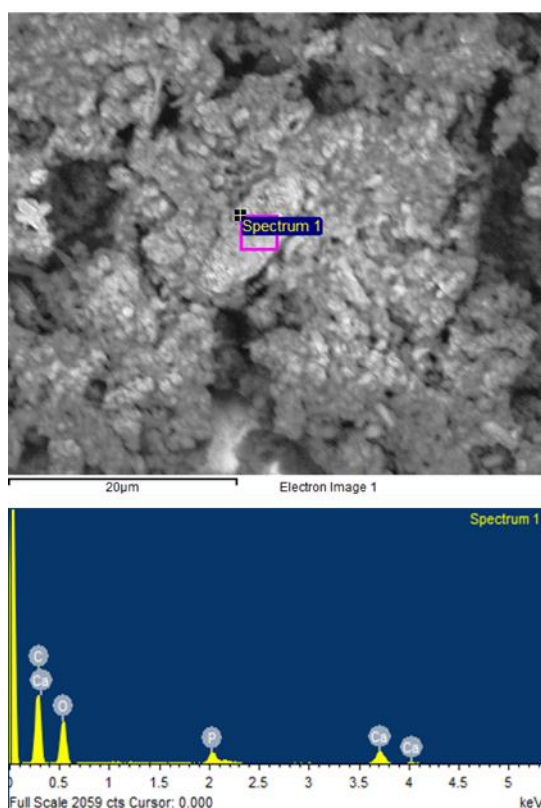


**Figure 6.13: FTIR of polymicrobial floc EPS.** A wide range of function groups were detected via FTIR reflecting the complex composition of the EPS identified via chemical and microscopic methods.

Floc dry weight (%)	Dry weight volatile solids (%)	Dry weight ash content (%)	Dry weight per L (g DW L <sup>-1</sup> )	Volatile solids per L (g VS L <sup>-1</sup> )
1.56	44.46	55.54	15.54	6.91

**Table 6.6: Dry weight, volatile solids and ash content of polymicrobial flocs.** The flocs had a large inorganic content possibly due to the binding of calcium to the EPS components.

SEM investigations into the morphology of the flocs showed crystalline areas within the EPS materials. Subsequent analysis of these areas (Figure 6.14) via EDS revealed them to be composed elementally of calcium, carbon and oxygen indicating calcium carbonate precipitation. The ability of microbes to link microbial metabolism and the precipitation of calcite has been shown in the lithification processes of microbial mats (138) and could have an potential impact upon radionuclide migration as uranium has been shown to co-precipitate with calcite (139).



Element	(%) Weight
C	41.2
O	37.7
Ca	16.3
P	4.8

**Figure 6.14: Elemental composition of EPS based crystalline precipitate.** The area analysed was mainly composed calcium, carbon and oxygen indicating calcium carbonate precipitation.

The calcium content of the liquid component of the floc microcosm was  $1.6 \text{ g L}^{-1}$  which was lower than that of the abiotic comparison which measured  $4.3 \text{ g L}^{-1}$ . Investigation into the calcium binding capacity of dialysed EPS (Figure 6.15) indicated that the EPS was able to bind  $0.173 \text{ mg calcium per mg of EPS}$ . Analysis of the dialysed EPS materials showed a total of  $0.203 \text{ mg of calcium per mg of EPS}$  was still bound even after the extraction procedure which gave the floc EPS a total calcium binding capacity of  $0.376 \text{ mg calcium per mg of EPS}$ .

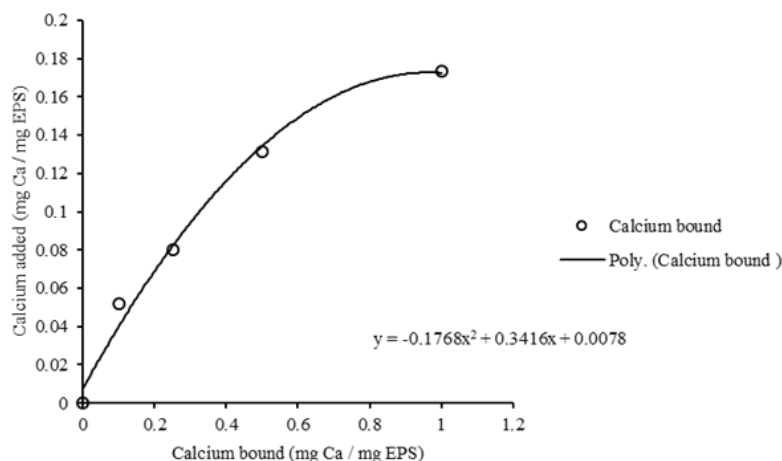


**Figure 6.15: Polymicrobial floc EPS calcium binding curve.** EPS was able to bind calcium from solution reinforcing the importance of calcium EPS interactions in biofilm formation and stability.

The calcium binding assay undertaken here (Figure 6.15) showed the ability of the dialysed EPS to bind calcium from solution to be similar to that found in EPS produced by *D. autotrophicum* of 0.15 mg calcium per mg EPS and a *Desulfovibrio sp.* of 0.12 mg calcium per mg EPS (244). Investigations using atomic absorption spectroscopy revealed a portion of calcium to be still bound to the EPS even after dialysis with the total calcium bound by the EPS similar but lower than that reported for the EPS of a hypersaline non-lithifying microbial mat of between 0.60 and 0.66 mg calcium per mg EPS (289). The ability of the EPS components to bind calcium appears to greatly facilitate the formation of flocs and biofilm, with the addition of calcium also shown to increase sludge granulation in a USAB reactor (Yu et al., 2001). Analysis via FTIR revealed a range of functional groups with the potential to interact with cations under alkaline conditions (244, 289). eDNA within the floc EPS is capable of interacting with calcium cations in a thermodynamically favourable manner and has been shown to assist in bacterial aggregation through acid-base interactions and cationic bridging (102).

#### 6.2.4 Survival of microorganisms within polymicrobial flocs.

Subcultures (see Section 5.9.2 for details) showed the ability of the flocs to grow at pH 11.0 and pH 11.5 and survive at pH 12 (Figure 6.16). At pH 13 the flocs were able to maintain detectable ATP levels for two weeks after which no ATP could be detected. Optimal cell growth was reported at pH 11.0 and no increase in ATP values were reported from control microcosms. The ability of this survival was attributed to protection offered by the

encapsulation of the cells within EPS possibly forming a lower pH niche microsite. Using micro-electrodes, the pH profiles through the flocs were able to be investigated. In their cultured state at pH 11, the flocs had an internal pH of 10.4 with subsequent subculturing forcing this internal pH value to rise as the external pH rose (Figure 6.17). Zeta potential measurements (Figure 6.18) indicated that floc formation was favoured at pH values close to the internal pH of the flocs (pH 10-11) with floc formation likely maintained across all the pH values tested due to the tight binding of calcium to the EPS. Survival of the flocs was observed at pH 11.5, with a reduced biomass compared to pH 11.0 and is likely associated with more energy being diverted into the maintenance of the internal floc pH, which had an approximate value of pH 10.7. The subculturing of flocs at pH 12.0 resulted in the loss of biomass, whilst the flocs remained stable as determined via zeta potential work and microscopy analysis (Figure 6.19). At pH 12.0 the internal floc pH rose to pH 11.6 and suggests that only the most alkaliphilic microorganisms were present with a large portion of the energetic process likely used to maintain the internal floc pH and cytoplasmic pH homeostasis (47, 48). Although the shift in pH may only have been 0.4 – 0.8 units, at these extremes of pH the differential in hydroxyl ion concentration between the internal and external floc surfaces was substantial (between 0.25 to 4.0 mM).

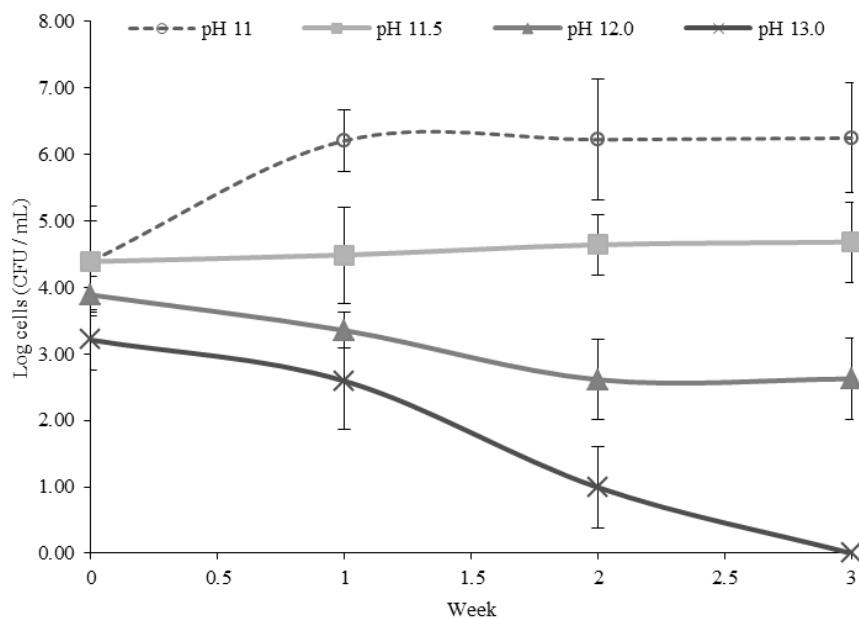


**Figure 6.16: pH survival curves of polymicrobial flocs.** The ability of the flocs to survive decreased as the external pH increased. Microbes within flocs were able to grow at pH 11.0 and pH 11.5 and survive at pH 12.0. At pH 13 microbes survived for a short period of up to 2 weeks before dying

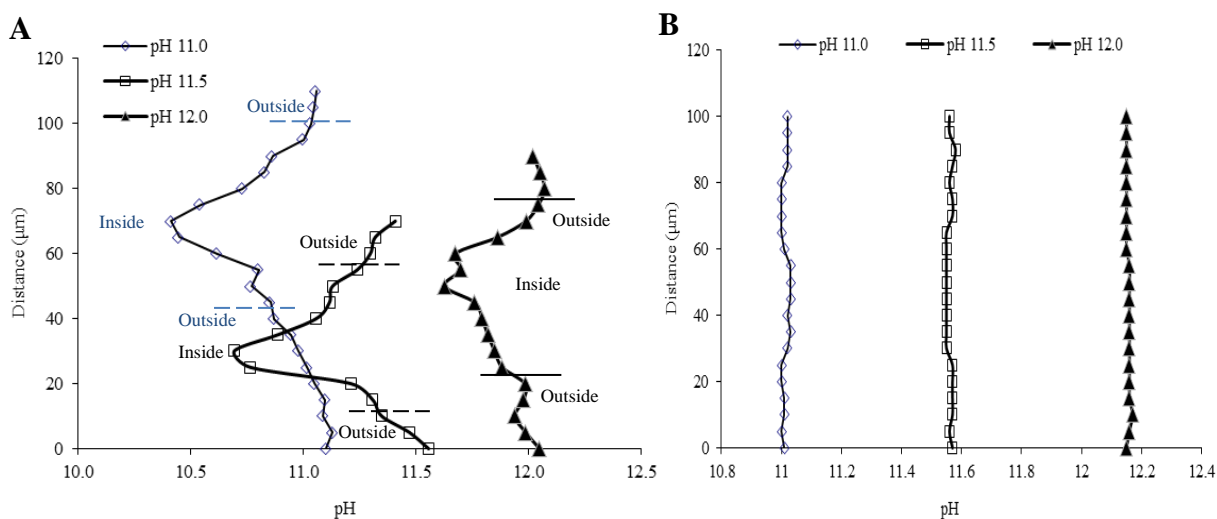


**Figure 6.17: pH profiles through polymicrobial flocs.** [A] Large pH drops within the interior of the floc were seen at both pH 11.0 and 11.5 with a lesser drop measured at pH 12.0. This lower pH site within the floc may contribute towards microbial survival. Lines and annotations show estimated boundaries of the flocs. [B] Controls through agar showed no major shifts in pH value.

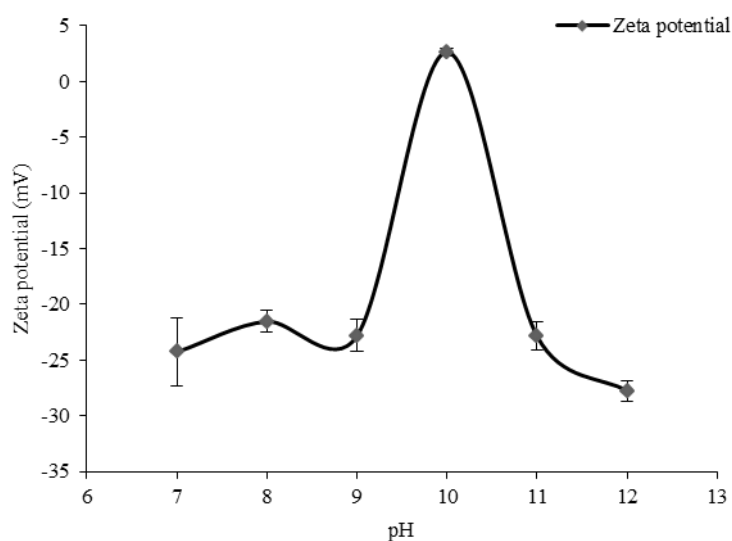


**Figure 6.18: Zeta potential measurements of polymicrobial flocs at different pH values.** The zeta potential showed the flocs favoured aggregation at all pH values tested and showed the strongest tendency to aggregate at pH 10. The ability to retain floc stability as the pH shifts may be linked to tightly bound calcium stabilising the EPS structure.

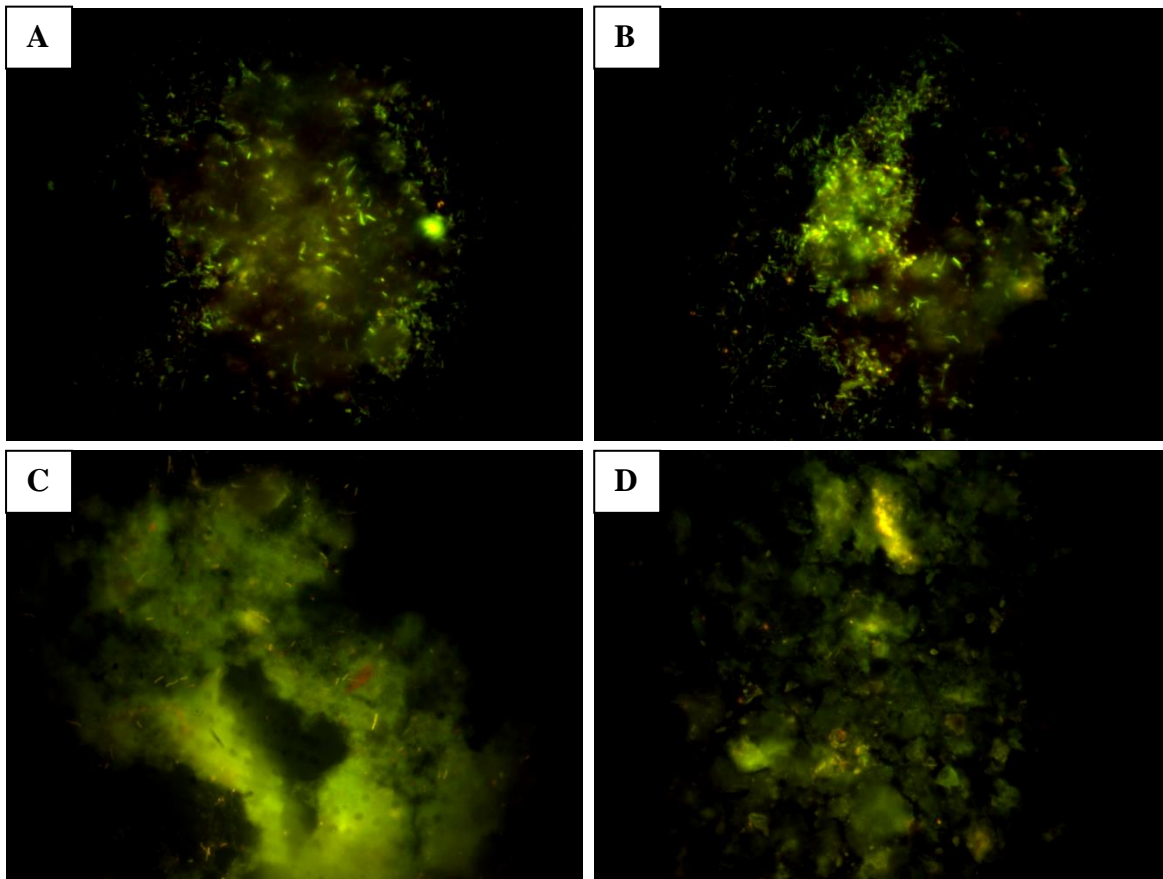


**Figure 6.19: Live/dead images of polymicrobial flocs after pH survival testing period.** The amount of visible live cells decreased as the external pH increased reflecting the ATP results. (green = live cells, red = dead cells). [A] pH 11. [B] pH 11.5. [C] pH 12.0. [D] pH 13.0.

The ability of microbes to modify the internal pH of the floc is not unique to these circumstances with pH shifts between 0.4 – 2 pH units reported in *Bacillus laevolacticus* aggregates (290) and a shift of 1 pH unit in glucose acclimatised methanogenic aggregates from an upflow anaerobic sludge blanket (USAB) (291). In these examples, however, aggregate size was larger than those reported here and profiles were taken under pH neutral conditions. Similar shifts in pH are also seen in biofilm communities with drops of up to 1.4 pH units across distances of up to 50  $\mu\text{M}$  measured in *Pseudomonas* sp. biofilms (292) with further pH shifts seen across a variety of distances in a range of biofilms grown under different conditions (293-295). This study is, however, the first to show such pH changes in EPS under hyperalkaline conditions.

The mechanism by which the pH gradient is generated within the floc could be attributed to various factors such as the fermentation of ISA to acetate and hydrogen (81), the degradation

of EPS materials (289) or through the properties of various EPS components (99). CLSM imaging of the flocs suggested that the core of the flocs was composed primarily of lipids (Figure 6.9). The ability of lipids to increase the internal hydrophobicity of the floc at this area would reduce the transport of hydroxide ions into the floc, mediating the impact of the external alkaline environment. Acidic phospholipids are associated with alkaliphilic bacterial membranes and may also buffer against the external pH if incorporated into the EPS matrix. The excretion of specific proteins into the biofilm with the purpose of modifying the local pH has been observed in acid mine drainage biofilms (99) and the large protein content could potentially help to lower the internal pH as well mediating a wide range of other biofilm properties (85). Extracted proteins from the floc EPS were investigated towards this purpose using an isoelectric focussing approach to ascertain the isoelectric points of the extracted proteins (Figure 6.20). Unfortunately the technique failed to yield usable data due to suspected issues with protein solubility and possible DNA and carbohydrate based contaminants. The presence of uronic acids within bacterial extracellular polysaccharides has the potential to increase the acidity of EPS (296) and as such the monomer composition of the floc EPS was investigated (Table 6.7). The monomer composition, however only showed a low composition of uronic acids (4.3 %) with half the monomers dominated by mannose. Ribose and ribitol made up a further 20% and a varied range of sugars were identified in smaller amounts with the monomer composition similar to hyperalkaline biofilms harvested from calcite surfaces (297).

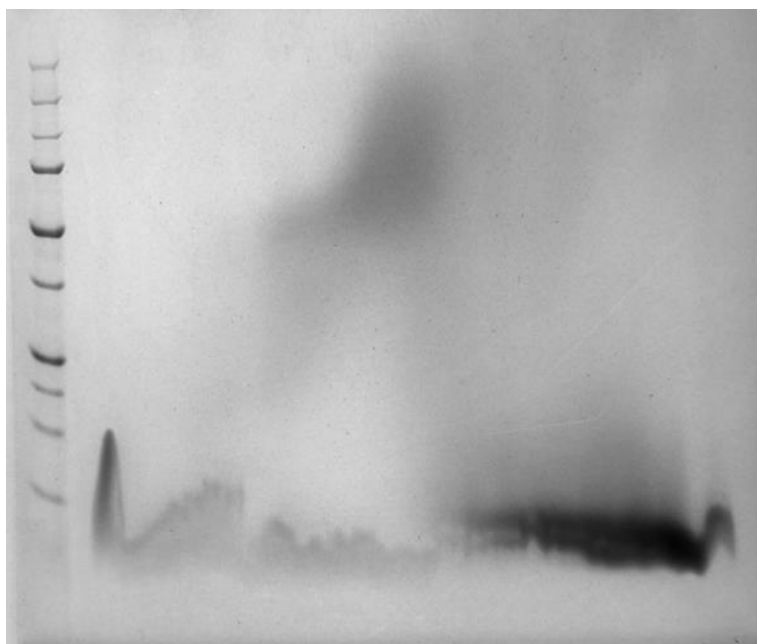


**Figure 6.20: Isoelectric focussing gel of extracted protein from polymicrobial flocculent EPS.** The technique failed to yield usable data due to issues with protein aggregation and possible contamination with DNA and carbohydrate component for which no solution could be found during the period of study.

Monomer unit	Composition (%)
Mannose	50.53
Ribose	9.89
Ribitol	9.73
Arabinose	5.71
Rhamnose	5.07
Galactose	4.45
Trehalose	4.45
Glucuronic	3.51
Xylose	2.91
Fucose	2.00
Glucose	0.99
Galacturonic	0.76

**Table 6.7: Monomer composition of polymicrobial flocculent EPS.** Monomers were mannose dominated and possessed a small total uronic acid fraction. The complex composition of the monomers may reflect the diverse microbial community present within the flocculent.

### 6.3 Conclusion

Using a cotton bait, biofilm was able to be cultured in-situ at the Buxton anthropogenic analogue site. The biofilm formed upon the cotton was dominated by Clostridia with the remaining microbial population containing a broad mix of bacterial species many related to previously described alkaliphilic species. The microbial consortia also contained an archaeal component which was dominated by hydrogenotrophic methanogens. ISA was found to be generated in-situ from the cellulose cotton with the generation of acetate and reduced conditions indicating active microbial metabolism despite the external pH value. A fermentative/methanogenic microcosm formed from the biofilm was able to demonstrate the degradation of all forms of ISA through a fermentation pathway with acetate and hydrogen as the end products. Investigations into the morphology of the microorganisms within the microcosm revealed cells to be existing in flocs or aggregates of EPS. Microscopy investigation of these flocs revealed them to be complex in composition consisting of eDNA, lipids, polysaccharides and protein. Enzymatic degradation of the eDNA component caused the flocs to lose structural integrity most likely due to a loss in calcium-eDNA interactions. The flocs were found to have a large inorganic component with elemental analysis showing these inorganic precipitates to be composed primarily of calcium, carbon and oxygen. Further work showed the ability of EPS extracted from the flocs to bind a large portion of its weight as calcium indicating a prevalent role of calcium in the facilitation of cell aggregation and biofilm formation (in this case as flocs). Localisation of microbes within the flocs via FISH showed most cells to be clustered with the central mass of the flocs with pH profiling showing this area to have a lower pH than the external value. It is likely that a combination of the properties of the EPS and microbial metabolism help to generate this microsite, with the formation of flocs facilitating long term microbial survival up to pH 12. The ability for flocs to survive short term (2 week) exposure to pH values of pH 13 may allow microbes in flocs to find lower pH niche areas with an ILW-GDF in which to colonise. Flocs may impact the long term performance of an ILW-GDF through the removal of radionuclide complexants such as ISA and allow biofilms to form, with the consequences of this discussed in Chapter 7.

The microbial community of the flocs was surprisingly diverse with a moderate component of low abundance mixed microbial species and was dominated by bacteria of the *Alishewanella*, *Dietzia* and Firmicutes lineages. The diversity of the flocs indicates that areas around an ILW-GDF within the alkaline disturbed zone could act as source of diverse alkaliphilic microbes with the potential to colonise and survive under the hyperalkaline conditions expected.

## 6.4 Key findings

- Biofilm is capable of forming upon cotton under hyperalkaline conditions in-situ at an anthropogenic analogue site for an ILW-GDF. The biofilm formed consisted of a mixed bacterial component which was dominated by Clostridia and an archaeal component that was dominated by hydrogenotrophic methanogens.
- Microcosms formed from colonised cotton were able to demonstrate the degradation of all forms of ISA at pH 11 with the generation of acetate and hydrogen as the end products.
- Polymicrobial flocs formed within this microcosm possessed a level of microbial diversity with a complex EPS composition. The formation of lower pH niche microsites within these flocs likely contributed to their survival under hyperalkaline conditions.
- The presence of calcium appears to facilitate cell aggregation and floc formation with probable crystals of calcium carbonate forming within the EPS of flocs. The ability of microbes to survive hyperalkaline conditions and precipitate calcium carbonate could have an impact upon the long term performance of an ILW-GDF.

The work presented here contributed to the following publications:

- **C. Charles, S. Rout, E. Garratt, K. Patel, A. Laws, P. Humphreys, (2015), The enrichment of an alkaliphilic biofilm consortia capable of the anaerobic degradation of isosaccharinic acid from cellulosic materials incubated within an anthropogenic, hyperalkaline environment. *FEMS Microbiology Ecology*, 91, 1574-6941.**

Here I contributed to the experimental design, data acquisition/analysis and manuscript preparation. S. Rout assisted with experimental design and manuscript preparation. E. Garratt and K. Patel assisted with data acquisition and A. Laws and P. Humphreys assisted with manuscript preparation.

- **C. Charles, S. Rout, K. Patel, S. Akbar, A. Laws, B. Jackson, S. Boxall, P. Humphreys, (2017), Floc formation reduces the pH stress experienced by microorganisms living in alkaline environments. *Applied and environmental microbiology*.**

Here I contributed to the experimental design, data acquisition/analysis and manuscript preparation. S. Rout assisted with experimental design and manuscript preparation. S. Akbar and K. Patel assisted with data acquisition and A. Laws and P. Humphreys assisted with manuscript preparation. B. Jackson and S. Boxall assisted with CLSM imaging and processing.

## **7. Biofilm based systems**

## 7.1 Rationale

The aim of this chapter was to assess the ability of the floc based system described in Chapter 6 to form biofilm within silica sand columns and to ascertain the impact fixed biofilm formation would have upon ISA degradation and microbial survival under ILW-GDF conditions. Initial experiments aimed at forming biofilm under pH 11 methanogenic conditions with subsequent experiments taking fully formed biofilms and exposing them to higher pH values. It is likely that low pH niche microsites could form within the near field which could facilitate microbial survival. If biofilm were to form in these niche areas then it could have an impact upon the surrounding local chemistry. By fixing NRVB columns with steel and graphite surfaces downstream from biofilm cultures, the ability of biofilms to colonise and modify ILW-GDF relevant surfaces under near field conditions was assessed.

## 7.2 Results and discussion

### 7.2.1 Formation of biofilm and the associated degradation of ISA under ILW-GDF conditions

Using a recirculation based system (Diagram 5.3) the formation of a biofilm within the sand column using the pH 11 floc based microcosm (Chapter 6) was possible, with flocs forming visible aggregates within an hour of circulation (Figure 7.1). A main flow channel formed within the biofilm sand column around which most of the biomass formed. After a 4 week period the biofilm reached a visible steady state in which growth appeared equal to loss. SEM investigation of the sand column (Figure 7.2) demonstrated significant biofilm formation in between and upon sand grains with distinct areas of rough and smooth biofilm most likely related to differences in shear experienced within the column (298). Within the smoother areas of biofilm, cells of different morphologies could clearly be seen (Figure 7.2C). Further microscopy investigations into the composition of the biofilm using CLSM (Figure 7.3) revealed it to be composed of a complex mixture of eDNA, polysaccharides, protein and lipids in an almost uniform distribution with a bias towards mannopyranosyl and  $\alpha$ -glucopyranosyl containing polysaccharides over  $\beta$ -1,4 and  $\beta$ -1,3 linked polysaccharides (Figure 7.3C & D).



**Figure 7.1: Time lapse pictures showing formation of biofilm in sand column at pH 11.** The biofilm was formed under a recirculation system which was under a 14 day feed/waste cycle with CDP. Floccs aggregated quickly within the sand column to form a stable biofilm after 4 weeks. A main water channel formed within the column around which most of biofilm formed.

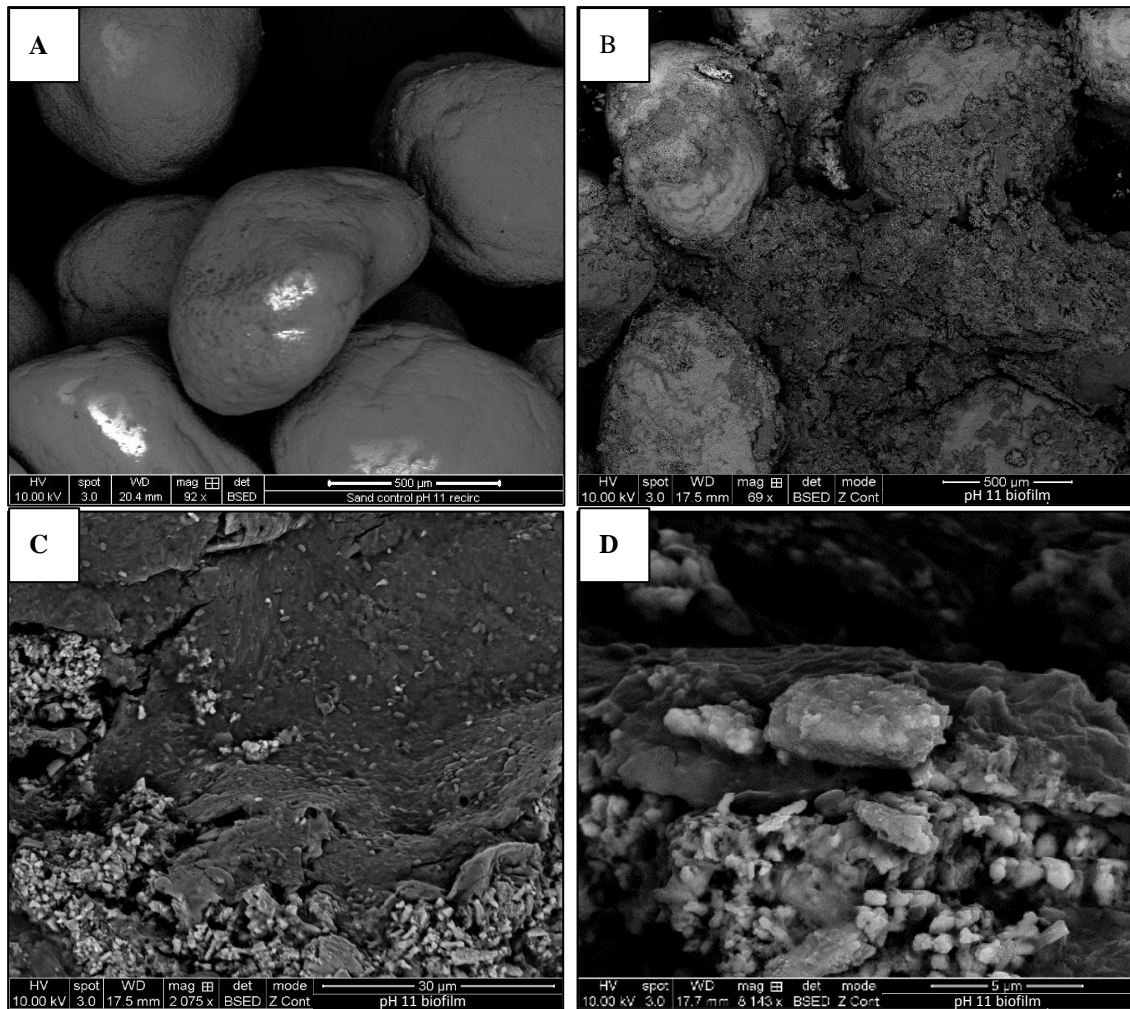


**Figure 7.2: SEM investigation into biofilm formed in sand column using recirculation system at pH 11. [A] Control sand column. [B] Biofilm can clearly be seen forming in between and upon sand grains. [C] Close up of the biofilm formed within sand column. Individual cells can be seen with both smooth and rough areas of biofilm. [D] A variety of cell morphologies can be seen within the biofilm.**

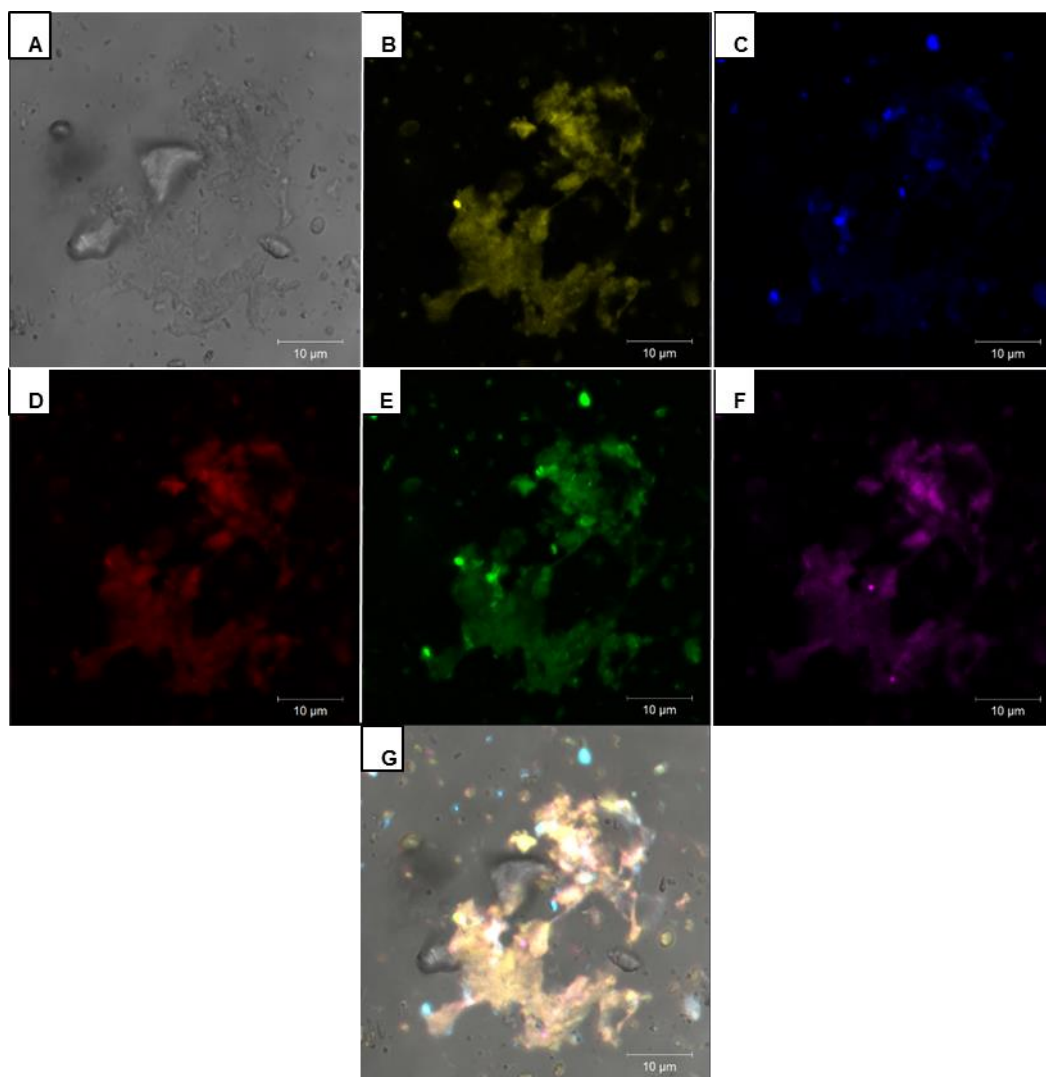


**Figure 7.3: CLSM images of biofilm formed in pH 11 sand column.** [A] Bright field image shows biofilm formed around small silica grain. The biofilm possessed a complex composition of EPS components including [B] Lipids, [C]  $\beta$ -1,4 and  $\beta$ -1,3 polysaccharides, [D] Mannopyranosyl,  $\alpha$ -glucopyranosyl, [E] Protein, [F] eDNA and cells. [G] Combined image.

The biofilm formed within the sand column was able to degrade all three forms of ISA, as determined by sampling of the liquid component of the recirculation system (Figure 7.4) with the first order rate constants of ISA degradation (Table 7.1) almost tenfold greater than those reported for the floc based system (Table 6.2). The rate constants reported for  $\alpha$ -ISA and  $\beta$ -ISA degradation are similar to those reported by Rout *et al* (80) in a pH 11 sediment based CDP driven microcosms of 0.17 and 0.11 day<sup>-1</sup> respectively. With the rate of ISA degradation greater than circumneutral communities forced to operate at pH 10 in liquid CDP driven microcosms (81). The degradation of ISA was through a fermentation pathway with methane

and hydrogen as the end products. Acetate was not detected within the system indicating that it was most likely immediately utilised possibly via syntrophic reactions between bacteria and methanogens within the system (120, 123). The level of hydrogen reduced within the headspace of the system after day 6 and was accompanied by a subsequent increase in methane. During this period levels of ISA were becoming depleted and could indicate that the hydrogenotrophic pathway was outpacing the acetotrophic pathway for methane production (154, 155). The TOC within the system decreased and was accompanied by an increase of IC indicating the production carbonate through fermentation of ISA. The small rise in IC only represented approximately 30 % of the total organic removed and is in line with the carbon flow of the floc based system (Chapter 6) and biofilms reported in sewer systems (280). Correspondingly only 4.1 % of the carbon supplied by degradation of ISA was converted to CH<sub>4</sub> again reflecting the large bias towards biomass development. The start and finish pH values are shown in Table 7.2 and confirm that the system remained alkaline throughout the testing period. A control system with a sterile sand column showed no signs of ISA degradation, gas production or major changes in pH or TOC/IC levels (Figure 7.4).

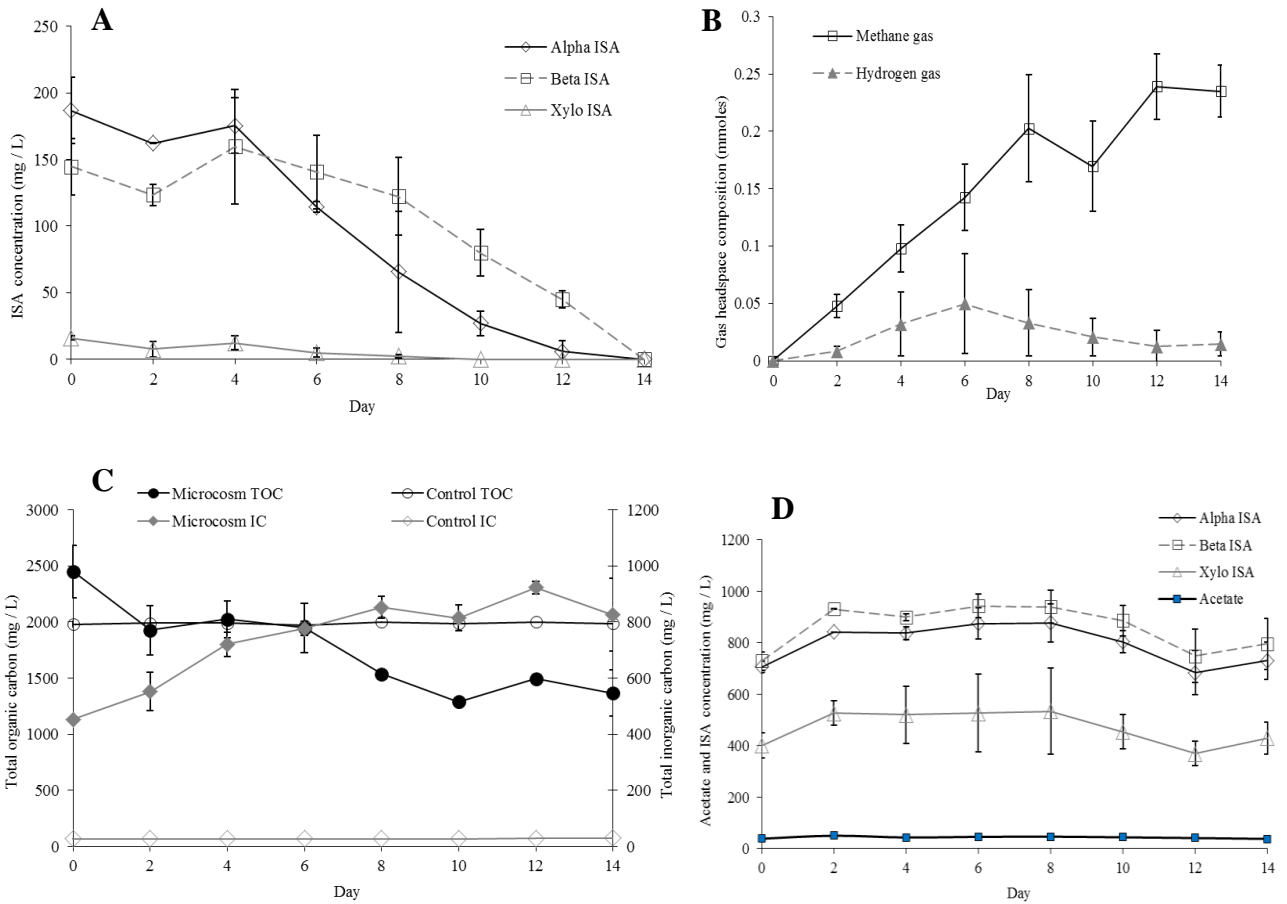


**Figure 7.4: Chemistry of pH 11 recirculation biofilm based system.** [A] The system was capable of the degradation  $\alpha$ -ISA,  $\beta$ -ISA and XISA. [B] Methane and hydrogen gas were produced as an end product from the degradation of ISA, hydrogen decreased after day 6 possibly due to hydrogen driven methanogenesis. [C] TOC correspondingly fell within the system and IC increased as ISA was degraded. Control systems showed no change. [D] Control systems also showed no evidence of ISA degradation.

	First order rate constant (day <sup>-1</sup> )					
	$\alpha$ -ISA	SE	$\beta$ -ISA	SE	XISA	SE
Recirculation system	0.203	0.021	0.098	0.000	0.251	0.064
Biofilm only	0.195	0.011	0.261	0.013	0.374	0.033
Liquid only	0.019	0.005	0.056	0.007	0.041	0.003

**Table 7.1: First order rate constants for the pH 11 biofilm based system.** The first order rate constants show that the biofilm component was the major site of the degradation of all forms of ISA. Biofilm only rates were calculated based on the average amount of ISA type removed at each 1.4 day period which equated to the passage of 100 mL of media through the system.

Biofilm recirculation system (pH)				Control system (pH)			
Start		Finish		Start		Finish	
Average	SE	Average	SE	Average	SE	Average	SE
11.0	0.00	10.6	0.04	11.03	0.00	11.01	0.00

**Table 7.2 : pH of recirculation biofilm based systems.** The pH of the recirculation system indicated it was still alkaline after the 14 day testing period.

As the recirculation system possessed both a liquid and a biofilm component, testing of these components individually of each other was required to ascertain the site of microbial activity. Testing of the biofilm component using a single pass system (Diagram 5.5) revealed the biofilm to be capable of the degradation of all three forms of ISA (Figure 7.5) with rate constants similar to the recirculation system (Diagram 5.3 & Table 7.1). The production of acetate and hydrogen and methane were detected as end products. The liquid only component was also able to degrade all three forms of ISA (Diagram 5.4 & Figure 7.6) however, showed an approximate tenfold reduction in the degradation rate constants for ISA (Table 7.1). The liquid component produced only hydrogen and methane as end products. The production of gas from the biofilm only component was lower than would be expected and was similar to the liquid only component. The absence of acetate within the liquid only component (Figure 7.6) may indicate the presence acetotrophic methanogens and the production of acetate from the biofilm only system (Figure 7.5) would suggest that methane production is primarily via the hydrogenotrophic pathway with the biofilm. Calculations by Bethke *et al* (38) suggest that methanogenesis driven via acetotrophic processes rather than hydrogen driven process are more thermodynamically favourable at elevated pH values. Hence if a pH microsite lower than that reported within the flocs (Figure 6.17) were present within biofilm then it could

favour hydrogen utilisation, especially given that double the amount of hydrogen compared to acetate can be produced from the fermentation of ISA (Equation 7.1).

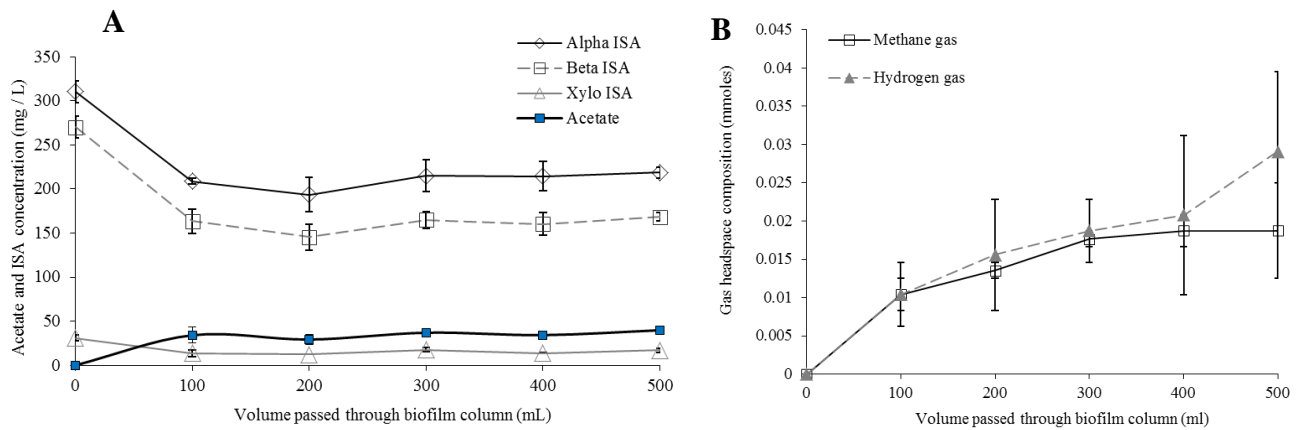


**Figure 7.5: Chemistry of biofilm only component of pH 11 recirculation system.** [A] Using a single pass system the biofilm was shown to degrade all three forms of ISA with the production of acetate as the sole VFA. Media was sampled at the Biocell outlet every 100 mL passed through the column (1.4 days). [B] Both methane and hydrogen gas were able to be produced driven by the degradation of ISA, with the concentration of both gases increasing the more ISA was delivered through the column.

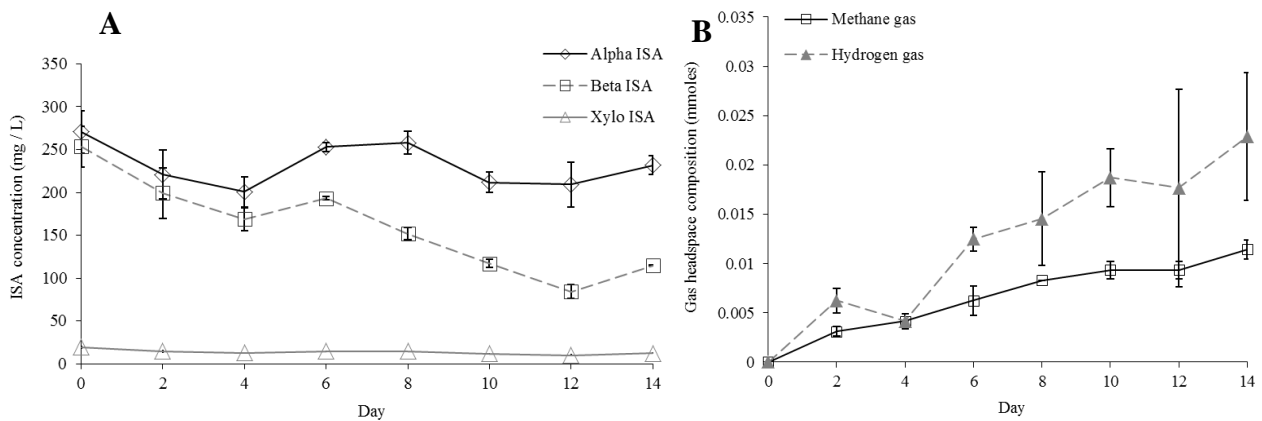
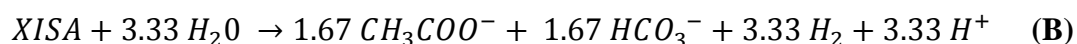
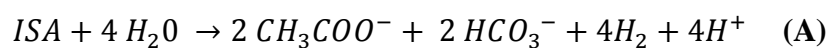


**Figure 7.6: Chemistry of the liquid only component of the pH 11 recirculation system.**

[A] Without a biofilm component the liquid component (which contained flocs produced from the biofilm) degraded mainly  $\beta$ -ISA. The liquid component showed small reductions in both  $\alpha$ -ISA and XISA, with ISA degradation on the whole operating at a much slower rate. [B] Both methane and hydrogen were able to be produced in a similar amount to the biofilm and could indicate acetotrophic methane production as no acetate was detected within the liquid only system.



**Equation 7.1: The fermentation of ISA to acetate.** [A] The fermentation of  $\alpha$ -ISA and  $\beta$ -ISA to acetate and hydrogen. [B] The fermentation of XISA to acetate and hydrogen.

Analysis of the morphology of the liquid component of the recirculation system revealed the cells to be existing within aggregates of EPS, with CLSM of these aggregate or flocs showing a similar composition to the biofilm from which they originated (Figure 7.7). This could indicate that sloughing of the biofilm was liberating a portion of biofilm material. In the context of an ILW-GDF this could allow biofilm in a micro niche to potentially seed other areas of an ILW-GDF.

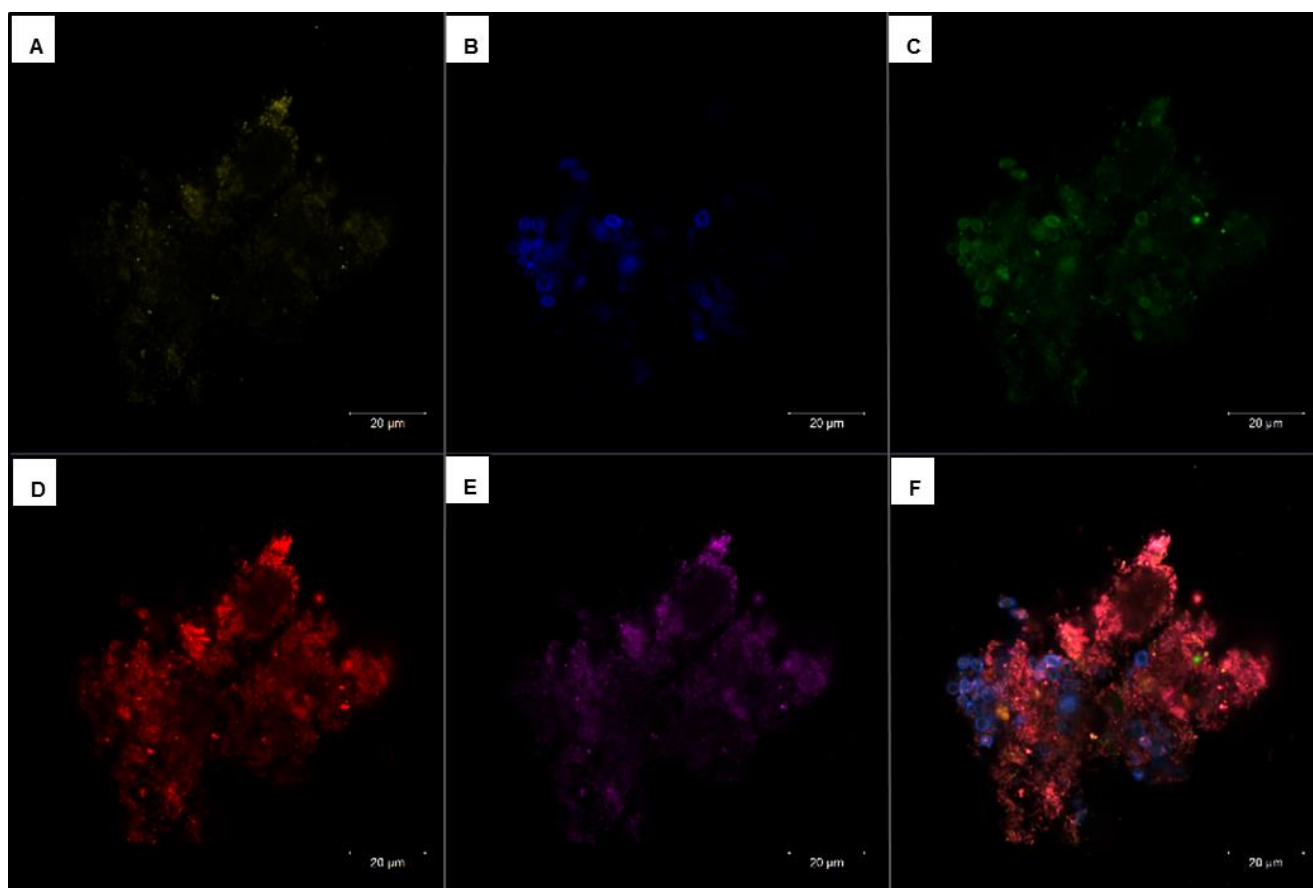


**Figure 7.7: CLSM investigation of EPS aggregates originating from biofilm.** The EPS aggregate or floc was composed of a complex mixture of EPS components including [A] Lipid, [B]  $\beta$ -1,4 and  $\beta$ -1,3 polysaccharides, [C] protein, [D] mannopyranosyl,  $\alpha$ -glucopyranosyl, glucopyranosyl, [E] eDNA and cells. [F] Combined image.

Analysis of the EPS material for its calcium binding capacity revealed it to be capable of binding 0.24 mg calcium per mg EPS with 0.27 mg calcium per mg EPS still bound after extraction. The total calcium bound was 0.51 mg calcium per mg EPS and is higher than reported for floc based communities (Chapter 6) under the same conditions and is close to values reported for a hypersaline non-lithifying microbial mat (289). The higher rate of ISA degradation coupled to the turnover of EPS substances could have contributed to this higher calcium content of the EPS through the mechanisms of calcium carbonate formation outlined in a conceptual model by Braissant *et al* (289). In support of this a small amount of both  $\alpha$ -ISA (0.34 mg g DW<sup>-1</sup>) and  $\beta$ -ISA (0.37 mg g DW<sup>-1</sup>) was able to be extracted from the biofilm material which would most likely be in a form associated with calcium.

### **7.2.2 The degradation of ISA by biofilms at hyperalkaline pH values**

A single pass system (Diagram 5.6) was used to investigate the survival of biofilms at pH values 11, 12 and 13 and their corresponding ability to degrade ISA. The development of the sand column biofilms used for these experiments is described in Section 5.9.6. Briefly: sterile units were placed downstream from a fully formed Biocell unit and allowed to grow for 10 weeks at pH 11. After this period units were then removed and placed into the single pass system described in Diagram 5.6. CDP media of the pH in question then flowed through the biofilm unit with an NRVB column placed downstream from this used to investigate the impact of biofilm upon different surfaces within the near field. Media was sampled at the outlet of the Biocell unit to ascertain microbial degradation rates of ISA and also at the outlet of the NRVB column. Under all three pH values biofilms were able to degrade all three forms of ISA, as determined by sampling of the media after the passage of 100 mL through the biofilm unit (1.4 days) (Figure 7.8) with rate constants shown in Table 7.3.

There was no impact upon the ability of the biofilm to degrade the  $\beta$ -ISA and XISA forms when the external pH increased from pH 11 to pH 12. Comparison of the rate constants between pH 11 and pH 12 biofilms revealed a small decline in the rate of  $\alpha$ -ISA degradation at pH 12 with small increases in the rates of both  $\beta$ -ISA and XISA degradation (Table 7.3). This could indicate the conditions within the biofilm were slightly more favourable for ISA degradation as the external pH approached pH 12. The rate constants for ISA degradation reduced by approximately a factor of 10 as the pH increased from pH 12 to pH 13 and could indicate a reduction in favourable conditions within the biofilm due to an increase in the local pH. Acetate was detected as an end product for pH 11 only (Figure 7.9) and could indicate acetotrophic processes are favoured within biofilms operating at higher pH values as per the

thermodynamic predications of Bethke *et al* (38). The production of both hydrogen and methane were detected as end products at both pH 11 and pH 12 (Figure 7.10) with a similar amount of methane produced at both pH values. More hydrogen was produced at pH 11 than at pH 12 and could be due to a higher rate of turnover of EPS substances. Correspondingly the pH drop of the liquid passing through the system was greater at pH 11 than at pH 12, with pH reductions at all pH values tested indicative of microbial activity (26) (Figure 7.11). This is the first demonstration of the degradation of all three forms of ISA under ILW-GDF conditions by biofilms and demonstrates that biofilm formation enhances the ability of microbes to survive and degrade ISA under hyperalkaline conditions.

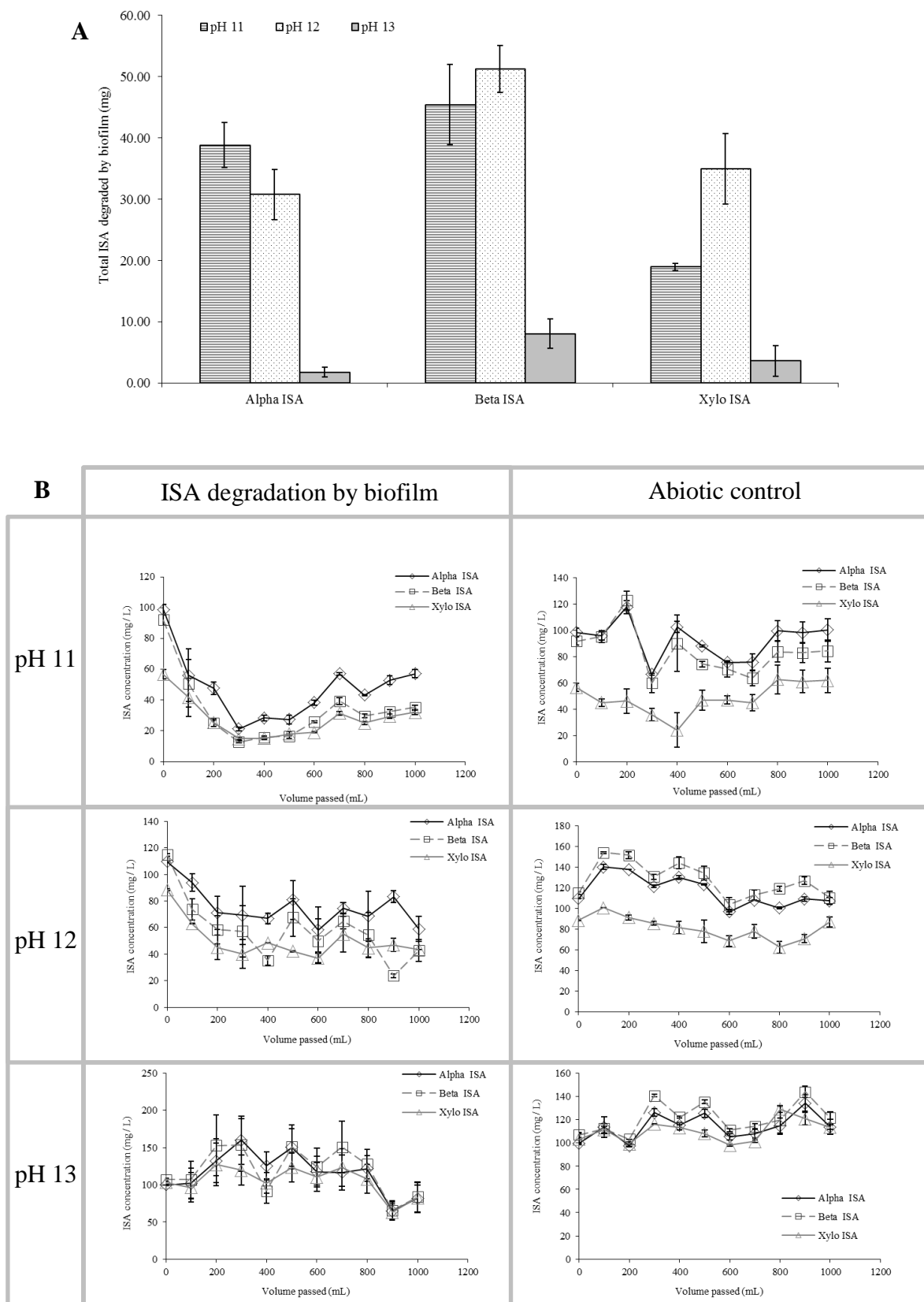


**Figure 7.8: ISA degradation by sand column biofilms at different pH values.** [A] The total amount of the different forms of ISA degraded at the different pH values. The largest amount of  $\alpha$ -ISA was degraded at pH 11 whereas greater amount of  $\beta$ -ISA and XISA were degraded at pH 12. pH 13 showed a large reduction in ISA degradation. The total amounts were calculated taking into account the abiotic removal of ISA within control columns. [B] ISA curves for both biotic and abiotic systems.

ISA type	First order rate constants (day <sup>-1</sup> )					
	pH 11		pH 12		pH 13	
	Average	SE	Average rate	SE	Average rate	SE
$\alpha$ -ISA	$2.87 \times 10^{-1}$	$1.04 \times 10^{-1}$	$1.96 \times 10^{-1}$	$1.94 \times 10^{-6}$	$1.11 \times 10^{-2}$	$5.74 \times 10^{-3}$
$\beta$ -ISA	$3.31 \times 10^{-1}$	$1.31 \times 10^{-1}$	$3.58 \times 10^{-1}$	$7.67 \times 10^{-2}$	$5.59 \times 10^{-2}$	$4.61 \times 10^{-2}$
XISA	$1.33 \times 10^{-1}$	$3.77 \times 10^{-2}$	$2.59 \times 10^{-1}$	$4.80 \times 10^{-2}$	$2.72 \times 10^{-2}$	$2.10 \times 10^{-2}$

**Table 7.3: First order rate constants for ISA degradation in biofilm at different pH values.** There are similar first order rate constants between pH 11 and 12 for all three forms of ISA with a tenfold decrease in these constants as the external pH raises to pH 13. Rate constants were calculated based on the average amount of ISA type removed at each 1.4 day period which equated to the passage of 100 mL of media through the system.

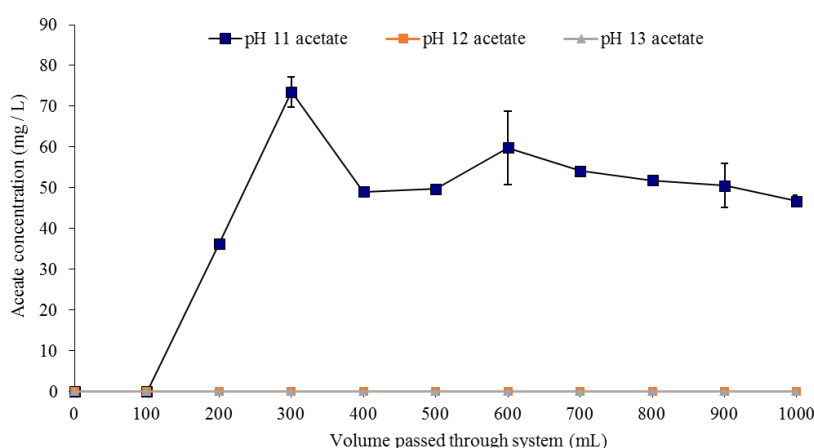


**Figure 7.9: VFA production from single pass biofilm systems.** Acetate was only detected within the pH 11 system. Controls showed no acetate production or removal.

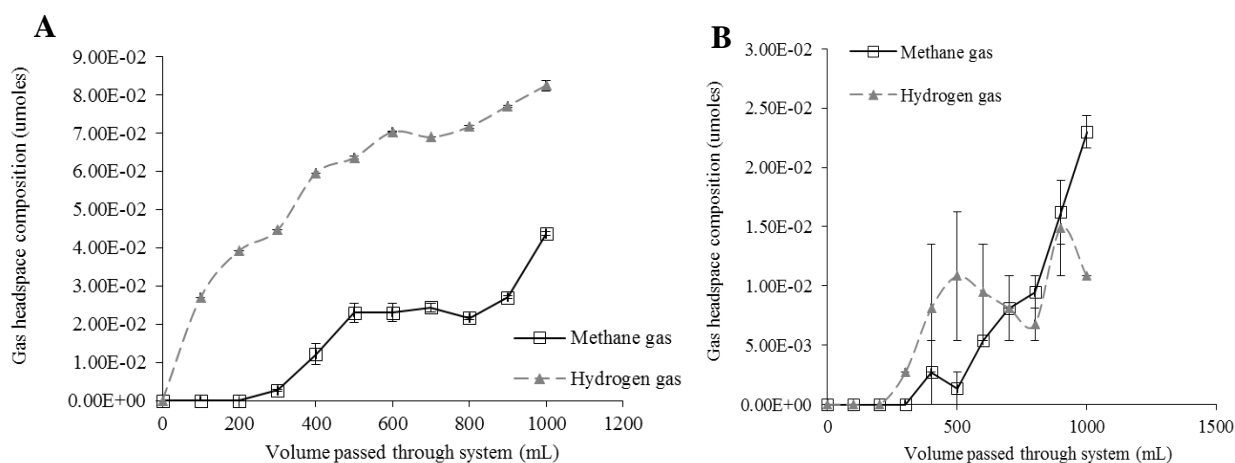


**Figure 7.10: Gas production from biofilms under hyperalkaline pH range.** [A] Both methane and hydrogen were able to be produced by ISA driven degradation at pH 11. [B] Less hydrogen and methane gas was produced at pH 12 even though a similar amount of ISA was degraded. This could indicate that EPS was been turned over at pH 11 to further drive methanogenesis. Control systems showed no gas generation.

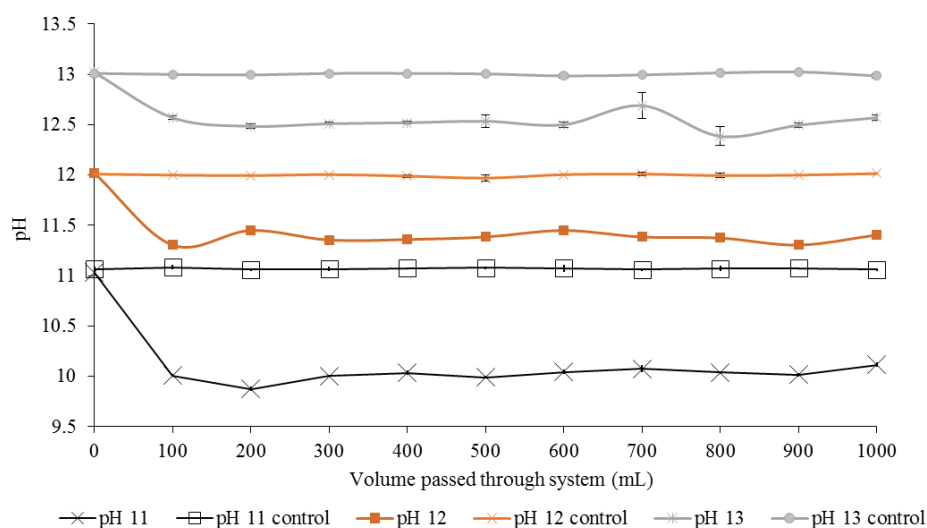


**Figure 7.11: pH measurements of single pass system under hyperalkaline range.** In all the biotic systems the biofilm was able to reduce the pH of the media flowing through it when compared to abiotic controls.

Microelectrode profiling through the biofilms at pH 11, 12 and 13 (Figure 7.12) revealed sharp pH gradients over the initial 50 - 100  $\mu\text{m}$ . Biofilms at both pH 11 and pH 12 experienced a reduction in the internal pH by approximately 1.5 pH points across 100  $\mu\text{m}$ , with internal biofilm pH remaining constant around approximately pH 9.5 and pH 10.4 after that point, respectively. Biofilm operating at pH 13 experienced a smaller drop of approximately 0.8 pH points across a 40  $\mu\text{m}$  distance before reaching a stable internal pH of approximately pH 12.2. The formation of biofilm within the sand column therefore appears to provide a level of protection from the external environment. Large drops in pH through biofilms have been recorded before (292-295) with similar changes recorded in sewer biofilms by Marjaka *et al* (299). This is the first time such pH profiles through biofilms have been reported under hyperalkaline conditions, with the lower internal pH possibly contributing to the rates of ISA degradation observed in this study (Table 7.3).

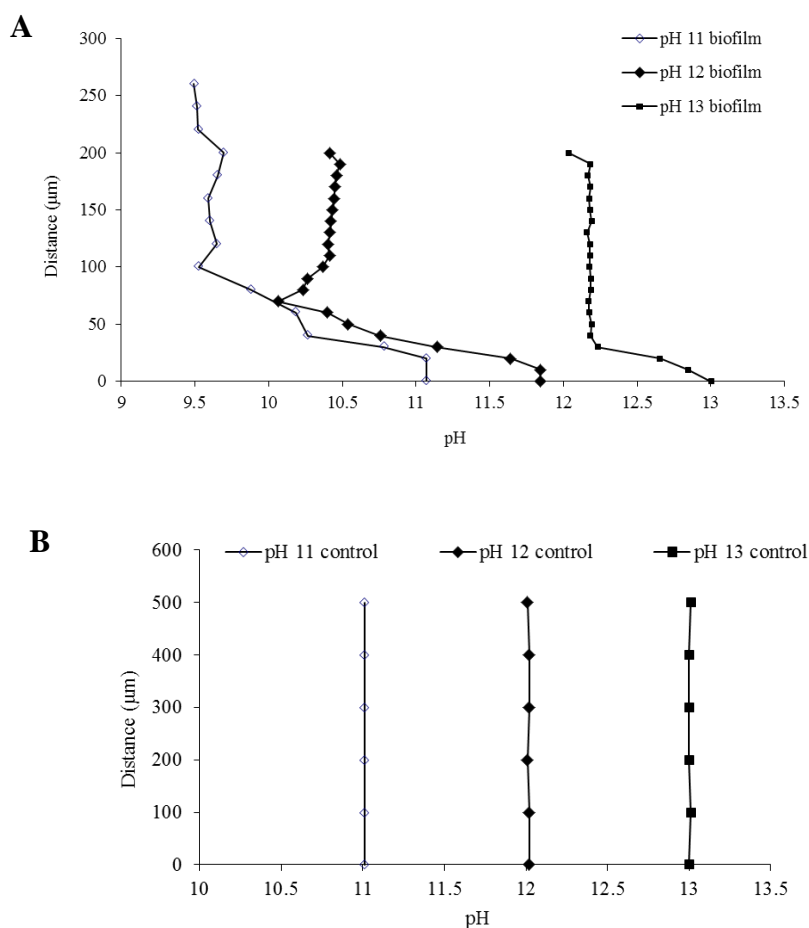


**Figure 7.12: Microelectrode pH profiles through sand column biofilm under hyperalkaline conditions.** [A] Profiles through the biofilm using a microelectrode at all pH values revealed steep pH gradients over 200 μm. [B] Control profiles through agar showed no large change in pH value.

Extraction and quantification of the EPS materials from the biofilms operating under hyperalkaline conditions is shown in Tables 7.4 & 7.5. The eDNA component increased as the external pH increased. Each biofilm had an almost equal composition of carbohydrates and lipids regardless of the external pH which only slightly decreased as the pH increased and the protein content of biofilms decreased as external pH increased. The inorganic matter content increased as the external pH rose (Table 7.6) and could reflect the large eDNA content as it would be able to bind more calcium from the media (102). FTIR analysis of the extracted EPS (Figure 7.13) was similar to the profile reported for floc based communities at pH 11 (Figure 6.13), with the profiles similar to those reported for tightly bound EPS produced by *Aeromonas hydrophila* under reducing conditions (281). The FTIR profiles identified functional groups such as carboxyl, amine and phosphoric groups which under the alkaline pH could contribute a negative charge to the EPS due to the deprotonation of these groups (287). Braissant *et al* (244) reviewed the pKa values of these groups and their ability

to bind cations at alkaline pH values. The wide range of functional groups identified here through FTIR allow the EPS to bind cation species at a wide range of pH values from acidic condition up to hyperalkaline values (244). Analysis of the elemental composition of the biofilms using EDS (Figure 7.14) revealed the biofilms to be mainly composed of carbon, oxygen, calcium and chloride with the biofilm thick enough the block detection of the silicon component of the sand (as seen in the controls). Both microbial cells and EPS materials can act as calcium carbonate nucleation sites (300) where the EPS can act as a buffer whereby a continuous supply of cations is needed to overcome its binding capacity for EPS for carbonates to form (301). Some crystals were visible within the biofilm and could indicate precipitation of calcium carbonate possibly facilitated by the local alkaline environment and presence of bicarbonate from microbial activity (302). For further reference a mathematical model which describes the precipitation of calcium carbonate by biofilms is given in work by Zhang *et al* (303). The precipitation of calcium carbonate could have an impact upon the solubility of radionuclides as they can be co-precipitated (139) with work by Warren *et al* (304) showing that up to 95 % of strontium and 30 % of uranium at concentration of 1 mM could be co-precipitated by *Bacillus pasteurii*.

EPS Component	pH 11				pH 12				pH 13			
	Sonication + ethanol (mg g VS <sup>-1</sup> )	SE	EDTA (mg g VS <sup>-1</sup> )	SE	Sonication + ethanol (mg g VS <sup>-1</sup> )	SE	EDTA (mg g VS <sup>-1</sup> )	SE	Sonication + ethanol (mg g VS <sup>-1</sup> )	SE	EDTA (mg g VS <sup>-1</sup> )	SE
Carbohydrate	21.99	7.71	7.00	2.96	5.27	0.16	7.34	0.05	2.83	0.22	5.43	0.11
eDNA	0.28	0.06	16.75	1.02	0.00	0.00	11.60	0.61	0.00	0.00	16.05	1.75
Protein	13.52	0.39	9.17	0.12	0.37	0.00	3.55	0.03	0.83	0.08	3.36	0.05
Lipid	29.11	6.32	0.95	0.51	7.39	0.43	3.04	0.43	7.35	0.15	1.25	0.15
Total	64.90	14.47	33.86	4.60	13.03	0.60	25.53	1.13	11.01	0.45	26.09	2.06

**Table 7.4: EPS extraction of sand column biofilms under hyperalkaline conditions.**

EPS component	(%)								
	pH 11			pH 12			pH 13		
	Sonication + ethanol	EDTA	Total	Sonication + ethanol	EDTA	Total	Sonication + ethanol	EDTA	Total
Carbohydrate	22.26	7.08	29.35	13.67	19.03	32.70	7.62	14.65	22.26
eDNA	0.29	16.96	17.24	0.00	30.08	30.08	0.00	43.26	43.26
Protein	13.69	9.28	22.97	0.96	9.20	10.16	2.24	9.05	11.29
Lipid	29.48	0.96	30.44	19.17	7.89	27.06	19.82	3.37	23.19

**Table 7.5: EPS percentage composition of sand columns biofilms under hyperalkaline condition.** The amount of eDNA contained within the biofilms increased as the external pH increased with other fractions decreasing. Protein was the most impacted of these fractions.

External pH	Biofilm dry weight (%)	Dry weight volatile solids (%)	Dry weight ash content (%)	Total volatile solids in sand column (g VS)
pH 11	73.20	2.00	98.00	0.48
pH 12	75.20	1.75	98.25	0.42
pH 13	77.23	1.62	98.38	0.39

**Table 7.6: Dry weight, inorganic content and volatile solids of sand columns biofilms under hyperalkaline conditions.** The volatile solid content of the biofilms fell as the external pH rose and could be indicative of alkaline lysis of the EPS materials or a greater extent of carbonation.

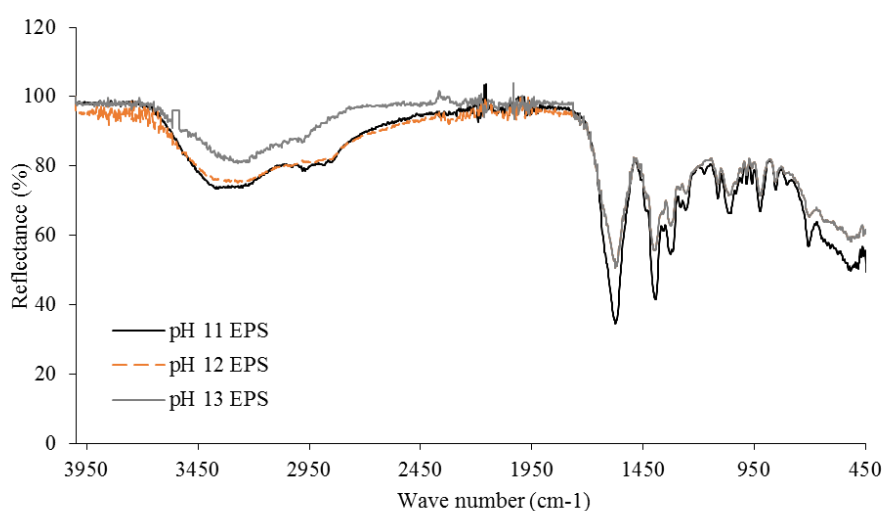


**Figure 7.13: FTIR analysis of biofilm EPS under different hyperalkaline pH values.** Profiles are similar reflecting the similar components of which the EPS is made up. There is a decrease in reflectance at pH 13 around  $3400\text{ cm}^{-1}$  to  $2400\text{ cm}^{-1}$  region which could reflect the small reduction in the carbohydrate content of the EPS.

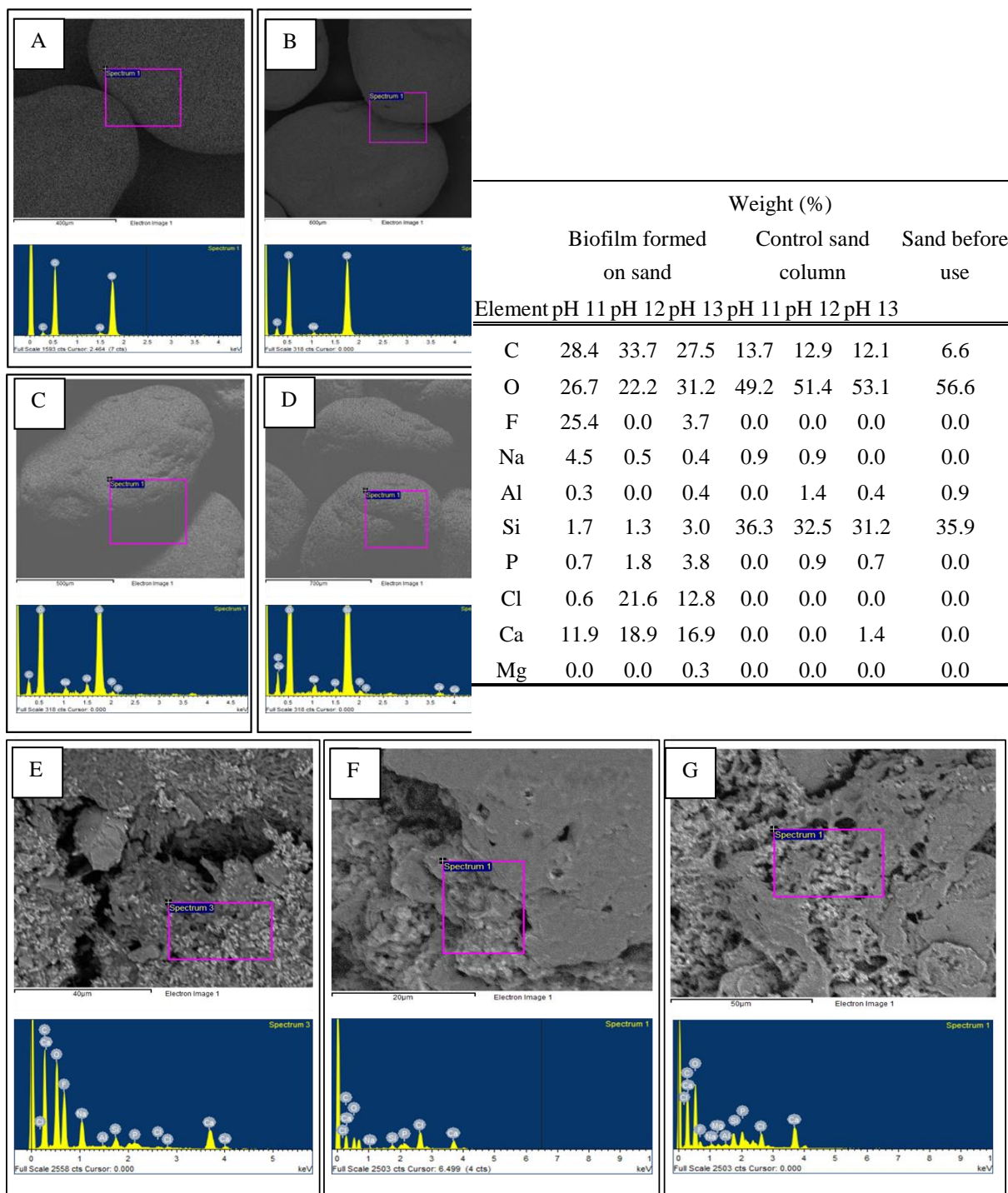


**Figure 7.14: EDS analysis of sand columns with and without biofilms under different hyperalkaline pH values.** [A] Sand before use. [B] pH 11 sand control. [C] pH 12 sand control. [D] pH 13 sand control. [E] pH 11 biofilm. [F] pH 12 biofilm. [G] pH 13 biofilm.

CLSM imaging of the biofilms under the different pH values (Figure 7.15) revealed them to have a complex composition consisting of eDNA, protein, polysaccharides and lipids. These findings tie in with the chemical extraction results explained previously (Table 7.4) and reflect the FTIR findings of a complex EPS with multiple functional groups (Figure 7.13). The different components of the biofilm EPS confer or mediate the different properties of the biofilm and are extensively reviewed by Flemming *et al* (85). In terms of hyperalkaline survival the lipid component could have conferred a level of hydrophobicity which could have helped to maintain the reported pH values within the biofilm. The lipid component of the biofilms was visible and equally abundant across all pH values and could indicate its importance in the production of a pH gradient with acidic phospholipid production reported in alkaliphilic *Bacillus* species (53). The protein component was visibly reduced as the pH increased and ties in with chemical extraction data of the EPS (Table 7.5). Proteins could play a role in the generation of a pH gradient with high isoelectric point proteins shown to be specifically secreted into the EPS materials of a biofilm under acidic conditions (99). The eDNA component was present under all pH values and most likely assisted biofilm stability through interactions with calcium cations (102). There appears to be an equal abundance of  $\beta$  1-3 and  $\beta$  1-4 linked polysaccharides within the biofilm EPS, which had a decreasing composition of mannopyranosyl linked sugars as the external pH increased. This may be due to changes in the community composition as internal and external pH increases may select for more alkaliphilic microorganisms. The relative abundance of the carbohydrate component may indicate its ability to buffer the internal pH with polysaccharides possessing acid monomers such as uronic acids (296). Monomer analysis of the polysaccharide component (Table 7.7) revealed the biofilm to be dominated by mannose monomer units with a wide range of different monomers as per the flocs used to seed the biofilms (Table 6.7) and biofilms formed upon calcite surfaces as reported by Perry *et al* (297). The total uronic acid content of the EPS from biofilms at pH 11 was 11.6 % and which is greater than reported for the flocs used to seed the biofilms which had uronic acid content of 4.3 %. At pH 12 the uronic content fell to 1.2% and at pH 13 the content was 5.4% these difference could be attributed to possible changes in the microbial community as shown in changes to the EPS composition of different acidophilic biofilm communities reported by Jiao *et al* (305).

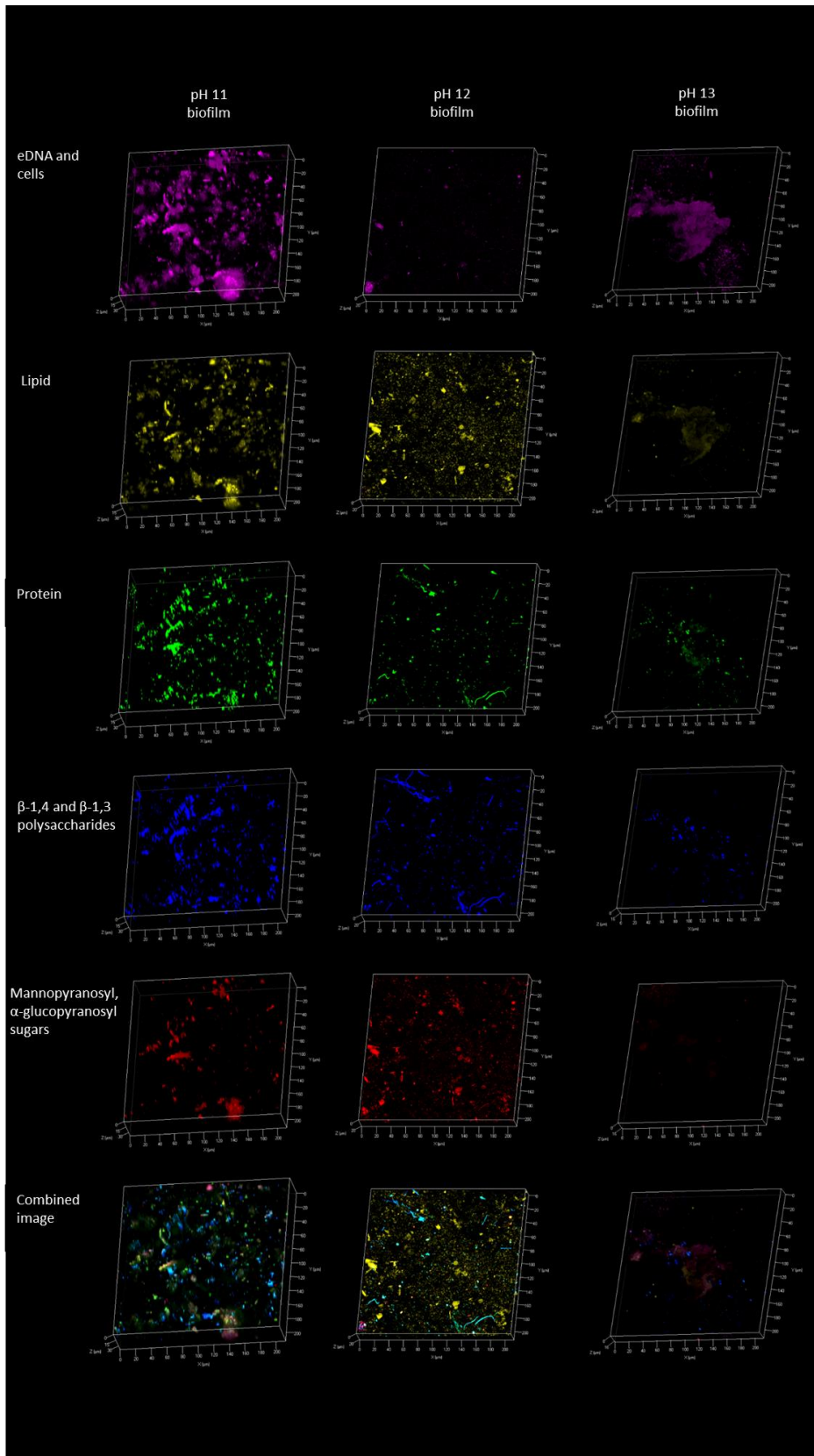


**Figure 7.15: CLSM imaging of sand column biofilms under different hyperalkaline pH values.** pH 11 and 12 biofilm showed an abundance of all EPS components tested for, whereas at pH 13 only eDNA, lipids and protein appeared abundant.

Monomer	Composition (%)		
	pH 11 biofilm	pH 12 biofilm	pH 13 biofilm
Mannose	39.4	50.6	40.2
Ribitol	25.5	21.2	16.9
Galacturonic	9.0	0.7	4.0
Galactose	6.6	7.1	2.8
Ribose	5.3	13.9	26.0
Xylose	3.8	0.0	0.0
Fucose	3.1	0.2	0.4
Glucuronic	2.6	0.5	1.4
Trehalose	2.1	0.0	0.0
Glucose	1.8	0.0	3.0
Rhamnose	0.5	5.7	5.4
Arabinose	0.4	0.0	0.0

**Table 7.7: Monomer analysis of the polysaccharide component of sand column biofilms under different hyperalkaline pH values.** All biofilm polysaccharides were dominated by mannose monomers with uronic acids present but not in a dominating amount at all external pH values.

Analysis of the microbial community of the biofilms at the different pH values using a MiSeq approach is shown in Figure 7.16. Statistical analysis of the microbial communities (Table 7.8) revealed that at a 95% confidence interval there was no significant difference between the pH 11 and pH 12 communities at a family level, however, there was a significant difference between pH 11 and pH 13 communities. There was also a significant difference between the biofilm communities at pH 12 and pH 13 indicating that the shift to pH 13 caused a shift in community composition with the conditions selecting for the most alkaliphilic microbes only.

	pH 11	pH 12	pH 13
pH 11 biofilm		0.073	0.043
pH 12 biofilm	0.073		0.050
pH 13 biofilm	0.043	0.050	

**Table 7.8: Statistical comparison of sand column biofilm communities under hyperalkaline pH values.** Biofilm communities at an external pH of pH 11 were similar to pH 12 communities and significantly different from pH 13 communities. Biofilm communities at an external pH of pH 12 were significantly different from pH 13 communities.

The key shifts in community across the pH range occurred in the Actinobacteria, Clostridia, Cytophagia,  $\alpha$ -Proteobacteria,  $\gamma$ -Proteobacteria and Methanobacteria. The Actinobacteria class was dominated by bacteria of the *Dietzia* genus which increased in community composition from 15.8 % at pH 11 to 27.7 % and 40.0 % at pH 12 and pH 13, respectively. *Dietzia* was dominant within the floc community (Figure 6.5B) which initially seeded the

biofilm and is clearly alkaliphilic. *Dietzia* is reported to degrade a range of carbohydrate sources and pollutants, it is capable of biofilm formation (273, 282) and has been reported in the alkaline calcium containing groundwater of Cabeço de Vide in the south of Portugal (306). The Clostridia increased in community composition from 11.3 % at pH 11 to 33.4 % and 26.4 % at pH 12 and pH 13, respectively. With the majority of these changes attributed to the genus *Anaerobranca* of the family XIV Incertae Sedis which increased from 2.5 % at pH 11 to 11.2 % and 20.5 % at pH 12 and pH 13, respectively. *Anaerobranca* formed a large portion of the Firmicutes population within the polymicrobial flocs described in Chapter 6 (Figure 6.5) and members of this genus have been isolated under a range of hyperalkaline conditions (307-310). The genus is reported to degrade a wide range of carbohydrates and polysaccharides such as cellulose under anaerobic conditions (307) with Engle *et al* (310) showing the products of fermentation from *Anaerobranca horikoshii* to be acetate, carbon dioxide and hydrogen gas. The Cytophagia class was entirely dominated by the genus *Fontibacter* of the Cyclobacteriaceae family which decreased from 14.2 % at pH 11 to 0.5 % and 4.5 % at pH 12 and pH 13, respectively. *Fontibacter* has previously been isolated from a hot spring at pH 8 (311) and a microbial fuel cell at pH 7.2 (312) with close relatives to *Fontibacter* reported at an alkaline lake in Kenya (313). The literature and the community analysis here suggest that *Fontibacter* cannot survive the hyperalkaline conditions as the pH increases with both the  $\alpha$ -Proteobacteria and  $\gamma$ -Proteobacteria showing similar results. The  $\alpha$ -Proteobacteria class was dominated by both Phyllobacteriaceae and Rhodobacteraceae families and decreased from 16.2 % at pH 11 to 6.2 % and 1.7 % at pH 12 and pH 13, respectively. The  $\gamma$ -Proteobacteria class was dominated by Alishewanella as per the floc community (Figure 6.5) and decreased from 15.3 % at pH 11 to 6.1 % and 2.4 % at pH 12 and pH 13, respectively. The methanogen component was entirely dominated by members of the Methanobacteriaceae family which increased as the external pH increased from 0.3 % at pH 11 to 1.4% and 2.1% at pH 12 and pH 13, respectively. Members of the Methanobacteriaceae have been previously isolated from alkaline areas (153, 158) and have been reported in pH 11 ISA degrading liquid methanogenic microcosms by Rout *et al* (80). The Bacillus class component remained stable across the pH range starting at 22.3 % at pH 11 then changing to 17.9 % and 22.2 % at pH 12 and pH 13, respectively. There is a wealth of literature of regarding the growth and survival of Bacillus species under alkaline conditions (48, 51, 314) , with alkaliphilic Bacillus species capable of both biofilm formation (297) and the degradation of a wide range of carbon sources (48, 314).

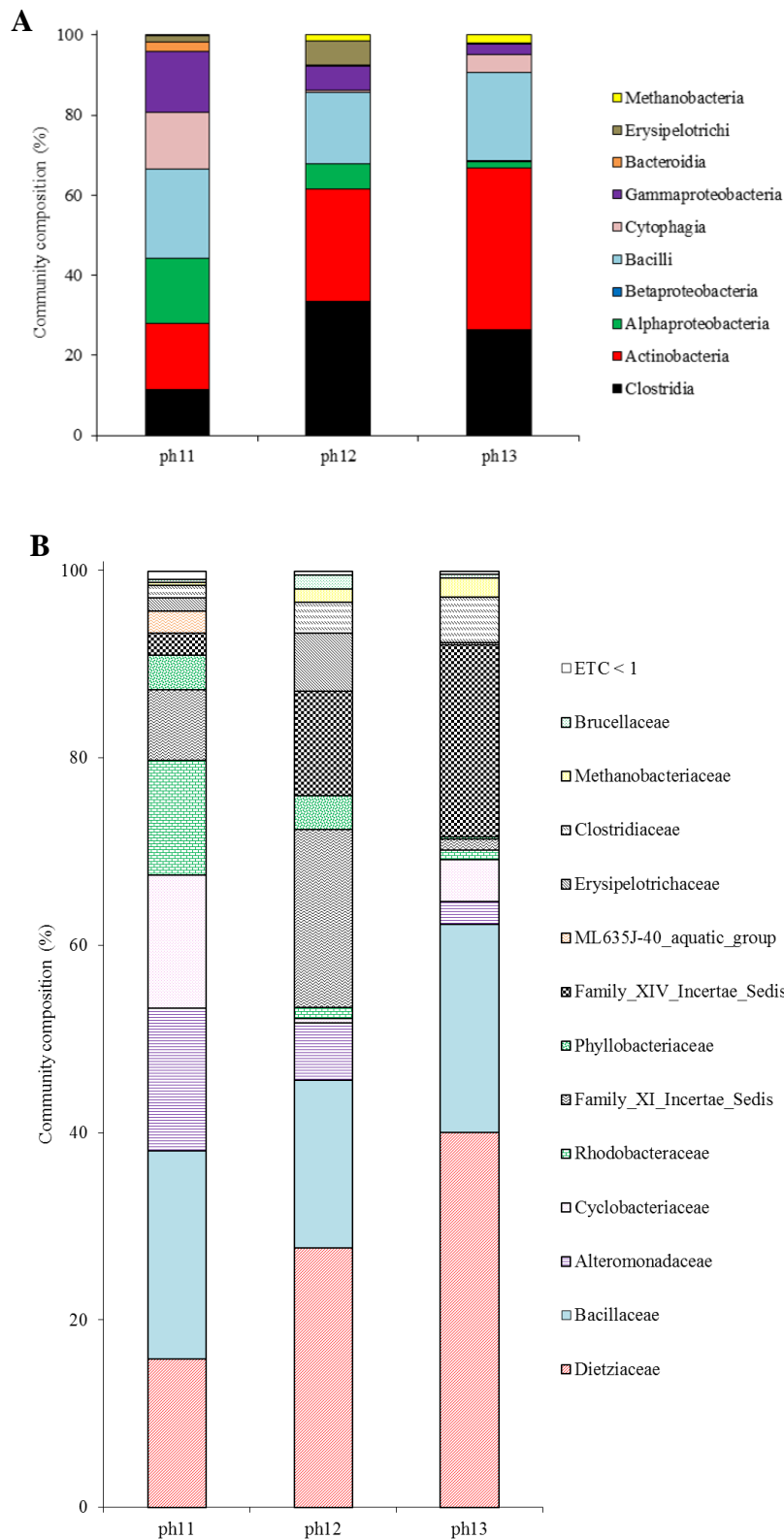


**Figure 7.16: 16S rRNA gene microbial community of sand column biofilms under different hyperalkaline pH values.** [A] Class distribution of sand column biofilms across different hyperalkaline pH values. *Bacillus*, *Clostridia* and *Actinobacteria* form a core component of the biofilms at all pH values tested. [B] Family distribution of biofilm communities. *Dietzia* dominates the *Actinobacteria*, *Bacillaceae* the *Bacillus* with the *Clostridia* composed of different proportions of families at each pH value. The *Clostridia* family XIV incertae sedis increased as the external pH value increased.

The changes in community composition could influence both the biofilm EPS composition and the ability to degrade ISA as the pH increases. The greater incorporation of methanogens into the biofilm may explain a higher eDNA content as archaeal biofilm are reported to be rich in eDNA (28). This, however, could also be a result of cell death from the lineages which could not survive as the pH rose. The biofilm composition of an unknown bacterium from the Incertae Sedis XI lineage increased to 19.0% at pH 12 and then decreased to 1.0 % at pH 13. This change could explain the reduction in ISA degradation at pH 13, however, the presence and stability of other alkaliphilic microorganisms across the entire pH range may indicate that ISA degradation was also impacted by the external conditions. The alpha diversity statistics (Table 7.9) showed a reduction in the number of OTU's as the pH rose with the Shannon diversity index decreasing accordingly. The rarefaction curves (Figure 7.17A) showed that the sampling depth was sufficient and this was reflected in the Goods coverage values. The rank abundance curves (Figure 7.17B) reflected the low diversity observed (226).

External pH	Valid reads	OTUs	Ace	Chao1	Shannon	Goods Coverage
11	26294	830	849.38	856.56	3.39	1.00
12	28914	792	813.19	817.14	3.03	0.99
13	29672	139	139.00	139.00	2.17	1.00

**Table 7.9: Alpha diversity statistics for sand column biofilm communities at different hyperalkaline pH values.** Diversity of the biofilm community decreased as the external pH increased with a reduction in OTU's, predicted OTU's and Shannon index.

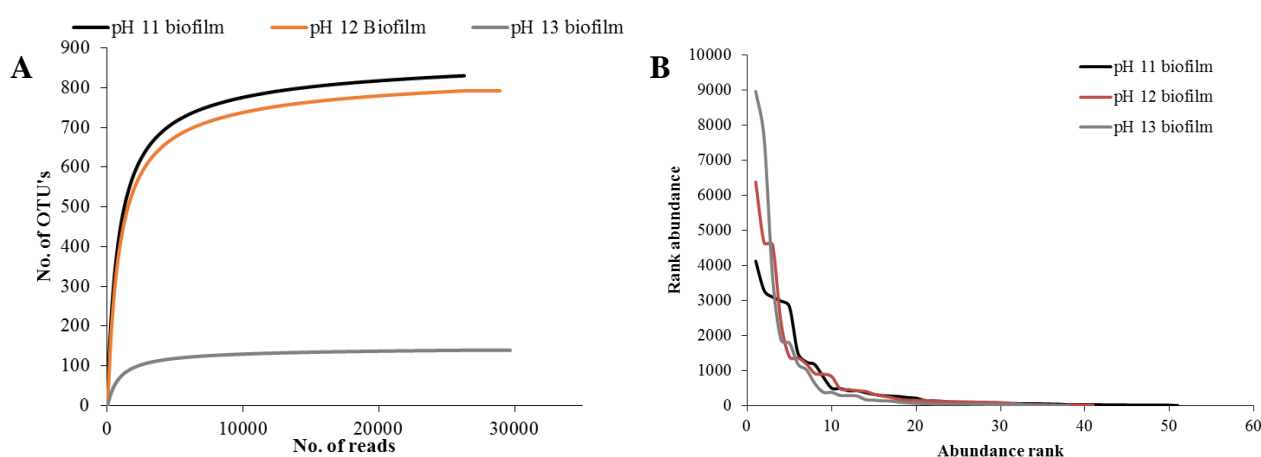


**Figure 7.17: Rarefaction and rank abundance curves for biofilm communities under different hyperalkaline pH values.** [A] Rarefaction curves show that sampling was sufficient to capture the diversity of all the biofilm communities. [B] Rank abundance curves reflect the low diversity at all pH values tested with the diversity decreasing as the external pH increased.

SEM imaging of the biofilms at different pH values (Figure 7.18) showed areas of both rough and smooth biofilm at all pH values and is most likely due to the difference in shear experienced within the flow cell as previously discussed (298). The amount of visible cells embedded with the biofilm decreased as the external pH increased and could indicate that only the most alkaliphilic organisms were surviving. ATP measurements (Table 7.10) of the biofilms reflected this finding showing a decrease in viable cells within the biofilms as the external pH rose. Redox profiling (Figure 7.19) demonstrated low values deep within the biofilm with approximate values of -350 mV, -200 mV and -180 mV reported where the pH was at its lowest in pH 11, 12 and 13 biofilms, respectively. These values indicate that the cells were active metabolically with reduction in redox associated with microbial activity (315). The increase in internal biofilm redox as the pH rose could be associated with a drop in viable cells and lower rates of metabolic activity.

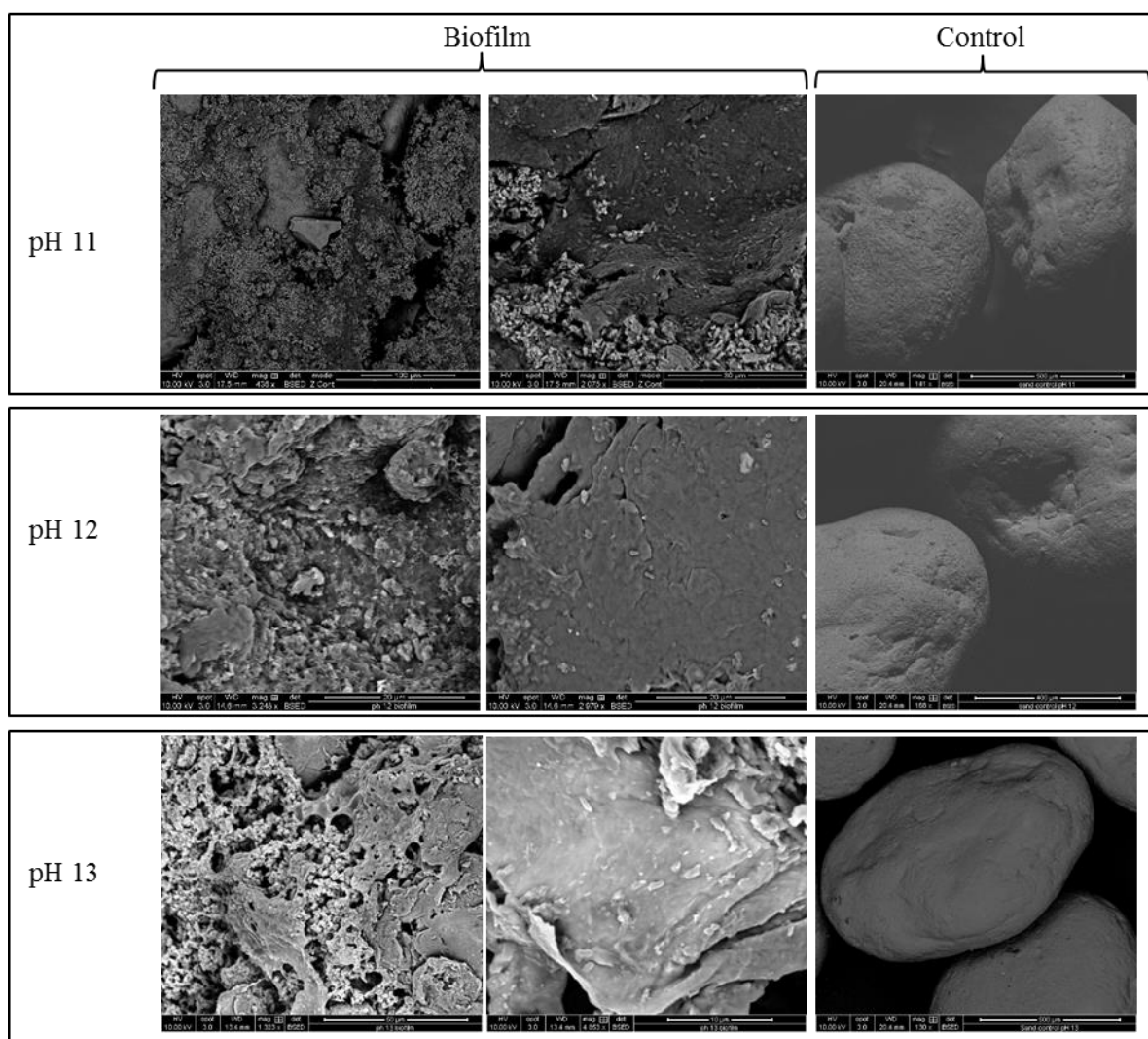


**Figure 7.18: SEM images of sand column biofilms under different hyperalkaline pH values.** A decreasing amount of cells can be seen as the external pH increases, with the biofilms possessing areas of rough and smooth surfaces possibly due to differences in shear within the sand column.

External pH	CFU g VS <sup>-1</sup>	SE	mg DW g VS <sup>-1</sup>	SE
pH 11	7.70 x 10 <sup>8</sup>	5.10 x 10 <sup>7</sup>	1.96	1.30 x 10 <sup>-1</sup>
pH 12	2.49 x 10 <sup>8</sup>	1.65 x 10 <sup>7</sup>	6.34 x 10 <sup>-1</sup>	4.21 x 10 <sup>-3</sup>
pH 13	7.79 x 10 <sup>6</sup>	3.27 x 10 <sup>5</sup>	1.99 x 10 <sup>-2</sup>	8.33 x 10 <sup>-4</sup>

**Table 7.10 : Viable cell measurements and related cell dry weight of sand column biofilms at different hyperalkaline pH values.** The amount of viable cells decreased as the external pH increased with a shift to pH 13 reducing the concentration of viable cells by a 100-fold.

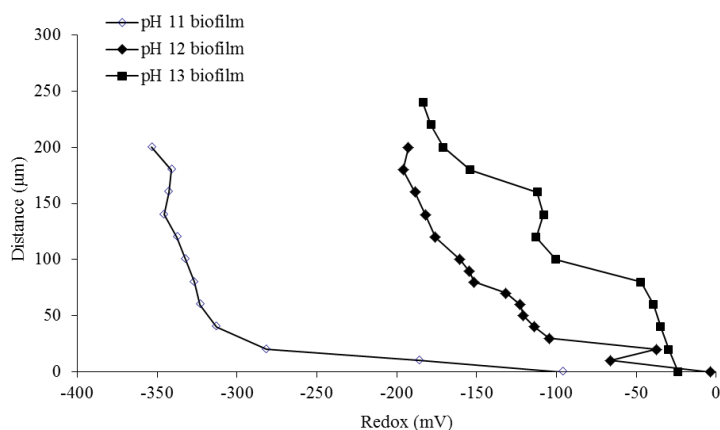


**Figure 7.19: Redox measurements in sand column biofilms under different pH values.** The redox values reached their lowest values deep within the biofilm where the lowest pH values were recorded for each biofilm. The biofilm redox increased as the pH increased possibly due to a reduction in metabolic activity.

### 7.2.3 Biofilms formation in the near field upon ILW-GDF relevant surfaces

ATP measurements downstream of the sand columns revealed aggregates of EPS material/flocs to be leaving the biofilm (Table 7.11) with live/dead investigations revealing the flocs to possess both alive and dead cells (Figure 7.20). After passage through the NRVB column flocs reduced in visible cells with ATP measurements showing an approximate 100-fold decrease of viable cells which could be linked to cells adhering to the surfaces within the NRVB column or dying through exposure to the higher pH values experienced within the NRVB column (Figure 7.21). The pH within the NRVB column component rose rapidly within the system and reflects findings by Butcher *et al* (12), with the pH increase most likely due to the dissolution of alkali metal hydroxides (7). Over the time scale of the experiment the pH within the NRVB component decreased within the columns exposed to a biological component (Figure 7.21) with carbonation staining revealing large areas of carbonation upon the surface of the NRVB column at all pH values (Figure 7.22).

External pH	Cell density (CFU mL <sup>-1</sup> )				Cell dry weight (µg mL <sup>-1</sup> )			
	Biofilm outlet	SE	NRVB Outlet	SE	Biofilm outlet	SE	NRVB Outlet	SE
pH 11	1.19 x 10 <sup>5</sup>	6.76 x 10 <sup>2</sup>	4.64 x 10 <sup>2</sup>	8.21	3.03 x 10 <sup>-1</sup>	1.72 x 10 <sup>-3</sup>	1.18 x 10 <sup>-3</sup>	2.09 x 10 <sup>-5</sup>
pH 12	9.02 x 10 <sup>4</sup>	2.87	1.24 x 10 <sup>2</sup>	1.76	2.30 x 10 <sup>-1</sup>	7.30 x 10 <sup>-6</sup>	3.17 x 10 <sup>-4</sup>	4.48 x 10 <sup>-6</sup>
pH 13	1.13 x 10 <sup>4</sup>	4.62	3.92 x 10 <sup>2</sup>	5.30	2.87 x 10 <sup>-2</sup>	1.18 x 10 <sup>-5</sup>	9.99 x 10 <sup>-4</sup>	1.35 x 10 <sup>-5</sup>

**Table 7.11: Cell density and dry weight measurements of flocs leaving sand column biofilms at different hyperalkaline values.** There were viable cells leaving the biofilms and entering the NRVB columns downstream from the biofilms. After passage through the NRVB column viable cells reduced by approximately 100-fold which could be due to cell death or adhesion to surfaces.

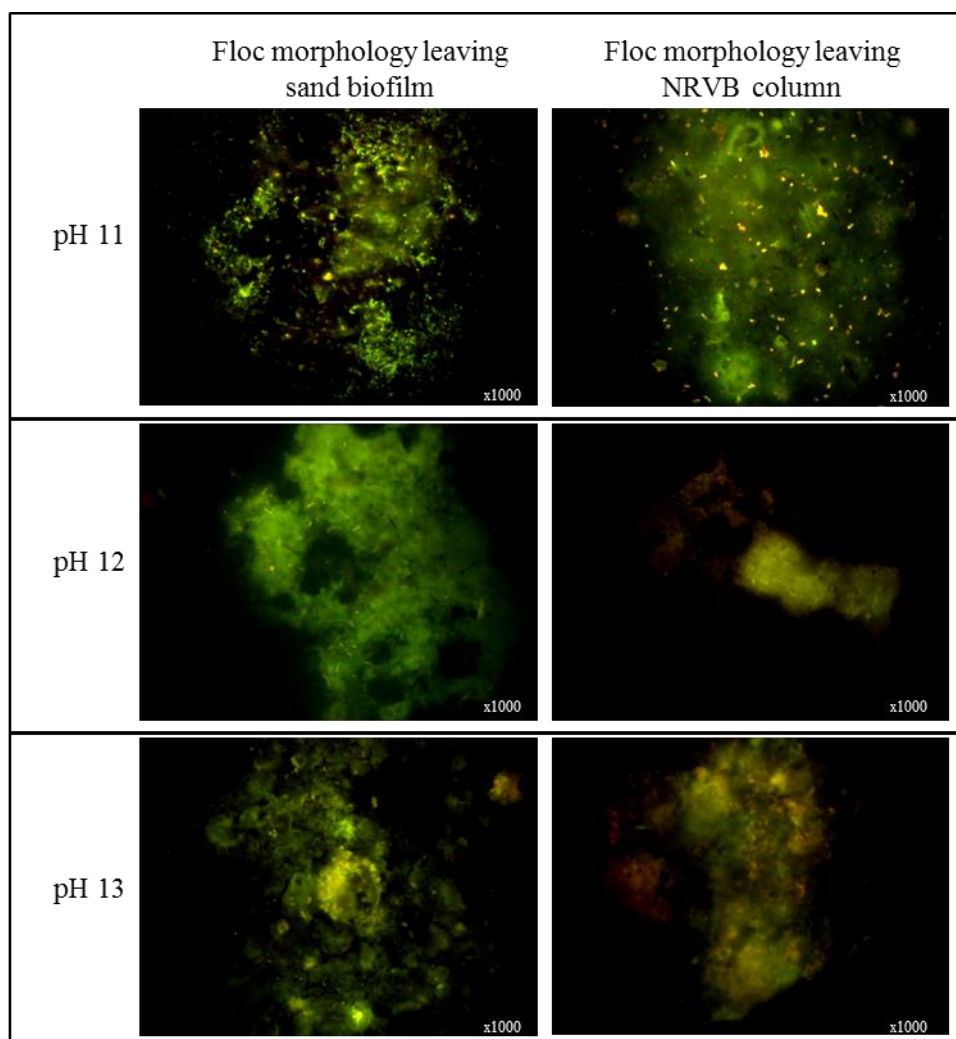


**Figure 7.20: Live/dead imaging of flocs leaving sand column biofilms at different hyperalkaline values.** At all pH values aggregates of EPS or flocs left the biofilms possibly as a transport vector for microbes to colonise new areas. After passage of these flocs through the NRVB column the amount of live cells decreased possibly due to exposure to the hyperalkaline conditions or loss due to adhesion to surfaces.

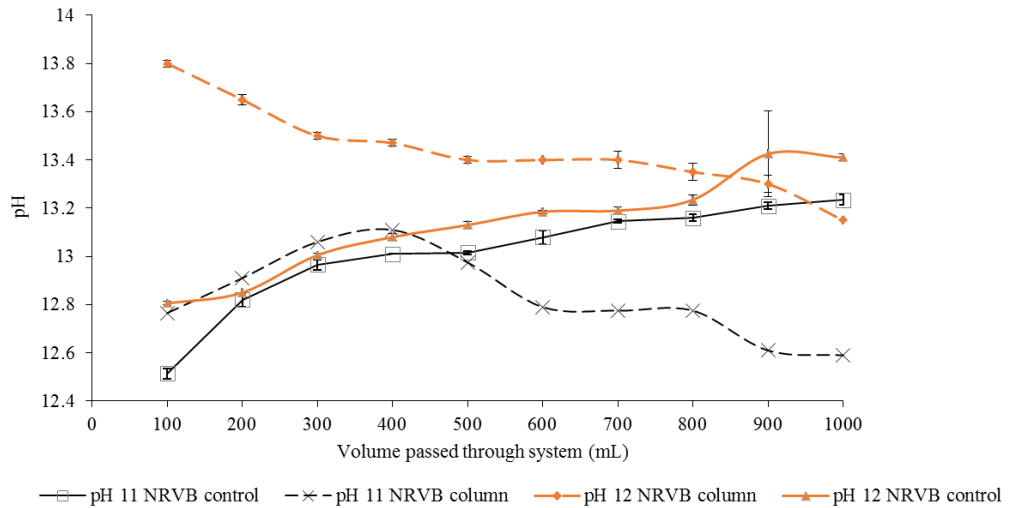


**Figure 7.21: pH measurements of NRVB column outlet.** The biofilm exposed NRVB columns decreased in pH as the experiment progressed whereas the controls increased in pH possibly due to the dissolution of alkali metal hydroxides. The reduction in pH in the biofilm exposed columns could indicate microbial processors beginning to establish a foothold within the NRVB column. The pH values of pH 13 systems were beyond the detectable limit of the pH probe due to a rise in pH due to the dissolution of alkali metal hydroxides.

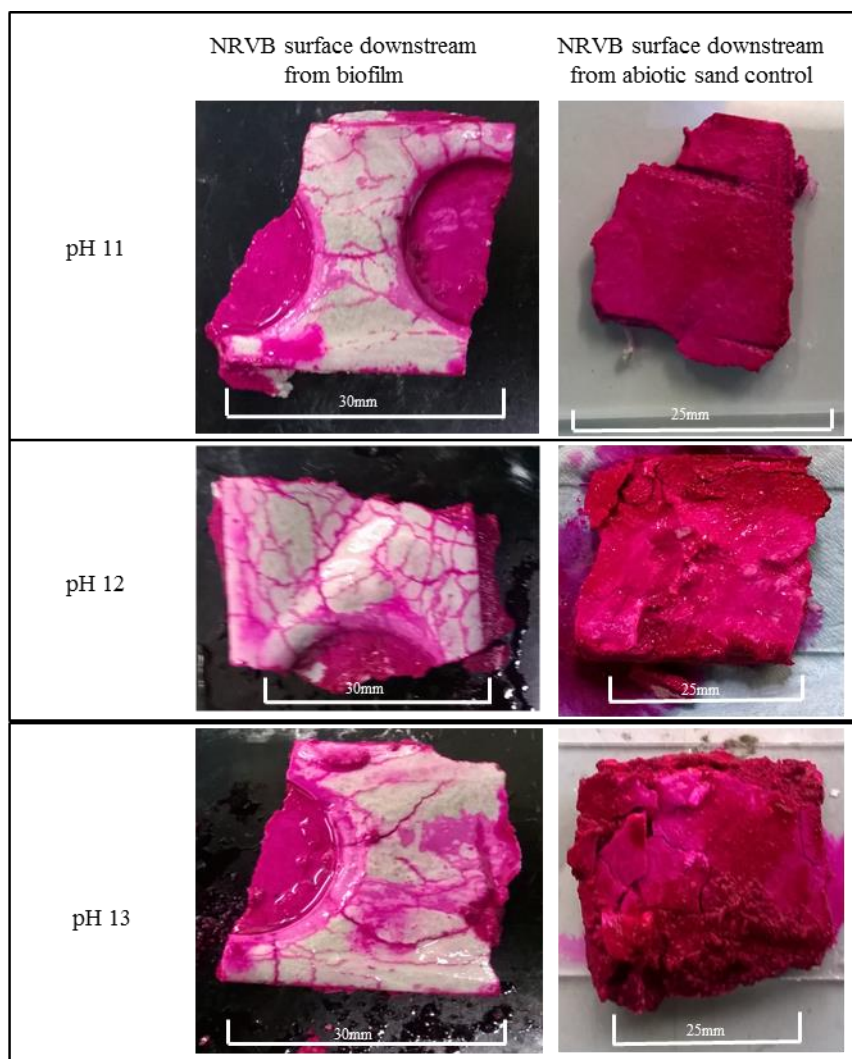


**Figure 7.22: Carbonation surface testing of NRVB columns.** At all three pH values tested, NRVB downstream from biofilm showed evidence of surface carbonation (clear areas). In contrast to this control columns showed no evidence of carbonation (purple areas).

SEM imaging (Figure 7.23) of the NRVB downstream from the biofilms showed a difference in surface morphology in comparison to the abiotic controls. The biotic exposed surfaces showed areas of greater surface roughness with EPS type materials and areas of possible carbonation with similarities between SEM investigations of carbonated NRVB reported by N.N.L. (316) and B.G.S.(317). Compared to the controls surface micro-cracks and pores appeared to be reduced in size and diameter with EDS of these areas (Figure 7.24) showing a composition similar to the biofilms grown upon the sand columns (Figure 7.14) but with a higher calcium content. This could indicate a higher rate of calcium carbonate formation upon the NRVB surface due to microbial activity with chicken wire mesh like patterns of carbonation as reported by B.G.S. (317) seen in some areas upon the NRVB surface (Figure

7.23). It should also be noted, however, that NRVB has a large calcium component. In both the EDS testing of sand biofilms and the biotic exposed NRVB surfaces a chloride component was present and could indicate that both biofilm formation and carbonation may have an impact upon the migration of  $^{36}\text{Cl}$  as reported by B.G.S. (141, 317). The chlorides in this instance are supplied by the mineral media (Table 5.1) which contains a range of chloride containing compounds such as ammonium chloride and magnesium chloride (235). The carbonation of NRVB impacts the migration of radioactive carbon dioxide through precipitation reactions (316) but also decreases the ability of the NRVB surface to interact and retard the migration of radionuclides (317, 318). However, the carbonation of NRVB has also been shown to seal cracks and pores reducing its permeability and therefore retarding the migration of radionuclides (319) with calcium carbonate precipitation shown to seal cracks in rocks at the Maquarin site (7). The sealing of cracks may, however, contribute to pressure issues due to the build of gases from the degradation or organic matter (319).

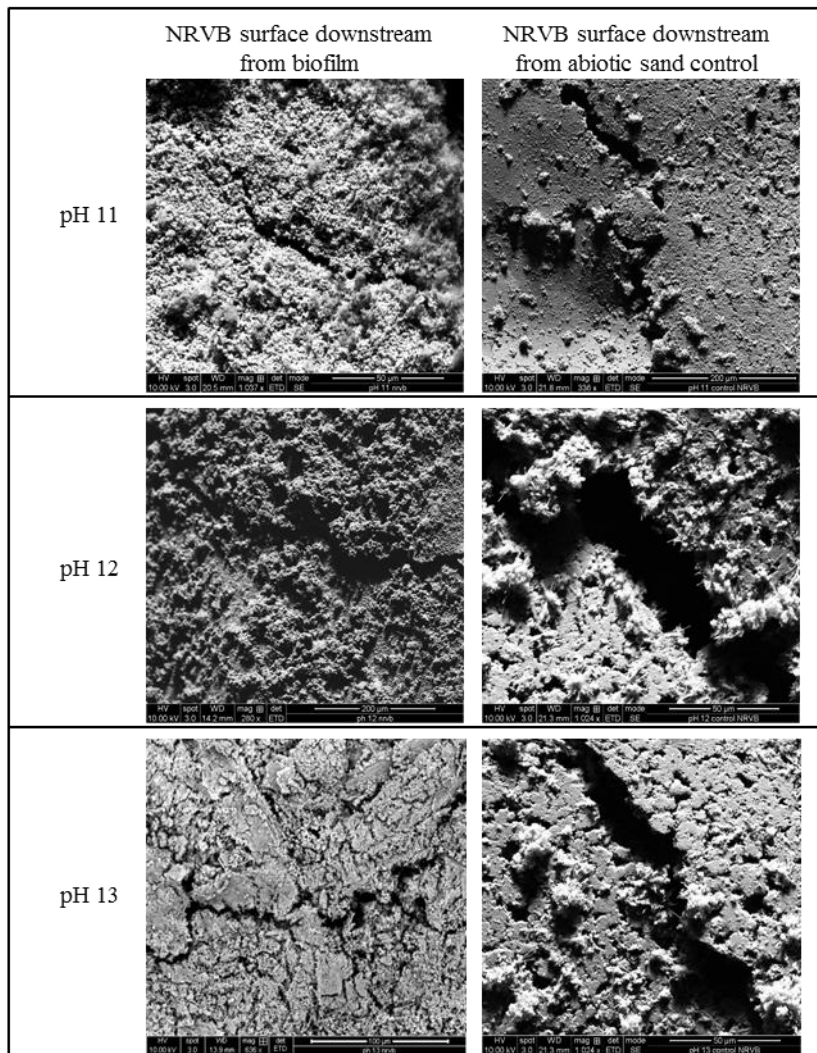
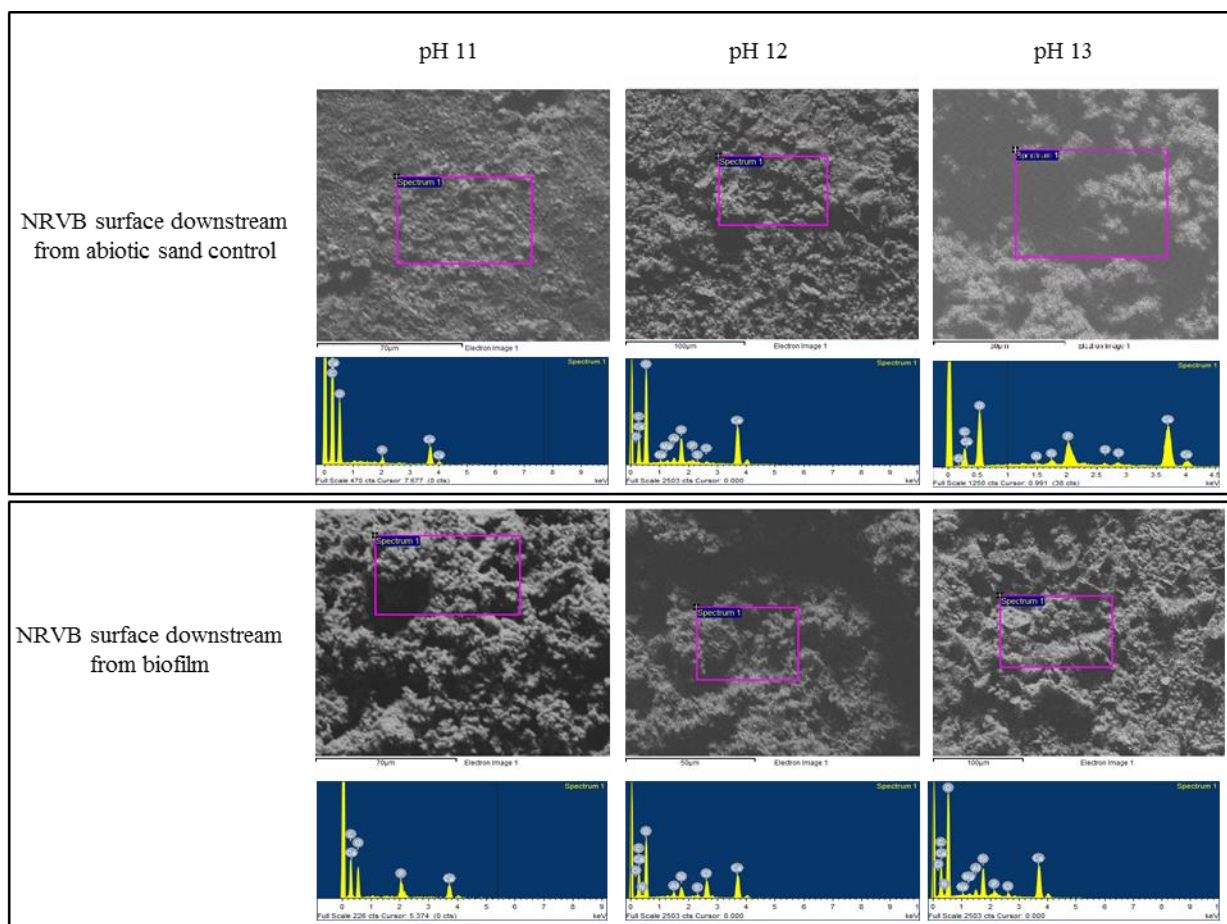


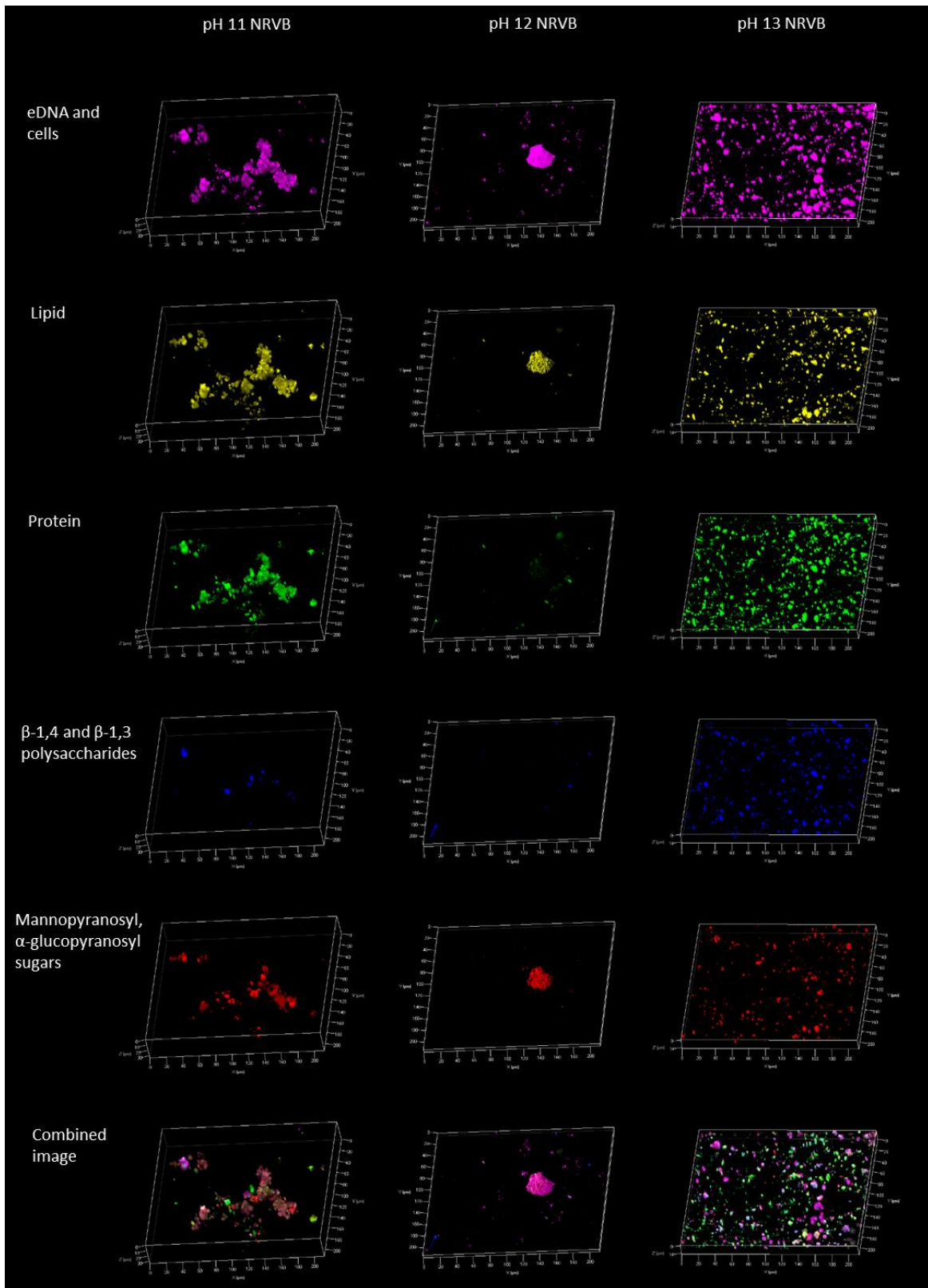
**Figure 7.23: SEM images of NRVB surfaces exposed at different hyperalkaline values under both abiotic and biotic conditions.** At all three pH values tested NRVB surfaces showed an increase in surface roughness with evidence of micro-fracture sealing possibly by carbonation.



Element	Weight (%)					
	Biofilm exposed NRVB surface			Control NRVB surface		
	pH 11	pH 12	pH 13	pH 11	pH 12	pH 13
C	36.4	17.7	12.1	52.0	10.4	5.9
O	35.2	39.9	49.7	31.0	49.5	40.3
Na	0.0	0.0	0.3	0.0	0.3	0.0
Mg	0.0	0.0	0.3	0.0	0.3	0.0
Al	0.0	0.9	1.1	0.0	0.9	0.3
Si	0.0	2.9	6.0	0.0	5.9	1.2
P	7.9	0.0	1.2	2.0	0.2	6.8
S	0.0	1.1	0.0	0.0	0.4	0.0
Cl	0.0	9.5	1.9	0.0	1.1	1.3
Ca	20.5	23.1	26.0	15.0	30.8	40.2
N	0.0	4.9	1.5	0.0	0.0	0.0

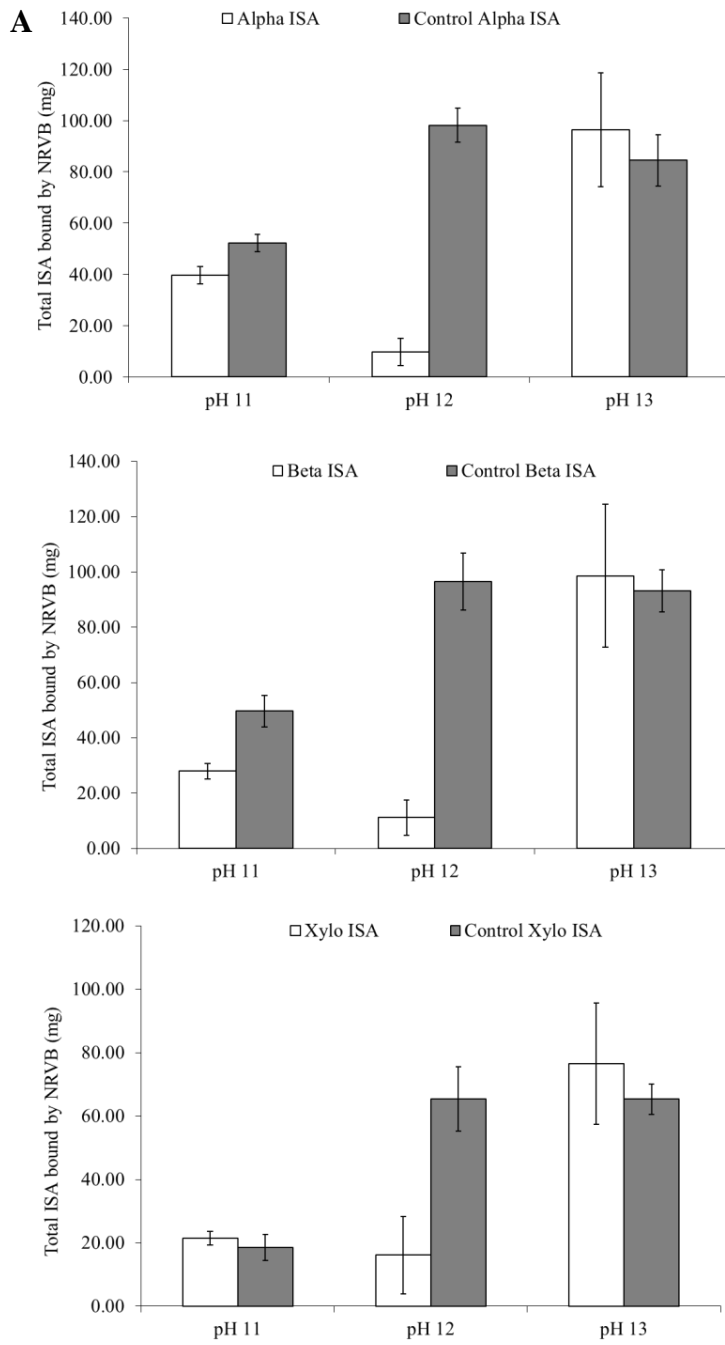
**Figure 7.24: Elemental composition of NRVB surfaces at different hyperalkaline pH values exposed to both biofilm and abiotic systems.** There is a difference between the composition of NRVB surfaces exposed to the biofilm system in comparison to the abiotic systems at all pH values tested. This could be due to biofilm formation or carbonation events.

CLSM imaging of the NRVB surfaces (Figure 7.25) showed the surfaces to possess organic components at all pH values. At pH 11 there appeared to be biofilm formed within crevices which had a similar composition to the sand biofilm reported at pH 11 (Figure 7.3). At pH 12 there appeared to be a reduced colonisation of the NRVB surface with a small patch of biofilm rich in eDNA, lipids and mannopyranosyl linked carbohydrates. pH 13 showed a greater degree of organic components spread across the surface of the NRVB and could indicate that EPS materials were sorbing to the surface. The volatile solids decreased within the biofilm sand columns (Table 7.6) as the pH increased which could indicate alkaline lysis of some of the EPS components. This may result in the surfaces becoming primed with organic materials (112) which could then further facilitate biofilm formation (113). The formation of biofilm upon the NRVB surfaces could lead to localised carbonation due to metabolic activity as seen in the microbially induced corrosion of concrete surfaces (320). Work by Grant *et al* (176) has previously shown that biofilm was able to form upon NRVB using ISA under nitrate reducing and hyperalkaline conditions. Grant *et al* (176) reported that once the NRVB surface was coated in a thin layer of organics, biofilm could form upon the surface in as little as 8 days with a thin carbonate layer reported between the biofilm and the NRVB surface. A review by Zhu *et al* (300) found that under hyperalkaline conditions microbial action mainly precipitates calcium carbonate in the form of calcite with work by Perry *et al* (297) showing that bacterial EPS consisting of polysaccharides with a similar monomer composition to those reported here which were capable of promoting biofilm adherence to calcite surfaces.



**Figure 7.25: CLSM imagery of NRVB surfaces under different hyperalkaline values exposed to biotic conditions.** NRVB surfaces at pH 11 and pH 12 showed areas of aggregated EPS upon the surfaces with a similar composition to the sand column biofilms. At pH 13 a large distribution of all EPS components were present across the surface of the NRVB.

Comparison of the ISA concentrations after passage of the media through the NRVB column between the biotic and abiotic system revealed the NRVB to be binding ISA to its surface, with comparison between the systems for each ISA type shown in Figure 7.26. Both pH 11 and pH 13 showed similar removal for all three types of ISA with NRVB at pH 13 binding more of all types of ISA to its surface under both abiotic and biotic conditions. In each instance at pH 11 and pH 13 the control bound similar amounts to the biotic system. At pH 12 the control bound significantly more of all three types of ISA than the biotic system and indicates at this pH the biological component had an effect upon the NRVB to bind ISA. The amounts of  $\alpha$ -ISA bound at these pH values are roughly similar to those reported by Van Loon *et al* (321) with this study the first to show the sorption of  $\beta$ -ISA and XISA to NRVB under hyperalkaline conditions (Table 7.12).



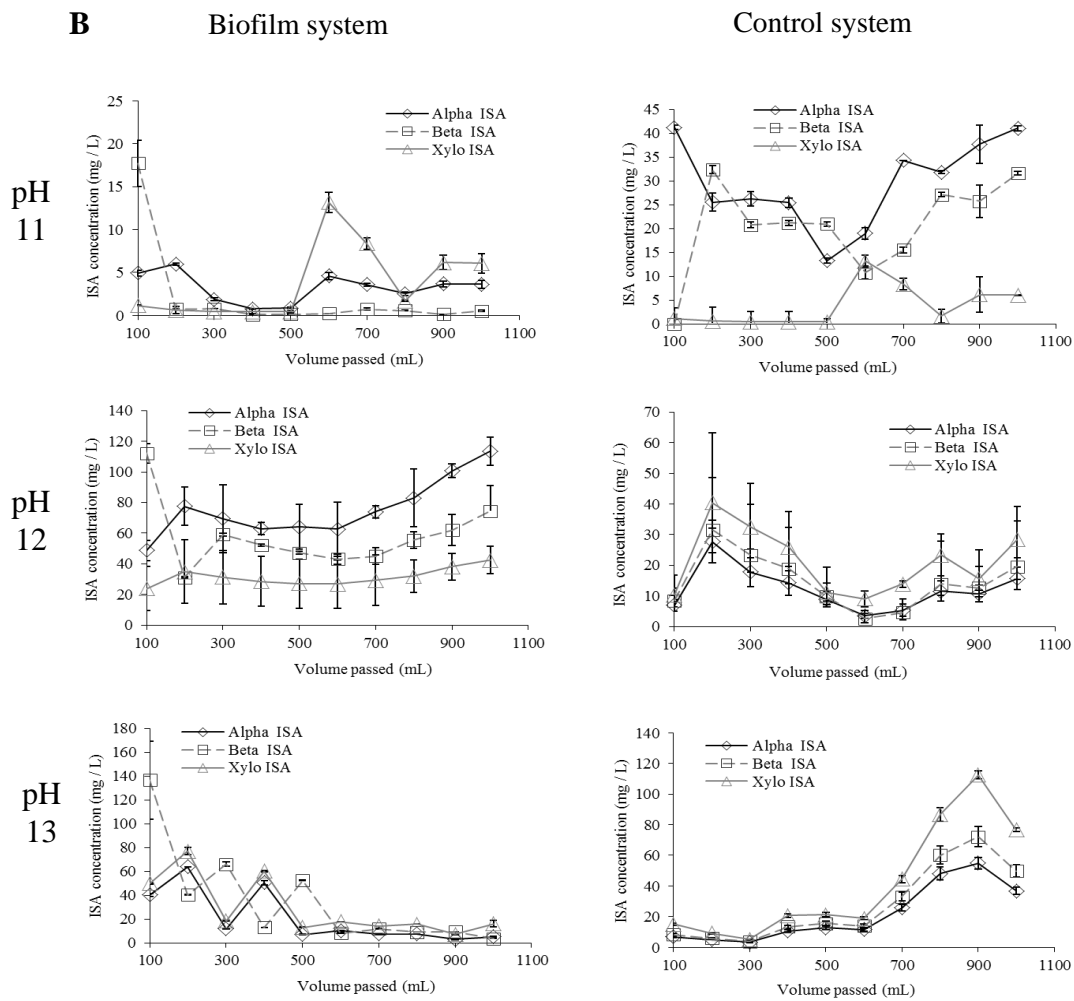


**Figure 7.26: Comparison of total ISA removed by passage through NRVB column at different hyperalkaline pH values.** [A] Control NRVB columns bound more  $\alpha$ -ISA and  $\beta$ -ISA at pH 11 and pH 12 with similar amounts of both types of ISA removed by both control and biofilm exposed NRVB at pH 13. At pH 11 and pH 13 XISA was removed in a similar amount by NRVB under control and biofilm systems, however at pH 12 the control bound more XISA. Values for the graphs were calculating by subtracting the ISA amount entering the NRVB column from the amount leaving. [B] Curves showing the ISA concentration of media leaving the NRVB column.

Total ISA removed by passage through NRVB column (mol kg <sup>-1</sup> )												
	Sample						Control					
	$\alpha$ -ISA	SE	$\beta$ -ISA	SE	XISA	SE	$\alpha$ -ISA	SE	$\beta$ -ISA	SE	XISA	SE
pH 11	2.14E-03	1.80E-04	1.51E-03	1.47E-04	1.39E-03	1.38E-04	2.82E-03	1.81E-04	2.68E-03	3.11E-04	1.20E-03	2.66E-04
pH 12	5.24E-04	2.82E-04	6.02E-04	3.44E-04	1.05E-03	7.92E-04	5.29E-03	3.61E-04	5.21E-03	5.55E-04	4.23E-03	6.55E-04
pH 13	5.20E-03	1.20E-03	5.32E-03	1.39E-03	4.96E-03	1.24E-03	4.56E-03	5.39E-04	5.03E-03	4.11E-04	4.23E-03	3.14E-04

**Table 7.12: Amount of ISA removed due to passage through NRVB column at different hyperalkaline pH values under both abiotic and biotic systems. All three forms of ISA were able to be bound to the NRVB surface**

Measurement of the TOC values through the system (Figure 7.27) revealed a similar amount of TOC to be removed by the biotic system at all three pH values. This result is likely a reflection of the increased ability of the NRVB to bind ISA and possibly other organics as the pH increased. The control TOC profiles reflected the control profile of NRVB binding ISA (Figure 7.26). The IC increased in both pH 11 and pH 12 biotic systems but not the pH 13 system and could be reflective of the degradation rates of ISA (Table 7.3). Within the abiotic control systems only pH 11 showed a rise in IC which could be due the lower pH media entering the column.

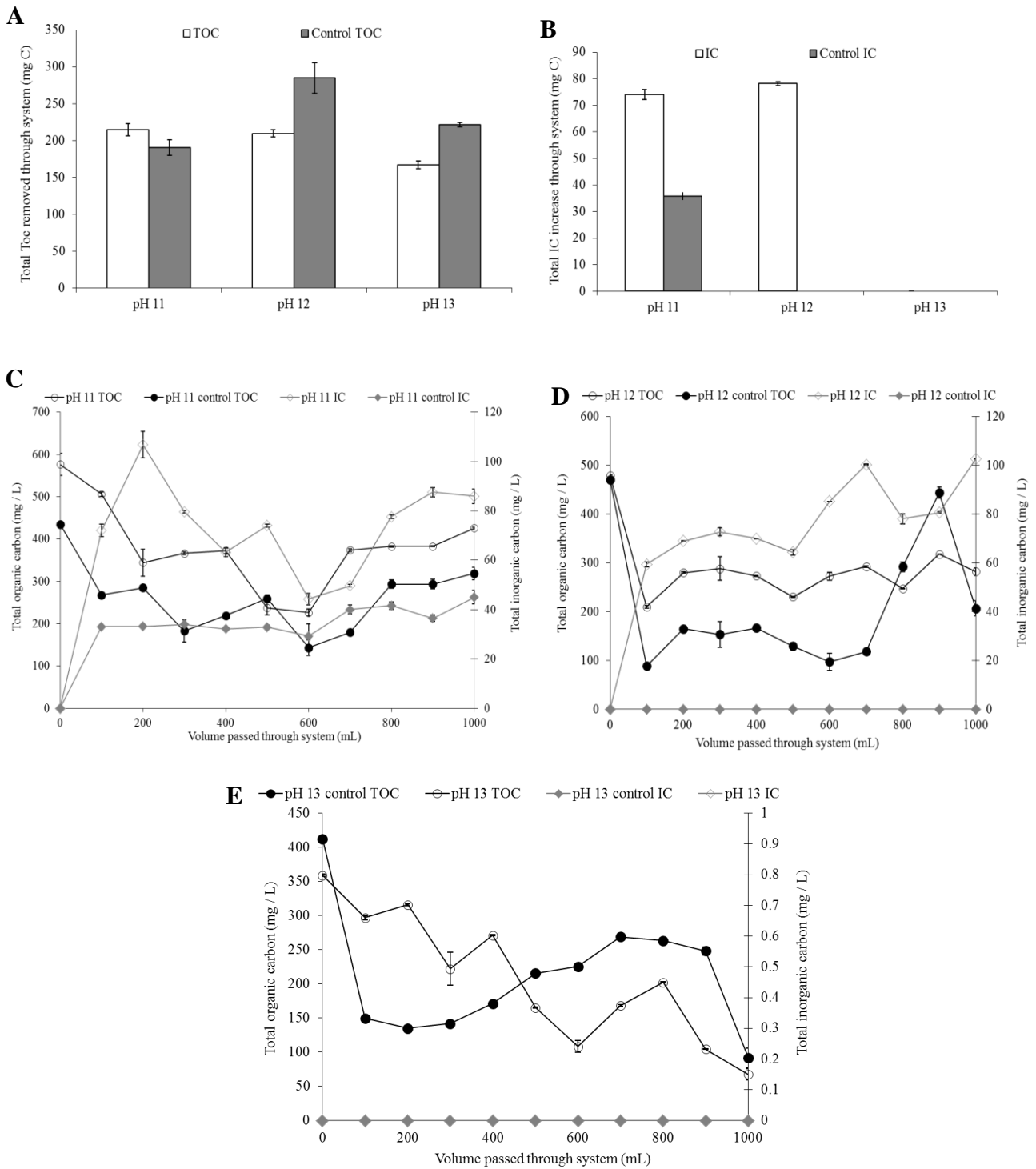


**Figure 7.27: TOC and IC measurements of biofilm and control systems at different hyperalkaline pH values.** [A] Total TOC decrease through both biofilm and control systems at all pH values tested. [B] Total IC increase through both biofilm and control systems at all pH values tested. [C] pH 11 TOC and IC curves for biofilm and control systems. [D] pH 12 curves. [E] pH 13 curves.

Graphite discs were also cast within the NRVB as graphite could potentially represent a surface for colonisation within an ILW-GDF (1). SEM investigation of the discs (Figure 7.28) showed that the biotic exposed surfaces looked different to the control surfaces but did not resemble SEM images of biofilms grown on a graphite anode as reported by Wang *et al* (322). EDS investigation of the biotic exposed graphite surfaces (Figure 7.29) revealed a drop in carbon and a rise in calcium and oxygen when compared to the controls at all pH values possibly indicating the formation of calcium carbonate upon the surface. CLSM investigation of the biotic exposed graphite surfaces (Figure 7.30) revealed a small amount of EPS present upon the graphite surface which had a similar composition to the biofilms formed within the sand column and decreased in surface coverage as the external pH rose. EPS present upon the graphite surface may therefore catalyse the formation of calcium carbonate with dissolved organic carbon released from biofilm materials shown to alter the saturation index of calcium carbonate favouring the precipitation of calcite (323). Reactor graphite is expected to release both  $^{14}\text{CO}_2$  and  $^{14}\text{CO}$  within an ILW-GDF (142). Biofilms forming upon its surface with an autotrophic component such as hydrogenotrophic methanogens could convert these to  $^{14}\text{CH}_4$  which is more likely to migrate through the engineered barriers and into the biosphere (142).

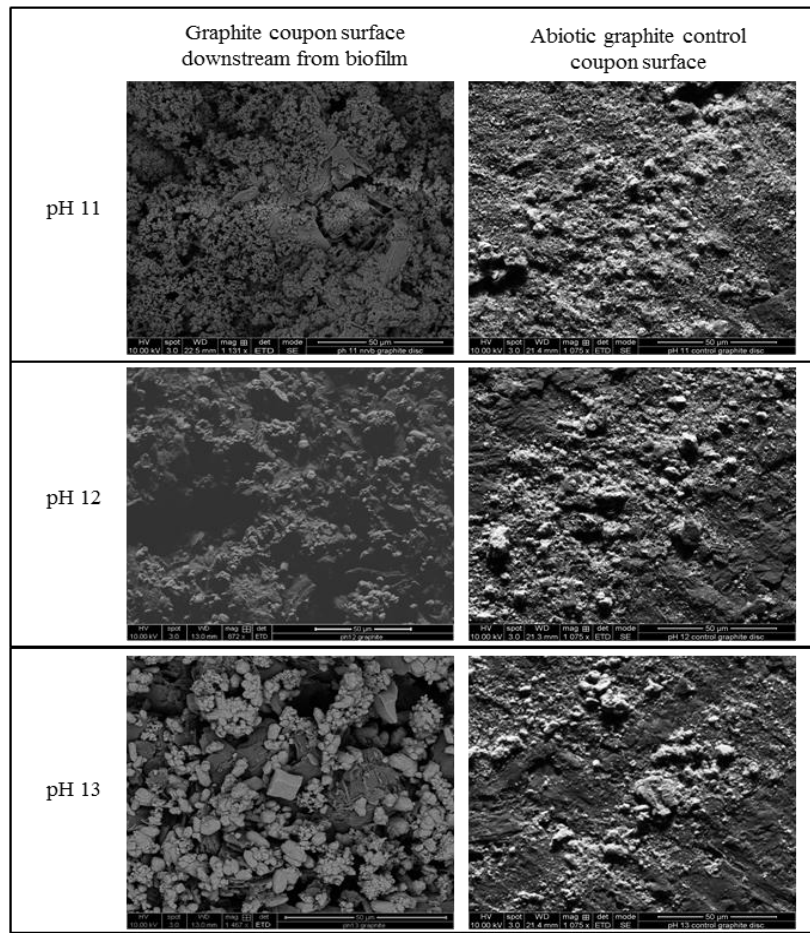
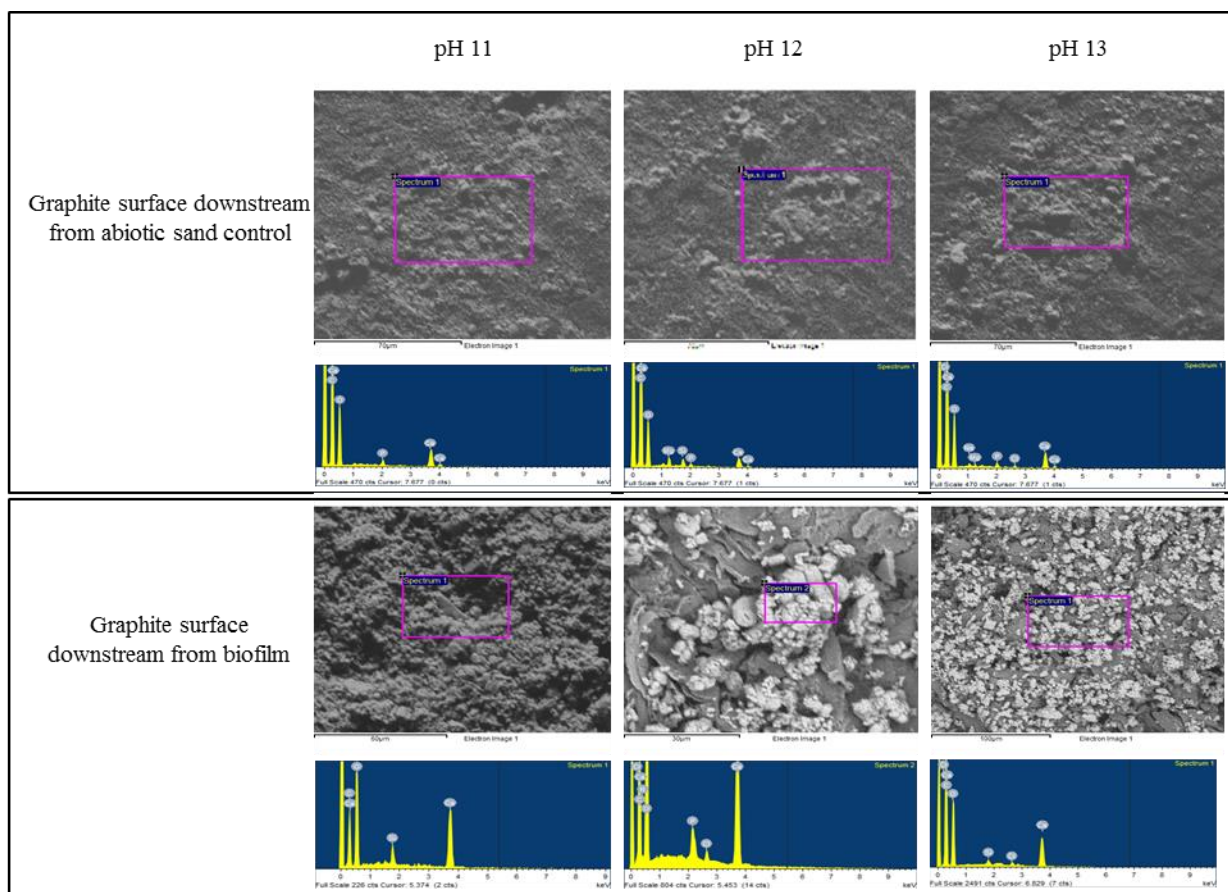


**Figure 7.28: SEM imaging of graphite discs under biofilm and control systems at various hyperalkaline pH values. At all pH values there appears to be an increase in surface roughness of the biofilm exposed surfaces compared to the controls.**



Element	Weight (%)					
	Biofilm exposed graphite surface			Control graphite surface		
	pH 11	pH 12	pH 13	pH 11	pH 12	pH 13
C	12.7	15.6	31.1	52.3	59.8	65.0
O	50.2	49.0	39.3	31.7	30.2	21.0
P	0.0	0.3	0.0	3.9	2.1	1.6
Cl	0.0	1.5	1.8	0.0	1.8	0.0
Si	2.7	0.0	0.6	0.0	0.0	2.0
Ca	34.4	31.5	27.2	12.1	4.9	8.0
N	0.0	2.1	0.0	0.0	0.0	0.0
Na	0.0	0.0	0.0	0.0	0.6	0.0
Mg	0.0	0.0	0.0	0.0	0.6	2.4

**Figure 7.29: EDS investigation into the elemental surface composition of graphite surfaces at different hyperalkaline pH values.** All graphite surfaces exposed to the biofilm system experienced a large increase in calcium and oxygen compared to abiotic controls, possibly indicating carbonate precipitation upon the surface.

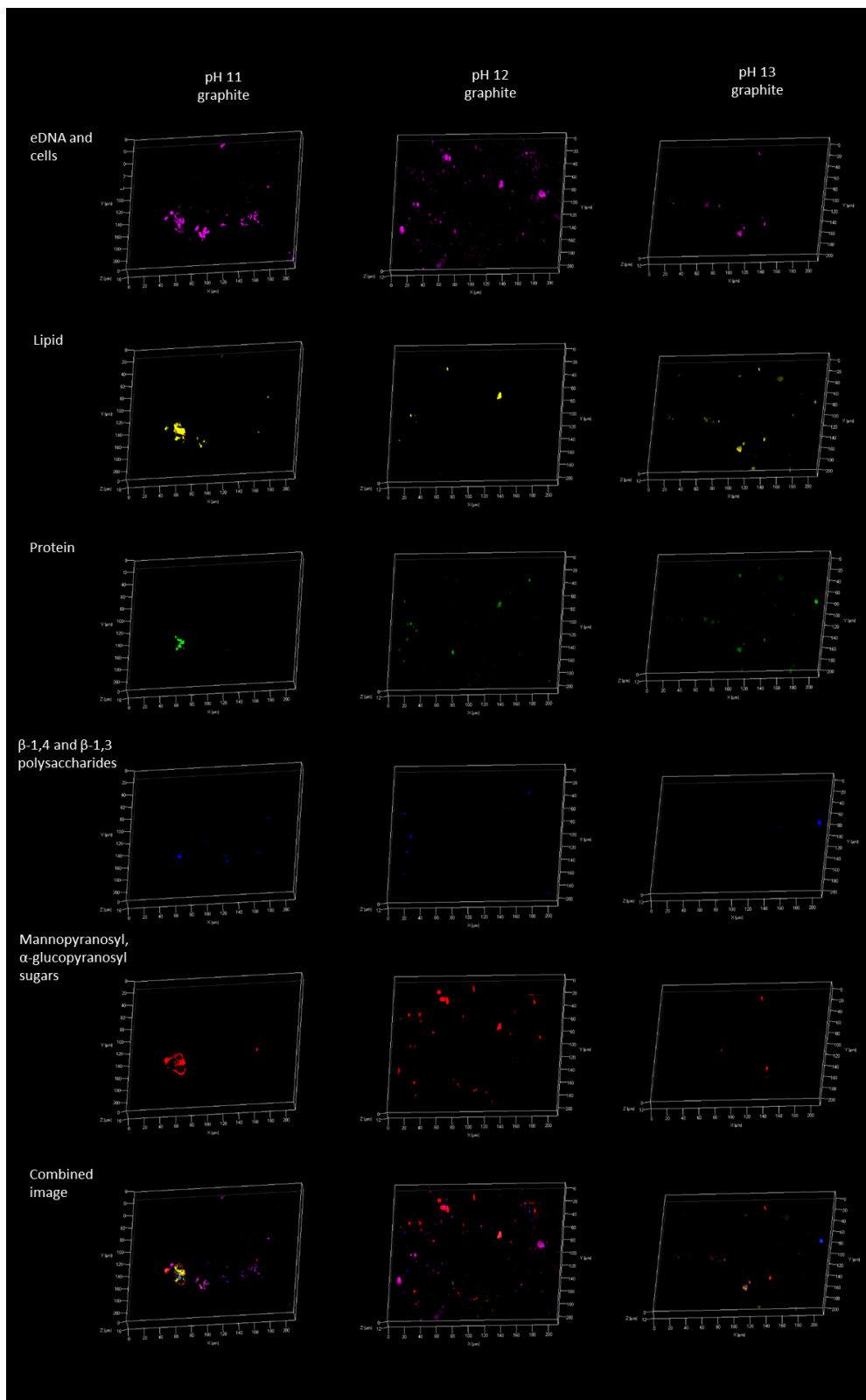


**Figure 7.30: CLSM imaging of biotic exposed graphite discs at different hyperalkaline pH values.** A small amount of EPS material with a similar composition to the sand column biofilms was detected upon the graphite surfaces. The amount of this EPS material decreased as the external pH increased.

Stainless steel discs (Grade 316 and 304) were also cast into the NRVB columns as steel is likely to be present with an ILW-GDF in a range of forms such as canister components, cladding and site equipment (1). SEM investigations of the steel discs (Figure 7.31) revealed the biotic exposed discs to have a different surface morphology to the control steel discs across all pH values. The discs appeared to have developed a rough surface interspersed with crystals with the elemental composition of the surface increasing in oxygen and calcium content across all three pH values (Figure 7.32). Iron was detected in very low levels on these surfaces compared to the controls indicating a thick coverage of possibly calcium carbonate and EPS materials. CLSM of the biotic exposed steel disc surfaces (Figure 7.33) revealed small portions of biofilm with a similar composition to that formed in the sand columns (Figure 7.3) to be present upon the surface at all pH values regardless of the steel grade. Investigation of these biofilms by SEM (Figure 7.34) revealed them to be small irregular shaped structures which became more compact as the external pH increased. These structure possessed sharp mineral like crystals similar to the needle fibre calcite crystal reported by Curry *et al* (324). Steel surfaces are likely to corrode under ILW-GDF and produce hydrogen gas (14), this hydrogen gas could drive autotrophic metabolism within biofilms formed upon the steel surfaces with a range of hydrogen utilising organisms reported under alkaline conditions including methanogens (153, 158) and bacteria such as *Hydrogenophaga* (67).

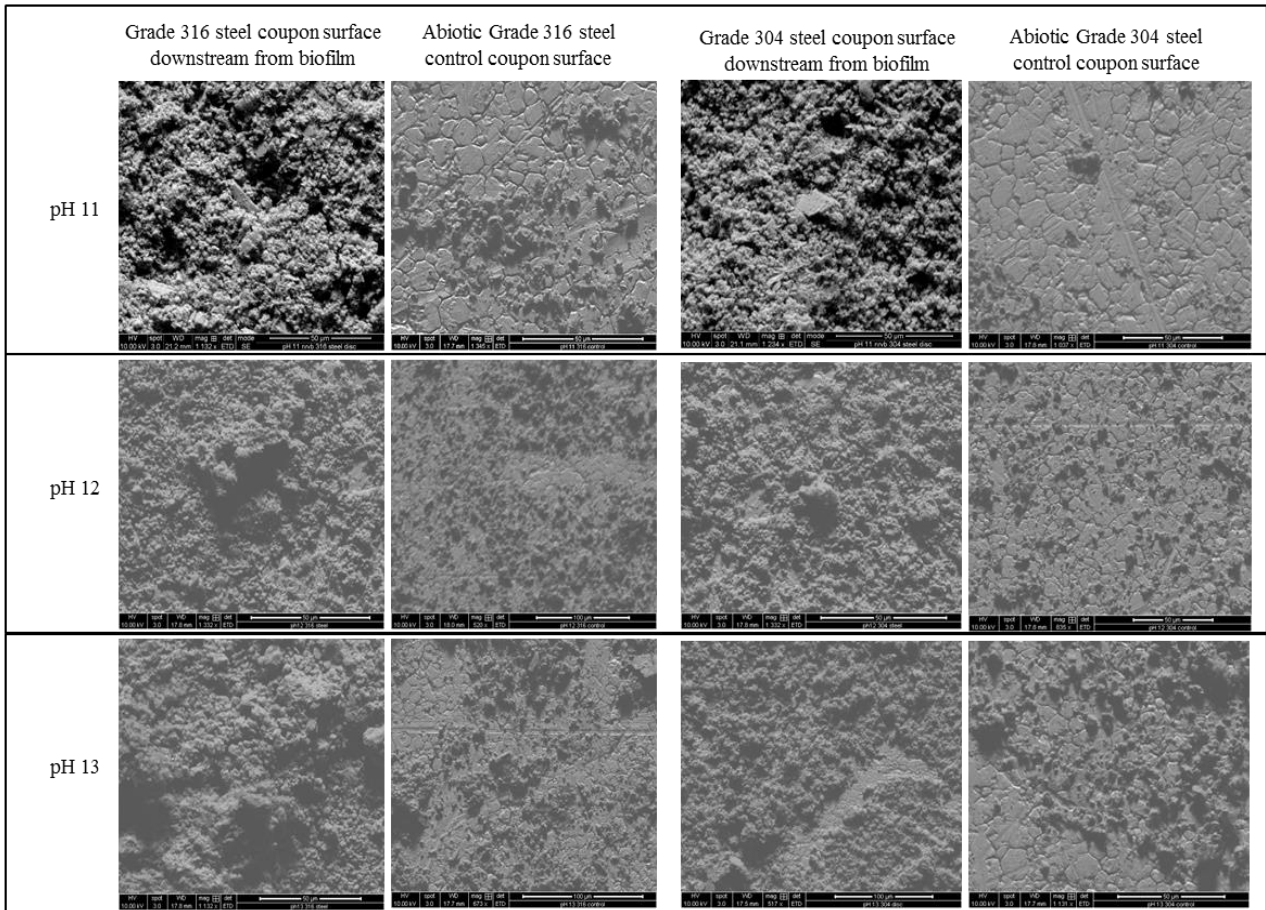
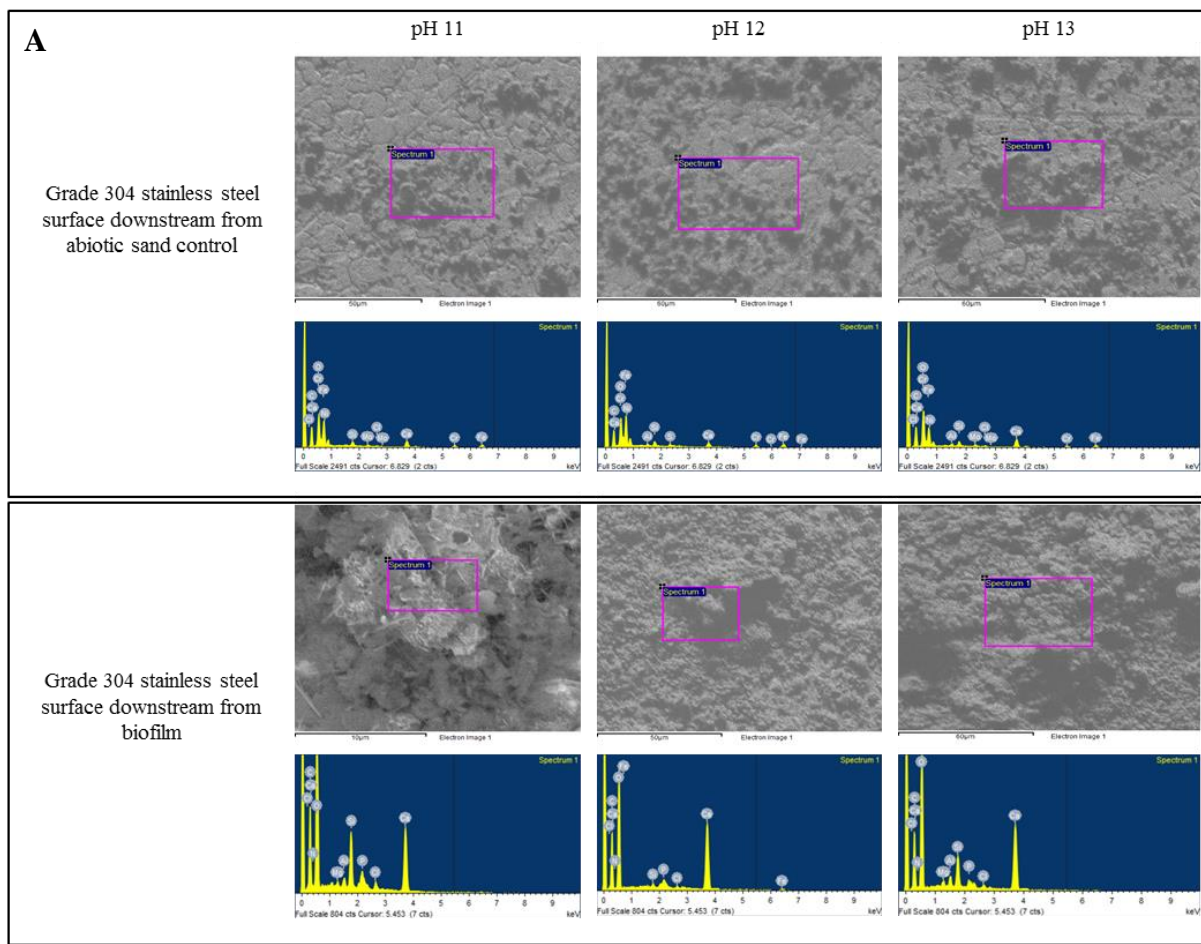
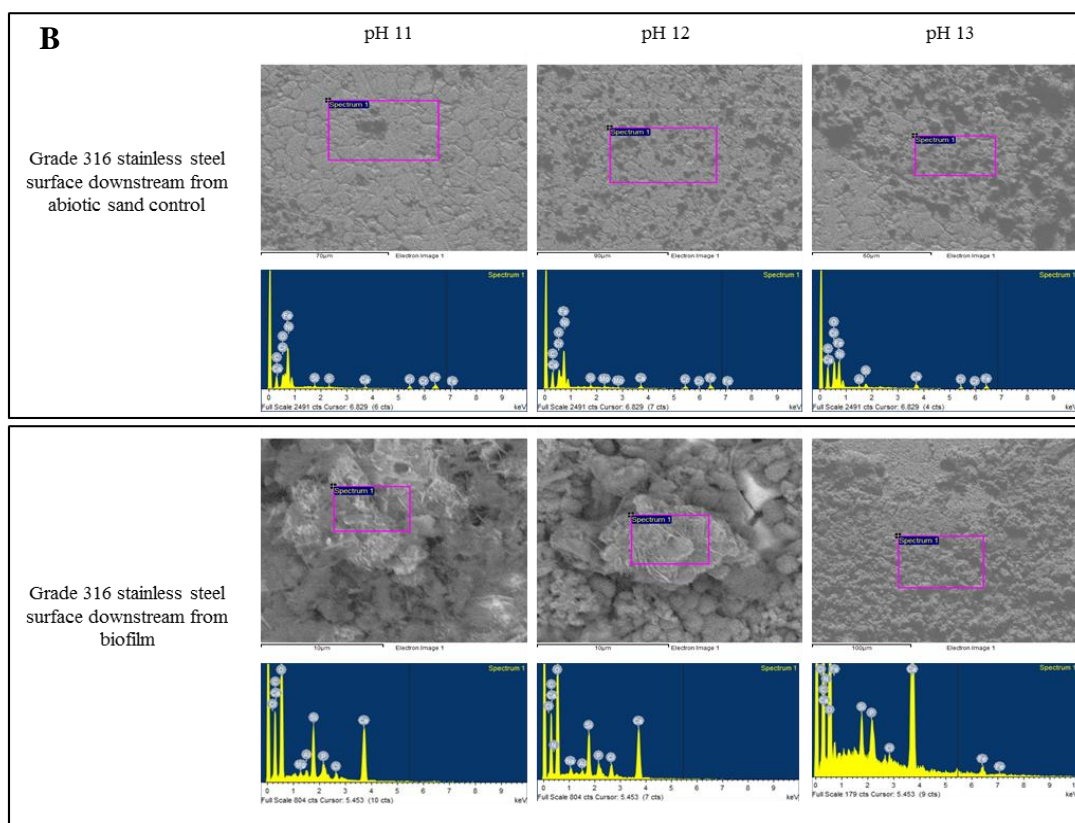


**Figure 7.31: SEM images of steel disc surfaces under different hyperalkaline values.** All steel discs regardless of grade or pH tested showed an increased surface roughness when exposed to biofilm systems. With a greater surface morphology change seen at pH 11 in comparison to the related control surfaces.



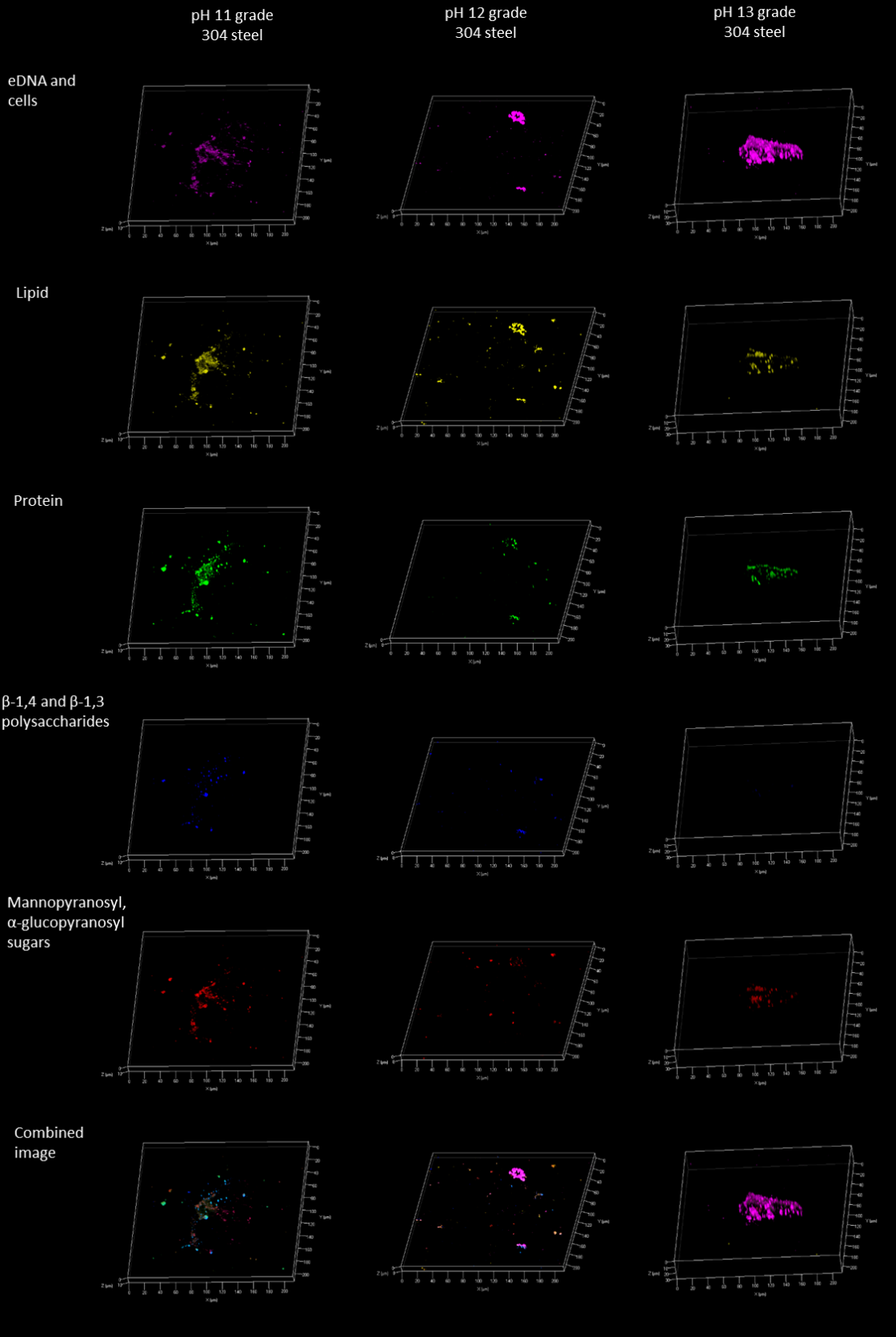
Element	Weight (%)					
	Grade 304 steel					
	Biotic exposed grade 304 steel surface			Control grade 304 steel surface		
	pH 11	pH 12	pH 13	pH 11	pH 12	pH 13
C	14.7	16.9	11.6	7.9	11.0	16.8
O	52.4	46.7	49.1	2.7	5.1	12.5
Al	0.8	0.5	1.2	0.0	0.0	0.3
P	0.8	0.7	0.7	0.0	0.0	0.0
Cl	1.6	3.9	1.1	0.0	0.0	0.0
Si	6.1	6.2	4.3	0.5	0.6	1.4
Ca	23.1	24.2	31.0	1.1	2.5	5.2
N	0.0	0.0	0.0	0.0	0.0	0.0
Na	0.0	0.9	0.0	0.0	0.0	0.0
Mg	0.4	0.0	0.7	0.0	0.0	0.0
Cr	0.0	0.0	0.0	15.1	11.4	0.0
Fe	0.0	0.0	0.0	60.2	56.8	52.8
Ni	0.0	0.0	0.0	12.2	11.0	11.2
Mo	0.0	0.0	0.0	0.0	1.7	0.0



Element	Weight (%)					
	Grade 316 steel					
	Biotic exposed grade 316 steel surface			Control grade 316 steel surface		
	pH 11	pH 12	pH 13	pH 11	pH 12	pH 13
C	14.1	12.5	18.7	13.8	11.9	16.3
O	53.6	46.5	42.8	13.0	10.5	20.2
Al	0.8	0.0	0.0	0.0	0.4	0.7
P	0.4	0.3	1.0	0.0	0.0	0.0
Cl	1.6	0.8	0.6	0.4	0.0	0.7
Si	5.6	0.5	1.5	1.4	1.5	1.8
Ca	23.5	37.4	28.7	5.8	4.1	9.6
N	0.0	0.0	0.0	0.0	0.0	0.0
Na	0.0	0.0	0.0	0.0	0.0	0.0
Mg	0.4	0.0	0.0	0.0	0.0	0.0
Cr	0.0	0.0	0.0	7.9	8.0	0.0
Fe	0.0	2.1	6.8	48.3	52.8	41.6
Ni	0.0	0.0	0.0	7.6	10.2	6.2
Mo	0.0	0.0	0.0	1.8	0.0	2.9

**Figure 7.32: Elemental composition of steel disc surfaces at different hyperalkaline pH values.** All steel discs regardless of grade or pH had an increased calcium and oxygen surface content possibly due to carbonation. [A] Grade 304 stainless steel discs. [B] Grade 316 stainless steel discs

**A**



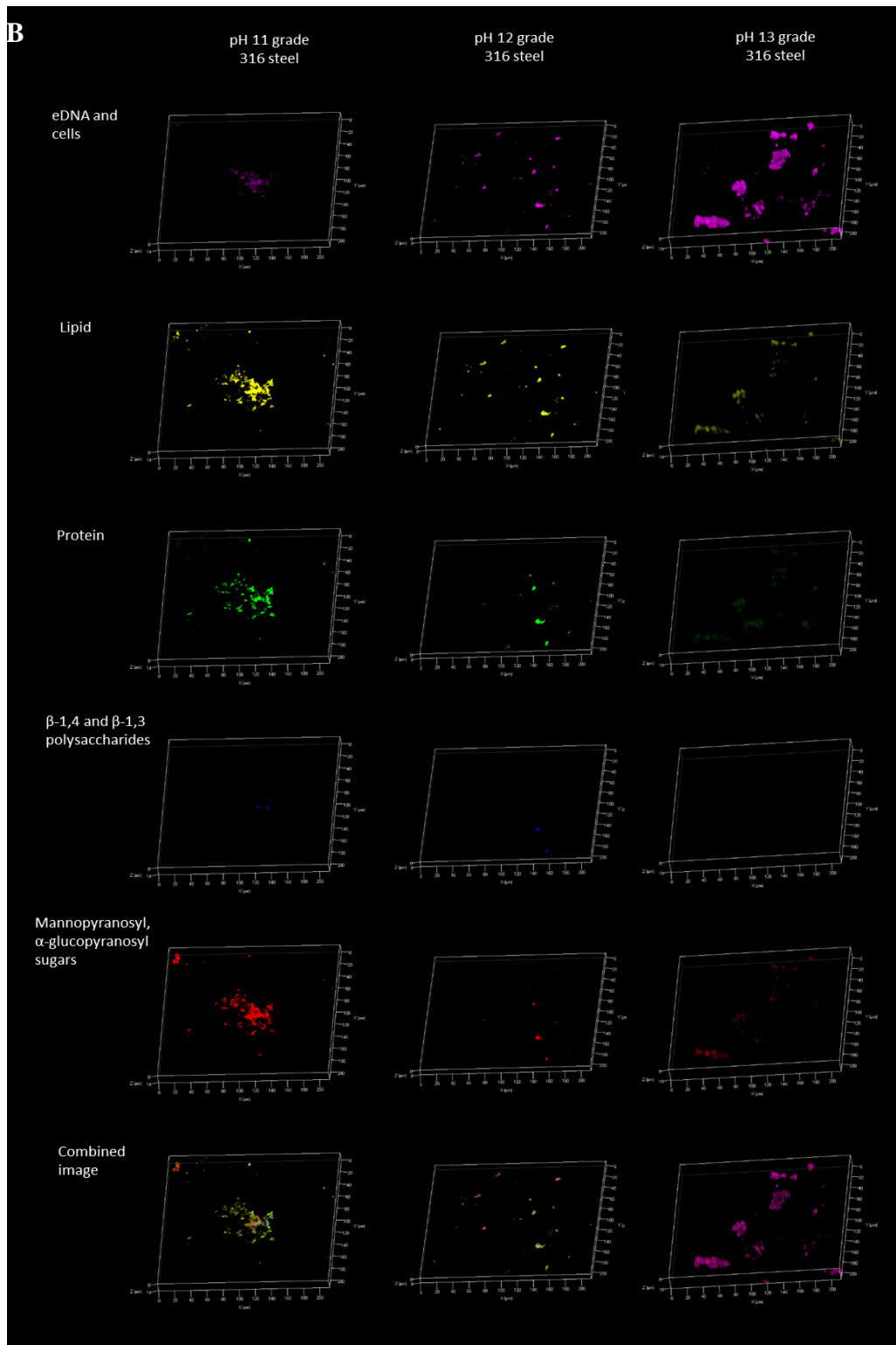


**Figure 7.33: CLSM investigation of steel surfaces exposed to biotic conditions under different hyperalkaline pH values.** There was no difference between the different grades of steel tested with EPS of similar composition to the sand column biofilms detected on the steel surfaces at all pH values tested. [A] Grade 304 stainless steel. [B] Grade 316 stainless steel.

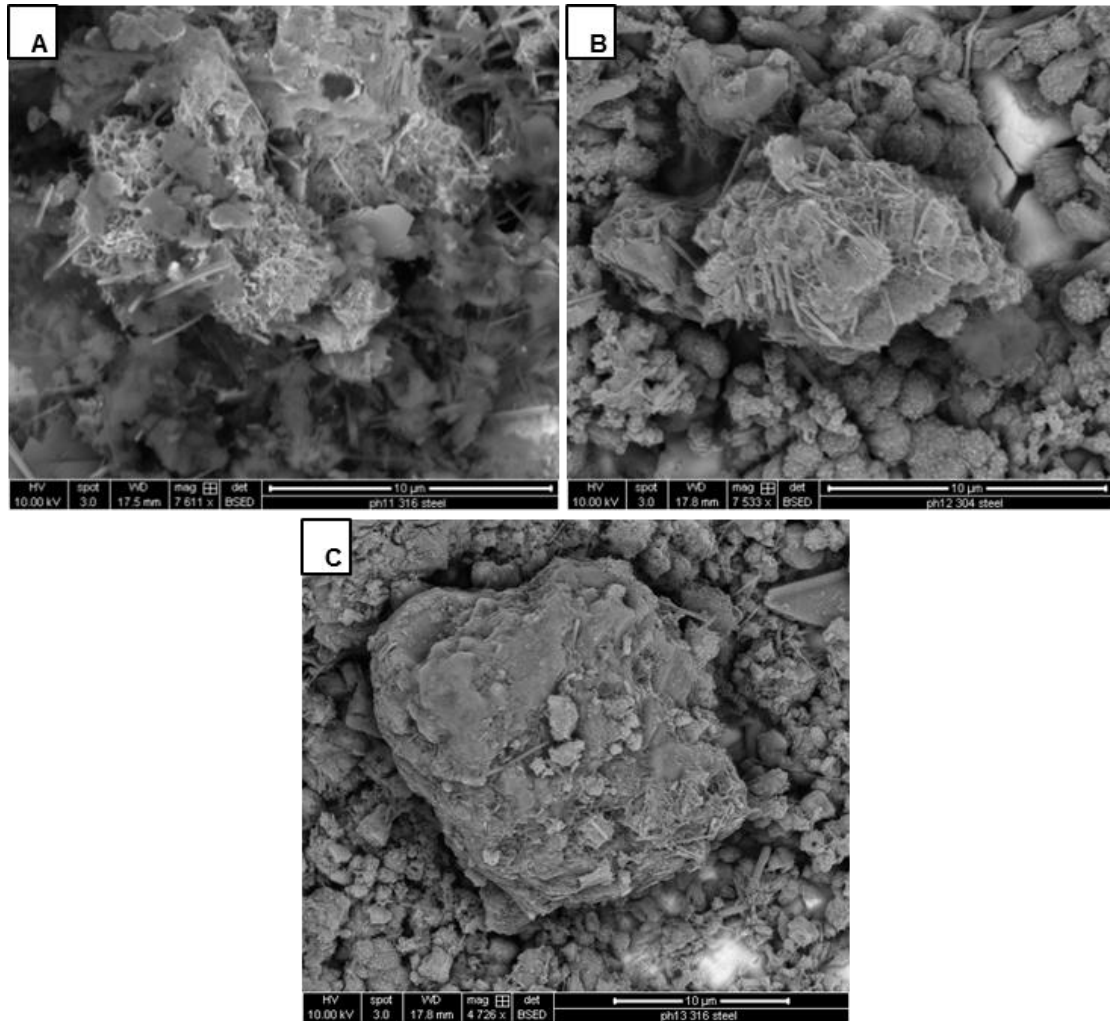


**Figure 7.34: SEM investigation of biofilm formed upon steel disc surfaces at different hyperalkaline pH values.** Suspected EPS aggregates appear to become more compact as the external pH increases. The aggregates possess small sharp needle like crystals and possible bacterial cells of different morphologies. [A] pH 11 surface. [B] pH 12 surface. [C] pH 13 surface.

Although assessed using only a short time scale it appears that biofilms have an ability to impact surfaces relevant to a ILW-GDF. This may be through the formation of biofilm or through carbonation. Carbonation is an important component of radionuclide immobilisation within an ILW-GDF concept (7). The carbonation of NRVB surfaces downstream from a biofilm could possibly alter the ability of NRVB to interact with radionuclides as well decrease its porosity (319). This may lead to issues associated with pressure due to gas build up but could also reduce the migration of potential radionuclides by increasing hydraulic retention (319). Further steel and graphite surfaces may provide sites for colonisation as well releasing nutrient sources such as  $\text{CO}_2$  and  $\text{H}_2$  which could fuel potential microbial metabolisms. The production of  $\text{CH}_4$  from the methanogenic component of the biofilms

reported here could provide a mechanism for the release of  $^{14}\text{C}$  from an ILW-GDF due to its lack of interaction with the engineered and natural barriers (142).

The formation of biofilm within and around an ILW-GDF could alter its long performance by aiding hydraulic retention through the blocking of pore throats (135) and altering the binding properties of host rocks for radionuclides (137). The diverse nature of microbial communities appears to have facilitated the production of a complex EPS. The ability flocs to adhere to the surfaces through the production of eDNA, proteins and polysaccharides (85) clearly enhances biofilm formation on surfaces under these conditions with sloughing or floc production by biofilms representing a transport mechanism for microbes within an ILW-GDF. Chapter 6 showed the ability flocs to survive short term exposure at pH 13 which could increase the probability of low pH niche areas becoming colonised and a biofilm becoming established. Low pH niches could be formed under hyperalkaline conditions through the fermentation of ISA by biofilms with some microbes deep within the EPS possibly entering quiescence and becoming more resistance to environmental stresses (325). Cells entering quiescence could be akin to ‘persister’ like cells as described by Dawson *et al* (326) which could act as a potential seed bank to establish microbial communities once more favourable conditions are attained.

### **7.3 Conclusion**

Thick biofilm was able to form at pH 11 with its formation enhancing the rates of all three forms of ISA degradation. The formation of biofilm at pH 11 also facilitated the production of methane which was likely driven by the fermentation products of ISA. The modification of the internal biofilm environment through both the properties of the EPS and microbial metabolic processes appeared to be a key driver behind these observations.

As the external pH increased, the microbial community shifted to select for alkaliphilic microbial species with large increases in *Dietzia*, *Anaerobranca* and Archaea from the Methanobacteriaceae family. These shifts were accompanied with changes in EPS composition with eDNA increasing in content and protein decreasing. The lipid and carbohydrate components only decreased slightly as the pH increased which may implicate them in the production or buffering of the lower pH within the biofilm. Change in the internal biofilm pH and community composition as the external pH increased may have both impacted the rates of ISA degradation.

Surfaces downstream from the biofilms at all three pH values showed evidence of EPS components similar to the original biofilm formed within the sand column with evidence of

carbonation on all the surfaces exposed to a biological component. The formation of biofilm within a repository could therefore have a wide range of impacts upon the chemistry of the local area. This could include the carbonation of surfaces which would reduce the ability of engineered barriers to interact with radionuclides and lead to the filling of cracks and pores. This could increase hydraulic retention of radionuclides but also lead to issues associated with pressure because of gas build up. The removal of ISA within the near field would impact the migration of radionuclides, however, the production of methane could provide a vector for the transport of  $^{14}\text{C}$  into the biosphere.

Aggregate or flocs leaving the biofilm could have the potential to migrate through an ILW-GDF and colonise other niche areas. Under hyperalkaline conditions the growth rates and metabolic activity of such biofilms are slow but given the times scales of an ILW-GDF may have an impact upon its long term performance.

#### **7.4 Key findings**

- Flocs are able to form biofilm at pH 11 within sand columns, with biofilm formation increasing the rate of ISA degradation of  $\alpha$ -ISA,  $\beta$ -ISA and XISA. Correspondingly methane was able to be produced from the by-products of ISA fermentation.
- Microbes in biofilm were able to survive at pH 12 and 13 with ISA degradation and methane production only impacted when the external pH rose above pH 12.
- A lower pH environment compared the external pH was experienced within the biofilm which was theorised to contribute towards an increased ability of microbes to survive under hyperalkaline conditions. The mechanisms of this ability were most likely due to the properties of the EPS and microbial metabolic processes such as fermentation of both ISA and EPS components.
- Biofilms were able to produce flocs which could colonise NRVB, graphite and steel surfaces at all pH values. These surfaces experienced carbonation when downstream from biofilms.
- NRVB was able to bind all three forms ISA to its surfaces with the amount of ISA bound to its surface increasing with pH.

## **8. ISA degradation under sulphate reducing conditions**

## 8.1 Rationale

The ability of microbes cultured from biofilm formed in-situ at the Buxton, Harpur Hill analogue site to degrade ISA under methanogenic conditions was demonstrated in liquid culture in Chapter 6 and in biofilm systems in Chapter 7. The most likely abundant TEA's under ILW-GDF conditions may include both CO<sub>2</sub> and sulphate due to the depletion of higher energy TEA's as inundating ground water passes through the geosphere's thermodynamic ladder. This chapter will focus on the ability of microbes cultured in-situ at the Buxton analogue site to degrade ISA under sulphate reducing conditions within both liquid and biofilm systems. The aim of this work was to ascertain the ability of these systems to couple the degradation of ISA to the utilisation of sulphate as a TEA with the subsequent production of sulphide. Sulphide could have an impact upon the long term performance of an ILW-GDF through the corrosion of steel surfaces such as those used to contain ILW.

## 8.2 Results and discussion

### 8.2.1 Liquid microcosm investigation under ILW-GDF conditions

Using colonised cotton from the Buxton analogue site (as described in Chapter 6.2.1.) a liquid CDP driven microcosm (Diagram 5.1) was set up as per the methanogenic system described in Chapter 6.2.2. This liquid microcosm was run alongside the methanogenic system (Chapter 6.2.2) under the same conditions but contained sulphate as a potential TEA (see Chapter 5.9.1 for additional details). Over a 2 week feed/waste cycle the microcosm demonstrated the ability to degrade all three forms of ISA with the first order rate constants given in Table 8.1 similar but lower than those reported under methanogenic conditions (Table 6.2). The degradation of ISA resulted in the generation of both acetate and hydrogen as end products (Figure 8.1) indicating a fermentation based pathway as previously reported in Chapters 6 & 7 and by Rout *et al* (80). There was a corresponding decrease in TOC and an increase in IC (Figure 8.1) which were similar in proportion to the methanogenic systems (Figure 6.4D). The system remained alkaline during the testing period (Table 8.2) and control microcosms amended with chloramphenicol (Figure 8.1) showed no ISA removal, acetate or hydrogen generation, changes to TOC or IC and its pH remained stable. Sulphate measurements of the microcosm fluid at the end of the testing period revealed a small portion of sulphate was utilised (6.6 %) with the production of sulphide (Table 8.3).

ISA	Rate (day <sup>-1</sup> )	SE
Alpha	$2.18 \times 10^{-2}$	$6.10 \times 10^{-3}$
Beta	$2.34 \times 10^{-2}$	$7.57 \times 10^{-3}$
Xylo	$3.15 \times 10^{-2}$	$1.87 \times 10^{-2}$

**Table 8.1: First order rate constants for ISA degradation under sulphate reducing conditions.**

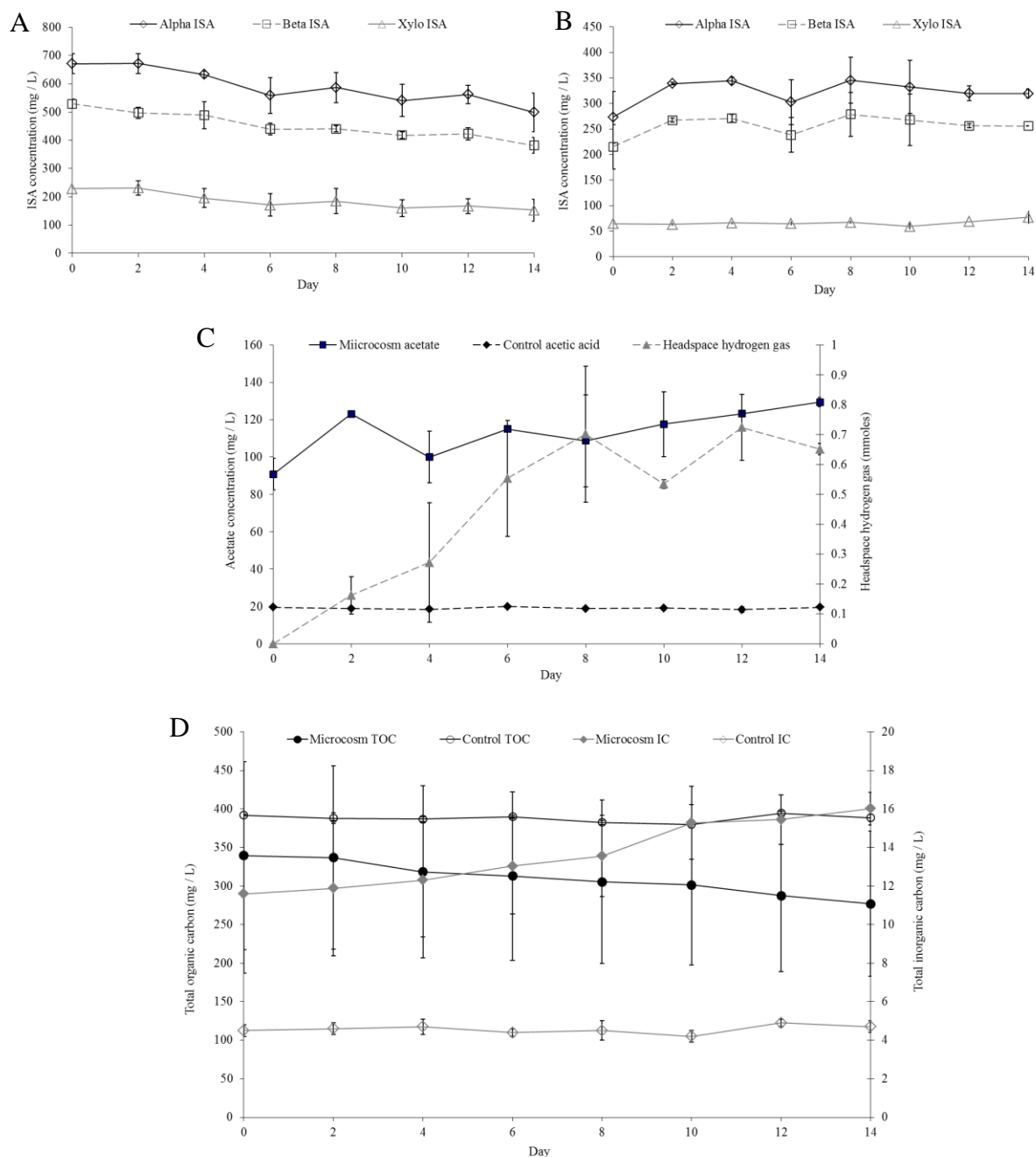


**Figure 8.1: Chemistry of pH 11 sulphate reducing liquid microcosm.** [A] The pH 11 microcosm was able to degrade all three forms of ISA at a similar rate. [B] Controls showed no ISA degradation. [C] The degradation of ISA formed acetate and hydrogen as end products. [D] Microcosm TOC decreased whilst microcosm IC increased due to the fermentation of ISA. Control TOC and IC showed no change.

Microcosm				Control			
Start		Finish		Start		Finish	
Average	SE	Average	SE	Average	SE	Average	SE
11.0	0.0	10.9	0.0	11.0	0.0	11.0	0.0

**Table 8.2: pH measurements of pH 11 sulphate reducing microcosm.** The pH 11 microcosm remained alkaline during the testing the period with the control showing no change in pH.

	(mg L <sup>-1</sup> )		(mMoles)	
	Average	SE	Average	SE
Initial sulphate	617.27	42.50	1.61	0.12
Sulfate degraded	41.01	1.43	0.11	0.00
Control sulfate degraded	0.64	0.79	0.00	0.00
Sulfide produced	6.79	4.50	0.05	0.03
Control sulfide	0.00	0.00	0.00	0.00

**Table 8.3: Sulphate and sulphide measurements of pH 11 sulphate reducing microcosm.**

A small amount of sulfate was degraded with a corresponding production of sulphide.

Controls showed no sulphate removal or sulphide generation.

Investigation into the morphology of the pH 11 ISA degrading microcosm under sulphate reducing conditions (Figure 8.2) revealed the microbes to be existing in flocs of EPS as per the fermentative/methanogenic microcosms reported in Chapter 6. Fluorescence microscopy revealed these flocs to possess a similar polysaccharides and eDNA matrix (Figure 8.2C) in comparison to methanogenic flocs (Figure 6.7) with digestion of the eDNA component causing the sulphate reducing system flocs to also lose structural integrity (Figure 8.2D). SEM investigation into the sulphate reducing system flocs showed areas of possible mineral precipitate (Figure 8.2B) with EDS (Figure 8.3) investigation into the flocs revealing them to possess a high calcium, carbon and oxygen content indicating possible calcium carbonate formation. Sulfur was also detected and could indicate that sulphate was becoming incorporated into or sorbed onto the EPS materials (85). The dry weight and volatile solid content of the flocs reflected these finding with 71.2 % of the dry weight consisting of inorganic matter (Table 8.4).

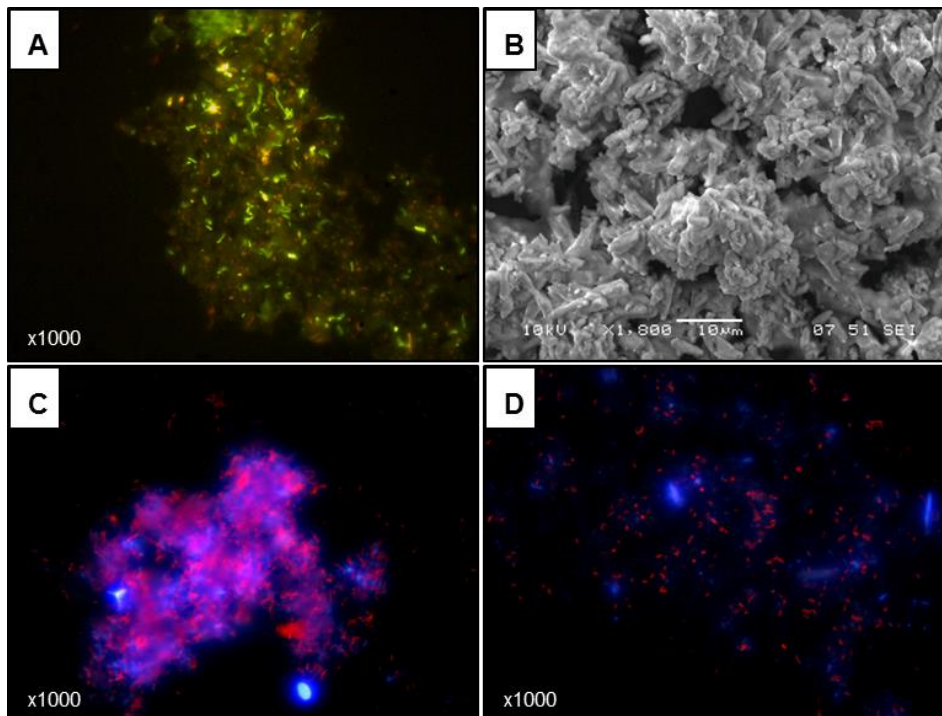


**Figure 8.2: Microscopy investigation into the morphology of sulphate reducing microcosm.** [A] Live/dead stain of flocs showing range of cell morphologies (alive cells (green), dead cells (red)). [B] SEM image of flocs showing aggregates of EPS, cells and precipitate. [C] Ethidium bromide and Calcofluor white stain of bacterial floc showing individual cells and eDNA (red) and extracellular polysaccharides (blue). [D] DNase digest of flocs stained with ethidium bromide and Calcofluor white. Treatment with DNase caused flocs to lose structural integrity.

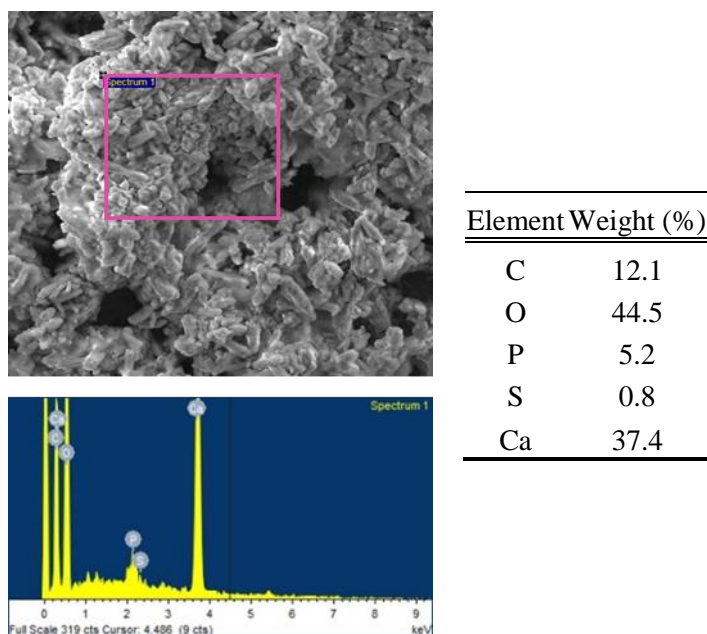


**Figure 8.3: Elemental composition of pH 11 sulphate reducing system flocs.** Flocs had a composition of carbon, oxygen, calcium and small amount of sulfur. This may indicate calcium carbonate precipitate and the sorption of sulphate to the EPS.

Floc dry weight (%)	Dry weight volatile solids (%)	Dry weight ash content (%)	Dry weight per L (g DW L <sup>-1</sup> )	Volatile solids per L (g VS L <sup>-1</sup> )
2.08	29.81	70.19	20.80	6.20

**Table 8.4 : Dry weight, volatile solids and inorganic matter of sulphate reducing system flocs.**

Using a micro pH electrode, a pH profile through a floc within the sulphate reducing system revealed a lower pH micro-site within the interior of the floc which reached a minimum value of pH 10.5 (Figure 8.4). This value was similar to that reported within methanogenic flocs (Figure 6.17A) and could be attributed either to the production of metabolic acids through the fermentation of ISA (47, 51) or through the properties of the EPS components (99). Calculations by Bethke *et al* (38) suggest that acetate driven rather than hydrogen driven sulphate reduction is possible under hyperalkaline conditions, however, the usable energy this process generates decreases as the external pH increases. Work by Rizoulis *et al* (60) using sediments from the Hapur Hill, Buxton site with acetate and lactate as electron donors suggest sulphate reduction was not possible above pH 10. Studies into the sulphur cycle of different hyperalkaline soda lakes, however, suggest that sulphate reduction may be possible above pH 10 (63, 165) with biofilms operating at pH 10.2 able to produce sulphide from sulphate within the alkaline waters at a Danish district heating plant (169). The low pH microsite and syntrophic interactions between microbes within the flocs may offer a micro-niche site for sulphate reduction to occur within this system.

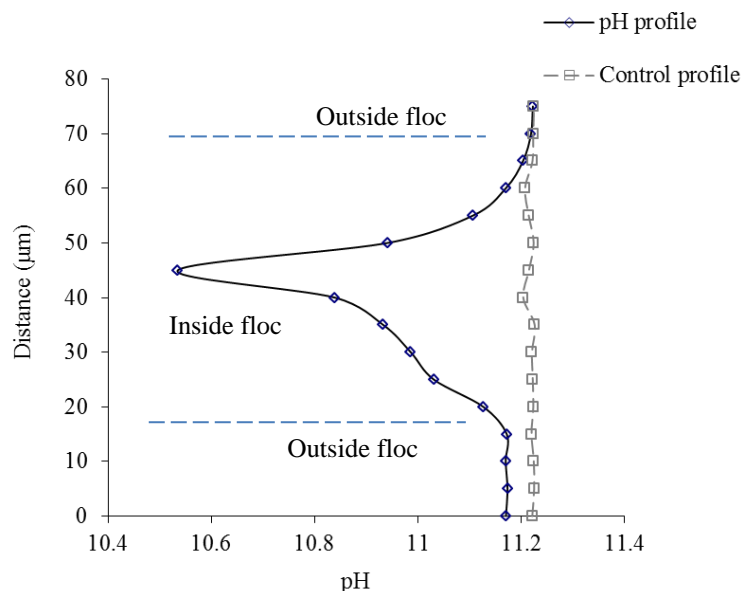


**Figure 8.4: pH profile through sulphate reducing floc at pH 11.** The pH experienced a sharp drop within the interior of the floc. The pH values reported here may be lower than measured as the method is limited by the resolution of the electrode. Control profiles showed no major pH changes.

Extraction of the EPS components (Figure 8.5) revealed the sulphate reducing system flocs to have a complex EPS composition with EDTA treatment removing more eDNA and protein and ethanol treatment removing more carbohydrate and lipid. This could indicate that under sulphate reducing conditions the formation of EPS is stabilised by both hydrophobic and ionic interactions. FTIR analysis of the extracted EPS (Figure 8.6) reflected this complex composition with a wide range of groups including carboxyl, amine and phosphoric groups and is similar to the FTIR results of floc EPS from fermentative/methanogenic systems (Figure 6.13). Under the alkaline pH these groups could contribute a negative charge to the EPS due to the deprotonation of these components (287) which could bind cations such as  $\text{Ca}^{2+}$  (102). The binding of calcium by components such as eDNA is thermodynamically favourable and assists in bacterial aggregation through acid-base interactions and cationic bridging (102). The loss of structural integrity of the floc through DNase treatment (Figure 8.2D) and the extraction of eDNA by EDTA treatment (Figure 8.5) indicate eDNA plays a key role in biofilm formation and development through interactions with calcium. Components such as lipids and carbohydrates can increase the hydrophobicity of the EPS which could reduce wetting (85, 327) and assist in maintaining the internal pH of the floc. Both components may also possess acidic subunits with uronic acids often present within polysaccharides (296) and acidic phospholipids associated with some alkaliphilic bacteria (53). Monomer analysis of the polysaccharide component of these flocs (Table 8.5) revealed the composition to be similar to alkaliphilic biofilms extracted from the surfaces of calcite (297) and those reported from floc and biofilm communities under methanogenic hyperalkaline conditions in Chapters 6 & 7 (Tables 6.7 & 7.7). The polysaccharide component in this instance had a total uronic acid content of 10.25 %, was mannose dominated (42.27%) and lacked some of the monomer units which were in a smaller composition within the methanogenic floc EPS (Table 6.7.). These included arabinose, trehalose, rhamnose and xylose.

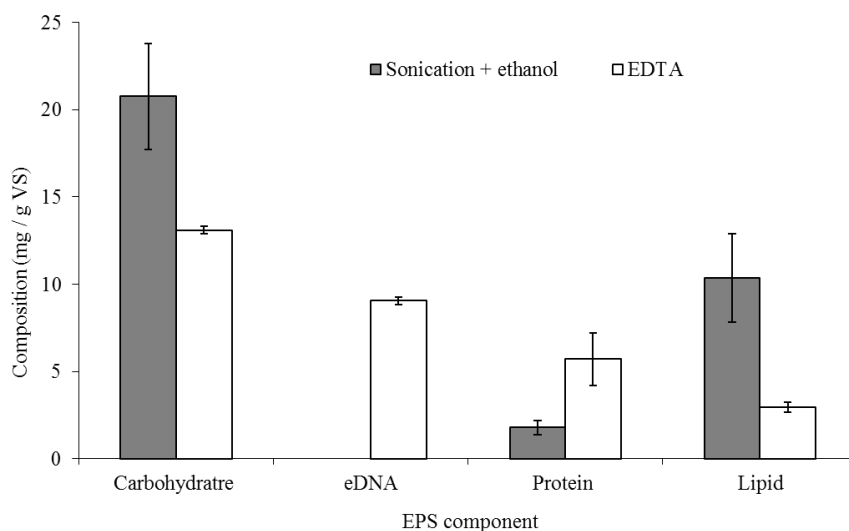


**Figure 8.5: Extraction of EPS components from flocs under hyperalkaline sulphate reducing conditions.** Sonication and ethanol treatment were able to extract more carbohydrate and lipids whereas EDTA treatment extracted more eDNA and protein.

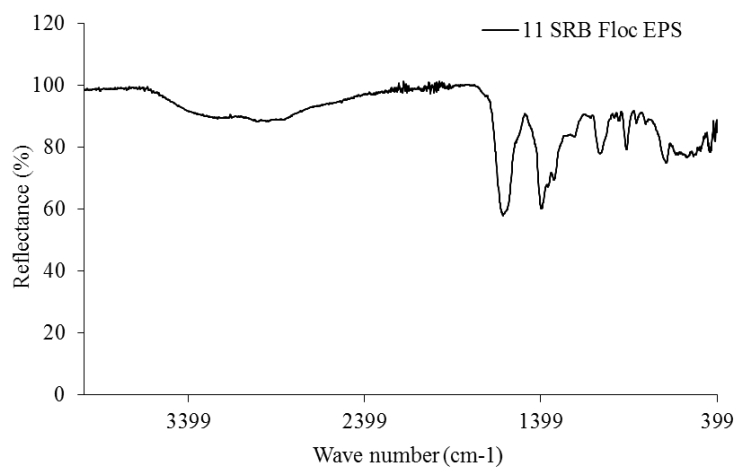


**Figure 8.6: FTIR of EPS extracted from flocs under hyperalkaline sulphate reducing conditions.** The profile is similar to EPS extracted from methanogenic floc communities and biofilms under hyperalkaline conditions with a range of functional groups.

Monomer unit	Composition (%)
Mannose	42.27
Ribose	21.34
Ribitol	19.50
Galacturonic	9.22
Galactose	3.16
Glucose	3.12
Glucuronic	1.04
Fucose	0.35

**Table 8.5: Monomer analysis of polysaccharide component extracted from floc EPS under sulphate reducing hyperalkaline conditions.** The monomers are dominated by mannose with a uronic acid component which may confer acidity to the EPS and protect against the external pH.

### 8.2.2 Free drift study.

Despite 2 years under a 2 weekly feed/waste cycle the pH 11 microcosm under sulphate reducing conditions still demonstrated sulphate reduction and sulphide production albeit at a very low concentration. Under ILW-GDF conditions low pH niches may form through chemical and biological processes. The lowering of the pH under these conditions with sulphate present may release the constraints upon sulphate reduction. By allowing the pH to drift (i.e. acidify due to ISA fermentation) the ability of the microbes present within the subculture microcosm to reduce sulphate under the above circumstances was assessed. Further information regarding the details and set-up of this work can be found in Section 5.9.4.

All three forms of ISA were able to be degraded fully over the 26 day testing period by the sulphate reducing subculture microcosms (Figure 8.7). The subculture microcosms amended with molybdenum (Figure 8.7) which inhibits sulphate uptake (260) showed a similar amount of ISA degradation to the sulphate reduction subculture microcosms up to day 16. After this period the sulphate reduction microcosms with no molybdenum quickly degraded all the remaining ISA in a period of 4 - 6 days. This increase in degradation of ISA resulted in a large drop in pH and an increase in acetate (Figure 8.8AB). Up to day 16 both the sulphate reducing subcultures and the molybdenum amended subcultures showed a steady rate of ISA degradation of all three forms of ISA (Figure 8.7) indicating that the degradation was through a fermentation pathway which sulphate did not influence.

Acetate was produced as the end product of ISA degradation and accumulated within the molybdenum amended reactor following the trend of the ISA degradation (Figure 8.8B). Within the sulphate reducing subculture acetate remained at a low level below that of the

molybdenum treated sub-cultures until day 16 indicating its removal through microbial action. During this period the sulphate concentration decreased within the subculture (Figure 8.8C) and aqueous sulfide concentration increased within the system (Figure 8.8D). The sulphate concentration appeared to reach a plateau after day 10, however, sulfide continued to rise. This may be related to turnover of EPS materials which had sulphate bound to them with its uptake onto EPS and its liberation from EPS masking the true sulphate concentrations. Investigations into the morphology of the subcultures at different time points throughout the testing period (Figure 8.9) would appear to support that the turnover of EPS substances was occurring as the external pH value decreased. Both the protein and polysaccharides components decreased as the number of cells increased, with a larger increase in cells and EPS turnover seen in the sulphate reducing subcultures compared to the molybdenum treated subcultures (Figure 8.9). After day 22 the sulphate levels within the sulphate reducing microcosm dropped sharply and the increased acetate levels generated from the degradation of ISA were reduced to zero, indicating sulphate reduction. The pH at this point was neutral at  $\text{pH } 7.7 \pm 0.1$ . The actions of acetotrophic methanogens could have resulted in the removal of acetate, however, if this process was occurring then it was at a low rate as seen by its lack of impact upon acetate accumulation within the molybdenum treated subcultures (Figure 8.8B). Gas headspace composition could not be assessed due to the nature of the experiment; this was due to gassing of the headspace with nitrogen in order to access the reaction vessel to measure the pH.

TOC measurements showed organic carbon to remain fairly stable throughout the experiment (Figure 8.8E) and could be related to release of organic carbon from the turnover of EPS substances masking the TOC removed by microbial processes. IC increased within the molybdenum treated subcultures but remained stable within the sulphate reducing subcultures (Figure 8.8F). This may be due to the precipitation of calcium carbonate facilitated by sulphate reduction under the initial alkaline phases (244, 289) and the loss of carbon through carbon dioxide generation as the pH values became more neutral. Molybdenum treated subcultures showed a small reduction of sulphate which could be related to sorption onto freshly made EPS as no sulphide was produced (Figure 8.8C). Chloramphenicol controls failed to show evidence of ISA degradation, sulphate reduction, sulphide production, acetate production or removal and showed no changes in TOC or IC (Figure 8.8).

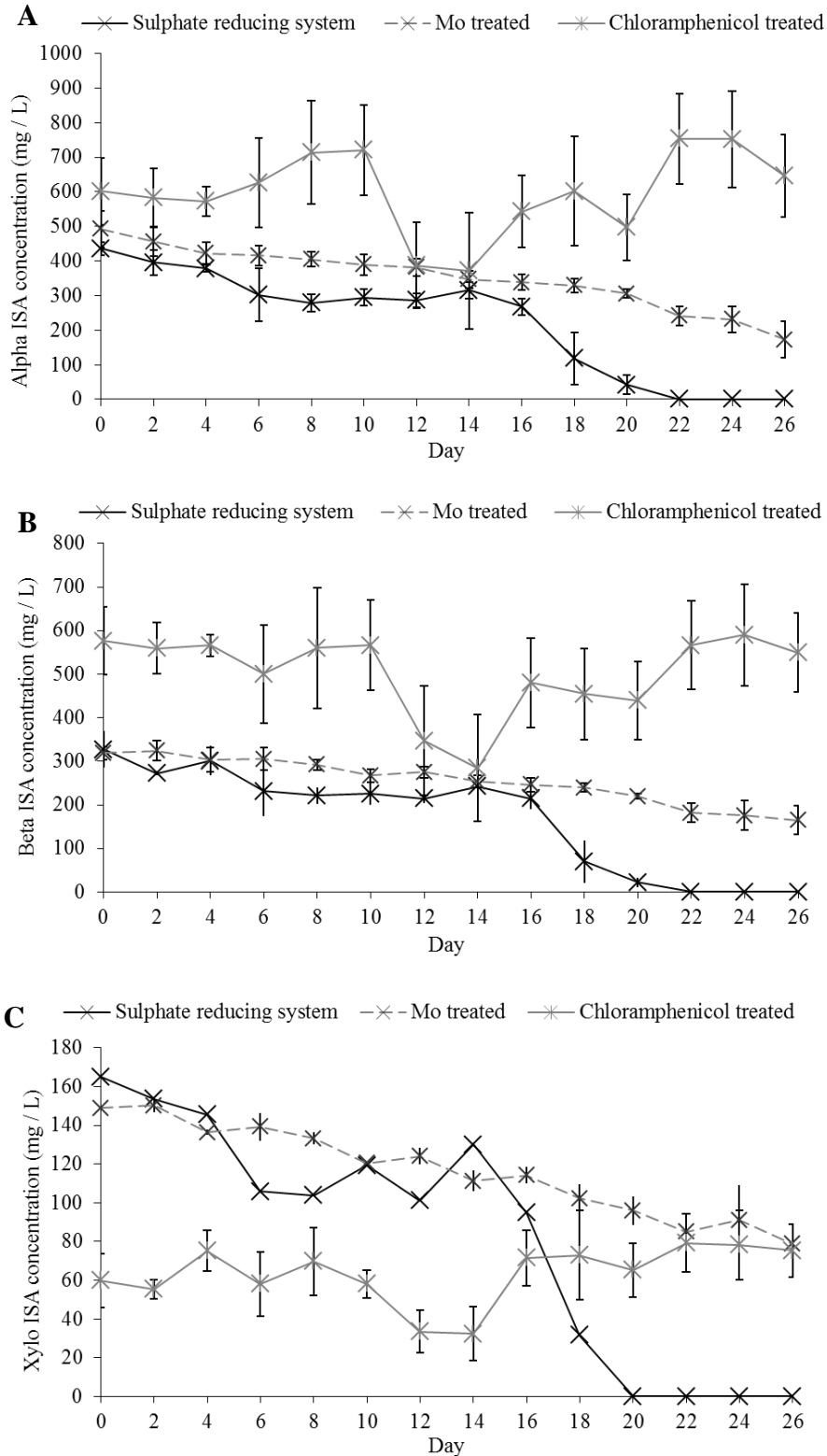


**Figure 8.7: ISA degradation within free drift systems.** The sulphate reducing system was able to degrade all three forms of ISA after day 20. The molybdenum treated system was able to degrade all three forms of ISA but not to the same extent of the sulphate reducing system. Chloramphenicol controls showed no obvious signs of ISA degradation. [A]  $\alpha$ -ISA. [B]  $\beta$ -ISA. [C] XISA.

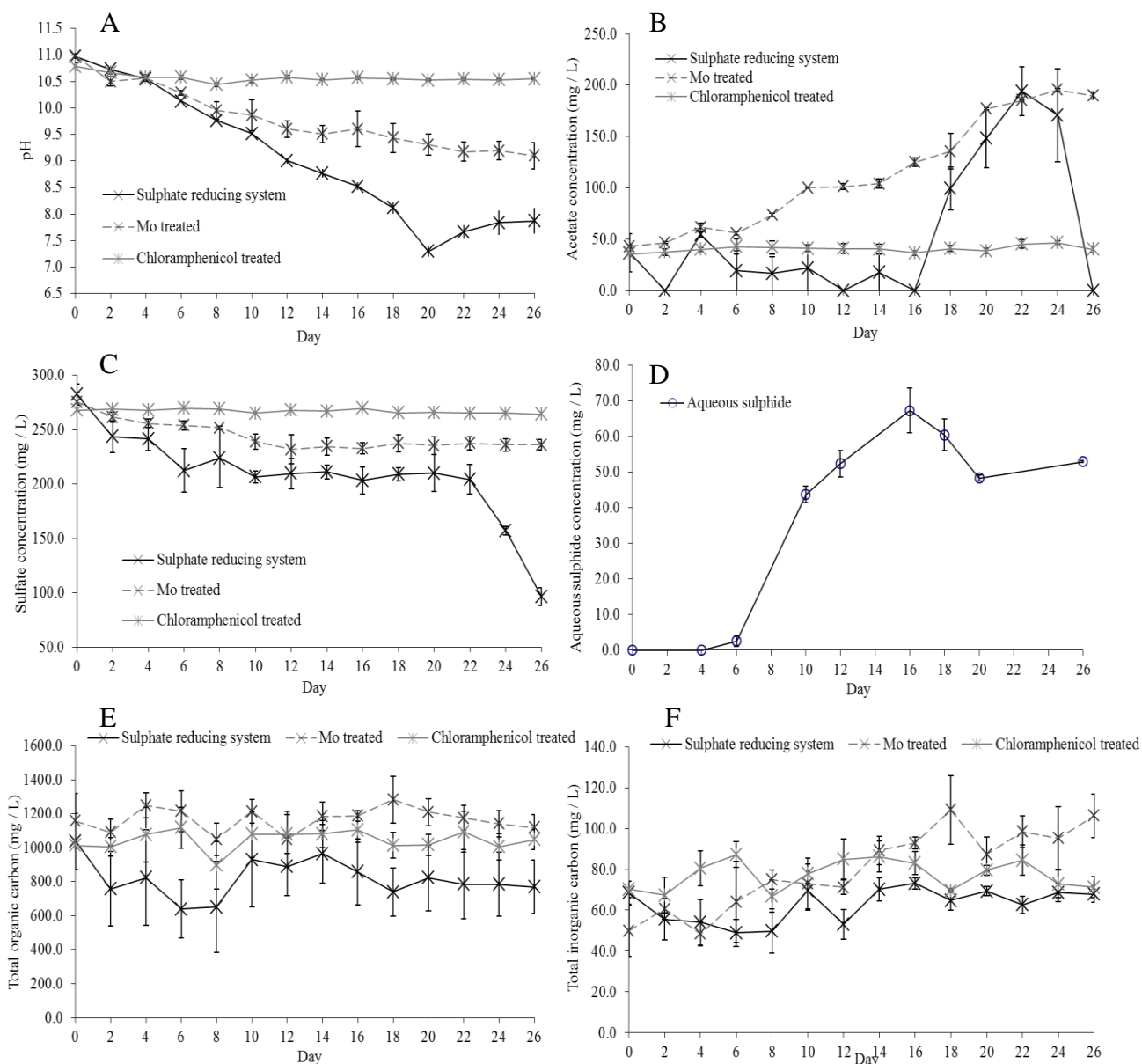


**Figure 8.8: Chemistry of free drift systems.** [A] The microcosm pH fell as ISA was fermented in both sulphate reducing and molybdenum treated subcultures. [B] Acetate was produced as an end product of ISA fermentation in both sulphate reducing and molybdenum treated subcultures. [C] Sulphate was predominantly utilised within the sulphate reducing subcultures and experienced a large drop in concentration as the pH became neutral. [D] Aqueous sulphide was produced as sulphate was reduced and was only detected within the sulphate reduction subcultures. [E] TOC measurements of all three different subculture systems. [F] TIC measurements of all three different subculture systems.

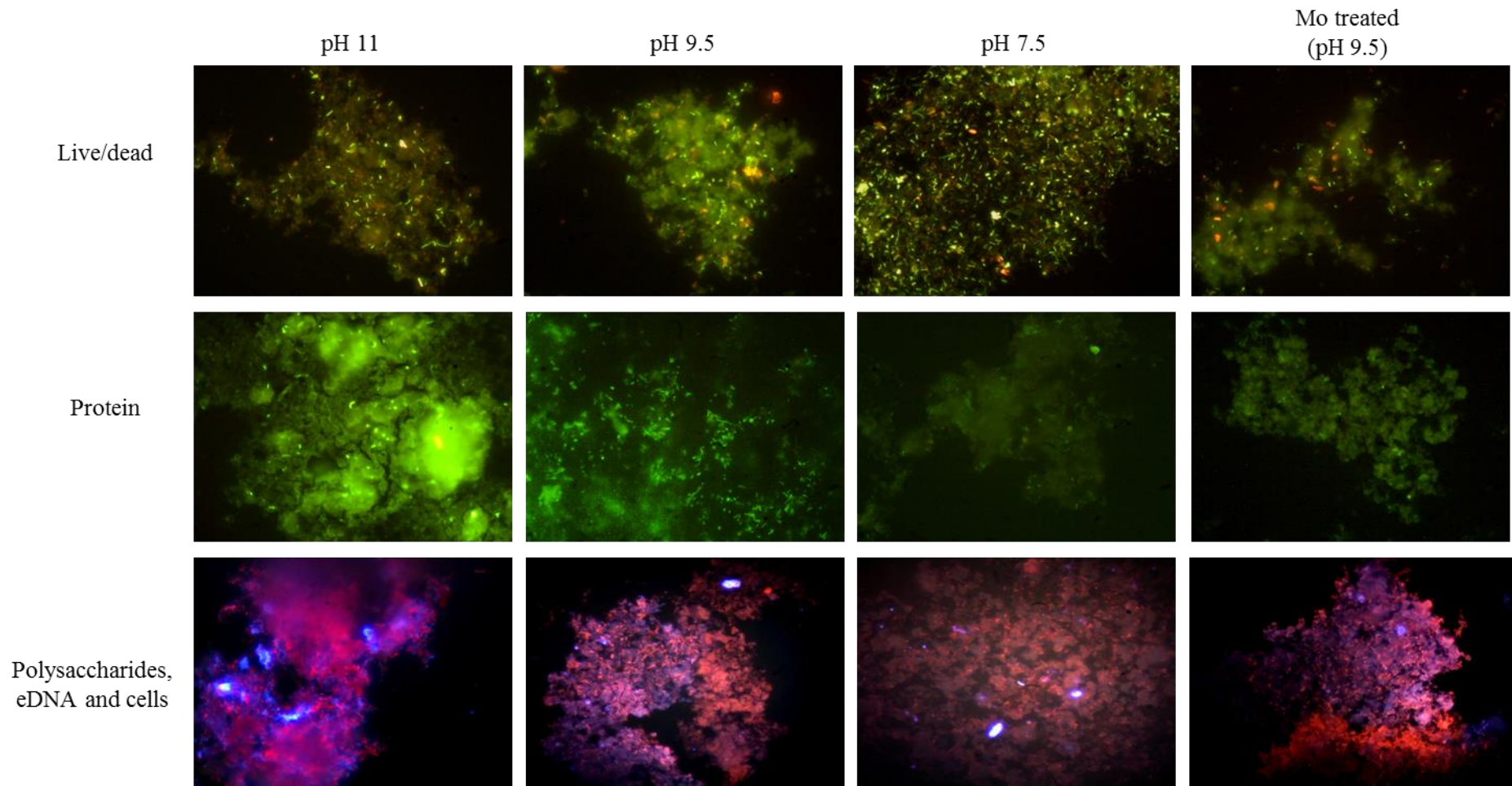


**Figure 8.9: Morphology of the free drift subcultures.** The morphology of the sulphate reducing subculture system is shown at pH 11, pH 9.5 and pH 7.5. The live/dead staining shows an increase in cells as the pH becomes more neutral with a reduction in the protein and polysaccharide components. The morphology of the subculture treated with molybdenum is viewed the end of the experiment at approximately pH 9.5. The morphology of the molybdenum treated flocs is similar to the sulphate reducing pH 9.5 morphology (all images are at x1000 magnification).

Comparison of sulphate, sulphide and acetate with theoretical values is shown in Figure 8.10 and is based on the assumptions that all sulphate utilised is coupled to acetate oxidation with subsequent sulphide generation (*161*) and all ISA degraded goes to acetate. From the comparison of the acetate levels it is clear that a large proportion of ISA was used for biomass generation with carbon flow calculation estimating 71.6 % of the ISA carbon flowing to biomass. The theoretical sulphide showed a similar trend to the measured sulphide indicating that acetate was removed through sulphate reduction.

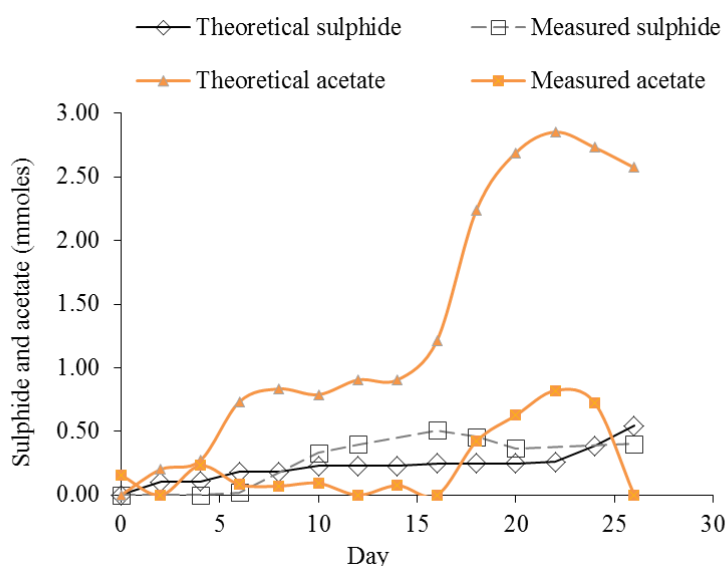


**Figure 8.10: Comparison of theoretical and system acetate and sulphide within sulphate reducing free drift system.** The theoretical values are based on the assumptions that all sulphate utilised is coupled to acetate oxidation with sulphide generation and all ISA degraded goes to acetate. The theoretical acetate is higher than the measured acetate suggesting a portion of ISA degradation goes to biomass.

Using qPCR methods the number of *dsrA* genes and transcripts were determined at a range of pH values (Figure 8.11). As the pH decreased from pH 11 the number of *dsrA* gene copies increased slowly from  $5.1 \pm 0.1$  log gene copy  $\mu\text{L template}^{-1}$  to  $5.8 \pm 0.1$  log gene copy  $\mu\text{L template}^{-1}$  (Figure 8.11B). Transcripts of the *dsrA* gene also increased as the pH decreased starting at  $3.4 \pm 0.1$  log gene copy  $\mu\text{L template}^{-1}$  at pH 11 and increasing to  $6.4 \pm 0.4$  log gene copy  $\mu\text{L template}^{-1}$  at pH 7.5. The qPCR approach here shows that sulphate reduction processes were active at pH 11 with the ratio of genes to transcripts suggesting a portion of microbial community was capable of sulphate reduction but did not undertake this activity at the higher pH values (Figure 8.11C). Sulphate reducing bacteria are metabolically diverse (*161*) and it could be that some undertook fermentation or turned over EPS (*289*) at the

higher pH values and became active sulphate reducers as the pH fell. This is reflected in the changes between the ratio of genes to transcripts as the external pH decreased (Figure 8.11C).

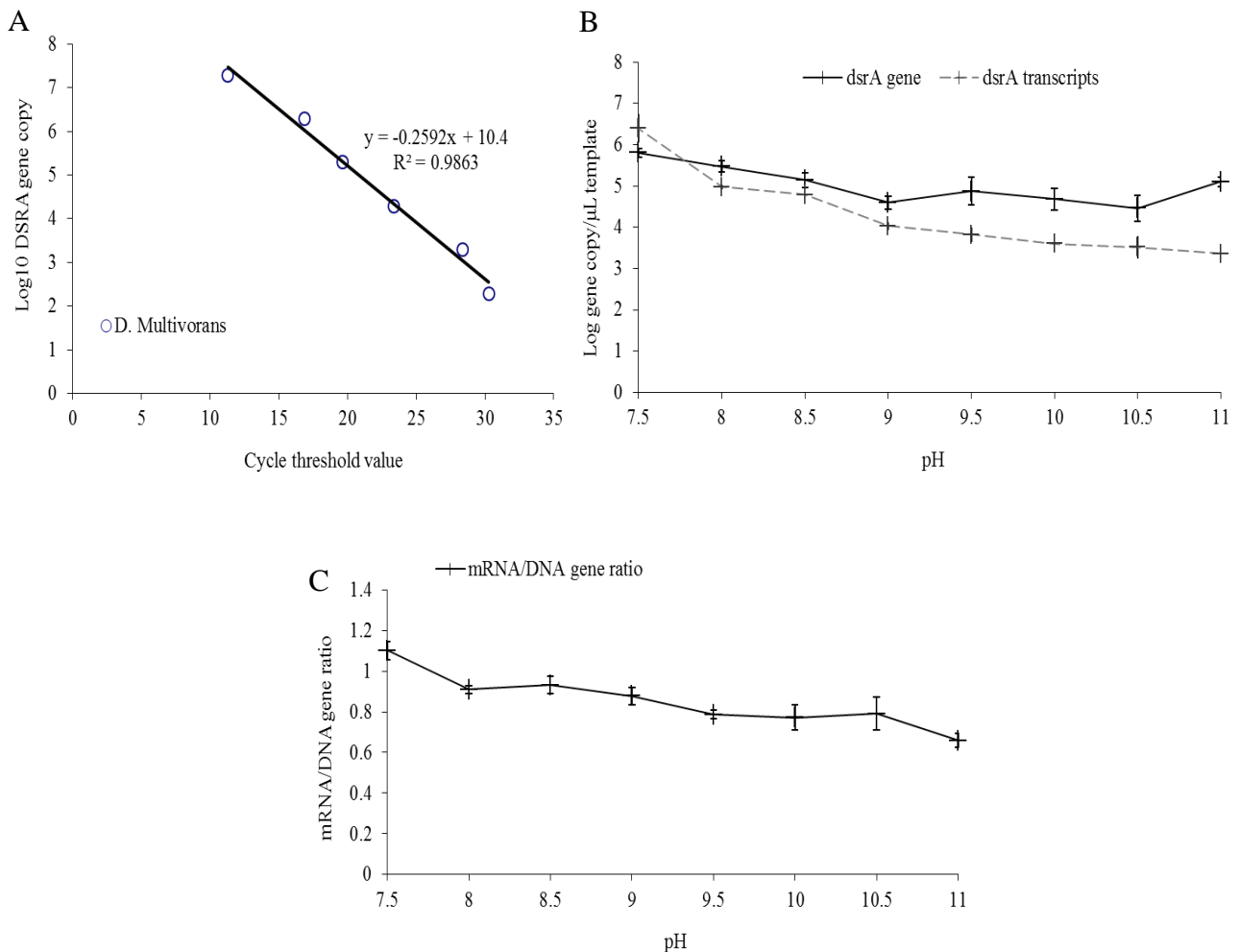


**Figure 8.11: qPCR analysis of the *dsrA* gene and its transcripts within the free drift sulphate reducing subculture.** [A] *Desulfococcus multivorans* calibration curve. [B] Both the *dsrA* gene and its transcripts were detected at all pH ranges and increased as the external pH decreased. [C] mRNA to DNA ratios show that not all *dsrA* genes were active under hyperalkaline conditions.

At the class level the microbial community changed in composition as the external pH value dropped with classes containing alkaliphilic families such as the Bacilli and the Actinobacteria decreasing in community composition (Figure 8.12A). The Actinobacteria class at pH 11 was dominated by the Corynebacteriaceae (Figure 8.12B) rather than the Dietziaceae as reported in methanogenic flocs in Chapter 6 (Figure 6.5). Alkaliphilic Corynebacteriaceae have been reported to grow up to pH 9.0 within microbial fuel cells (328) with *Corynebacterium humireducens* reported to grow up to pH 11 (329). Interestingly the

addition of sulfur compounds to growth media has been shown to enhance the growth of *Corynebacterium spp.* (330) with *Corynebacterium glutamicum* shown to be able to reduce sulphate via an assimilatory pathway to sulfide to produce both homocysteine and methionine using C<sub>1</sub> carbon sources (331). The provision of sulphate in this instance seems to have facilitated the growth of the Corynebacteriaceae possibly enabling assimilatory sulphate reduction under hyperalkaline conditions. As the pH decreased the community composition of the Actinobacteria fell from 52.8 % at pH 11 to 23.7 % and 8.2 % at pH 9.5 and pH 7.5, respectively. Additionally the Bacilli class, which has a wide range of reported alkaliphilic species (51, 314) fell from 3.8 % at pH 11 to 0.9 % and 0.3 % at pH 9.5 and pH 7.5, respectively. The Betaproteobacteria were dominated by the Alcaligenaceae family and fell from 9.1 % at pH 11 to nearly undetectable levels at pH 9.5 and pH 7.5. Members of the Alcaligenaceae family are reported to form biofilm (332) and have been reported in the hyperalkaline sediments at the Harpur Hill, Buxton analogue site (56) and were found in greater abundance as the pH became more alkaline in CDP driven microcosms reported by Rout *et al* (81). The loss of the aforementioned lineages identifies them to be strict alkaliphilic microorganisms where as a range of alkali-tolerant microbes were able to increase in abundance as the pH fell. The Clostridia class was diverse at all pH values tested and increased in community composition as the external pH fell to neutral conditions. At pH 11 the Clostridia were primarily composed of microbes from the *Anaerovirgula* (12.5 %), *Tissierella* (7.7 %) and *Anaerobranca* (3.8 %) lineages. As the pH began to fall the community composition of alkaliphilic Clostridia fell, with lineages such as *Anaerovirgula* which is widely reported under hyperalkaline conditions (265) falling to 11.8 % at pH 9.5 % and to 2.3 % at pH 7.5. Other Clostridia lineages such as the Ruminococcaceae increased from very low abundance at pH 11 (0.1 %) to high levels as the pH became more neutral with an increase to 8.3 % at pH 9.5 and 24.7 % at pH 7.5. As the pH reached pH 7.5 Clostridia lineages associated with the reduction of sulfur compounds began to increase in community composition with *Desulfitobacterium* (2.1 %) and *Desulfotomaculum* (2.3 %) reported at pH 7.5, both of which are capable of dissimilatory sulphate reduction (333, 334). As the pH fell some alkaliphilic microorganisms decreased in community composition where as other alkali-tolerant microbes increased in composition and the ability to degrade ISA did not diminish (Figure 8.12). It is likely that a range of microorganism possess the ability to degrade ISA with work by Rout *et al* (80, 81, 177) showing the ability of microbial communities from both neutral and hyperalkaline conditions to degrade ISA despite different community compositions.

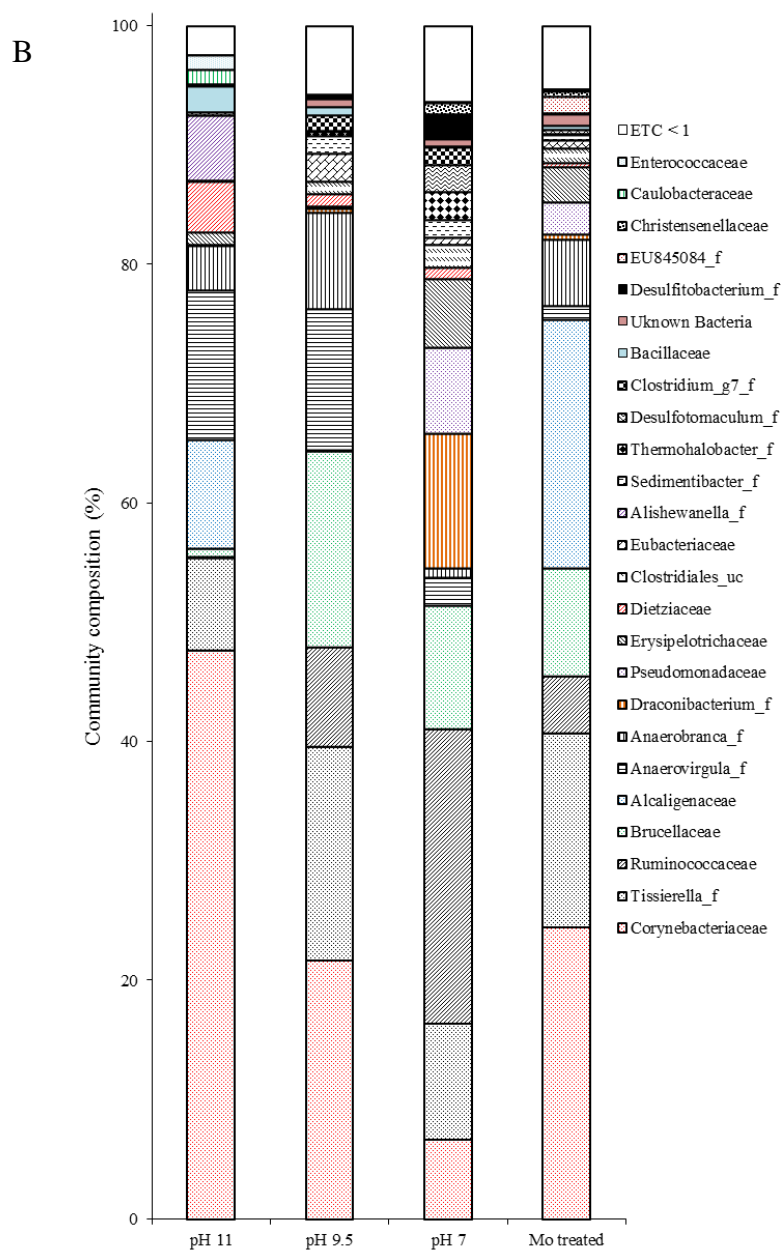
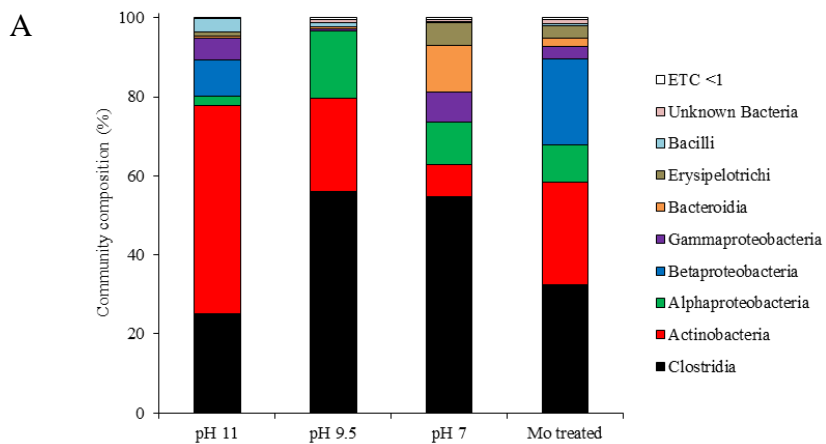


**Figure 8.12: Community composition of free drift subcultures.** [A] Class distribution of sulphate reducing subculture system at pH 11.0, pH 9.5 and pH 7.5 and molybdenum treated system at the end of the experiment at approximately pH 9.5. [B] Family level distribution.

The subcultures amended with molybdenum showed a similar composition to the pH 11 sulphate reducing starting culture (Figure 8.12) but with increased Bacilli and Clostridia class compositions and a decrease in Actinobacteria. These results were most likely due to the reduction in pH caused by the fermentation of ISA. The differences between the molybdenum treated subcultures and the sulphate reducing subcultures were not significantly different at a 95 % confidence interval and neither were the changes to community structure as the pH changed from alkaline to neutral within the sulphate reducing subcultures (Table 8.6). The alpha diversity statistics (Table 8.7) showed that as the external pH decreased the number of OTU's increased and the Shannon index correspondingly showed an increase in diversity. The SRB floc community at pH 11 showed a similar number of OTU's in comparison to the methanogenic floc community (Table 6.4) and had a slightly higher Shannon index indicating that the addition of sulphate may facilitate the growth of more organisms under these conditions. The rarefaction curves (Figure 8.13A) suggest that sampling in all instances did not reach saturation with regard to the identified OTU's with Goods Coverage values (Table 8.7) suggesting >10 % of OTU's were still left to be found. Rank abundance curves (Figure 8.13B), however, show a diverse microbial populations in each instance with ACE and Chao1 values indicating that the remaining OTU's to be found were probably rare low read species (226).

	pH 11.0	pH 9.5	pH 7.5	Mo treated (pH 9.5)
pH 11.0		0.21	0.11	0.24
pH 9.5	0.21		0.22	0.27
pH 7.5	0.11	0.22		0.24
Mo treated (pH 9.5)	0.24	0.27	0.24	

**Table 8.6: P value distribution for the comparison between different free drift subcultures.** There was no significant difference between any of the systems at the family level.

	Valid reads	OTUs	Ace	Chao1	Shannon	Goods Coverage
pH 11.0	18860	1463	10054.50	4748.01	4.55	0.84
pH 9.5	10122	2231	21204.97	10696.13	5.31	0.84
pH 7.5	11522	2707	20607.96	10709.53	6.06	0.83
Mo treated (pH 9.5)	11664	2257	19982.16	11771.48	5.25	0.86

**Table 8.7: Alpha diversity statistics of different free drift systems.** As the pH increased as did the diversity of the sulphate reducing subcultures. The subcultures treated with molybdenum were similar to the sulphate reducing subculture system at pH 9.5.

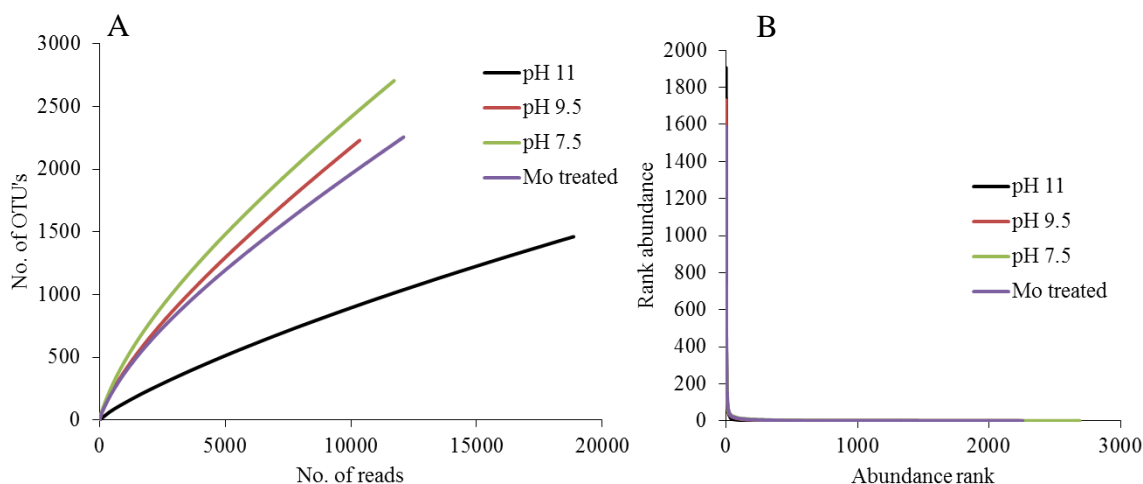


**Figure 8.13: Rarefaction and rank abundance curves of different free drift subculture systems.** [A] Rarefaction curves show sampling did not reach saturation with respect to OTU identification. [B] Rank abundance reflects findings of a diverse microbial community.

### 8.2.3 Steel surface biofilm investigation under ILW-GDF conditions

The ability of sulphate reducing floc communities to form biofilm upon steel surfaces may lead to microbial induced corrosion issues through the production of sulphide (170). Methanogenic floc communities were shown to have an increased ability to degrade ISA when in biofilm (Chapter 7) with the ability to create low pH microsites within the biofilm attributed to this ability. If biofilm were to form upon steel under ILW-GDF conditions then a lower pH within the biofilm may allow for sulphate reduction and sulphide production to occur under hyperalkaline conditions. In order to investigate this grade 304 and grade 316 austenitic stainless steel discs were incubated in a pH 11 CDP microcosm for 3 months (see Section 5.9.3 for more details).

After the incubation period the steel disc reactor was able to degrade all three forms of ISA with first order rate constants shown in Table 8.8. The first order rate constant for both  $\alpha$ -ISA and  $\beta$ -ISA were slightly higher than those reported for related floc communities with the XISA constant ten-fold higher (Table 8.1). Compared to the methanogenic sand column biofilms under a recirculation system, the rate constants for both  $\alpha$ -ISA and  $\beta$ -ISA are ten-fold lower with the XISA constant half the value of the sand column biofilm (Table 7.1). This is probably related to the density of the biofilms formed within the different systems with thick dense biofilms forming in between and upon sand grains within the sand column systems (Figure 7.2) and only thin surface based biofilms forming upon the steel surfaces within this system.

ISA	Rate (day <sup>-1</sup> )	SE
$\alpha$ -ISA	$3.26 \times 10^{-2}$	$9.27 \times 10^{-3}$
$\beta$ -ISA	$3.59 \times 10^{-2}$	$1.04 \times 10^{-2}$
XISA	$1.54 \times 10^{-1}$	$8.39 \times 10^{-2}$

**Table 8.8: First order rate constants for ISA degradation within steel disc system.** The rate constants are higher than those reported for floc based systems under similar conditions.

The degradation of ISA resulted in the production of acetate, hydrogen gas and methane as end products (Figure 8.14). Sulphate was able to be utilised at a steady rate (Figure 8.14E) with  $0.07 \pm 0.01$  mmol removed over the 14 day testing period with a corresponding sulphide production of  $0.06 \pm 0.02$  mmol, The pH of the disc microcosm remained alkaline throughout the testing period (Table 8.9) and abiotic microcosms showed no evidence of ISA degradation, gas generation, acetate production or degradation or changes in TOC and IC (Figure 8.14). The generation of both acetate and hydrogen has the potential to drive methanogenesis, however the rise in both acetate and methane with the corresponding loss of hydrogen gas from the headspace after day 10 would suggest methanogenesis is occurring through the hydrogenotrophic pathway. Under circumneutral conditions sulphate reduction generally outpaces methanogenesis with greater rates of hydrogen and acetate utilisation seen in the SRB compared to the methanogenic archaea (335, 336). Under these conditions, however, it would seem both systems can co-exist which may be due to the low activity of the SRB seen here. The co-occurrences of both processes has been reported before in coal bed reservoirs (337) and co-cultures of hydrogenotrophic sulphate reducing bacteria and acetotrophic methanogens (338). In this case however, it would appear the opposite way around with the co-occurrence of acetotrophic sulphate reduction and hydrogenotrophic methanogenesis.

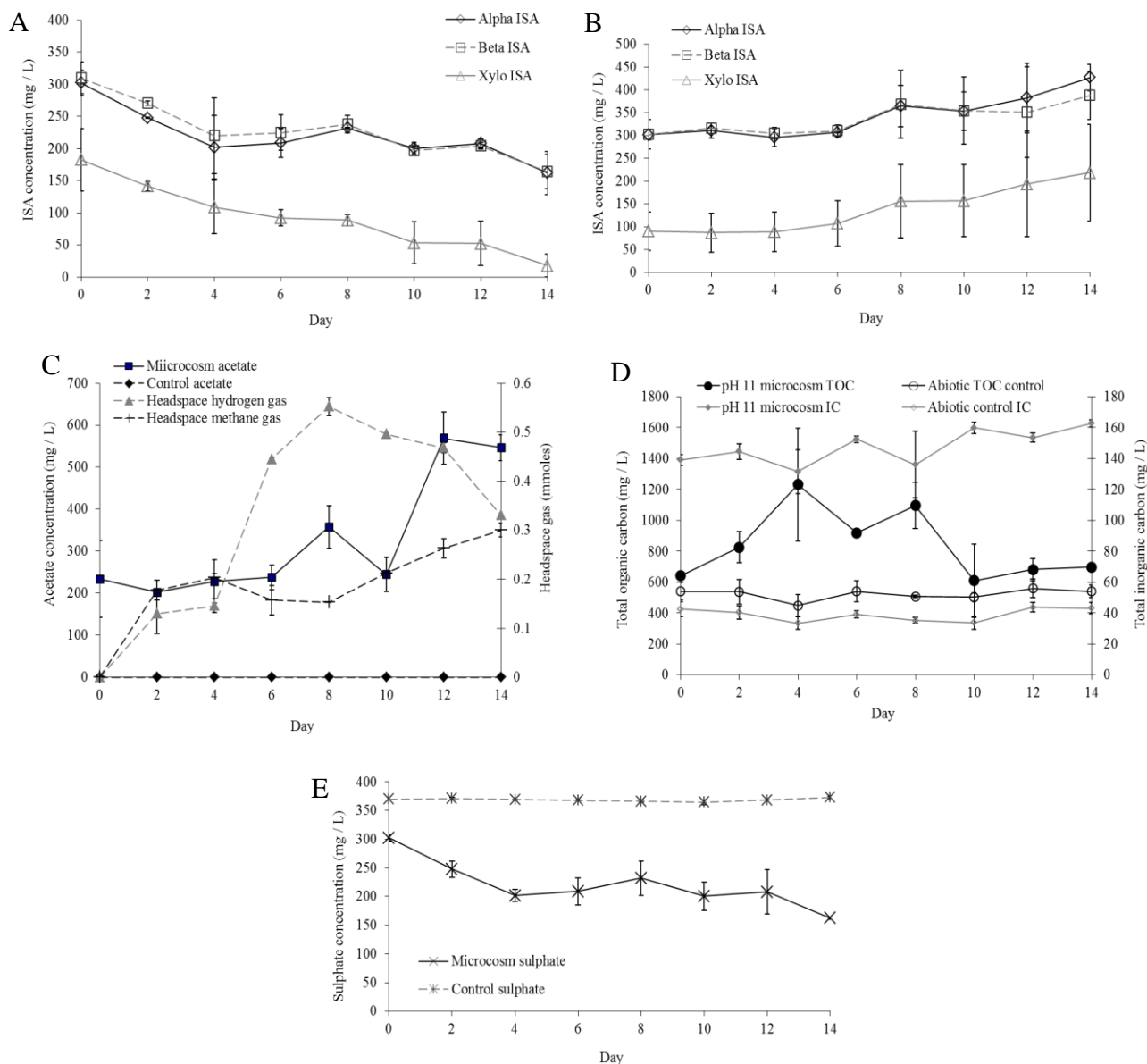


**Figure 8.14: Chemistry of hyperalkaline steel disc microcosm under sulphate reducing conditions.** [A] All three forms of ISA were able to be degraded by the steel biofilms. [B] The controls showed no evidence of ISA degradation. [C] The fermentation of ISA was able to produce acetate and hydrogen as end products which further fuelled methane production. [D] The TOC and IC measurements within the steel disc system and the controls. [E] Sulphate was able to be utilised throughout the testing period.

Microcosm				Control			
Start		Finish		Start		Finish	
Average	SE	Average	SE	Average	SE	Average	SE
11.0	0.0	10.5	0.0	11.0	0.0	11.0	0.0

**Table 8.9: pH values of sulphate reducing disc reactor under hyperalkaline conditions.**

Analysis of the steel discs by CLSM revealed the biofilm formed upon the steel surface to be composed of a complex mixture of eDNA, polysaccharides, lipids and protein (Figure 8.15). The grade 304 disc had more biofilm coverage compared to the grade 316 disc but both discs had a biofilm of a similar EPS composition with large amounts of protein, lipid and eDNA with a bias towards  $\alpha$ -Mannopyranosyl and  $\alpha$ -glucopyranosyl sugars within the polysaccharide component. These biofilms were similar in composition to biofilms formed upon steel discs reported in Chapter 7 (Figure 7.33) with the EPS possessing a range of functional groups able to become deprotonated under the hyperalkaline conditions gaining a negative charge (287). These groups are then able to interact with cations such as  $\text{Ca}^{2+}$ , with components such as eDNA interacting with  $\text{Ca}^{2+}$  to favour biofilm aggregation and formation (102).

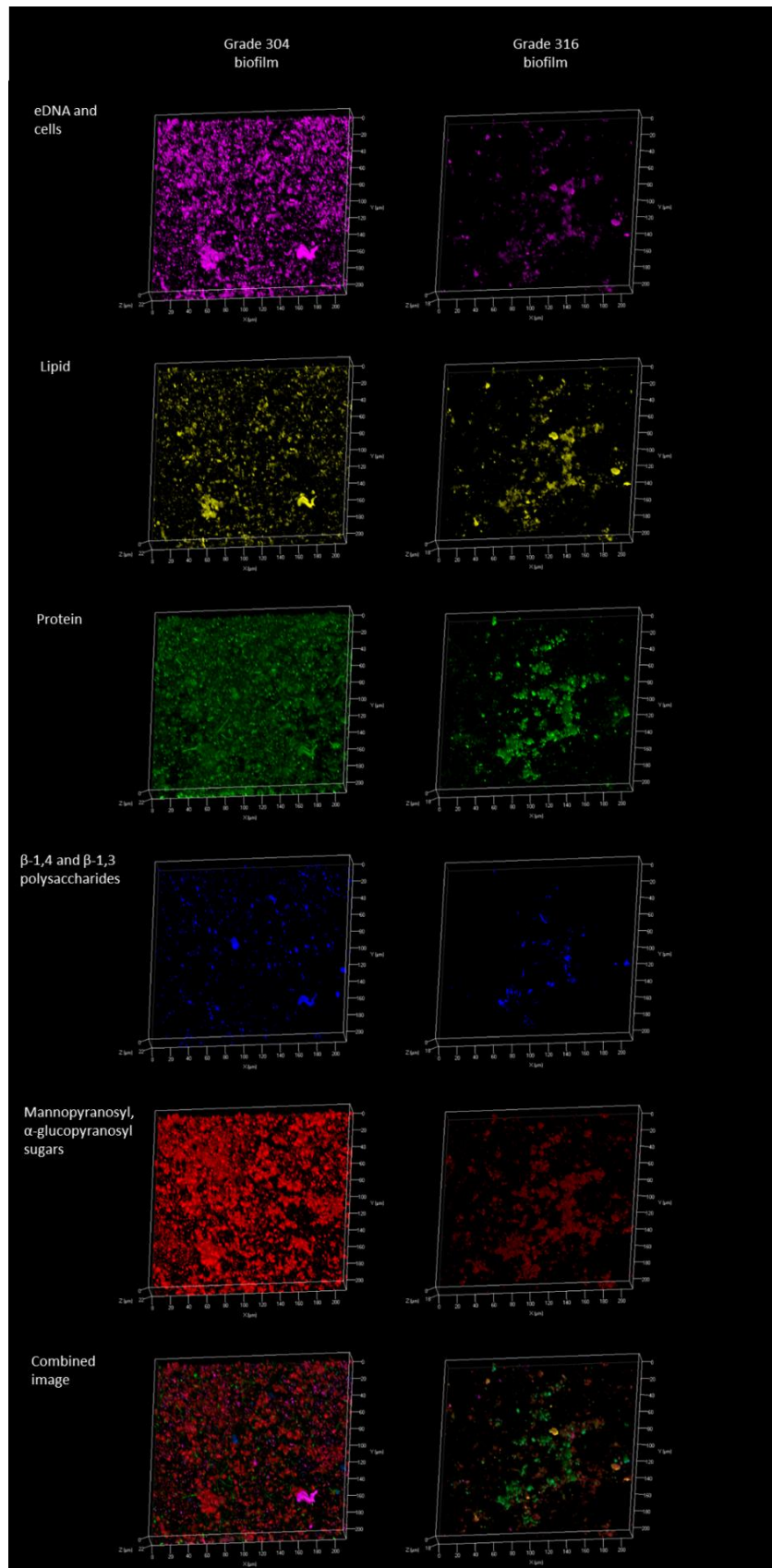


**Figure 8.15: CLSM imaging of biofilms formed upon steel discs under ILW-GDF conditions.** Biofilm formed upon both grade 304 and 316 steel discs is shown, with both biofilms having a similar EPS compositions.

Analysis of the microbial community of the biofilm formed upon the steel discs showed no significant difference between the biofilms formed upon the different grades of steel at a 95 % confidence interval with a P value of 0.498. The alpha diversity statistics (Table 8.10) reflected the similarity between the two biofilms formed upon the different grades of steel showing very little difference between the different statistics. The formation of biofilm upon the steel discs by floc communities at pH 11 resulted in a decrease in OTU's and a corresponding drop in the Shannon index. This indicates that as per the methanogenic systems (Chapters 6 & 7) a proportion of floc community was unable to transfer to a fixed surface based biofilm. Similar findings are shown in the work by Niederdorfer *et al* (276) who showed aggregate based communities had higher diversity than biofilm communities formed from the aggregates. The rarefaction curves (Figure 8.16A) showed that sampling did not reach saturation with respect to OTU detection; however, the Goods Coverage values suggest a large proportion of the OTU's were detected. The Rank abundance curves (Figure 8.16B) showed a diverse microbial community and Ace and Choa1 values indicated that only rare low abundance species were left to find (226).

	Valid reads	OTUs	Ace	Chao1	Shannon	Goods Coverage
Grade 304 biofilm	15056	633	8181.75	25857	3.26	0.94
Grade 306 biofilm	16116	637	8201	26014	3.28	0.94

**Table 8.10: Alpha diversity statistics for biofilms grown on steel discs under hyperalkaline conditions.** There appears to be little difference between the grade of steel and the alpha diversity statistics of the biofilms communities. The biofilms were less diverse than the floc based communities which formed the biofilms.

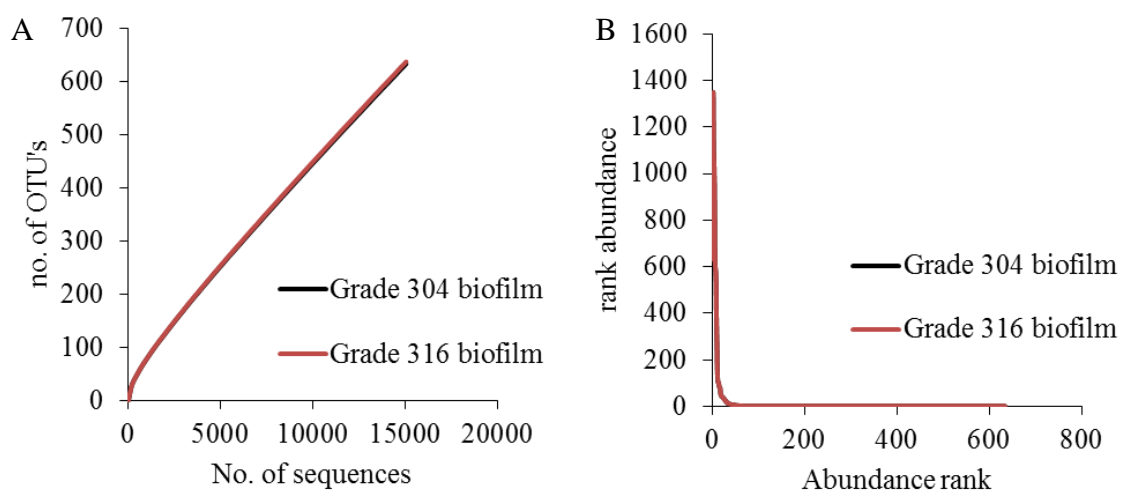


**Figure 8.16 : Rarefaction and rank abundance curves of steel disc biofilms grown under hyperalkaline conditions.** Both biofilms from the different grades of steel show similar results. [A] Rarefaction curves show sequencing did not reach saturation with respect to OTU's. [B] Rank abundance curves reflected the diversity of the microbial population.

At the class level the average steel disc biofilm composition was predominantly represented by Clostrida (34.3 %),  $\alpha$ -Proteobacteria (24.0 %),  $\gamma$ -Proteobacteria (13.2 %), Actinobacteria (11.9 %), Bacteroidia (8.2 %) and Bacilli (3.8 %) (Figure 8.17A). The Clostridia contained fewer families compared to the related floc communities at pH 11 (Figures 8.12B & 8.17B) and was dominated by reads closely related to the *Anaerobranca* (18.6 %) and *Anaerovirgula* (13.9 %) lineages which are reported to survive under a range of alkaline conditions and can ferment a broad range of carbohydrates (265, 308, 309). In terms of sulphate utilisation there has been no reported instances for these lineages with only the use of thiosulphate as an electron acceptor by *Anaerobranca gottschalkii* (307). The  $\alpha$ -Proteobacteria were dominated by the Rhodobacteraceae family which were below the 1 % cut-off within the related pH 11 floc community (Figure 8.12B). The Rhodobacteraceae were comprised predominantly of two non-phototrophic lineages: *Defluviimonas* (6.3 %) and *Ochrobactrum* (15.8 %) which are both associated with denitrification processes (339, 340) with clones related to *Ochrobactrum grignonense* identified within sediment microcosms representative of the UK Sellafield site (339). Clones relating to *Ochrobactrum anthropi* were also identified within the biofilms grown in-situ upon cotton within the Buxton analogue site (Figure 6.3). The Gamma-Proteobacteria were dominated by bacteria from the *Alishewanella* lineage which was a common component in the methanogenic flocs (Figure 6.5) and the methanogenic biofilms at pH 11 (figure 7.16B). *Alishewanella* species are reported to grow under alkaline conditions

and utilise a wide range of substrates (271, 272) with sulphate reduction by an *Alishewanella* species demonstrated recently by Xia *et al* (341). The Actinobacteria were comprised of bacteria from both the Corynebacteriaceae family (7.3 %) and the Dietziaceae family (4.1 %). Bacteria from the Corynebacteriaceae family were also present within the pH 11 sulphate reducing floc community (Figure 8.12B) and possess the ability to generate sulfur containing proteins and also the ability to generate sulfide through the assimilatory sulphate reducing pathway (330, 331). Bacteria from the Dietziaceae family were also reported within methanogenic floc communities and biofilms where they appeared to favour hyperalkaline conditions (Figure 7.16B). Members of the *Dietzia* lineages have been reported under hyperalkaline conditions and can form biofilm as well as degrade a wide range of carbon based substrates (273, 282, 306). The Bacteroidia class were mainly made up of bacteria from the *Draconibacterium* lineage with clones relating to *Draconibacterium orientale* identified in pH 7.5 and pH 9.5 clone libraries of CDP driven microcosms reported by Rout *et al* (81). The ability for sulphate reduction through the assimilatory pathway is also present within the genome of *Draconibacterium orientale* reported by Li *et al* (342). The Bacilli class were made up predominantly of the Bacillaceae family (3.7 %) of which many alkaliphilic bacteria are reported with the family possessing the ability to utilise a wide range of substrates and form biofilm (48, 297, 314). Methanogenic archaea were detected in as a small quantity of the total community (0.05%) and were completely dominated by the *Methanobacteria* genus. Different *Methanobacteria* species have previously been isolated from alkaline environments and are hydrogenotrophic rather than acetotrophic (153, 158).

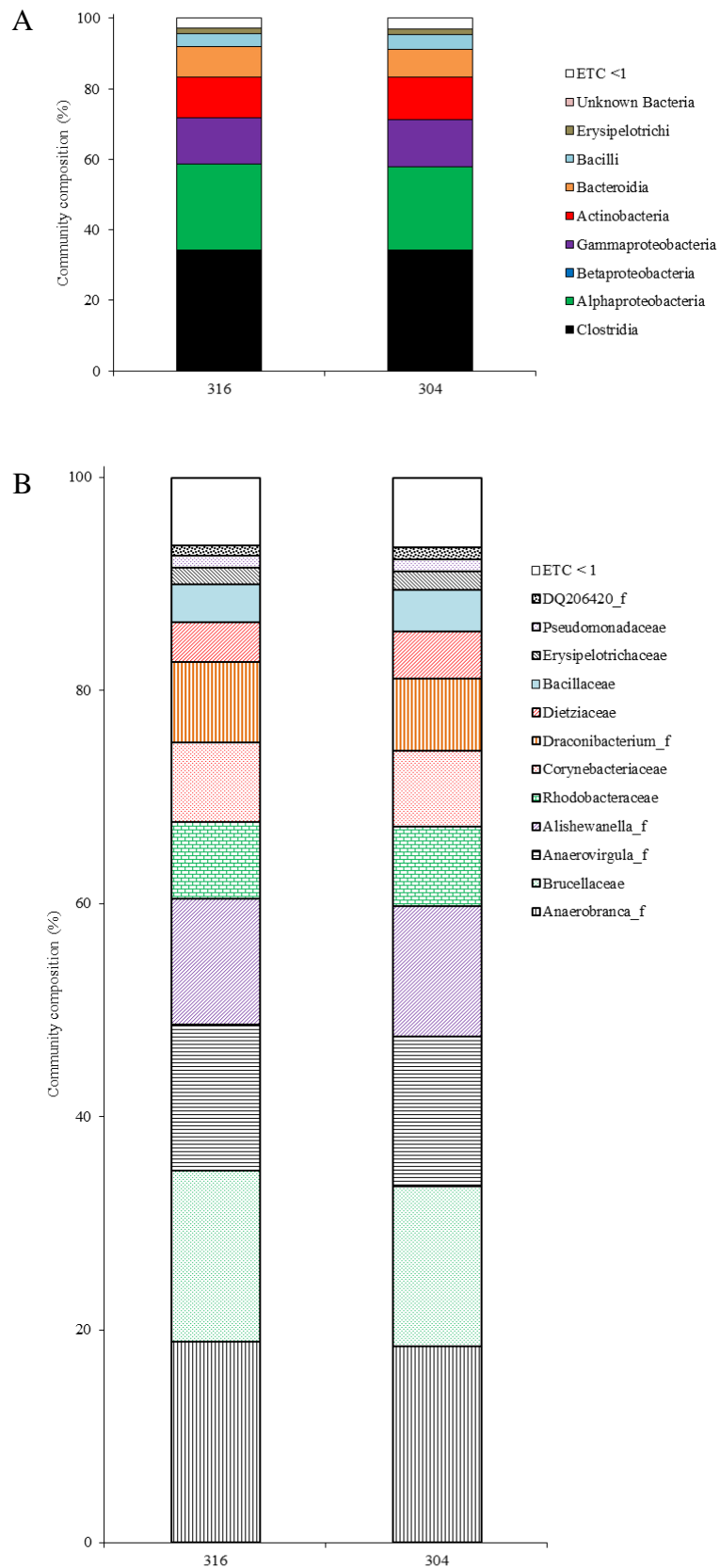


**Figure 8.17: 16S rRNA gene community analysis of biofilms formed upon steel discs under hyperalkaline conditions. At both the class [A] and family [B] levels the biofilms from the different grades of steel appeared almost identical.**

Sulphide was detected within the steel disc system (Figure 8.17) with the microbial community analysis showing the potential for sulphide generation through both the assimilatory and dissimilatory pathways, which could lead to the corrosion of the steel surfaces (170). It appears that under these circumstances despite the lack of traditional sulphate reducing genera (161), bacteria from lineages such as the *Alishewanella* and *Corynebacteria* were able to produce sulphide through sulphate reducing processes (330, 341).

SEM imaging of the biofilm formed upon the steel discs (Figure 8.18) reflected the CLSM findings (Figure 8.15) and showed wide coverage by biofilms which appeared to be similar in appearance to sulphate reducing biofilms grown on steel reported by both Marques *et al* (343) and Rajala *et al* (344). SEM showed the biofilms were interspersed with precipitate with EDS of the biofilm (Figure 8.19A) revealing a composition of primarily carbon, oxygen, calcium and a small sulphur component. This could indicate the precipitation of calcium carbonate within the biofilm as sulphate reduction can facilitate calcium carbonate precipitation by altering the saturation index of calcium carbonate to favour precipitation (244, 289). The detection of sulphur could indicate the sorption of sulphate to the biofilm or the generation of gypsum due to sulphide generation (345). The value of sulphur detected here is lower than steel coupon biofilms under neutral conditions reported by Al'Abbas *et al* (346) which may be a reflection of the lower rate of sulfide production under these conditions.

Removal of the biofilm formed upon the steel surfaces revealed small dark patches and pits when compared to the control (Figure 8.19AB). The patches and pits are somewhat similar to microbial induced steel corrosion images produced by Fan *et al* (347) and Rajala *et al* (344) with EDS investigation into the pits (Figure 8.19A) showing sulphur present in small quantities which could indicate the formation of iron sulphide due to microbial corrosion processes (161).

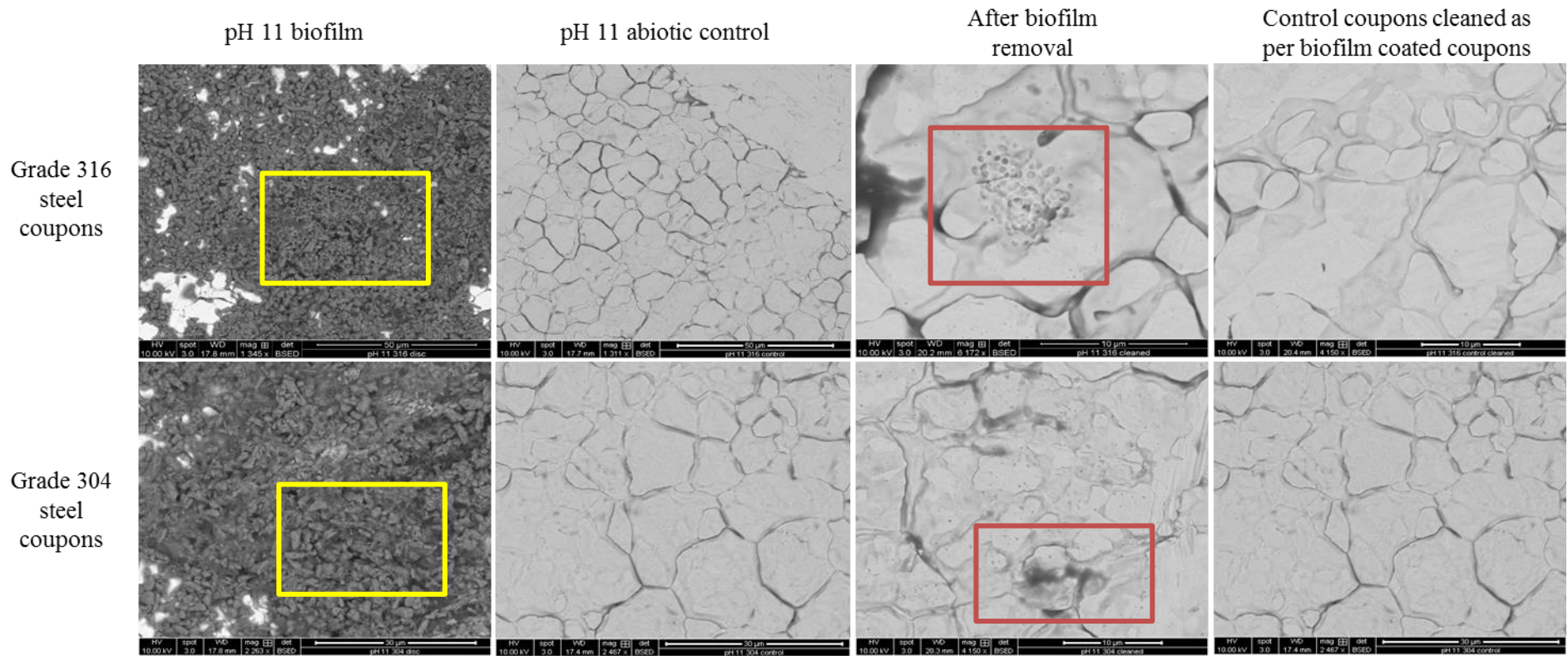
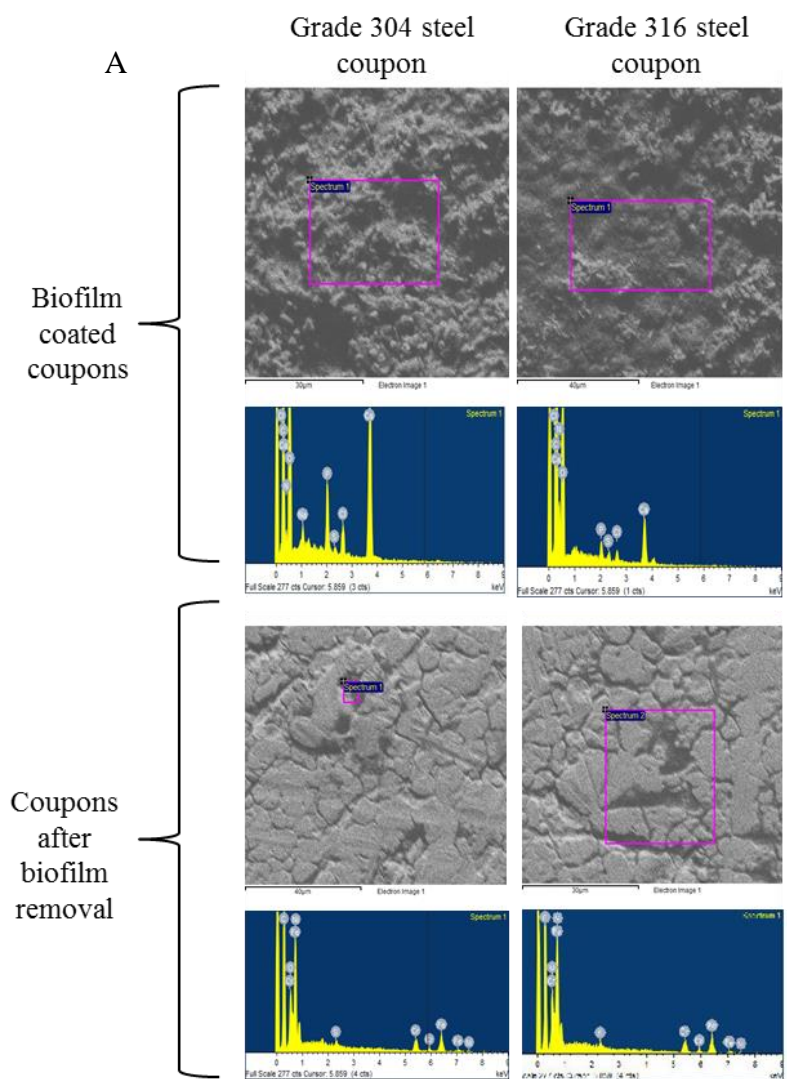
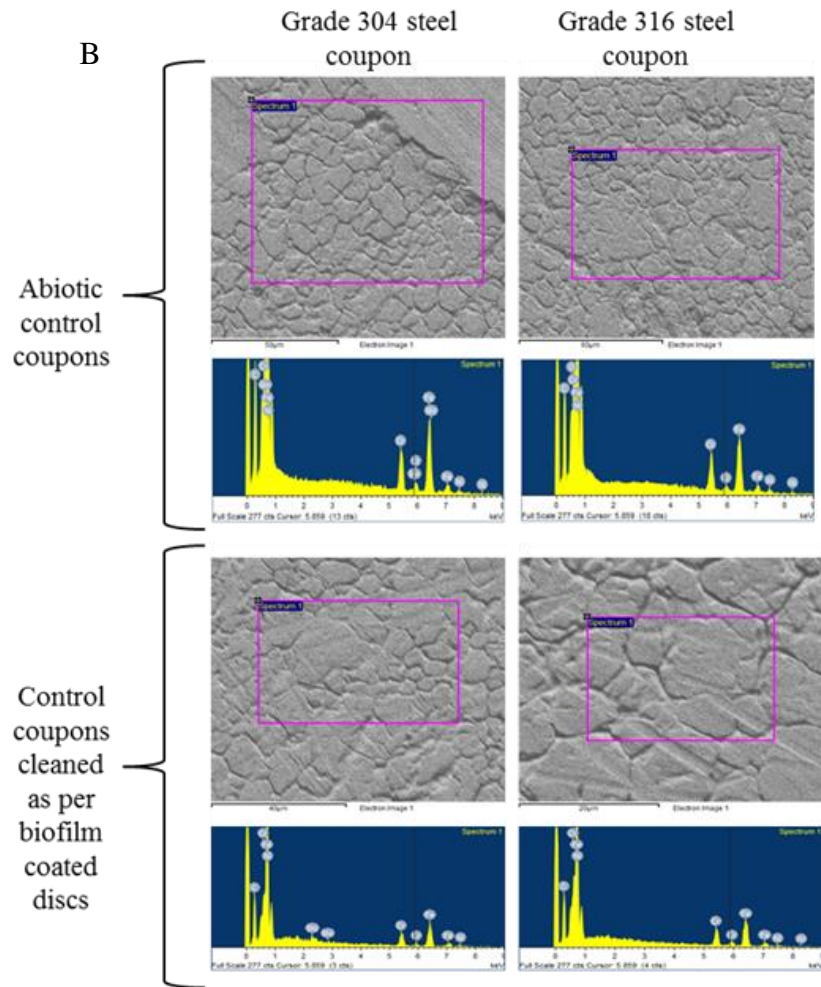


**Figure 8.18: SEM imaging of biofilm coated steel discs before and after biofilm removal.** The surface of the steel discs was covered in biofilm (yellow box). Removal of this biofilm revealed dark areas and pits which may be associated with microbial induced corrosion of the steel surfaces through sulphide generation (red box).



Weight (%)

Element	Steel coupon biofilm		Cleaned biofilm coupon	
	Grade 304	Grade 316	Grade 304	Grade 316
C	44.0	23.3	34.6	18.3
O	34.9	43.3	3.4	8.1
Cr	0	0	12.4	0.0
Fe	0	0	43.6	60.9
Ni	0	0	5.7	8.5
Mn	0	0	0.0	0.0
P	0.8	3.5	0.0	0.0
S	0.4	0.4	0.3	0.5
Cl	0.6	2.0	0.0	0.0
Ca	4.6	20.9	0.0	3.8
Na	0.0	0.6	0.0	0.0



Element	Weight (%)			
	Control steel coupon		Cleaned control steel coupon	
	Grade 304	Grade 316	Grade 304	Grade 316
C	8.4	7.7	7.6	8.1
Cr	18.7	18.2	17.3	18.2
Fe	60.6	65.0	61.7	63.7
Ni	10.6	9.1	12.3	10.0
Mo	1.7	0	0	0
S	0	0	0.0	0.0
O	0	0	1.1	0.0
Ca	0	0	0.0	0.0

**Figure 8.19: Elemental composition of steel discs coated by biofilm and controls.** [A] Elemental composition of biofilm coated discs with and without biofilm. [B] Control discs before and after cleaning as per the biofilm discs.

The ability of both floc based systems and biofilm system to produce sulphide through the reduction of sulphate driven by the products of ISA fermentation could have an impact upon the long term performance of an ILW-GDF. Steel surfaces have the potential to be colonised by sulphide producing biofilms which in turn could lead to the corrosion of these surfaces.

Steel canisters which encase ILW could therefore be compromised by microbial action especially given the long time scales associated with an ILW-GDF (348). There may be more than one mechanism for sulphide generation with these systems with different bacterial species identified able to undertake dissimilatory and assimilatory sulphate reduction. The ability to produce sulfur containing proteins through assimilatory sulphate reduction may produce sulphide when degraded via microbial action (349).

The work undertaken here regarding the potential for sulphate reduction to occur under ILW-GDF conditions is produced as consequence of the ISA degradation work and further deeper investigations regarding sulphate reduction and its related steel corrosion is beyond the scope of this thesis. It does; however, lay the foundations for further work within this area especially regarding the impact of sulphate reducing biofilms may have under ILW-GDF conditions.

### 8.3 Conclusion

Using colonised cotton from the Harpur Hill, Buxton analogue site a pH 11 floc based system was able to be formed under sulphate reducing conditions. Although only utilising small amounts of sulphate and producing a correspondingly small amount of sulfide the community was able to link the fermentation of ISA to sulphate reducing processes under ILW-GDF conditions. Experiments using molybdenum showed that fermentation of ISA by the addition of sulphate under hyperalkaline conditions ( $\text{pH} > 9.5$ ) was not impacted suggesting sulphate reduction was driven by the products of ISA fermentation. The addition of sulphate allowed members of the Corynebacteriaceae to become a large portion of microbial community with the Corynebacteriaceae possessing the ability to undertake assimilatory sulphate reduction to form sulphur containing proteins. Degradation of these proteins could lead to an alternative sulphide generation pathway.

Allowing the pH to fall using a free drift system revealed a proportion of the microbial community were alkali-tolerant and rare species at pH 11 such as members of the Ruminococcaceae became dominant as the pH moved towards neutral. Despite these shifts in population the ability to degrade all forms of ISA across these pH ranges was retained. Sulphate reduction driven by acetate became a more dominant process as the pH reached neutral conditions with the corresponding emergence of bacteria related to known sulphate reducers. The presence of *drsA* transcripts were detected at all pH values and increased in number as the external pH fell. This indicated dissimilatory sulphate reduction was active under pH 11 possibly facilitated by lower pH microsites formed by the EPS materials.

Flocs were able to form biofilm upon steel surfaces at pH 11 with correspondingly small increases in the ability to degrade all three forms of ISA. Sulphide was able to be produced under these conditions alongside methane, which may be possibly due to the low rate of sulphate utilisation by the consortia. Small areas of possible corrosion were formed upon the steel surfaces and indicate microbial induced corrosion of steel through sulphate reduction may be possible under ILW-GDF conditions, albeit at a very low rate.

### 8.4 Key findings

- Colonised cotton from the Harpur Hill, Buxton analogue site was able to form liquid floc based microcosms which were able to degrade all three forms of ISA with the subsequent production of acetate and hydrogen. Sulphate utilisation within these systems was then able to produce a small amount sulphide.

- *dsrA* transcripts were detected at pH 11 and increased in number as the external pH fell. The ability to reduce sulphate could be facilitated by low pH microsites formed within the EPS.
- The addition of sulphate allowed members of the Corynebacteriaceae to become a large portion of microbial community with the Corynebacteriaceae possessing the ability to undertake assimilatory sulphate reduction to form sulphur containing proteins. Degradation of these proteins could lead to an alternative sulphide generation pathway.
- Biofilm formed upon steel at pH 11 under ILW-GDF conditions was able to degrade all three forms of ISA and produce sulphide whilst utilising sulphate. Removal of the biofilm revealed possible corrosion pits similar to those caused by microbial action.

## **9. Analogue site investigations**

## 9.1 Rationale

Since the location of any UK based ILW-GDF is as yet undecided, analogue sites for an ILW-GDF present an opportunity to investigate the potential microbial ecology and metabolic processes operating under the geochemical conditions in which ILW is to be stored. Investigations of natural analogues such as the Hyperalkaline Allas springs in Cyprus (67) and the Maqarin site in northern Jordan (71) have reported multiple microbial communities and metabolic profiles through laboratory sub-culture and 16S rRNA techniques. In addition to natural analogues, anthropogenic analogues also offer a unique opportunity to study the microbial ecology and evolution of microbial populations under hyperalkaline conditions. Recent studies have shown that a microbially diverse population exists within the hyperalkaline soils present at a site in Harpur Hill, Buxton, UK, (Site-B) where historical (ca. 140 y) calcium rich waste deposits have been made (56, 83, 84). The highly alkaline pH of both the soils and saturating water coupled to the observation of ISA generation in-situ (80), suggest that alkaline environments contaminated with calcium rich wastes provide a strong analogue to an ILW-GDF. Biofilm formation under these conditions could provide a degree of protection to microbes from the harsh environment (95). The production of EPS is likely to constitute a protective layer in which microbes are able to survive under ILW-GDF conditions through the formation of a lower pH internal environment. EPS exists as an encapsulating gel like matrix composed of multiple components such as lipids, carbohydrates, proteins and eDNA (85). With EPS components such as eDNA enhancing the formation and stability of biofilm through thermodynamically favourable interactions with  $\text{Ca}^{2+}$  (102). Previous work in Chapter 6 demonstrated that the use of a cellulose cotton 'bait' allowed for the culturing of biofilm forming consortia within an anthropogenic analogue whose constituents were capable of ISA degradation under laboratory conditions. Therefore, further investigations into the ability of microbes to form biofilms under the alkaline conditions associated with analogue sites could provide an insight into microbial survival within an ILW-GDF.

The aim of the work within this chapter was to assess the suitability of two further sites contaminated with calcium rich wastes at varying time points as potential analogue sites with further work assessing in-situ biofilm production. These sites were both located in North Yorkshire, with the first of these two sites (Site-H) having a lagoon formed from an old quarry sinking that had been worked for the Greywacke stone. This lagoon was used as a dumping ground for lime kiln waste which started in the 1940's and is now hyperalkaline

with a tufa sediment base and crusts around the interface between the organic perimeters. The last site (Site-T) was also adjacent to a limestone quarry and featured a hyperalkaline spring generated by rain water percolation through historical waste deposits which is channelled into an engineered drainage basin. The formation of this site was approximately 10 years ago, making it the youngest of the three. All three sites had an interface area where the alkaline waters inundated a vegetated marginal area. The emplacement of cellulose cotton within these potential analogue sites aimed to provide a substrate for microbial colonisation and biofilm formation. Microscopic techniques were coupled to 16S rRNA sequencing of biofilm communities in order to provide a comparison of both the morphology and composition of the biofilms alongside the active microbial communities present (through cDNA generation of rRNA extracted). Overall, the data generated from this study are likely to provide an insight into the biofilm communities that are likely to form within the cellulosic components of an ILW-GDF and inform of any potential impact this may have with respect to its operational safety.

## 9.2 Results and discussion

### 9.2.1 Chemical analysis of analogue sites

Pictures of the sites surveyed are shown in Figure 9.1 and borehole location plans are shown in Figures 5.1 to 5.3. The sites possessed a wide range of terminal electron acceptors with predominantly hyperalkaline waters with a high concentration of calcium compared to sodium ions (Table 9.1).

At Site-B Boreholes B-BH3 and B-BH4 were dry and were excluded from the study. The porewaters of the remaining boreholes had an average pH of  $12.4 \pm 0.1$  with related sediments having an average reduction potential of  $-76.0 \pm 4.0$  mV. Both  $\alpha$ -ISA and  $\beta$ -ISA was able to be detected in equal amounts at both B-BH1 and B-BH2 with a concentration of  $0.04 \text{ mg L}^{-1}$ .

The hyperalkaline lagoon at Site-H had porewater with an average pH  $12.5 \pm 0.5$  and sediment pH's which ranged from pH 10.6 to pH 12.9 (Table 9.1). The sediments were slightly reduced with an average reduction potential of  $-34.5 \pm 18.1$ .  $\alpha$ -ISA was detected in the porewater of only one borehole at site HQ-BH4 and was only able to be extracted from the sediments from this area along with a small amount of  $\beta$ -ISA. The slightly alkaline overflow pond had an average porewater pH of  $8.3 \pm 0.2$  and a sediment pH of  $8.4 \pm 0.2$ , no

ISA of any form was detected in the pore water or sediments in this area (Table 9.1). Borehole HQ-BH1 was lost and was excluded from the study.

The hyperalkaline spring at Site T had large areas of hyperalkaline porewater ranging from pH 12.2 to pH 13.1 but also had an area of lower pH of 8.2 at TQ-BH3, an area which was dominated by plant life (Figure 9.1C, Table 9.1). The sediments in hyperalkaline areas were correspondingly high with an average pH of  $12.2 \pm 0.5$  and were slightly reduced with an average reduction potential of  $-61.3 \pm 28.8$ .  $\alpha$ -ISA was detected in small quantities from the porewater at TQ-BH2 in the porewater and the sediments of TQ-BH4 (Table 9.1).



**Figure 9.1: Photographs of hyperalkaline areas tested at different analogue sites. Each site possesses hyperalkaline waters (blue) with tufa deposits (white) and hyperalkaline sediments with organic rich perimeters. [A] Harpur Hill, Buxton (Site-B) [B] Horton-in-Ribblesdale (Site-H). [C] Tarmac quarry, Grassington (Site-T).**

	Porewater analysis (mg L <sup>-1</sup> )											Sediment analysis (mg g DW <sup>-1</sup> )			
	pH	$\alpha$ -ISA	$\beta$ -ISA	Acetate	Propionate	Fe (II)	Fe (III)	Sulphate	Nitrate	Calcium*	Sodium*	pH	Eh	$\alpha$ -ISA	$\beta$ -ISA
HQ-BH2	12.8	0.00	0.00	0.00	0.00	24.39	3.58	0.46	0.00	271.59	14.50	10.6	-25.0	0.00	0.00
HQ-BH3	12.8	0.00	0.00	0.00	0.00	22.61	2.79	0.21	2.83	353.03	26.45	12.9	-53.0	0.00	0.00
HQ-BH4	11.8	11.98	0.00	13.70	0.00	13.51	1.27	0.08	2.08	643.94	19.42	11.0	-46.0	4.34	0.00
HQ-BH5	8.4	0.00	0.00	33.63	0.00	28.09	2.30	0.20	1.89	907.58	21.25	8.3	-211.0	0.00	1.61
HQ-BH6	8.1	0.00	0.00	0.00	0.00	17.11	1.88	0.35	3.02	594.70	22.89	8.6	-166.0	0.00	0.00
															0.00
LQ-BH1	12.2	0.00	0.00	2.65	1.74	2.09	0.66	33.45	18.72	79.92	17.18	11.6	-24.0	0.00	
LQ-BH2	13.0	1.00	0.00	12.73	6.55	2.77	6.93	22.23	36.27	75.00	30.28	12.7	-78.0	0.00	0.00
LQ-BH3	8.2	0.00	0.00	20.27	12.23	2.25	8.81	13.77	1.40	67.42	10.53	7.8	-243.0	0.00	0.00
LQ-BH4	13.1	0.00	0.00	58.10	7.40	7.22	1.71	13.01	9.13	54.17	12.70	12.5	-89.0	0.14	0.00
LQ-BH5	13.1	0.00	0.00	0.00	0.00	0.87	0.45	18.69	14.74	15.91	13.96	12.0	-54.0	0.00	0.00
															0.00
B-BH1	12.4	0.01	0.01	0.00	0.00	3.81	11.94	16.51	3.75	364.02	23.23	11.4	-72.0	0.04	0.04
B-BH2	12.3	0.02	0.02	2.00	0.00	5.32	12.89	21.02	9.38	331.06	21.52	11.5	-80.0	0.04	0.04

\* Sample measured after equilibration with air.

**Table 9.1: Chemical analysis of different potential ILW analogue sites.** Analysis of porewater and sediments before cotton emplacement show a wide range of available TEA's and the generation of  $\alpha$ -ISA and  $\beta$ -ISA in some instances. The presence of both acetate and propionate and sediments with negative redox potentials indicate an active microbial population within the sediments of the different sites despite the hyperalkaline conditions.

There was considerable variation both within and between sites when compared on the availability of nitrate, iron and sulphate (Table 9.1). Site-H had lower average levels of sulphate ( $\bar{x} = 0.26 \text{ mg L}^{-1}$ ) and nitrate ( $\bar{x} = 1.96 \text{ mg L}^{-1}$ ) compared to Site-B (sulphate  $\bar{x} = 18.77$  & nitrate  $\bar{x} = 16.05 \text{ mg L}^{-1}$ ) and Site-T (sulphate  $\bar{x} = 18.77$  & nitrate  $\bar{x} = 16.05 \text{ mg L}^{-1}$ ). Site B and Site T had similar average levels of sulphate (T  $\bar{x} = 20.23 \text{ mg L}^{-1}$ ) and iron (II) (B  $\bar{x} = 4.57$  & T  $\bar{x} = 3.04 \text{ mg L}^{-1}$ ) with Site-T having the highest average levels of nitrate and Site-B the highest average levels of iron (III) (B  $\bar{x} = 12.41$ , H  $\bar{x} = 3.71$ , T  $\bar{x} = 2.36 \text{ mg L}^{-1}$ ). Site-H had the highest average levels of iron (II) ( $\bar{x} = 21.14 \text{ mg L}^{-1}$ ). The situation with ferric iron is more complex than the situation with nitrate and sulphate since it is likely to be present as colloids at this pH and the surrounding sediment may contain significant quantities of mineral iron that was not quantified in this investigation. The presence of acetic acid and ferrous iron, does however, indicate the presence of active microbial populations within the hyperalkaline sediments (310, 312).

After a 3 month period, cotton samples incubated in all three sites showed evidence of alkaline cellulose hydrolysis with  $\alpha$ -ISA and/or  $\beta$ -ISA being extracted from the cotton and present within the associated pore waters (Table 9.2). These findings are in line with those previously discussed in Chapter 6 and as per those reported by Bassil *et al* (178) and Rout *et al* (80) who both showed ISA generation from the incubation of cellulosic materials under similar hyperalkaline conditions. In the majority of samples the presence of ISA was associated with the detection of acetate within the porewater and could indicate its utilisation via a fermentation pathway as reported by Rout *et al* (80). The pH values of the porewaters remained hyperalkaline and were similar to the initial readings before cotton emplacement (Table 9.1). Average sulphate decreased at Site-T and Site-B (B  $\bar{x} = 12.26$  & T  $\bar{x} = 5.82 \text{ mg L}^{-1}$ ) and increased at Site-H ( $\bar{x} = 31.78 \text{ mg L}^{-1}$ ). Average nitrate increased at Site-H ( $\bar{x} = 10.38 \text{ mg L}^{-1}$ ), decreased at Site-B ( $\bar{x} = 2.35 \text{ mg L}^{-1}$ ) and remained stable at Site-T ( $\bar{x} = 15.91 \text{ mg L}^{-1}$ ). Average iron (II) levels dropped at all three sites to a similar concentration (B  $\bar{x} = 0.3$ , H  $\bar{x} = 0.14$ , T  $\bar{x} = 0.59 \text{ mg L}^{-1}$ ) and iron (III) increased at Site-H ( $\bar{x} = 5.56 \text{ mg L}^{-1}$ ) and Site-T ( $\bar{x} = 10.15 \text{ mg L}^{-1}$ ) and decreased at Site-B ( $\bar{x} = 5.26 \text{ mg L}^{-1}$ ). The oldest Site-B appeared to show a greater ability to utilise the different available TEA's in comparison to the two younger sites, however these differences could also be attributed to other factors such as dilution rates, geographical location, local geochemistry and local weather patterns.

	Porewater analysis (mg L <sup>-1</sup> )									Cotton extract (mg g DW <sup>-1</sup> )	
	pH	$\alpha$ -ISA	$\beta$ -ISA	Acetate	Propionate	Fe (II)	Fe (III)	Sulphate	Nitrate	$\alpha$ -ISA	$\beta$ -ISA
HQ-BH2	13.5	6.04	6.41	6.04	0.00	0.44	4.40	37.83	9.76	0.69	0.71
HQ-BH3	13.6	14.06	12.54	140.65	0.00	0.09	7.39	37.83	8.26	0.59	0.65
HQ-BH4	13.6	12.38	13.83	2.48	0.00	0.18	5.19	52.96	8.51	1.91	2.09
HQ-BH5	8.0	0.00	0.00	4.01	0.00	0.00	4.24	0.00	10.36	0.00	0.00
HQ-BH6	8.5	0.00	0.00	5.75	0.00	0.00	6.60	30.27	15.01	0.00	0.00
TQ-BH1	13.1	0.00	0.00	24.32	14.12	0.89	12.73	1.88	13.26	1.97	0.98
TQ-BH2	12.8	1.95	1.80	0.00	0.00	0.18	4.87	17.83	12.26	1.75	1.74
TQ-BH3	7.1	4.76	0.00	22.91	12.34	0.44	18.54	2.81	17.51	0.00	0.00
TQ-BH4	12.7	1.14	1.97	51.03	5.61	1.06	6.76	2.35	19.52	1.40	1.40
TQ-BH5	12.4	4.26	0.00	0.00	0.00	0.35	7.86	4.22	17.01	1.62	1.61
B-BH1	12.0	0.45	0.49	0.00	0.00	0.62	5.19	12.51	2.35	0.18	0.19
B-BH2	12.1	2.06	2.40	7.87	6.55	0.09	5.34	12.01	2.35	0.06	0.05

**Table 9.2: Chemical analysis after 3 month cotton incubation period at different potential analogue sites.** There was a general increase in both  $\alpha$ -ISA and  $\beta$ -ISA within the porewater at the different sites after cotton emplacement indicating chemical hydrolysis of the cellulose fibres. ISA was correspondingly extracted from cotton samples exposed to hyperalkaline conditions. The presence of VFA's and ferrous iron may be indicative of microbial metabolic activity.

### 9.2.2 Analysis of colonised cotton at different analogue sites

Cotton samples from all three sites developed biofilms during their emplacement, with the biofilm matrix being composed of a complex mixture of proteins, polysaccharides, cells, extracellular DNA and lipids (Figure 9.2). Cotton from Site-B was highly colonised with the biofilm EPS having a uniform distribution of proteins, high levels of eDNA, cells and lipid. The polysaccharide component of the biofilm was dominated by  $\alpha$ -Mannopyranosyl and  $\alpha$ -glucopyranosyl sugars with smaller discrete areas of  $\beta$ -1,4 and  $\beta$ -1,3 polysaccharides (Figure 9.2). The composition of the biofilm formed here was similar to the EPS composition of floc communities determined using CLSM as reported in Chapter 6 (Figure 6.9) and biofilm formed from these floc communities reported in Chapter 7 (Figure 7.15). Cotton from Site-H showed the lowest levels of overall colonisation (Figure 9.2) with biofilm having a complex EPS composition similar to the Site-B biofilm but with lower levels of lipids and  $\alpha$ -Mannopyranosyl and  $\alpha$ -glucopyranosyl sugars. Cotton from Site-T showed a higher level of colonisation than Site-H but lower than Site-B (Figure 9.2). The biofilm EPS possessed lipid, eDNA,  $\beta$ -1,4 and  $\beta$ -1,3 polysaccharide and protein components with a lower content of  $\alpha$ -Mannopyranosyl and  $\alpha$ -glucopyranosyl sugars compared to Site-B and Site-H biofilms.

In all cases the biofilms (Figure 9.2) were a complex mixture of polysaccharides, protein, lipids, eDNA and cells, with wide spread protein and lipid components regardless of the degree of colonisation. Proteins play a number of key roles in biofilm formation including the sorption of inorganic and organic ions, enzymatic reactions and protection from environmental conditions (85). Bacteria associated with acidophilic biofilms have been shown to use alkaline proteins in the biofilm matrix in order to increase the ambient pH (99). To date there is no evidence that alkaline biofilms contain acidic proteins to reduce the ambient pH, however this may be a useful area of future research. The production of lipids within the biofilm will increase hydrophobicity which improves attachment between organisms and favours aggregation as seen in activated sludge flocs (350). Increased hydrophobicity will reduce wetting (327) which will in turn reduce the impact of the alkaline pore waters. Lipids may also maintain the pH buffering capacity of the biofilm matrix if the acidic phospholipids reported in the membranes of alkaliphilic bacteria (53) have been employed within the matrix construction.

The diversity of EPS components observed within these biofilms may provide an array of functional groups which ally themselves to survival of the community at alkaline pH. Such groups include carboxyl and amine groups which deprotonate under alkaline pH, contributing

a negative charge to the EPS (287). This negative charge will bind cation species such as  $\text{Ca}^{2+}$  to the EPS and in turn enhance the adhesive and structural properties of the biofilm (351). eDNA was present in all three biofilms and although acidic in nature due to the linkage of nucleotides by the 3' - 5' phosphodiester bond it is likely to provide structural support possibly via thermodynamically favourable interactions with  $\text{Ca}^{2+}$  ions (102).

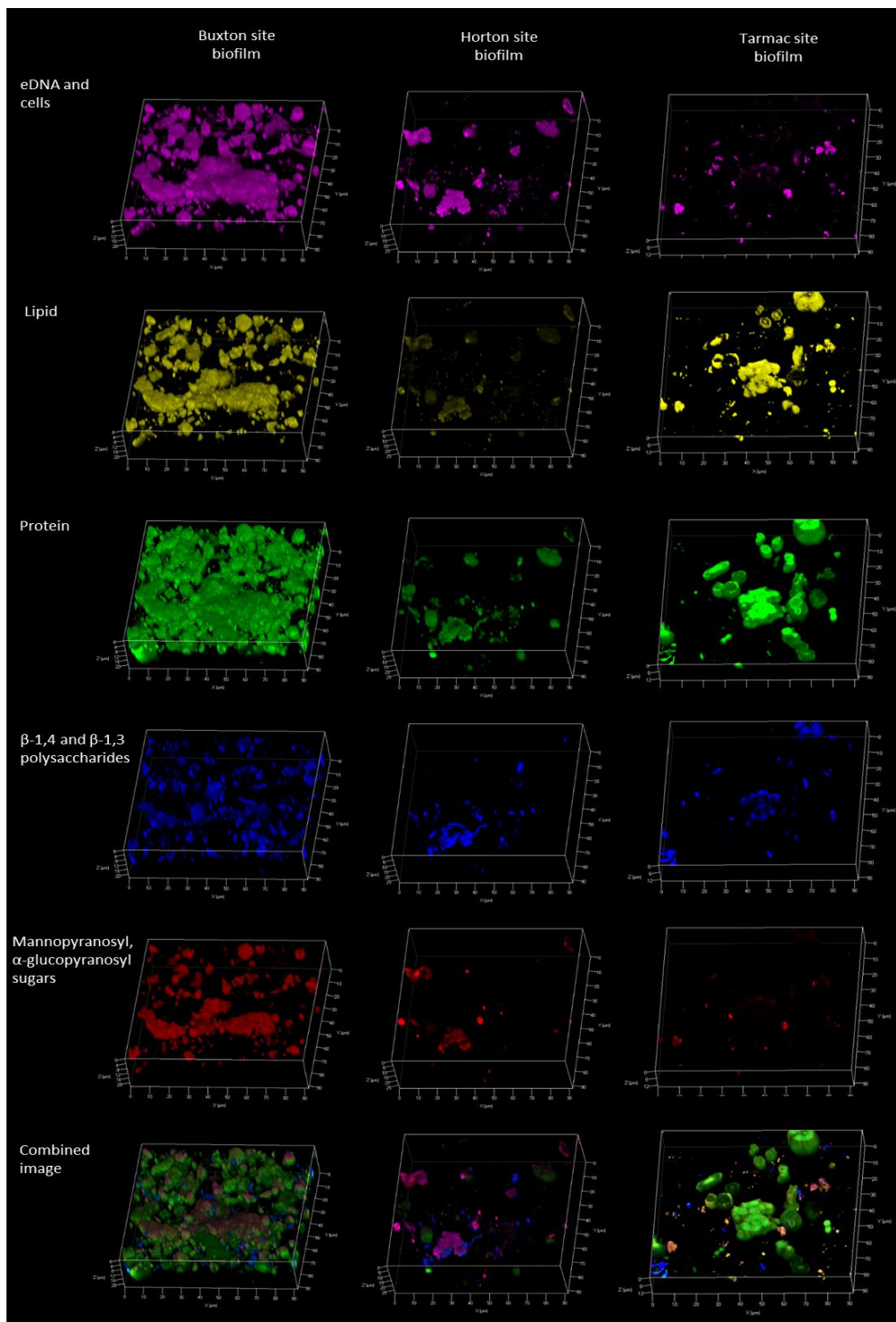


**Figure 9.2: CLSM imaging of biofilm formed upon cotton after 3 month incubation period at different potential analogue sites.** The Buxton site (Site-B) cotton showed the largest amount of colonisation with a biofilm with a complex EPS composition. The cotton samples from the younger sites showed lower levels of colonisations with biofilms possessing similar complex EPS compositions.

SEM investigation of the colonised cotton samples showed areas of biofilm that were punctuated with mineral deposits (Figure 9.3ABC). With EDS of these areas (Figure 9.4)

showing a predominant composition of carbon, calcium and oxygen possibly indicating calcium carbonate formation. In all cases the biofilms were associated with calcium rich precipitates which had formed on the fibres. These fibres lacked evidence of the pits and grooves associated with microbial anaerobic cellulose degradation reported by McDonald *et al* (262) which suggests any degradation of these fibres would be chemical rather than biological. The precipitation of calcium carbonate has relevance to the long term performance of an ILW-GDF as radionuclides can co-precipitate with calcium (139) with carbonation altering the surface chemistry and porosity of NRVB (316, 317) leading to changes in hydraulic retention and pressure issues related to gas build up (319). The ability of biofilm to sequester  $\text{Ca}^{2+}$  may also impact on pH buffering by the partial prevention of calcium carbonate precipitation (301). The small areas of calcium containing precipitate observed here might be related to areas of lower biofilm density which are likely to calcify compared to denser sections as reported by Arp *et al* (301).

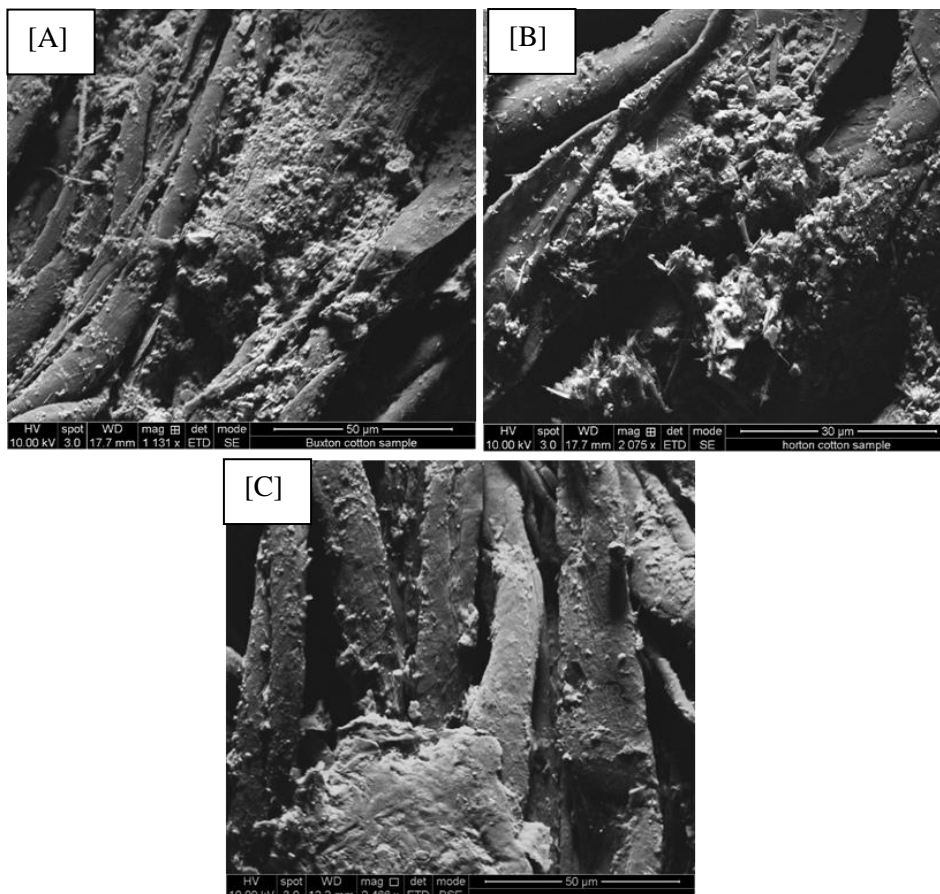
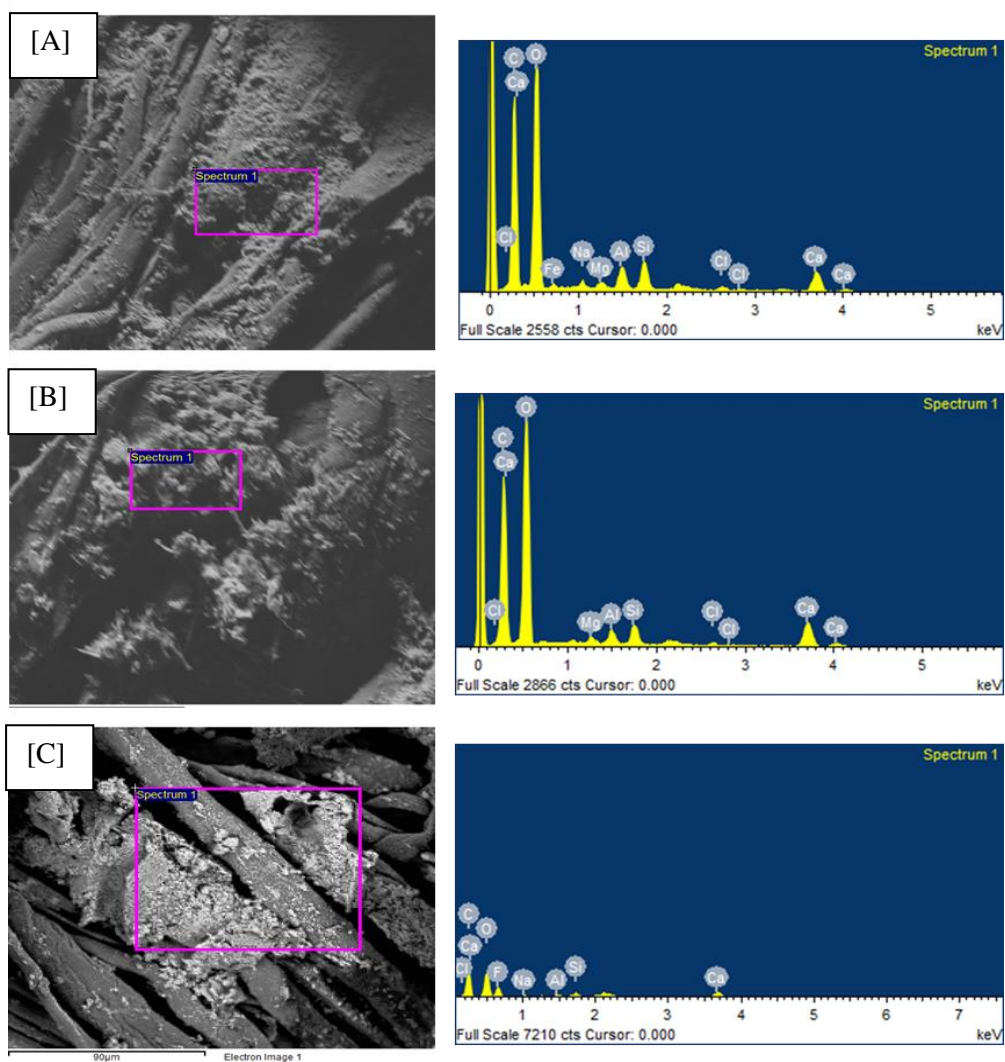


**Figure 9.3: SEM imaging of biofilm formed upon cotton after a 3 month incubation period at different potential analogue sites. Clumps of biofilm can be seen formed upon and in-between cotton fibres with small sections inorganic precipitate. [A] Site-B. [B] Site-H. [C] Site-T.**



Element	(% ) Weight		
	Site-B	Site-H	Site-T
Al	2.2	1.5	1.1
C	35.5	31.5	29.7
Ca	7.7	10.6	12.8
Cl	0.9	0.8	1.0
F	0.0	0.0	18.8
Fe	3.6	0.0	0.0
Mg	0.5	0.6	0.0
Na	0.6	0.0	0.4
O	45.8	52.5	34.1
Si	3.4	2.6	2.3

**Figure 9.4: EDS investigation into the composition of biofilms from upon cotton from different potential analogue sites. Mineral precipitates and biofilm were composed primarily of carbon, calcium and oxygen. [A] Site-B. [B] Site-H. [C] Site-T.**

In order to extract sufficient rRNA from the cotton, samples from hyperalkaline boreholes at each individual site were pooled and the microbial community analysis reported here is based upon cDNA generated from pooled rRNA. This was undertaken in-order to investigate the active microbial biofilm community only. Investigations into the taxonomy of the biofilms revealed a diverse range bacteria present at each site location with lower proportions and diversity of archaea (Figure 9.5AB & Figure 9.6AB). At the class level each biofilm had a similar composition but differed in the representation of the different classes of bacteria present. The archaea were dominated by the Methanobacteria and Methanomicrobia classes at all three sites with archaea from the Thermoplasmata and MBGB classes only present in biofilm from Site-T.

The biofilm from Site-B (Figure 9.6AB) was dominated by taxa from the phylum Firmicutes (58.9 %), and in particular taxa from the classes Clostridia, Bacilli and designation AB476673 which represented 37.0 %, 15.9 % and 6.0 % of the total bacterial community, respectively. Within the Clostridia the families Desulfitobacterium (17.7 %), Veillonellaceae (6.9 %), Christensenellaceae (5.3 %), Hydrogenispora (3.2 %) and Ruminococcaceae (2.1 % of the total community) were most abundant. The Family Desulfitobacterium contained amplicons with sequence similarity to *Desulfitobacterium hafniense*, an anaerobic spore former associated with methanogenic biofilms (352). The Veillonellaceae comprised a number of species within the genera *Anaerospira* and *Dendrosporobacter* which again have been associated with anaerobic consortia (353). The taxa within Christensenellaceae, *Hydrogenispora* and Ruminococcaceae showed species sequence homology to *Clostridium clariflavum*, *Kroppenstedtia eburnean*, *Hydrogenispora ethanolica* and *Clostridium cellulolyticum*, micro-organisms associated with the anaerobic degradation of carbohydrates and complex polymers, including cellulose (354-357) Reads associated with Class designation AB476673 was poorly described and contained two genera designated *FJ269100* and *AB476673* within the EZtaxon database.

Bacillaceae family associated taxa dominated the reads associated with the Bacilli representing 65.6 % of this class and 10.4 % of the total community. Many of the sequences associated with Bacillaceae showed sequence similarity to that *Bacillus pseudofirmus*, an alkaliphilic bacterium capable of growth up to pH 11.4 with the ability to degrade a range of carbohydrates (314, 358). The remaining Bacilli class were classified within the Families Vulcanibacillus and Paenibacillaceae representing 3.0 % and 1.5 % of the total community. These Families contained a number of reads showing sequence similarity to the alkaliphilic

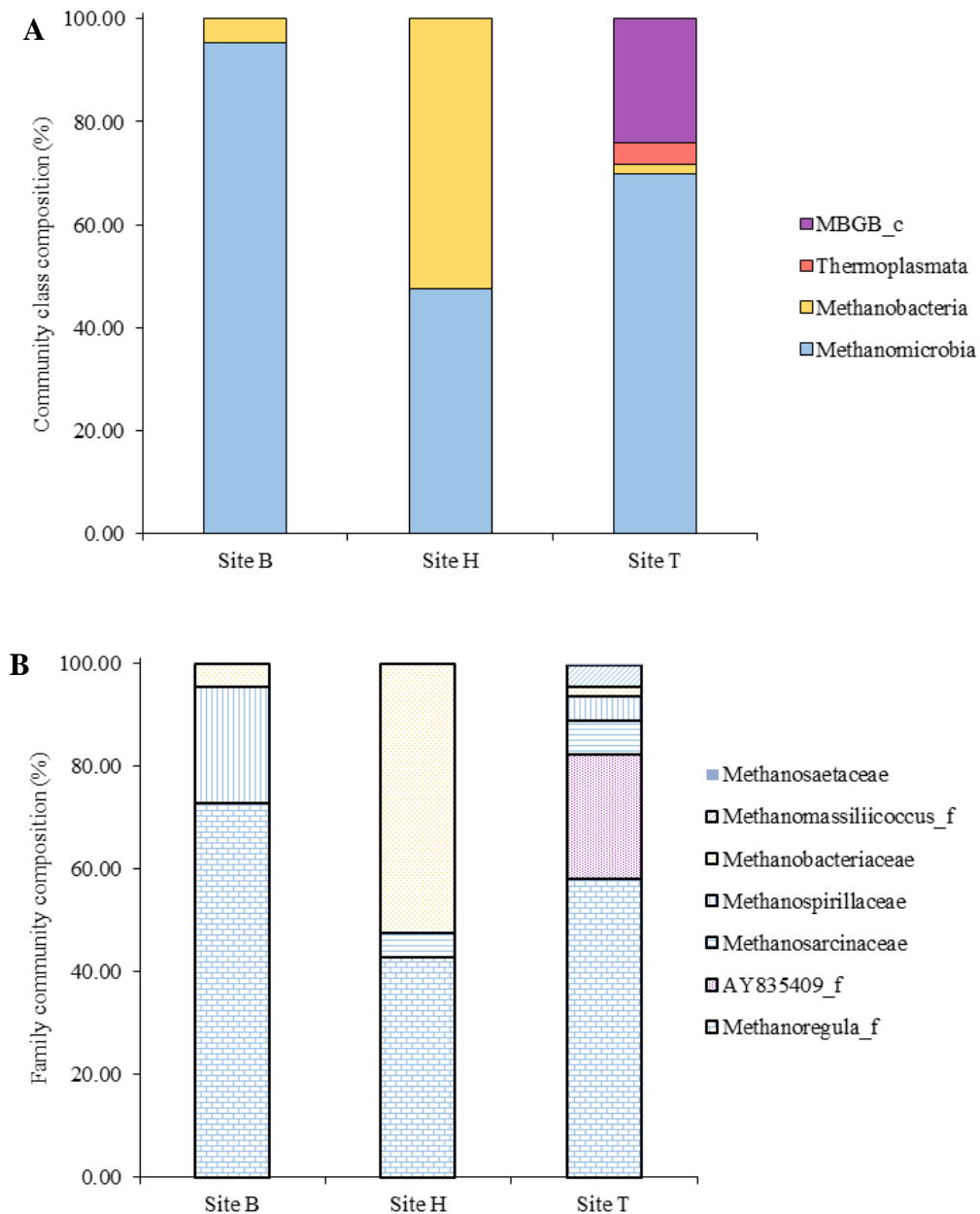
species *Bacillus solimangrovi* and *Paenibacillus daejeonensis* (359, 360). Within AB476673, the reads associated with this class showed greatest sequence similarity to *Caloramator boliviensis* and *Dethiobacter alkaliphilus* species (361, 362). Betaproteobacteria also constituted a significant portion of the active biofilm community at Site-B, where it represented 21.8 % of the total reads. The majority of these reads were associated with taxa of the family Comamonadaceae (17.9 %), which largely showed similarity to sequences associated with the autotrophic hydrogen-oxidizers present within the genus *Hydrogenophaga* (363). Organisms from the Dietziaceae comprised the most part of the reads associated with the class Actinobacteria, which comprised 8.5 % of the total community, sequences within the Dietziaceae showed greatest sequence similarity to the psychrophilic alkaliphile *Dietzia psychralcaliphila* (273). Sequence reads associated with the bacterial phyla Acidobacteria (2.3 %) Bacteroidetes (1.9 %) and Planctomycetes (1. %) were also present within the library where their representation was >1.0 %.

The biofilm from Site-H was dominated by taxa from the phyla Firmicutes and Actinobacteria representing 35.3 % and 33.1 % of the total community (Figure 5). The Firmicutes were again represented by Bacilli, Clostridia and designation AB476673 which represented 21.3 %, 10.5 % and 3.4 % of the total bacterial community, respectively. Within the Bacilli, the Bacillaceae again dominated representing 17.3 % of the total community structure, where again sequence similarity to *Bacillus pseudofirmus* was observed. The Families Vulcanibacillus and Paenibacillaceae were present within the community, where Vulcanibacillus represented 3.1 % of the total with the Paenibacillaceae being 0.05 % of the total community. Within the Clostridia the families Desulfitobacterium (2.2 %), Veillonellaceae (2.0 %), Ruminococcaceae (1.4 %) Hydrogenispora (1.3 %) and Anaerovirgula (1.1 % of the total community) were most abundant. At the species level, the families Desulfitobacterium and Hydrogenospora were also represented by *Desulfitobacterium hafniense* and *Hydrogenospora* as with Site-B. Within the Veillonellaceae members of the genera *Dendrosporobacter*, *Veillionella* and *Succinispira* were present alongside *Saccharofermentans* of the family Ruminococcaceae. *Alkaliphilus* and *Natronicola* represented the majority of reads within the family Anaerovirgula, where both these genera have been associated with anaerobic, alkaline sediments (364, 365). Within class designation AB476673, genus designation AB476673 was most prevalent. As observed with the Site-B cotton sample, the Actinobacteria associated taxa were almost exclusively Dietziaceae and showed sequence similarity to *Dietzia psychralcaliphila*. Proteobacteria

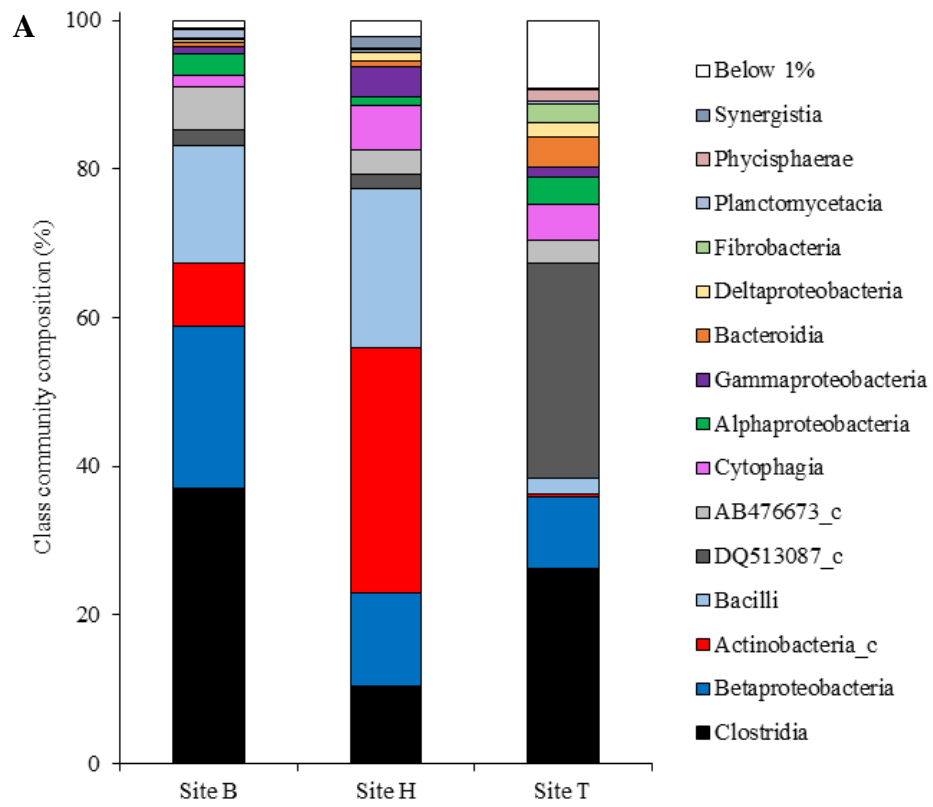
represented 13.3% of the total community, where reads associated with the Comamonadaceae (7.4 %) and Alishewanella (2.6 %) families. The Comamonadaceae were dominated by species from the genus *Hydrogenophaga* as had been observed at Site-B, with the family Alishewanella dominated by reads showing sequence similarity to *Alishewanella jeotgali*, previously associated with flocs degrading isosaccharinic acids described in Chapter 6. Bacteroidetes associated taxa represented 6.7% of the total Site-H community, dominated by the family Cyclobacteriaceae which in itself comprised 5.9% of the total community. The reads associated with this family showed greatest similarity to *Aquiflexum balticum*, which has been observed to grow up to a pH of 9 (366). Acidobacteria (2.0 %), and Synergistetes (1.5 %), were the remaining bacterial phyla detected at a cut off of 1.0 %.

Whereas taxa from the phylum Acidobacteria had represented 2.3 % and 2.1 % of the Site-B and Site-H biofilm communities, Acidobacteria represented 29.7 % of the total community at Site-T. Taxa from the family designation DQ513087 dominated the Acidobacteria representing 24.9 % of the total community of sequence similarity to the species of the genus *Thioprofundum* (Figure 9.6AB). Alongside Acidobacteria, Firmicutes also formed a significant proportion (31.3 %) of the Site T biofilm community. The Clostridia taxa of the Firmicutes were predominated by Veillonellaceae (12.6 %), Ruminococcaceae (5.6 %) and Christensenellaceae (3.0 % of the total community), where the Veillonellaceae associated reads showed greatest sequence similarity to *Succinispira*. *Saccharofermentans* sp. and *Clostridium sporogenes* were the dominant species matches within the Ruminococcaceae and Christensenellaceae families respectively. Family designation AB476673 and the Bacillaceae were also present within the phylum but the taxa associated with these represented only 2.4 % and 1.2 % of the total community. Proteobacteria represented 16.2 % of the active biofilm community and as with both Sites-B and Site-H, *Hydrogenophaga* of the family Comamonadaceae represented 6.2 % of the total. The family Acetobacteraceae was also prevalent, representing 2.2 % of the total community, where the reads showed greatest sequence similarity to *Sediminicoccus rosea*. Methylophilaceae (1.4 %) and Zoogloea (1.2 %) were also present within the Proteobacteria (Figure 9.6AB). Sequences showing greatest similarity to *Aquiflexum balticum* of the family Cyclobacteriaceae formed 4.8 % of the total community structure. These taxa alongside *Bacteroides luti* of the Bacteroidaceae (2.1 %) comprised the majority of the phylum Bacteroidetes, which represented 9.6 % of the total active community of Site-T. Organisms classified within the phylum Fibrobacteres composed 2.9 % of the total active community, and were almost exclusively of the family

Fibrobacteraceae. The sequences within this family all showed greatest sequence similarity to *Fibrobacter sp*, a genus closely associated with cellulolytic processes (262). Bacterial taxa composing >1.0 % of the total active community and were classified within the phyla: Planctomycetes (2.0 %), Verrumicrobia (1.6 %), and Lentisphaerae (1.0 %)



**Figure 9.5: Archaeal 16S rRNA community analysis of different potential analogue sites.** [A] Class level distribution shows relative dominance of Methanobacteria at all three sites with a larger abundance of Methanomicrobia at the two older sites. Site-T the youngest site had a methanogen component which was more diverse than the older sites. [B] Family level distribution showed the methanogen component was composed of a small number of families at all the sites.



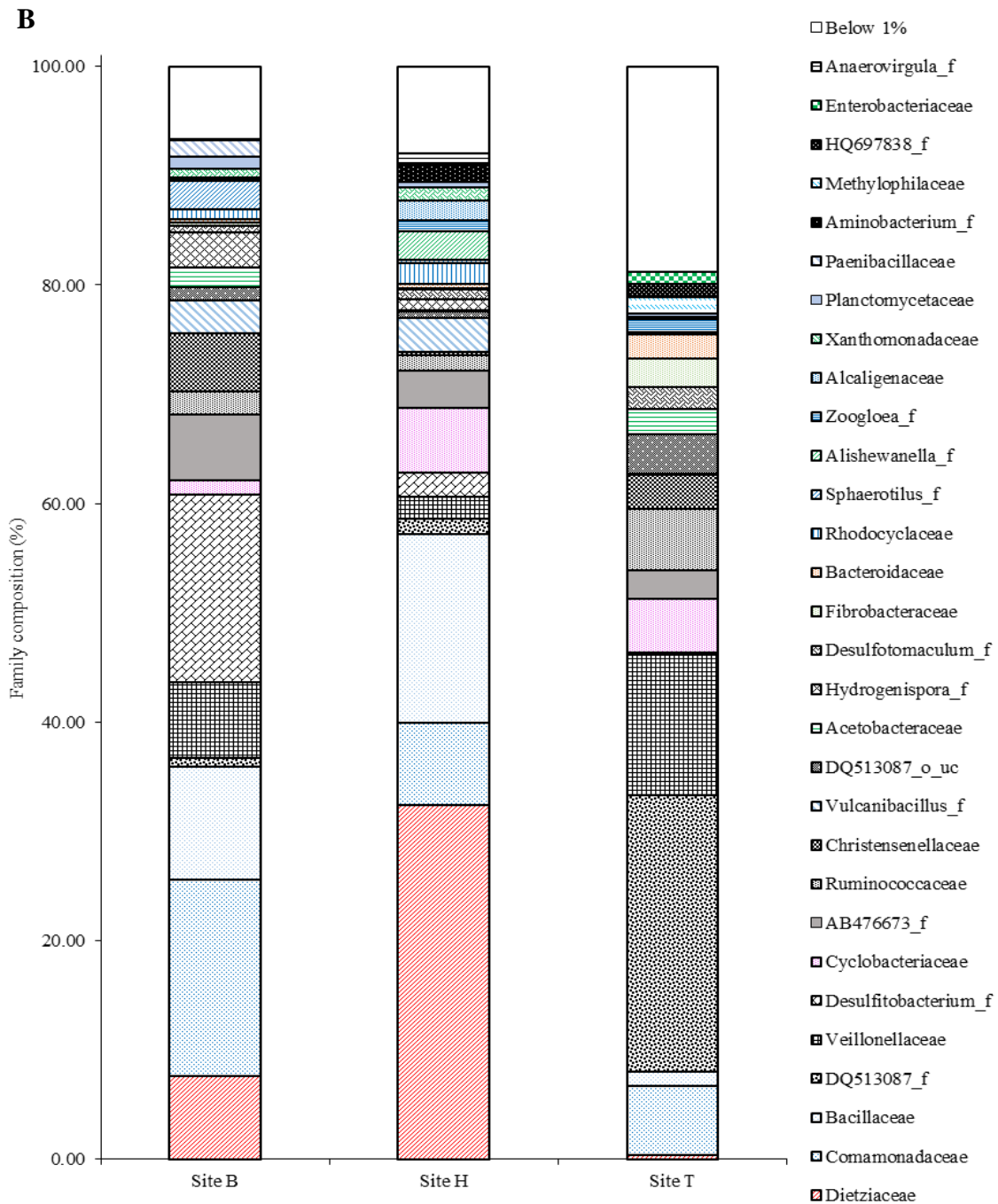


**Figure 9.6 : Bacterial 16S rRNA community analysis of different potential analogue sites.** [A] Class level distribution shows Site-B and Site H had a similar proportion of Clostridia, Betaproteobacteria, Actinobacteria and Bacilli. The younger Site-T had both a Clostridia and Betaproteobacteria but lacked large Actinobacteria and Bacilli components. [B] Family level distribution shows many of the classes were dominated by a low number of families which were similar across the three biofilms.

16S rRNA analysis indicated the abundance of active Firmicutes and Proteobacteria within all three sites, implicating these taxa with the generation and establishment of these cellulose

associated biofilms (Figure 9.6AB). The abundance of Proteobacteria, and in particular *Hydrogenophaga* also suggest that the degradation of cellulose and cellulose degradation products (both microbial and alkaline) results in the generation of hydrogen which is subsequently utilised by these hydrogenotrophic micro-organisms. *Hydrogenophaga* appears to be a common taxa observed within natural alkaline sites including the Allas Springs in Cyprus (67, 143), Leka Ophiolite in Norway (42) and at two continental serpentinite hosted alkaline seeps at the Tablelands Ophiolite, Newfoundland (43). The presence of hydrogenotrophic methanogens also support that the generation of hydrogen is occurring within the biofilm community. Species of the *Methanoregula* genus were observed which have previously been reported to produce methane through the H<sub>2</sub>/CO<sub>2</sub> pathways rather than via the utilisation of acetate (367). Hydrogenotrophic Methanobacteria were present at all sites but were most abundant in the biofilms from Site-H with methanogens from this class previously isolated and reported under alkaline conditions (153, 158).

Biofilms from all three sites showed a large degree of species richness with similar OTU numbers of 1868 and 1881 for Site-B and Site-H, respectively, and a lower number of 1244 for Site-T (Table 9.3). Sampling of the sites did not reach saturation according to the rarefaction curve (Figure 9.5A), however, the rank abundance curves (Figure 9.5B) indicate that the most abundant OTU's were sufficiently detected (226) with a corresponding Goods coverage of between 0.94 and 0.96 across all three sites (Table 3). The Shannon indices were similar for biofilms from Site-B and Site-H with values of  $5.52 \pm 0.03$  and  $5.28 \pm 0.03$ , respectively, with Site-T biofilms having the lowest value of  $4.48 \pm 0.03$  (Table 9.3). The Shannon indices here are larger than those reported for biofilms formed from floc communities as reported in Chapter 7 (Table 7.9) as is probably a reflection of the inevitable loss of some microorganisms due to culturing methods (368) and the in-situ availability of TEA's at the sites. Despite the harsh conditions the in-situ biofilms possessed a level of diversity similar to biofilms developed from circumneutral floodplains and stream communities under laminar and turbulent flows reported by Niederdorfer *et al* (276).

Analogue site biofilm	Valid reads	OTUs	Ace	Chao1	Shannon	Goods Lib. Coverage
Site-B	19085	1868	9115.75	6385.88	5.52	0.94
Site-H	19088	1881	9084.58	6274.59	5.28	0.94
Site-T	19534	1244	5402.19	3760.60	4.48	0.96

**Table 9.3: Alpha diversity statistics for biofilms formed at different potential analogue sites.** The biofilms formed at older sites possessed a similar level of diversity and had higher numbers of OTU's and diversity scores in comparison to the biofilm formed at the younger site.

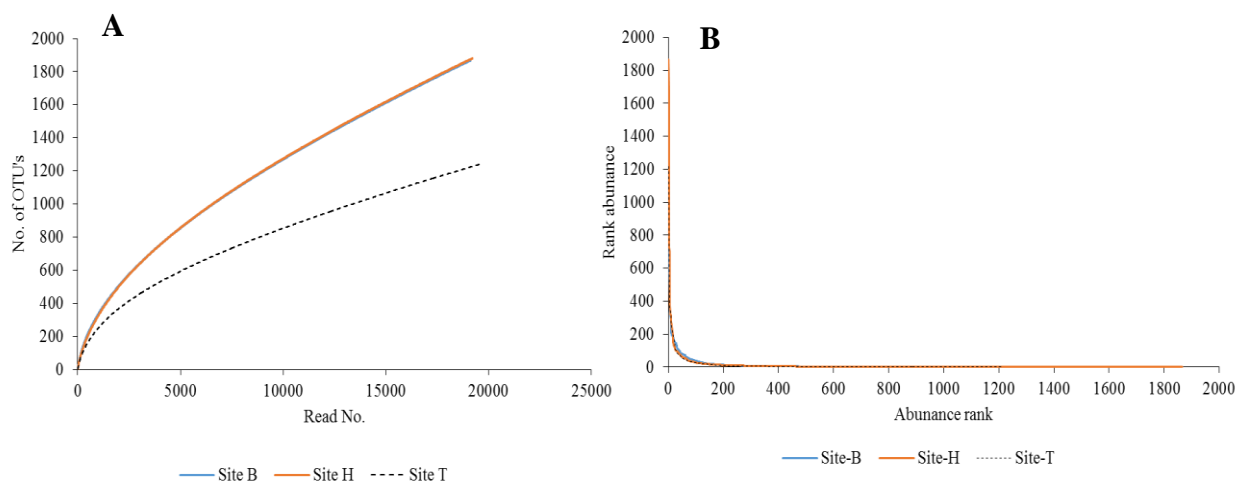


**Figure 9.7: Rarefaction and rank abundance curves of biofilms formed in-situ at different potential analogue sites.** [A] Rarefaction curves shows sampling did not reach saturation, however, Goods Coverage values indicate the vast majority of OTU's were identified. [B] Rank abundance curves show a diverse microbial community.

Probability testing showed that there was no significant difference between the biofilms at all 3 sites at the family level using a 95% confidence interval (Table 9.4). The biofilms at all three sites only shared 5.8 % of the total detected OTU's (Figure 9.8A) but this shared common component accounted for 48.8 % of all the sequence reads (Figure 9.8B). The total sequence reads not shared occurring at all individual site was 11.9 %, with 88.1 % of the sequence reads shared between two or more sites. From the above, it is clear that the shared component between the sites, despite only consisting of a small portion of the total OTU's contained a significant portion of the microbial community.

	Site-B	Site-H	Site-T
Site B		0.143	0.148
Site H	0.143		0.094
Site T	0.148	0.094	

**Table 9.4: Probability testing for the comparison of biofilm communities at different potential analogue sites.**

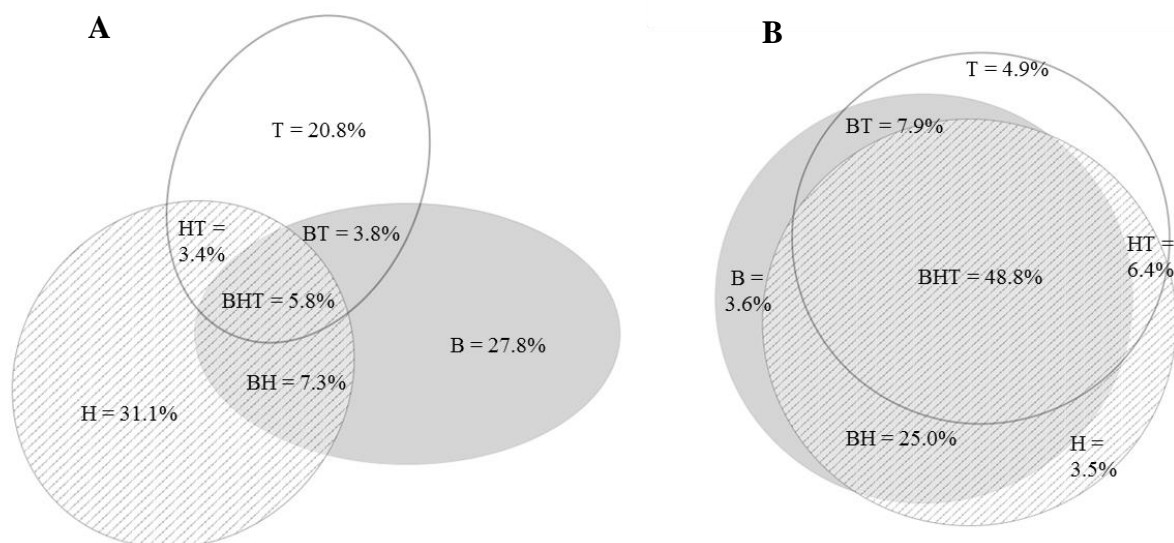


**Figure 9.8: Distribution of the shared OTU's and sequence reads across biofilms from different potential analogue sites.** [A] Distribution of OTU's show only a small portion of the total OTU's were shared between the biofilms from different sites. [B] Read distribution, however, shows that this small portion of shared OTU's represented the majority of microbial community.

Deeper investigation into the shared OTU's between all biofilms and the related taxonomy (Table 9.5) revealed bacteria from the classes Clostridia, Betaproteobacteria and Bacilli to be the most dominant with a 22.6 %, 6.7 % and 5.3 % representation of the total sequence reads, respectively. A further 23 different classes of bacteria and 2 classes of archaea made up the rest of the shared OTU's.

Order	Class	Sequence reads	OTU95	Total contribution (%)	Shared contribution (%)
Firmicutes	Clostridia	13911	33	22.6	29.7
Proteobacter	Betaproteobacter	4109	15	6.7	13.5
Firmicutes	Bacilli	3243	9	5.3	8.1
Bacteroidetes	Cytophagia	1957	4	3.2	3.6
Actinobacteria	Actinobacteria_c	1865	7	3.0	6.3
Acidobacteria	DQ513087_c	1027	3	1.7	2.7
Firmicutes	AB476673_c	712	1	1.2	0.9
Bacteroidetes	Bacteroidia	536	4	0.9	3.6
Fibrobacteres	Fibrobacteria	518	3	0.8	2.7
Proteobacter	Alphaproteobacter	363	6	0.6	5.4
Synergistetes	Synergistia	295	1	0.5	0.9
Proteobacter	Deltaproteobacter	273	3	0.4	2.7
Euryarchaeota	Methanomicrobia	172	1	0.3	0.9
Proteobacter	Gammaproteobacter	162	2	0.3	1.8
Verrucomicrobia	Opitutae	140	4	0.2	3.6
Cyanobacteria	Vampirovibrio_c	123	2	0.2	1.8
Chloroflexi	SAR202_c	112	1	0.2	0.9
Chloroflexi	Anaerolineae	108	1	0.2	0.9
Fibrobacteres	JN697815_c	83	1	0.1	0.9
Acidobacteria	EU881314_c	68	2	0.1	1.8
Firmicutes	Erysipelotrichi	65	1	0.1	0.9
Lentisphaerae	GU196224_c	63	1	0.1	0.9
WS3	AQSL_c	54	1	0.1	0.9
Fibrobacteres	JF304641_c	28	1	0.0	0.9
Armatimonadetes	EU266864_c	14	1	0.0	0.9
Planctomycetes	Phycisphaerae	13	1	0.0	0.9
Euryarchaeota	Methanobacteria	9	1	0.0	0.9
Spirochaetes	Spirochaetes_c	9	1	0.0	0.9

**Table 9.5: Shared OTU's between biofilms from different potential analogue sites.** The majority of the shared OTU's were from Clostridia, Betaproteobacter and Bacilli lineages.

Heat mapping of the shared genera between all three biofilms (Figure 9.9) revealed *Aquiflexum*, *Bacillus\_g6*, *Hydrogenophaga* and an uncultured genus *DQ513087* of the order Acidobacteria to be present in all three biofilms with a strong shared similarity. Biofilms from Site-B and Site-H showed a higher representation of *Dietzia* in comparison to Site-T. The expression of some individual genera was increased at specific sites such as seen in the increased abundance of *Malikia* at Site-B and uncultured genus of the *Christensenellaceae* family at Site-H. Only 2 archaeal genera were shared between the sites with *Methanobacterium* expressed similarly in biofilms across all sites and *Methanoregula* the

most dominant at Site-T compared to Site-B and Site-H.

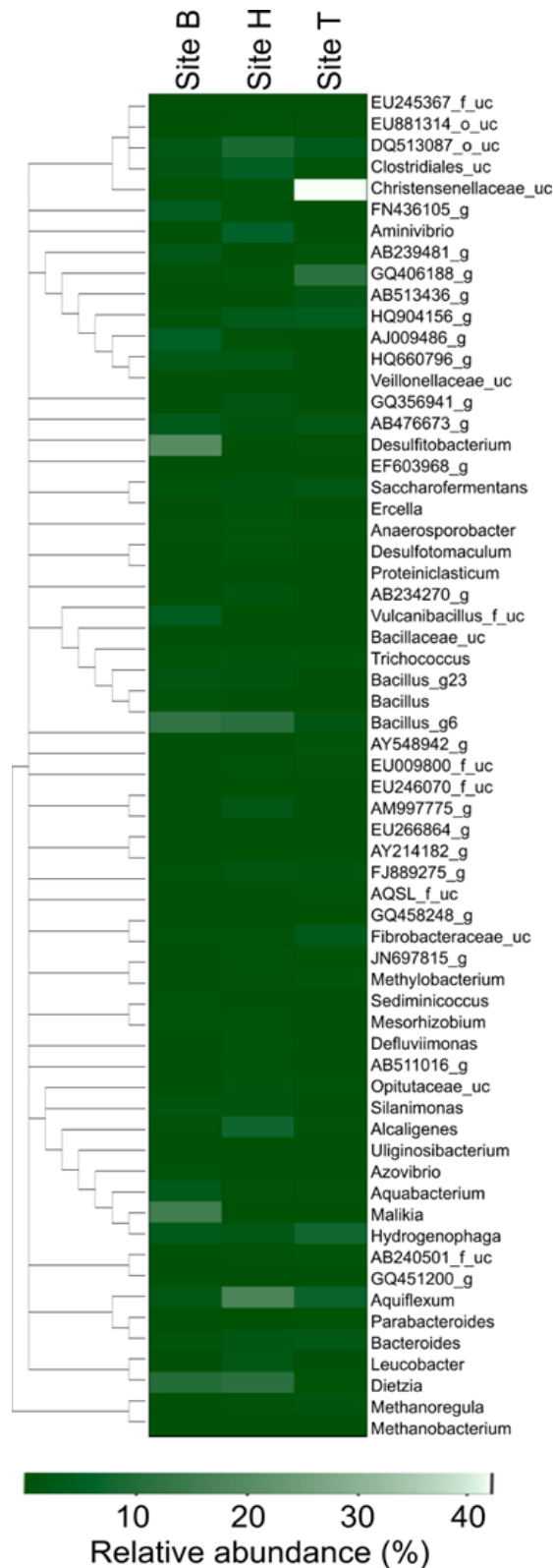


Figure 9.9: Heat map at the genus level of shared OTU's between biofilms at different potential analogue sites.

All three sites shared a small proportion of the total OTU's and of this shared proportion, OTU's of the Clostridia made up its majority (Table 9.5). Clostridia have been widely reported previously at both natural (43, 67) and anthropogenic alkaline sites (82, 84) as well as being present in enrichment cultures generated from these sites (81, 84). The relative abundance of Clostridia under these conditions indicates that this highly versatile bacteria play a key role in carbon cycling and biofilm formation under hyper alkaline conditions. Each site possessed a distinct set of OTU's and also shared a smaller proportion of OTU's with the other two sites. The older sites (Site-B and Site-H) shared a higher proportion of OTU's than when compared to the younger Site-T. The older sites contained a similar and larger number of OTU's than Site-T and possessed a greater abundance of recognised alkaliphilic bacteria such as those from the *Bacillus* and *Dietzia* genera's (273, 314). These differences are a reflection of the time available for the local communities to adapt and evolve to the hyperalkaline conditions at these locations.

### 9.3 Conclusion

This work is the first to investigate the development of an active, polymicrobial biofilms on cellulosic materials within anthropogenic, hyper alkaline sites of different ages. The use of cotton 'bait' successfully simulated the role played by vegetation at the margins of these hyper alkaline sites in manner that allow site to site comparisons. All sites were able to form polymicrobial, anaerobic biofilms within a few months of incubation. In all cases alkaline cellulose hydrolysis contributed soluble, degradable organic carbon to the system. There was no obvious evidence of direct microbial cellulose hydrolysis although the microbial populations did contain genera with cellulolytic capabilities.

The biofilms formed were composed of a complex mixture of lipids, proteins, carbohydrates and eDNA with the complexity and extent of biofilm increasing as the age of the site increased. Changes in biofilm composition coincided with changes in microbial community composition with the presence or absence of alkaliphilic genera such as *Dietzia* possibly a key indicator of the biofilm EPS composition and maturity of the site. The microbial community analysis suggests that these hyperalkaline environments contain a small number of common microbes, with the number of these common microbes increasing as the age of the site increases. The genre *Hydrogenophaga* appears to be ubiquitous in these hyperalkaline sites and the Archaea are represented by a small number of hydrogenotrophic methanogenic genre. These observations have relevance to environments such as those predicted to develop in radioactive waste disposal sites since they indicate that complex polymicrobial biofilms

can develop with decades under hyper alkaline conditions provided cellulosic materials are present.

#### **9.4 Key findings**

- The additional two sites surveyed revealed a hyperalkaline calcium dominated environment which was able to generate ISA in-situ from cellulosic materials.
- Cotton incubated at these sites was able to be colonised by polymicrobial biofilms with complex EPS compositions. With the older sites showing a greater degree of colonisation and diversity of EPS components.
- All three biofilms analysed were diverse and contained a shared common component predominantly consisting of Clostridia, Betaproteobacteria and Bacilli. The older the site the more alkaliphilic microbes were present such as those from the *Dietzia* and *Bacillus* lineages.
- A range of hydrogen utilising microbes from both bacteria and archaea lineages common to all sites were identified.
- The presence cellulose under ILW-GDF conditions has the potential to generate a diverse biofilm community with a diverse metabolic range. The presence of biofilm and/or microbial action of these biofilm communities has the potential to locally form mineral precipitates with a composition similar to calcium carbonate.

## **10. Concluding remarks**

Using cotton 'baits', biofilm was able to be cultured in-situ at the Harpur Hill, Buxton analogue site for an ILW-GDF and two other potential analogue sites. At these sites ISA was able to be generated in-situ and the presence of various TEA's appears to have enable diverse microbial populations to form despite the external harsh conditions. Biofilms from all potential analogue sites tested possessed a common component of bacteria including Clostridia and Proteobacteria which align towards biofilm formation and carbohydrate fermentation. Microbial community analysis revealed that as areas contaminated with calcium rich wastes age the proportion of alkaliphilic microorganisms such as from those from *Dietzia* genus increase in abundance. The microbial community analysis of these biofilms indicates that in just a few decades alkaliphilic microorganisms can evolve and form a key component within biofilm communities.

Culturing of the biofilm formed upon cotton from the oldest anthropogenic site at Buxton, UK showed the ability of the microbial consortia to degrade all forms of ISA through a fermentation pathway to acetate and hydrogen. Liquid based CDP driven microcosms showed microbes formed floc based systems under both methanogenic and sulphate reducing systems, with the sulphate reducing system able to produce small quantities of sulphide. The floc communities formed within CDP driven microcosms possessed a good degree of diversity with large components of Actinobacteria, Clostridia and Proteobacteria. FISH probing showed that the vast majority of microbes were situated towards the centre of flocs where a lower pH microsite was present. This was produced probably by both the production of metabolic acids and the properties of the EPS matrix forming the flocs. The EPS matrix from which the flocs were formed was diverse and reflected the microbial community composition, with carbon flow showing a large portion of available carbon used for EPS production. The EPS was shown to partially shield the microbes from the external pH by allowing the formation of an area of a lower pH within the floc. This mechanism allowed microbial survival in flocs up to pH 12 and conferred short time survival at pH 13.

Floc systems were able to produce biofilm upon a range of ILW-GDF relevant surfaces including sand, NRVB, graphite and steel. Thick dense biofilm was able to form within sand columns under methanogenic conditions at pH 11 with the ability to degrade all three forms of ISA increasing due to biofilm formation. The production of methane alongside hydrogen was enhanced by biofilm formation possibly due low redox values and lower pH values within the interior of the biofilm compared to the floc communities. The protection biofilm conferred the microbes allowed bacterial survival up to pH 13, where ISA degradation and associated gas generation was only impacted by the transition from pH 12 to pH 13. This is most likely related to the rise in the internal pH of the biofilm with microbial community analysis showing a greater abundance of alkaliphilic microbes as the external pH increased.

Exposure of NRVB, graphite and steel surfaces downstream from biofilms under hyperalkaline conditions facilitated carbonation of these surfaces with the elemental composition analysis showing evidence of calcium, carbon and oxygen indicating possible calcium carbonate precipitate. CLSM imaging of these surfaces revealed EPS components to be present upon the surfaces indicating both biofilm formation and also possible priming of the surface from dissolved organic components. The NRVB surface showed a greater organic

coverage at pH 13 possibly due to alkaline lysis of some EPS components. As the priming of surfaces facilitates biofilm formation the ability of microbes to form biofilm upon NRVB surfaces may increase with exposure time. Biofilm under these conditions were able to decrease the pH of the surrounding environment which could facilitate microbial survival and propagation under ILW-GDF conditions. Further sloughing of the biofilm released flocs under all pH values tested which could act as a transport vector for biofilm colonisation elsewhere within an ILW-GDF.

The addition of sulphate to the liquid microcosm resulted in the enhanced growth of bacteria from the family *Corynebacteriaceae* which is capable of the assimilatory reduction of sulphate to form sulfur containing proteins. Degradation of these proteins could produce sulphide which could in turn facilitate the corrosion of metals. The detection of *drsA* transcripts at pH 11 revealed that dissimilatory sulphate reduction was possible under ILW-GDF conditions albeit at a very low rate.

Biofilm was able to form from floc communities upon steel surfaces under sulphate reducing conditions at pH 11. The grade of the steel had no significant impact upon the composition of the microbial community or biofilm EPS composition, with the biofilm system demonstrating the degradation of all forms of ISA. Sulphate was able to be degraded by this system and sulphide was subsequently produced. Removal of the biofilm from the steel discs showed small areas of possible microbial induced corrosion with elemental composition analysis showing small traces of sulphur. Only small amounts of sulphate were utilised with small amounts of sulphide produced. Interestingly methanogenesis was able to co-occur alongside sulphate reduction under this system possibly due to the low rates of sulphate reduction and sulphide generation.

The EPS matrices investigated under all systems showed a complex and similar composition with a range of functional groups which under the alkaline conditions could contribute a negative charge to the EPS. This negative charge could interact with cationic species such as  $\text{Ca}^{2+}$  and enhance biofilm aggregation, stability and formation. Components such as eDNA were shown to be integral in stability and formation of floc based aggregates most likely due to thermodynamically favourable interaction with  $\text{Ca}^{2+}$ . The EPS components likely facilitated the formation of lower pH values within biofilm and flocs, with carbohydrate and lipid fractions conferring a level of hydrophobicity and polysaccharides and possibly proteins possessing acidic monomer units.

The ability of microbes within biofilm to degrade ISA and survive under hyperalkaline conditions could have the following potential impacts when regarding the long term performance of an ILW-GDF:

- The removal of complexants such as ISA will have an impact upon the mobility radionuclides with the end products of ISA fermentation possibly fuelling methanogenesis and sulphate reduction processes. Methanogenesis could allow for the transport of  $^{14}\text{C}$  out an ILW-GDF through the formation of  $^{14}\text{CH}_4$ . Sulphide generation may lead to corrosion of steel surfaces such as those encasing ILW.

- Microbes cultured from an ILW-GDF analogue site have the ability to form biofilm upon a range of ILW-GDF surfaces, with biofilm formation enhancing ISA degradation. Biofilm formation upon host rock and NRVB surfaces may alter its ability to interact with radionuclides and cause changes to the surface chemistry. With the clogging of pore throats by biofilm altering hydraulic retention.
- Carbonation of NRVB surfaces caused by microbial action will lead to a lowering of the NRVB porosity which will alter hydraulic retention and possibly cause pressure issues due to gas build up. Carbonation of NRVB may also alter its ability to interact and immobilise radionuclides.
- The formation of calcium carbonate may trap radionuclides and also seal cracks and fissures leading to changes in hydraulic retention.
- The generation of hydrogen may further fuel microbial metabolism which in turn could facilitate biofilm formation and support a range of microbial metabolic processes including methanogenesis.

## 11. References

1. N.D.A., (2011), The 2010 UK Radioactive Waste Inventory: Main Report, NDA/ST/STY(11)0004. Nuclear Decommissioning Authority (Radioactive Waste Management Directorate), Harwell, Didcot, Oxfordshire, UK.
2. N.D.A., (2014), Radioactive Wastes in the UK: A Summary of the 2013 Inventory, NDA/ST/STY(14)0006. Nuclear Decommissioning Authority (Radioactive Waste Management Directorate), Harwell, Didcot, Oxfordshire, UK.
3. L. L. LTD, (2016), <http://llwrsite.com/national-repository/>, LLWR Lpository LTD. [November 2016].
4. I. Beadle, P. N. Humphreys, C. Pettit, J. Small, (2000), Integrating microbiology into the Drigg Post-closure radiological safety assessment. *Materials Research Society Proceedings*. 663, 665.
5. N.D.A., (2010), Geological Disposal: An Introduction To The Generic Disposal System Safety Case, Nuclear Decommissioning Authority (Radioactive Waste Management Directorate), Harwell, Didcot, Oxfordshire, UK. .
6. N.D.A., (2010), Geological Disposal: Generic Disposal System Technical Specification, NDA/RWMD/044. Nuclear Decommissioning Authority (Radioactive Waste Management Directorate), Harwell, Didcot, Oxfordshire, UK. .
7. N.D.A., (2010), Near-field Evolution Status Report, NDA/RWMD/033. Nuclear Decommissioning Authority (Radioactive Waste Management Directorate), Harwell, Didcot, Oxfordshire, UK.
8. V. V. Romyantsev, (1992), High-level radioactive waste vitrification. *Atomnaya Tekhnika za Rubezhom*. 24-26.
9. D.E.C.C., (2014), Implementing Geological Disposal: A Framework For The Long-term Management Of Higher Activity Radioactive Waste, URN 14D/235. Department of Energy and Climate Change, London, UK.
10. N.D.A., (2010), Geological Disposal: Package Evolution Status Report, NDA/RWMD/031. Nuclear Decommissioning Authority (Radioactive Waste Management Directorate), Harwell, Didcot, Oxfordshire, UK.
11. U. R. Berner, (1992), Evolution of pore water chemistry during degradation of cement in a radioactive waste repository environment. *Waste Management*. 12, 201-219.
12. E. J. Butcher, J. Borwick, N. Collier, S. J. Williams, (2012), Long term leachate evolution during flow-through leaching of a vault backfill (NRVB). *Mineralogical Magazine*. 76, 3023-3031.
13. N. Chapman, A. Hooper, (2012), The disposal of radioactive wastes underground. *Proceedings of the Geologists' Association*. 123, 46-63.
14. M. Libert, O. Bildstein, L. Esnault, M. Jullien, R. Sellier, (2011), Molecular hydrogen: An abundant energy source for bacterial activity in nuclear waste repositories. *Physics and Chemistry of the Earth, Parts A/B/C*. 36, 1616-1623.
15. N.D.A., (2010), Geological Disposal: Geosphere Status Report, NDA/RWMD/035. Nuclear Decommissioning Authority (Radioactive Waste Management Directorate), Harwell, Didcot, Oxfordshire, UK.
16. N.D.A., (2010), Geological Disposal: Radionuclide Behaviour Status Report, NDA/RWMD/034. Nuclear Decommissioning Authority (Radioactive Waste Management Directorate), Harwell, Didcot, Oxfordshire, UK.
17. T. D. H. Bugg, M. Ahmad, E. M. Hardiman, R. Rahmanpour, (2011), Pathways for degradation of lignin in bacteria and fungi. *Natural product reports*. 28, 1883-1896.
18. L. R. Van Loon, M. A. Glaus, (1998), Experimental and theoretical studies on alkaline degradation of cellulose and its impact on the sorption of radionuclides, Paul Scherrer Institut Villigen, Switzerland.
19. W. Astbury, M. Davies, (1944), Structure of cellulose. *Nature*. 154, 84.

20. P. N. Humphreys, A. P. Laws, J. Dawson, (2010), A review of cellulose degradation and the fate of degradation products under repository conditions, SERCO/TAS/002274/001. Nuclear Decommissioning Authority (Radioactive Waste Management Directorate), Harwell, Didcot, Oxfordshire, UK. .
21. H. V. Scheller, P. Ulvskov, (2010), Hemicelluloses. *Plant Biology*. 61, 263.
22. C. J. Knill, J. F. Kennedy, (2003), Degradation of cellulose under alkaline conditions. *Carbohydrate Polymers*. 51, 281-300.
23. I. Pavasars, J. Hagberg, H. Borén, B. Allard, (2003), Alkaline degradation of cellulose: mechanisms and kinetics. *Journal of Polymers and the Environment*. 11, 39-47.
24. M. A. Glaus, L. R. Van Loon, S. Achatz, A. Chodura, K. Fischer, (1999), Degradation of cellulosic materials under the alkaline conditions of a cementitious repository for low and intermediate level radioactive waste: Part I: Identification of degradation products. *Analytica Chimica Acta*. 398, 111-122.
25. L. R. Van Loon, M. A. Glaus, (1997), Review of the kinetics of alkaline degradation of cellulose in view of its relevance for safety assessment of radioactive waste repositories. *Journal of Environmental Polymer Degradation*. 5, 97-109.
26. P. N. Humphreys, J. M. West, R. Metcalfe, (2010), Microbial effects on repository performance, Quintessa contractors report prepared for the Nuclear Decommissioning Authority (Radioactive Waste Management Directorate), Harwell, Didcot, Oxfordshire, UK.
27. M. Almond, P. B. Shaw, P. N. Humphreys, M. J. Chadha, K. Niemela, A. P. Laws, (2012), Behaviour of xyloisosaccharinic acid and xyloisosaccharino-1,4-lactone in aqueous solutions at varying pHs. *Carbohydr Res*. 363, 51-57.
28. M. Randall, B. Rigby, O. Thomson, D. Trivedi, (2013), Assessment of the effects of cellulose degradation products on the behaviour of europium and thorium 12239 Part A Issue 4. National Nuclear Laboratory Chadwick House, Warrington, UK. .
29. P. B. Shaw, G. F. Robinson, C. R. Rice, P. N. Humphreys, A. P. Laws, (2012), A robust method for the synthesis and isolation of  $\beta$ -gluco-isosaccharinic acid ((2R, 4S)-2, 4, 5-trihydroxy-2-(hydroxymethyl) pentanoic acid) from cellulose and measurement of its aqueous pKa. *Carbohydr Res*. 349, 6-11.
30. B. F. Greenfield *et al.*, (1994), The identification and degradation of isosaccharinic acid, a cellulose degradation product. *Materials Research Society Proceedings*. 353, 1151.
31. B. F. Greenfield, M. H. Hurdus, M. W. Spindler, H. P. Thomason, (1997), The effects of the products from the anaerobic degradation of cellulose on the solubility and sorption of radioelements in the near field, 376. UK NIREX Report NSS, Harwell, Didcot, Oxfordshire, UK.
32. K. Vercammen, M. A. Glaus, L. R. Van Loon, (2001), Complexation of Th (IV) and Eu (III) by  $\alpha$ -isosaccharinic acid under alkaline conditions. *Radiochimica Acta International journal for chemical aspects of nuclear science and technology*. 89, 393.
33. J. Tits, E. Wieland, M. H. Bradbury, (2005), The effect of isosaccharinic acid and gluconic acid on the retention of Eu(III), Am(III) and Th(IV) by calcite. *Applied geochemistry*. 20, 2082-2096.
34. P. Warwick, N. Evans, T. Hall, S. Vines, (2003), Complexation of Ni (II) by  $\alpha$ -isosaccharinic acid and gluconic acid from pH 7 to pH 13. *Radiochimica Acta/International journal for chemical aspects of nuclear science and technology*. 91, 233-240.

35. P. Warwick, N. Evans, T. Hall, S. Vines, (2004), Stability constants of uranium (IV)- $\alpha$ -isosaccharinic acid and gluconic acid complexes. *Radiochimica Acta/International journal for chemical aspects of nuclear science and technology*. 92, 897-902.
36. X. Gaona, V. Montoya, E. Colàs, M. Grivé, L. Duro, (2008), Review of the complexation of tetravalent actinides by ISA and gluconate under alkaline to hyperalkaline conditions. *Journal of Contaminant Hydrology*. 102, 217-227.
37. E. Wieland, J. Tits, J. P. Dobler, P. Spieler, (2002), The effect of  $\alpha$ -isosaccharinic acid on the stability of and Th (IV) uptake by hardened cement paste. *Radiochimica Acta*. 90, 683-688.
38. C. M. Bethke, R. A. Sanford, M. F. Kirk, Q. Jin, T. M. Flynn, (2011), The thermodynamic ladder in geomicrobiology. *American Journal of Science*. 311, 183-210.
39. P. P. Kanekar, S. S. Nilegaonkar, S. S. Sarnaik, A. S. Kelkar, (2002), Optimization of protease activity of alkaliphilic bacteria isolated from an alkaline lake in India. *Bioresource Technology*. 85, 87-93.
40. K. Takai, D. P. Moser, T. C. Onstott, N. Spoelstra, S. M. Pfiffner, A. Dohnalkova, J. K. Fredrickson, (2001), Alkaliphilus transvaalensis gen. nov., sp. nov., an extremely alkaliphilic bacterium isolated from a deep South African gold mine. *International journal of systematic and evolutionary microbiology*. 51, 1245-1256.
41. B. E. Jones, W. D. Grant, A. W. Duckworth, G. G. Owenson, (1998), Microbial diversity of soda lakes. *Extremophiles*. 2, 191-200.
42. F. L. Daae, I. Økland, H. Dahle, S. L. Jørgensen, I. H. Thorseth, R. B. Pedersen, (2013), Microbial life associated with low-temperature alteration of ultramafic rocks in the Leka ophiolite complex. *Geobiology*. 11, 318-339.
43. W. J. Brazelton, B. Nelson, M. O. Schrenk, (2012), Metagenomic evidence for H<sub>2</sub> oxidation and H<sub>2</sub> production by serpentinite-hosted subsurface microbial communities. *Frontiers in microbiology*. 268, 75-86.
44. I. P. Sarethy, Y. Saxena, A. Kapoor, M. Sharma, S. K. Sharma, V. Gupta, S. Gupta, (2011), Alkaliphilic bacteria: applications in industrial biotechnology. *Journal of industrial microbiology & biotechnology*. 38, 769-790.
45. E. Padan, E. Bibi, M. Ito, T. A. Krulwich, (2005), Alkaline pH Homeostasis in Bacteria: New Insights. *Biochimica et biophysica acta*. 1717, 67-88.
46. I. R. Booth, (1985), Regulation of cytoplasmic pH in bacteria. *Microbiological Reviews*. 49, 359-378.
47. J. L. Slonczewski, M. Fujisawa, M. Dopson, T. A. Krulwich, (2009), Cytoplasmic pH measurement and homeostasis in bacteria and archaea. *Advances in microbial physiology*. 55, 1-317.
48. M. G. Sturr, A. A. Guffanti, T. A. Krulwich, (1994), Growth and bioenergetics of alkaliphilic Bacillus firmus OF4 in continuous culture at high pH. *Journal of bacteriology*. 176, 3111-3116.
49. T. Hamamoto, M. Hashimoto, M. Hino, M. Kitada, Y. Seto, T. Kudo, K. Horikoshi, (1994), Characterization of a gene responsible for the Na<sup>+</sup>/H<sup>+</sup> antiporter system of alkaliphilic Bacillus species strain C-125. *Molecular microbiology*. 14, 939-946.
50. T. H. Swartz, S. Ikewada, O. Ishikawa, M. Ito, T. A. Krulwich, (2005), The Mrp system: a giant among monovalent cation/proton antiporters? *Extremophiles*. 9, 345-354.
51. T. A. Krulwich, R. Gilmour, D. B. Hicks, A. A. Guffanti, M. Ito, (1998), Energetics of Alkaliphilic Bacillus Species: Physiology and Molecules. *Advances in microbial physiology*. 40, 401-438.

52. R. Aono, M. Ito, T. Machida, (1999), Contribution of the cell wall component teichuronopeptide to pH homeostasis and alkaliphily in the alkaliphile Bacillus lentus C-125. *Journal of bacteriology.* 181, 6600-6606.
53. K. Enomoto, N. Koyama, (1999), Effect of growth pH on the phospholipid contents of the membranes from alkaliphilic bacteria. *Current microbiology.* 39, 270-273.
54. G. S. Roadcap, R. A. Sanford, Q. Jin, J. R. Pardinas, C. M. Bethke, (2006), Extremely alkaline (pH > 12) ground water hosts diverse microbial community. *Ground Water.* 44, 511-517.
55. C. M. Linklater *et al.*, (1998), A Natural Analogue Study of Cement-buffered, Hyperalkaline Groundwaters and Their Interaction with a Repository Host Rock Phase II, UK Nirex Limited, Harwell, Didcot, Oxfordshire, UK.
56. I. T. Burke, R. J. G. Mortimer, S. Palaniyandi, R. A. Whittleston, C. L. Lockwood, D. J. Ashley, D. I. Stewart, (2012), Biogeochemical reduction processes in a hyper-alkaline leachate affected soil profile. *Geomicrobiology Journal.* 29, 769-779.
57. H. C. Rees, W. D. Grant, B. E. Jones, S. Heaphy, (2004), Diversity of Kenyan soda lake alkaliphiles assessed by molecular methods. *Extremophiles.* 8, 63-71.
58. J. C. M. Scholten, S. B. Joye, J. T. Hollibaugh, J. C. Murrell, (2005), Molecular Analysis of the Sulfate Reducing and Archaeal Community in a Meromictic Soda Lake (Mono Lake, California) by Targeting 16S rRNA, mcrA, apsA, and dsrAB Genes. *Microbial ecology.* 50, 29-39.
59. R. S. Oremland, S. E. Hoefft, J. M. Santini, N. Bano, R. A. Hollibaugh, J. T. Hollibaugh, (2002), Anaerobic oxidation of arsenite in Mono Lake water and by a facultative, arsenite-oxidizing chemoautotroph, strain MLHE-1. *Applied and environmental microbiology.* 68, 4795-4802.
60. A. Rizoulis, H. M. Steele, K. Morris, J. R. Lloyd, (2012), The potential impact of anaerobic microbial metabolism during the geological disposal of intermediate-level waste. *Mineralogical Magazine.* 76, 3261-3270.
61. C. P. Antony, D. Kumaresan, S. Hunger, H. L. Drake, J. C. Murrell, Y. S. Shouche, (2013), Microbiology of Lonar Lake and other soda lakes. *The ISME journal.* 7, 468-476.
62. S. B. Humayoun, N. Bano, J. T. Hollibaugh, (2003), Depth distribution of microbial diversity in Mono Lake, a meromictic soda lake in California. *Applied and environmental microbiology.* 69, 1030-1042.
63. M. Foti *et al.*, (2007), Diversity, activity, and abundance of sulfate-reducing bacteria in saline and hypersaline soda lakes. *Applied and environmental microbiology.* 73, 2093-2100.
64. V. P. Surakasi, A. A. Wani, Y. S. Shouche, D. R. Ranade, (2007), Phylogenetic analysis of methanogenic enrichment cultures obtained from Lonar Lake in India: isolation of Methanocalculus sp. and Methanoculleus sp. *Microbial ecology.* 54, 697-704.
65. S. B. Joye, T. L. Connell, L. G. Miller, R. S. Oremland, R. S. Jellison, (1999), Oxidation of ammonia and methane in an alkaline, saline lake. *Limnology and oceanography.* 44, 178-188.
66. J. B. Moody, (1976), Serpentinization: a review. *Lithos.* 9, 125-138.
67. A. Rizoulis, A. E. Milodowski, K. Morris, J. R. Lloyd, (2016), Bacterial diversity in the hyperalkaline Allas Springs (Cyprus), a natural analogue for cementitious radioactive waste repository. *Geomicrobiology Journal.* 33, 73-84.
68. J. G. Blank, S. J. Green, D. Blake, J. W. Valley, N. T. Kita, A. Treiman, P. F. Dobson, (2009), An alkaline spring system within the Del Puerto Ophiolite (California, USA): a Mars analog site. *Planetary and Space Science.* 57, 533-540.

69. A. H. Bath, N. Christofi, C. Neal, J. C. Philp, M. R. Cave, I. G. McKinley, U. Berner, (1987), Trace element and microbiological studies of alkaline groundwaters in Oman, Arabian Gulf: a natural analogue for cement pore-waters, Nationale Genossenschaft fuer die Lagerung Radioaktiver Abfaelle (NAGRA),
70. H. N. Khoury *et al.*, (1992), A natural analogue of high pH cement pore waters from the Maqarin area of northern Jordan. I: introduction to the site. *Journal of Geochemical Exploration*. 46, 117-132.
71. K. Pedersen, E. Nilsson, J. Arlinger, L. Hallbeck, A. O'Neill, (2004), Distribution, diversity and activity of microorganisms in the hyper-alkaline spring waters of Maqarin in Jordan. *Extremophiles*. 8, 151-164.
72. W. M. Mayes, A. P. Jarvis, I. T. Burke, M. Walton, V. Feigl, O. Klebercz, K. Gruiz, (2011), Dispersal and attenuation of trace contaminants downstream of the Ajka bauxite residue (red mud) depository failure, Hungary. *Environ Sci Technol*. 45, 5147-5155.
73. R. Turpeinen, T. Kairesalo, M. M. Häggblom, (2004), Microbial community structure and activity in arsenic-, chromium-and copper-contaminated soils. *FEMS Microbiology Ecology*. 47, 39-50.
74. M. Hiroki, (1992), Effects of heavy metal contamination on soil microbial population. *Soil Science and Plant Nutrition*. 38, 141-147.
75. Y. Crouau, P. Chenon, C. Gisclard, (1999), The use of *Folsomia candida* (Collembola, Isotomidae) for the bioassay of xenobiotic substances and soil pollutants. *Applied Soil Ecology*. 12, 103-111.
76. C. L. Hemme *et al.*, (2010), Metagenomic insights into evolution of a heavy metal-contaminated groundwater microbial community. *The ISME journal*. 4, 660-672.
77. C. Viti, A. Pace, L. Giovannetti, (2003), Characterization of Cr (VI)-resistant bacteria isolated from chromium-contaminated soil by tannery activity. *Current microbiology*. 46, 0001-0005.
78. K. B. Hallberg, (2010), New perspectives in acid mine drainage microbiology. *Hydrometallurgy*. 104, 448-453.
79. A. E. Milodowski, R. P. Shaw, D. I. Stewart, (2013), The Harpur Hill Site: its geology, evolutionary history and a catalogue of materials present CR/13/104. British Geological Survey, Keyworth, Nottinghamshire, UK.
80. S. P. Rout, C. J. Charles, E. J. Garratt, A. P. Laws, J. Gunn, P. N. Humphreys, (2015), Evidence of the generation of isosaccharinic acids and their subsequent degradation by local microbial consortia within hyper-alkaline contaminated soils, with relevance to intermediate level radioactive waste disposal. *PLoS One*. 10, e0119164.
81. S. P. Rout *et al.*, (2015), Anoxic Biodegradation of Isosaccharinic Acids at Alkaline pH by Natural Microbial Communities. *PLoS One*. 10, e0137682.
82. A. J. Williamson, K. Morris, S. Shaw, J. M. Byrne, C. Boothman, J. R. Lloyd, (2013), Microbial reduction of Fe (III) under alkaline conditions relevant to geological disposal. *Applied and environmental microbiology*. 79, 3320-3326.
83. N. M. Bassil, N. Bryan, J. R. Lloyd, (2015), Microbial degradation of isosaccharinic acid at high pH. *The ISME journal*. 9, 310-320.
84. I. A. Kyeremeh, C. J. Charles, S. P. Rout, A. P. Laws, P. N. Humphreys, (2016), Microbial Community Evolution Is Significantly Impacted by the Use of Calcium Isosaccharinic Acid as an Analogue for the Products of Alkaline Cellulose Degradation. *PLoS One*. 11, e0165832.
85. H. C. Flemming, J. Wingender, (2010), The biofilm matrix. *Nature Reviews Microbiology*. 8, 623-633.

86. M. Jacob, (2006), Biofilms, a new approach to the microbiology of dental plaque. *Odontology*. 94, 1-9.
87. M. Whiteley, J. R. Ott, E. A. Weaver, R. J. C. McLean, (2001), Effects of community composition and growth rate on aquifer biofilm bacteria and their susceptibility to betadine disinfection. *Environmental Microbiology*. 3, 43-52.
88. H. W. Jannasch, C. O. Wirsen, (1981), Morphological survey of microbial mats near deep-sea thermal vents. *Applied and environmental microbiology*. 41, 528-538.
89. D. A. R. Meyer-Dombard, W. Swingley, J. Raymond, J. Havig, E. L. Shock, R. E. Summons, (2011), Hydrothermal ecotones and streamer biofilm communities in the Lower Geyser Basin, Yellowstone National Park. *Environmental Microbiology*. 13, 2216-2231.
90. S. M. Hinsla-Leasure, C. Koid, J. M. Tiedje, J. N. Schultzhaus, (2013), Biofilm formation by *Psychrobacter arcticus* and the role of a large adhesin in attachment to surfaces. *Applied and environmental microbiology*. 79, 3967-3973.
91. W. Pohl, J. Schneider, (2002), Impact of endolithic biofilms on carbonate rock surfaces. *Geological Society, London, Special Publications*. 205, 177-194.
92. H. C. Flemming, T. R. Neu, D. J. Wozniak, (2007), The EPS matrix: the “house of biofilm cells”. *Journal of bacteriology*. 189, 7945-7947.
93. H. C. Flemming, J. Wingender, (2001), Relevance of microbial extracellular polymeric substances (EPSs)-Part I: Structural and ecological aspects. *water science and technology*. 43, 1-8.
94. R. D. Waite, A. Papakonstantinou, E. Littler, M. A. Curtis, (2005), Transcriptome analysis of *Pseudomonas aeruginosa* growth: comparison of gene expression in planktonic cultures and developing and mature biofilms. *Journal of bacteriology*. 187, 6571-6576.
95. M. E. Davey, G. A. O'Toole, (2000), Microbial biofilms: from ecology to molecular genetics. *Microbiology and molecular biology reviews*. 64, 847-867.
96. P. S. Stewart, J. W. Costerton, (2001), Antibiotic resistance of bacteria in biofilms. *The lancet*. 358, 135-138.
97. R. W. Care, (2008), A study of biofilm-based wound management in subjects with critical limb ischaemia. *Journal of wound care*. 17, 145.
98. J. M. Vroom *et al.*, (1999), Depth penetration and detection of pH gradients in biofilms by two-photon excitation microscopy. *Applied and environmental microbiology*. 65, 3502-3511.
99. Y. Jiao *et al.*, (2011), Identification of biofilm matrix-associated proteins from an acid mine drainage microbial community. *Applied and environmental microbiology*. 77, 5230-5237.
100. I. W. Sutherland, (2001), Biofilm exopolysaccharides: a strong and sticky framework. *Microbiology*. 147, 3-9.
101. T. Das, P. K. Sharma, H. J. Busscher, H. C. van der Mei, B. P. Krom, (2010), Role of extracellular DNA in initial bacterial adhesion and surface aggregation. *Applied and environmental microbiology*. 76, 3405-3408.
102. T. Das, S. Sehar, L. Koop, Y. K. Wong, S. Ahmed, K. S. Siddiqui, M. Manefield, (2014), Influence of calcium in extracellular DNA mediated bacterial aggregation and biofilm formation. *PLoS One*. 9, e91935.
103. F. Ahimou, M. J. Semmens, G. Haugstad, P. J. Novak, (2007), Effect of protein, polysaccharide, and oxygen concentration profiles on biofilm cohesiveness. *Applied and environmental microbiology*. 73, 2905-2910.

104. A. M. Romani, K. Fund, J. Artigas, T. Schwartz, S. Sabater, U. Obst, (2008), Relevance of polymeric matrix enzymes during biofilm formation. *Microbial ecology*. 56, 427-436.
105. L. Montanaro, A. Poggi, L. Visai, S. Ravaioli, D. Campoccia, P. Speziale, C. R. Arciola, (2011), Extracellular DNA in biofilms. *The International journal of artificial organs*. 34, 824-831.
106. X. Zhang, P. L. Bishop, (2003), Biodegradability of biofilm extracellular polymeric substances. *Chemosphere*. 50, 63-69.
107. B. G. Plósz, C. Vogelsang, K. Macrae, H. H. Heiaas, A. Lopez, H. Liltved, K. H. Langford, (2010), The BIOZO process—a biofilm system combined with ozonation: occurrence of xenobiotic organic micro-pollutants in and removal of polycyclic aromatic hydrocarbons and nitrogen from landfill leachate. *water science and technology*. 61, 3188-3197.
108. M. Schorer, M. Eisele, (1997), Accumulation of inorganic and organic pollutants by biofilms in the aquatic environment. *Water, Air, and Soil Pollution*. 99, 651-659.
109. H. C. Flemming, (1995), Sorption sites in biofilms. *water science and technology*. 32, 27-33.
110. J. Schmitt, H. C. Flemming, (1999), Water binding in biofilms. *water science and technology*. 39, 77-82.
111. L. R. Johnson, (2008), Microcolony and biofilm formation as a survival strategy for bacteria. *Journal of Theoretical Biology*. 251, 24-34.
112. W. M. Dunne, (2002), Bacterial Adhesion: Seen Any Good Biofilms Lately? *Clinical Microbiology Reviews*. 15, 155-166.
113. R. M. Donlan, (2002), Biofilms: microbial life on surfaces. *Emerg Infect Dis*. 8,
114. Y. H. An, R. B. Dickinson, R. J. Doyle, (2000), in *Handbook of Bacterial Adhesion*. Springer, pp. 1-27.
115. C. Hannig, M. Hannig, (2009), The oral cavity—a key system to understand substratum-dependent bioadhesion on solid surfaces in man. *Clinical oral investigations*. 13, 123-139.
116. I. W. Wang, J. M. Anderson, R. E. Marchant, (1993), Platelet-mediated adhesion of Staphylococcus epidermidis to hydrophobic NHLBI reference polyethylene. *Journal of biomedical materials research*. 27, 1119-1128.
117. J. W. Leung, Y. L. Liu, T. Desta, E. Libby, J. F. Inciardi, K. Lam, (1998), Is there a synergistic effect between mixed bacterial infection in biofilm formation on biliary stents? *Gastrointestinal Endoscopy*. 48, 250-257.
118. C. Solano, M. Echeverz, I. Lasa, (2014), Biofilm dispersion and quorum sensing. *Current Opinion in Microbiology*. 18, 96-104.
119. C. T. O'Loughlin, L. C. Miller, A. Siryaporn, K. Drescher, M. F. Semmelhack, B. L. Bassler, (2013), A quorum-sensing inhibitor blocks Pseudomonas aeruginosa virulence and biofilm formation. *Proceedings of the National Academy of Sciences*. 110, 17981-17986.
120. M. Felchner-Zwirello, J. Winter, C. Gallert, (2013), Interspecies distances between propionic acid degraders and methanogens in syntrophic consortia for optimal hydrogen transfer. *Applied microbiology and biotechnology*. 97, 9193-9205.
121. A. Oren, (2011), Thermodynamic limits to microbial life at high salt concentrations. *Environmental Microbiology*. 13, 1908-1923.
122. T. M. Hoehler, M. J. Alperin, D. B. Albert, C. S. Martens, (2001), Apparent minimum free energy requirements for methanogenic Archaea and sulfate-reducing bacteria in an anoxic marine sediment. *FEMS Microbiology Ecology*. 38, 33-41.

123. B. E. Jackson, M. J. McInerney, (2002), Anaerobic microbial metabolism can proceed close to thermodynamic limits. *Nature*. 415, 454-456.
124. W. Michaelis *et al.*, (2002), Microbial reefs in the Black Sea fueled by anaerobic oxidation of methane. *Science*. 297, 1013-1015.
125. D. Ren, J. S. Madsen, S. J. Sørensen, M. Burmølle, (2015), High prevalence of biofilm synergy among bacterial soil isolates in cocultures indicates bacterial interspecific cooperation. *The ISME journal*. 9, 81-89.
126. E. Diaz, R. Amils, J. L. Sanz, (2003), Molecular ecology of anaerobic granular sludge grown at different conditions. *water science and technology*. 48, 57-64.
127. H. Satoh, Y. Miura, I. Tsushima, S. Okabe, (2007), Layered structure of bacterial and archaeal communities and their in situ activities in anaerobic granules. *Applied and environmental microbiology*. 73, 7300-7307.
128. I. W. Sutherland, (2001), The biofilm matrix—an immobilized but dynamic microbial environment. *Trends in microbiology*. 9, 222-227.
129. P. Stoodley, I. Dodds, J. D. Boyle, H. M. Lappin-Scott, (1998), Influence of hydrodynamics and nutrients on biofilm structure. *Journal of applied microbiology*. 85,
130. S. R. Wood, J. Kirkham, P. D. Marsh, R. C. Shore, B. Nattress, C. Robinson, (2000), Architecture of intact natural human plaque biofilms studied by confocal laser scanning microscopy. *Journal of Dental Research*. 79, 21-27.
131. P. L. Bond, S. P. Smriga, J. F. Banfield, (2000), Phylogeny of microorganisms populating a thick, subaerial, predominantly lithotrophic biofilm at an extreme acid mine drainage site. *Applied and environmental microbiology*. 66, 3842-3849.
132. B. Lanoil *et al.*, (2009), Bacteria beneath the West Antarctic ice sheet. *Environmental Microbiology*. 11, 609-615.
133. T. R. Kulp *et al.*, (2008), Arsenic (III) fuels anoxygenic photosynthesis in hot spring biofilms from Mono Lake, California. *Science*. 321, 967-970.
134. M. Quéméneur, A. Palvadeau, A. Postec, C. Monnin, V. Chavagnac, B. Ollivier, G. Erauso, (2015), Endolithic microbial communities in carbonate precipitates from serpentinite-hosted hyperalkaline springs of the Voltri Massif (Ligurian Alps, Northern Italy). *Environmental Science and Pollution Research*. 22, 13613-13624.
135. S. W. Taylor, P. R. Jaffé, (1990), Biofilm growth and the related changes in the physical properties of a porous medium: 3. Dispersivity and model verification. *Water Resources Research*. 26, 2171-2180.
136. M. O. Cuthbert, M. S. Riley, S. Handley-Sidhu, J. C. Renshaw, D. J. Tobler, V. R. Phoenix, R. Mackay, (2012), Controls on the rate of ureolysis and the morphology of carbonate precipitated by *S. Pasteurii* biofilms and limits due to bacterial encapsulation. *Ecological Engineering*. 41, 32-40.
137. C. Anderson, K. Pedersen, A.-M. Jakobsson, (2006), Autoradiographic comparisons of radionuclide adsorption between subsurface anaerobic biofilms and granitic host rocks. *Geomicrobiology Journal*. 23, 15-29.
138. C. Dupraz, P. T. Visscher, (2005), Microbial lithification in marine stromatolites and hypersaline mats. *Trends Microbiol*. 13, 429-438.
139. Y. Kitano, T. Oomori, (1971), The coprecipitation of uranium with calcium carbonate. *Journal of the Oceanographical Society of Japan*. 27, 34-42.
140. E. Vincke, N. Boon, W. Verstraete, (2001), Analysis of the microbial communities on corroded concrete sewer pipes—a case study. *Applied microbiology and biotechnology*. 57, 776-785.
141. A. E. Milodowski, C. A. Rochelle, G. Purser, (2013), Uptake and retardation of Cl during cement carbonation. *Procedia Earth and Planetary Science*. 7, 594-597.

142. C. Doulgeris, P. Humphreys, S. Rout, (2015), An approach to modelling the impact of <sup>14</sup>C release from reactor graphite in a geological disposal facility. *Mineralogical Magazine*. 79, 1495-1503.
143. S. L. Smith, A. Rizoulis, J. M. West, J. R. Lloyd, (2016), The Microbial Ecology of a Hyper-Alkaline Spring, and Impacts of an Alkali-Tolerant Community During Sandstone Batch and Column Experiments Representative of a Geological Disposal Facility for Intermediate-Level Radioactive Waste. *Geomicrobiology Journal*. 1-13.
144. S. L. Smith, C. Boothman, H. A. Williams, B. L. Ellis, J. Wragg, J. M. West, J. R. Lloyd, (2016), Microbial impacts on <sup>99m</sup>Tc migration through sandstone under highly alkaline conditions relevant to radioactive waste disposal. *Science of The Total Environment*.
145. Nirex, (1997), Sellafield Geological and Hydrogeological Investigations: the Hydrochemistry of Sellafield UK NIREX Ltd, Harwell, Oxfordshire, UK.
146. M. T. Madigan, H. Gest, (1978), Growth of a photosynthetic bacterium anaerobically in darkness, supported by "oxidant-dependent" sugar fermentation. *Archives of Microbiology*. 117, 119-122.
147. R. K. Thauer, K. Jungermann, K. Decker, (1977), Energy conservation in chemotrophic anaerobic bacteria. *Bacteriological reviews*. 41, 100.
148. K. Y. Teh, A. E. Lutz, (2010), Thermodynamic analysis of fermentation and anaerobic growth of baker's yeast for ethanol production. *J Biotechnol*. 147, 80-87.
149. V. Müller, (2008), Bacterial fermentation. *eLS*. 1-7.
150. E. Shock, A. Poret-Peterson, P. A. Canovas, K. Robinson, P. Marsala, (2012), Methanogenesis and Methanotrophy in Serpentinizing Systems. *AGU Fall Meeting Abstracts*. 1, 0509.
151. A. J. Williamson, K. Morris, C. Boothman, K. Dardenne, G. T. W. Law, J. R. Lloyd, (2015), Microbially mediated reduction of Np (V) by a consortium of alkaline tolerant Fe (III)-reducing bacteria. *Mineralogical Magazine*. 79, 1287-1295.
152. R. K. Thauer, A.-K. Kaster, H. Seedorf, W. Buckel, R. Hedderich, (2008), Methanogenic archaea: ecologically relevant differences in energy conservation. *Nature Reviews Microbiology*. 6, 579-591.
153. S. Worakit, D. R. Boone, R. A. Mah, M.-E. Abdel-Samie, M. M. El-Halwagi, (1986), Methanobacterium alcaliphilum sp. nov., an H<sub>2</sub>-utilizing methanogen that grows at high pH values. *International journal of systematic and evolutionary microbiology*. 36, 380-382.
154. J. H. Thiele, J. G. Zeikus, (1988), Control of interspecies electron flow during anaerobic digestion: significance of formate transfer versus hydrogen transfer during syntrophic methanogenesis in flocs. *Applied and environmental microbiology*. 54, 20-29.
155. H. Penning, P. Claus, P. Casper, R. Conrad, (2006), Carbon isotope fractionation during acetoclastic methanogenesis by Methanosaeta concilii in culture and a lake sediment. *Applied and environmental microbiology*. 72, 5648-5652.
156. J. G. Ferry, (2010), The chemical biology of methanogenesis. *Planetary and Space Science*. 58, 1775-1783.
157. R. S. Oremland, L. Marsh, D. J. DesMarais, (1982), Methanogenesis in Big Soda Lake, Nevada: an alkaline, moderately hypersaline desert lake. *Applied and environmental microbiology*. 43, 462-468.
158. D. R. Boone, S. Worakit, I. M. Mathrani, R. A. Mah, (1986), Alkaliphilic methanogens from high-pH lake sediments. *Systematic and Applied Microbiology*. 7, 230-234.

159. R. S. Oremland, L. G. Miller, (1993), Biogeochemistry of natural gases in three alkaline, permanently stratified (meromictic) lakes. *The future of energy gases, USGS Paper*. 1570, 439-452.
160. U. Sydow, P. Wohland, I. Wolke, H. Cypionka, (2002), Bioenergetics of the alkaliphilic sulfate-reducing bacterium *Desulfonatronovibrio hydrogenovorans*. *Microbiology*. 148, 853-860.
161. G. Muyzer, A. J. M. Stams, (2008), The ecology and biotechnology of sulphate-reducing bacteria. *Nature Reviews Microbiology*. 6, 441-454.
162. Y. Liu, W. B. Whitman, (2008), Metabolic, phylogenetic, and ecological diversity of the methanogenic archaea. *Annals of the New York Academy of Sciences*. 1125, 171-189.
163. H. D. Peck, (1961), Enzymatic basis for assimilatory and dissimilatory sulfate reduction. *Journal of bacteriology*. 82, 933-939.
164. A. S. Bradley, W. D. Leavitt, D. T. Johnston, (2011), Revisiting the dissimilatory sulfate reduction pathway. *Geobiology*. 9, 446-457.
165. D. Y. Sorokin, (2011), The microbial sulfur cycle at extremely haloalkaline conditions of soda lakes. *Frontiers in microbiology*. 2, 44.
166. D. E. Canfield, (1989), Sulfate reduction and oxic respiration in marine sediments: implications for organic carbon preservation in euxinic environments. *Deep Sea Research Part A. Oceanographic Research Papers*. 36, 121-138.
167. T. R. Kulp *et al.*, (2006), Dissimilatory arsenate and sulfate reduction in sediments of two hypersaline, arsenic-rich soda lakes: Mono and Searles Lakes, California. *Applied and environmental microbiology*. 72, 6514-6526.
168. R. L. Smith, R. S. Oremland, (1987), Big Soda Lake (Nevada). 2. Pelagic sulfate reduction. *Limnology and oceanography*. 32, 794-803.
169. D. M. Goeres, P. H. Nielsen, H. D. Smidt, B. Frølund, (1998), The effect of alkaline pH conditions on a sulphate reducing consortium from a Danish district heating plant. *Biofouling*. 12, 273-286.
170. T. S. Rao, T. N. Sairam, B. Viswanathan, K. V. K. Nair, (2000), Carbon steel corrosion by iron oxidising and sulphate reducing bacteria in a freshwater cooling system. *Corrosion Science*. 42, 1417-1431.
171. C. E. Courchene, (1998), The tried, the true, and the new-getting more pulp from chips modifications to the kraft process for increased yield.
172. S.-H. Wang, J. L. McCarthy, J. F. Ferguson, (1993), Utilization of glucoisosaccharinic acid and components of Kraft black liquor as energy sources for growth of anaerobic bacteria. *Holzforchung-International Journal of the Biology, Chemistry, Physics and Technology of Wood*. 47, 141-148.
173. S. E. Strand, J. Dykes, V. Chiang, (1984), Aerobic microbial degradation of glucoisosaccharinic acid. *Applied and environmental microbiology*. 47, 268-271.
174. A. Pekarovičová, M. Mikulášová, (1991), Biodegradation of black liquor hydroxyacids by *Micrococcus lylae*. *Journal of chemical technology and biotechnology*. 52, 539-543.
175. M. J. Bailey, (1986), Utilization of glucoisosaccharinic acid by a bacterial isolate unable to metabolize glucose. *Applied microbiology and biotechnology*. 24, 493-498.
176. W. D. Grant, G. J. Holtom, N. O. Kelly, J. Malpass, A. Rosevear, P. Watkiss, D. Widdowson, (2002), Microbial Degradation of Cellulose derived Complexants Under Repository Conditions AEAT/ERRA-0301. AEA Technology plc, Harwell, Didcot, Oxfordshire, UK.

177. S. P. Rout, J. Radford, A. P. Laws, F. Sweeney, A. Elmekawy, L. J. Gillie, P. N. Humphreys, (2014), Biodegradation of the alkaline cellulose degradation products generated during radioactive waste disposal. *PLoS One*. 9, e107433.
178. N. M. Bassil, A. D. Bewsher, O. R. Thompson, J. R. Lloyd, (2015), Microbial degradation of cellulosic material under intermediate-level waste simulated conditions. *Mineralogical Magazine*. 79, 1433-1441.
179. M. S. Rappe, S. J. Giovannoni, (2003), The uncultured microbial majority. *Annual Reviews in Microbiology*. 57, 369-394.
180. M. Nedelkova, M. L. Merroun, A. Rossberg, C. Hennig, S. Selenska-Pobell, (2007), Microbacterium isolates from the vicinity of a radioactive waste depository and their interactions with uranium. *FEMS Microbiology Ecology*. 59, 694-705.
181. S. Fukunaga *et al.*, (2005), Investigation of microorganisms in bentonite deposits. *Geomicrobiology Journal*. 22, 361-370.
182. J. M. Horn, B. A. Masterson, A. Rivera, A. Miranda, M. A. Davis, S. Martin, (2004), Bacterial growth dynamics, limiting factors, and community diversity in a proposed geological nuclear waste repository environment. *Geomicrobiology Journal*. 21, 273-286.
183. M. Kalab, A.-F. Yang, D. Chabot, (2008), Conventional scanning electron microscopy of bacteria. *Infocus Magazine*. 10, 42-61.
184. K. Wouters, H. Moors, P. Boven, N. Leys, (2013), Evidence and characteristics of a diverse and metabolically active microbial community in deep subsurface clay borehole water. *FEMS Microbiology Ecology*. 86, 458-473.
185. D. A. Brown, D. C. Kamineni, J. A. Sawicki, T. J. Beveridge, (1994), Minerals associated with biofilms occurring on exposed rock in a granitic underground research laboratory. *Applied and environmental microbiology*. 60, 3182-3191.
186. F. Reith, S. L. Rogers, D. C. McPhail, D. Webb, (2006), Biomining of gold: biofilms on bacterioform gold. *Science*. 313, 233-236.
187. E. Chicote, A. M. García, D. A. Moreno, M. I. Sarró, P. I. Lorenzo, F. Montero, (2005), Isolation and identification of bacteria from spent nuclear fuel pools. *Journal of Industrial Microbiology and Biotechnology*. 32, 155-162.
188. M.-Y. Chen, D.-J. Lee, J.-H. Tay, K.-Y. Show, (2007), Staining of extracellular polymeric substances and cells in bioaggregates. *Applied microbiology and biotechnology*. 75, 467-474.
189. G. Hwang *et al.*, (2016), Simultaneous spatiotemporal mapping of in situ pH and bacterial activity within an intact 3D microcolony structure. *Scientific Reports*. 6,
190. A. Bridier, F. Dubois-Brissonnet, A. Boubetra, V. Thomas, R. Briandet, (2010), The biofilm architecture of sixty opportunistic pathogens deciphered using a high throughput CLSM method. *Journal of Microbiological Methods*. 82, 64-70.
191. T. D. Ainsworth, M. Fine, L. L. Blackall, O. Hoegh-Guldberg, (2006), Fluorescence in situ hybridization and spectral imaging of coral-associated bacterial communities. *Applied and environmental microbiology*. 72, 3016-3020.
192. B. E. Ramirez, B. G. Malmström, J. R. Winkler, H. B. Gray, (1995), The currents of life: the terminal electron-transfer complex of respiration. *Proceedings of the National Academy of Sciences*. 92, 11949-11951.
193. H. S. C. Eydal, K. Pedersen, (2007), Use of an ATP assay to determine viable microbial biomass in Fennoscandian Shield groundwater from depths of 3–1000 m. *Journal of Microbiological Methods*. 70, 363-373.
194. S. Lydmark, K. Pedersen, (2011), Aespoe Hard Rock Laboratory Canister Retrieval Test. Microorganisms in buffer from the Canister Retrieval Test-numbers and metabolic diversity, Swedish Nuclear Fuel and Waste Management Co.,

195. Å. Frostegård, E. Bååth, A. Tunlio, (1993), Shifts in the structure of soil microbial communities in limed forests as revealed by phospholipid fatty acid analysis. *Soil Biology and Biochemistry.* 25, 723-730.
196. S. Stroes-Gascoyne, C. J. Hamon, P. Vilks, P. Gierszewski, (2002), Microbial, redox and organic characteristics of compacted clay-based buffer after 6.5 years of burial at AECL's Underground Research Laboratory. *Applied geochemistry.* 17, 1287-1303.
197. R. A. Hurt Jr, M. S. Robeson II, M. Shakya, J. G. Moberly, T. A. Vishnivetskaya, B. Gu, D. A. Elias, (2014), Improved yield of high molecular weight DNA coincides with increased microbial diversity access from iron oxide cemented sub-surface clay environments. *PLoS One.* 9, e102826.
198. R. I. Griffiths, A. S. Whiteley, A. G. O'Donnell, M. J. Bailey, (2000), Rapid method for coextraction of DNA and RNA from natural environments for analysis of ribosomal DNA-and rRNA-based microbial community composition. *Applied and environmental microbiology.* 66, 5488-5491.
199. M. W. Ariefdjohan, D. A. Savaiano, C. H. Nakatsu, (2010), Comparison of DNA extraction kits for PCR-DGGE analysis of human intestinal microbial communities from fecal specimens. *Nutrition journal.* 9, 1.
200. R. K. Saiki *et al.*, (1988), Primer-directed enzymatic amplification of DNA. *Science.* 239, 487-491.
201. J. M. S. Bartlett, D. Stirling, (2003), A short history of the polymerase chain reaction. *PCR protocols.* 3-6.
202. M. T. Suzuki, S. J. Giovannoni, (1996), Bias caused by template annealing in the amplification of mixtures of 16S rRNA genes by PCR. *Applied and environmental microbiology.* 62, 625-630.
203. S. J. Green *et al.*, (2012), Denitrifying bacteria from the genus Rhodanobacter dominate bacterial communities in the highly contaminated subsurface of a nuclear legacy waste site. *Applied and environmental microbiology.* 78, 1039-1047.
204. G. Lear *et al.*, (2009), Probing the biogeochemical behavior of technetium using a novel nuclear imaging approach. *Environ Sci Technol.* 44, 156-162.
205. K.-J. Chin, A. Esteve-Núñez, C. Leang, D. R. Lovley, (2004), Direct correlation between rates of anaerobic respiration and levels of mRNA for key respiratory genes in Geobacter sulfurreducens. *Applied and environmental microbiology.* 70, 5183-5189.
206. L. Villanueva, S. A. Haveman, Z. M. Summers, D. R. Lovley, (2008), Quantification of Desulfovibrio vulgaris dissimilatory sulfite reductase gene expression during electron donor-and electron acceptor-limited growth. *Applied and environmental microbiology.* 74, 5850-5853.
207. D. J. Strattan, (2010), Quantifying the expression of dissimilatory sulfite reductase as a metric for sulfate reduction rates. *Doctoral dissertation, University of Illinois at Urbana-Champaign.*
208. M. Johnson, I. Zaretskaya, Y. Raytselis, Y. Merezuk, S. McGinnis, T. L. Madden, (2008), NCBI BLAST: a better web interface. *Nucleic acids research.* 36, W5-W9.
209. C. R. Woese, G. E. Fox, (1977), Phylogenetic structure of the prokaryotic domain: the primary kingdoms. *Proceedings of the National Academy of Sciences.* 74, 5088-5090.
210. G. James, (2010), in *PCR for Clinical Microbiology: An Australian and International Perspective*, M. Schuller, T. P. Sloots, G. S. James, C. L. Halliday, I. W. J. Carter, Eds. Springer Netherlands, Dordrecht, pp. 209-214.
211. K. Knoche, D. Kephart, (1999), Cloning blunt-end Pfu DNA Polymerase-generated PCR fragments into pGEM®-T Vector Systems. *Promega Notes.* 71,

212. C. G. Lerner, M. Inouye, (1990), Low copy number plasmids for regulated low-level expression of cloned genes in Escherichia coli with blue/white insert screening capability. *Nucleic acids research*. 18, 4631.
213. K. Pedersen, (1996), Investigations of subterranean bacteria in deep crystalline bedrock and their importance for the disposal of nuclear waste. *Canadian Journal of Microbiology*. 42, 382-391.
214. T. Urich, A. Lanzén, J. Qi, D. H. Huson, C. Schleper, S. C. Schuster, (2008), Simultaneous assessment of soil microbial community structure and function through analysis of the meta-transcriptome. *PLoS One*. 3, e2527.
215. A. K. Kambura, R. K. Mwirichia, R. W. Kasili, E. N. Karanja, H. M. Makonde, H. I. Boga, (2016), Bacteria and Archaea diversity within the hot springs of Lake Magadi and Little Magadi in Kenya. *BMC microbiology*. 16, 136.
216. J. Chun, J.-H. Lee, Y. Jung, M. Kim, S. Kim, B. K. Kim, Y.-W. Lim, (2007), EzTaxon: a web-based tool for the identification of prokaryotes based on 16S ribosomal RNA gene sequences. *International journal of systematic and evolutionary microbiology*. 57, 2259-2261.
217. J. R. Cole *et al.*, (2013), Ribosomal Database Project: data and tools for high throughput rRNA analysis. *Nucleic acids research*. gkt1244.
218. C. Quast *et al.*, (2013), The SILVA ribosomal RNA gene database project: improved data processing and web-based tools. *Nucleic acids research*. 41, D590-D596.
219. P. D. Schloss *et al.*, (2009), Introducing mothur: open-source, platform-independent, community-supported software for describing and comparing microbial communities. *Applied and environmental microbiology*. 75, 7537-7541.
220. R. C. Edgar, B. J. Haas, J. C. Clemente, C. Quince, R. Knight, (2011), UCHIME improves sensitivity and speed of chimera detection. *Bioinformatics*. 27, 2194-2200.
221. J. Kuczynski, J. Stombaugh, W. A. Walters, A. González, J. G. Caporaso, R. Knight, (2012), Using QIIME to analyze 16S rRNA gene sequences from microbial communities. *Current protocols in microbiology*. 1E-5.
222. Y. Huang, B. Niu, Y. Gao, L. Fu, W. Li, (2010), CD-HIT Suite: a web server for clustering and comparing biological sequences. *Bioinformatics*. 26, 680-682.
223. C. A. Lozupone, R. Knight, (2008), Species Divergence and the Measurement of Microbial Diversity. *FEMS microbiology reviews*. 32, 557-578.
224. A. Chao, (1984), Nonparametric estimation of the number of classes in a population. *Scandinavian Journal of statistics*. 265-270.
225. R. L. Chazdon, R. K. Colwell, J. S. Denslow, M. R. Guariguata, (1998), Statistical methods for estimating species richness of woody regeneration in primary and secondary rain forests of northeastern Costa Rica, Man and the Biosphere Series no. Vol. 20,
226. J. B. Hughes, J. J. Hellmann, T. H. Ricketts, B. J. M. Bohannan, (2001), Counting the uncountable: statistical approaches to estimating microbial diversity. *Applied and environmental microbiology*. 67, 4399-4406.
227. C. J. Keylock, (2005), Simpson diversity and the Shannon–Wiener index as special cases of a generalized entropy. *Oikos*. 109, 203-207.
228. T. P. Boyle, G. M. Smillie, J. C. Anderson, D. R. Beeson, (1990), A sensitivity analysis of nine diversity and seven similarity indices. *Research Journal of the Water Pollution Control Federation*. 749-762.
229. M. C. Rea *et al.*, (2011), Effect of broad-and narrow-spectrum antimicrobials on Clostridium difficile and microbial diversity in a model of the distal colon. *Proceedings of the National Academy of Sciences*. 108, 4639-4644.

230. R. H. Whittaker, (1960), Vegetation of the Siskiyou mountains, Oregon and California. *Ecological monographs*. 30, 279-338.
231. C. Human Microbiome Project, (2012), Structure, function and diversity of the healthy human microbiome. *Nature*. 486, 207-214.
232. K. Rudi, T. Maugesten, S. E. Hannevik, H. Nissen, (2004), Explorative multivariate analyses of 16S rRNA gene data from microbial communities in modified-atmosphere-packed salmon and coalfish. *Applied and environmental microbiology*. 70, 5010-5018.
233. A. E. McCaig, L. A. Glover, J. I. Prosser, (2001), Numerical analysis of grassland bacterial community structure under different land management regimens by using 16S ribosomal DNA sequence data and denaturing gradient gel electrophoresis banding patterns. *Applied and environmental microbiology*. 67, 4554-4559.
234. D. R. Singleton, M. A. Furlong, S. L. Rathbun, W. B. Whitman, (2001), Quantitative comparisons of 16S rRNA gene sequence libraries from environmental samples. *Applied and environmental microbiology*. 67, 4374-4376.
235. B.S.I, (2005), BS ISO 14853:2005 Plastics. Determination of the ultimate anaerobic biodegradation of plastic materials in an aqueous system. Method by measurement of biogas production, British Standards Institute, London.
236. E. Viollier, P. W. Inglett, K. Hunter, A. N. Roychoudhury, P. Van Cappellen, (2000), The ferrozine method revisited: Fe (II)/Fe (III) determination in natural waters. *Applied geochemistry*. 15, 785-790.
237. B.S.I., (1999), BS ISO 6496:1999 Animal feeding stuffs. Determination of moisture and other volatile matter content, British Standards Institute, London.
238. K. M. Fagerbakke, M. Heldal, S. Norland, (1996), Content of carbon, nitrogen, oxygen, sulfur and phosphorus in native aquatic and cultured bacteria. *Aquatic Microbial Ecology*. 10, 15-27.
239. R. Monique, G. N. Elisabeth, P. Etienne, L. Dominique, (2008), A high yield multi-method extraction protocol for protein quantification in activated sludge. *Bioresource Technology*. 99, 7464-7471.
240. N. J. Kruger, (1994), in *Basic Protein and Peptide Protocols*, J. M. Walker, Ed. Humana Press, Totowa, NJ, pp. 9-15.
241. M. Dubois, K. Gilles, J. K. Hamilton, P. A. Rebers, F. Smith, (1951), A colorimetric method for the determination of sugars. *Nature*. 168,
242. E. G. Bligh, W. J. Dyer, (1959), A rapid method of total lipid extraction and purification. *Canadian journal of biochemistry and physiology*. 37, 911-917.
243. V. M. Marshall *et al.*, (2001), Exopolysaccharide-producing strains of thermophilic lactic acid bacteria cluster into groups according to their EPS structure. *Letters in applied microbiology*. 32, 433-437.
244. O. Braissant, A. W. Decho, C. Dupraz, C. Glunk, K. M. Przekop, P. T. Visscher, (2007), Exopolymeric substances of sulfate-reducing bacteria: interactions with calcium at alkaline pH and implication for formation of carbonate minerals. *Geobiology*. 5, 401-411.
245. B.S.I., (2005), BS ISO10390:2005 Soil quality. Determination of pH, British Standards Institute, London.
246. B.S.I., (2002), BS ISO 11271:2002 Soil quality. Determination of redox potential. Field method, London.
247. W. M. Brück, T. B. Brück, W. T. Self, J. K. Reed, S. S. Nitecki, P. J. McCarthy, (2010), Comparison of the anaerobic microbiota of deep-water *Geodia* spp. and sandy sediments in the Straits of Florida. *The ISME journal*. 4, 686-699.

248. W. Manz, R. Amann, W. Ludwig, M. Vancanneyt, K.-H. Schleifer, (1996), Application of a suite of 16S rRNA-specific oligonucleotide probes designed to investigate bacteria of the phylum cytophaga-flavobacter-bacteroides in the natural environment. *Microbiology*. 142, 1097-1106.
249. C. Roller, M. Wagner, R. Amann, W. Ludwig, K.-H. Schleifer, (1994), In situ probing of Gram-positive bacteria with high DNA G+ C content using 23S rRNA-targeted oligonucleotides. *Microbiology*. 140, 2849-2858.
250. U. Edwards, T. Rogall, H. Blöcker, M. Emde, E. C. Böttger, (1989), Isolation and direct complete nucleotide determination of entire genes. Characterization of a gene coding for 16S ribosomal RNA. *Nucleic acids research*. 17, 7843-7853.
251. S. Gantner, A. F. Andersson, L. Alonso-Sáez, S. Bertilsson, (2011), Novel primers for 16S rRNA-based archaeal community analyses in environmental samples. *Journal of Microbiological Methods*. 84, 12-18.
252. A. Klindworth, E. Pruesse, T. Schweer, J. Peplies, C. Quast, M. Horn, F. O. Glöckner, (2012), Evaluation of general 16S ribosomal RNA gene PCR primers for classical and next-generation sequencing-based diversity studies. *Nucleic acids research*. gks808.
253. M.-Y. Jung *et al.*, (2011), Enrichment and characterization of an autotrophic ammonia-oxidizing archaeon of mesophilic crenarchaeal group I. 1a from an agricultural soil. *Applied and environmental microbiology*. 77, 8635-8647.
254. J. G. Caporaso *et al.*, (2011), Global patterns of 16S rRNA diversity at a depth of millions of sequences per sample. *Proceedings of the National Academy of Sciences*. 108, 4516-4522.
255. R. Kondo, K. Shigematsu, J. Butani, (2008), Rapid enumeration of sulphate-reducing bacteria from aquatic environments using real-time PCR. *Plankton and Benthos Research*. 3, 180-183.
256. K. M. Ritalahti, B. K. Amos, Y. Sung, Q. Wu, S. S. Koenigsberg, F. E. Löffler, (2006), Quantitative PCR targeting 16S rRNA and reductive dehalogenase genes simultaneously monitors multiple Dehalococcoides strains. *Applied and environmental microbiology*. 72, 2765-2774.
257. K. Tamura, G. Stecher, D. Peterson, A. Filipinski, S. Kumar, (2013), MEGA6: molecular evolutionary genetics analysis version 6.0. *Molecular biology and evolution*. 30, 2725-2729.
258. A. P. Masella, A. K. Bartram, J. M. Truszkowski, D. G. Brown, J. D. Neufeld, (2012), PANDAseq: paired-end assembler for illumina sequences. *BMC bioinformatics*. 13, 1.
259. L. Micallef, P. Rodgers, (2014), euler APE: Drawing area-proportional 3-Venn diagrams using ellipses. *PLoS One*. 9, e101717.
260. D. R. Lovley, D. F. Dwyer, M. J. Klug, (1982), Kinetic analysis of competition between sulfate reducers and methanogens for hydrogen in sediments. *Applied and environmental microbiology*. 43, 1373-1379.
261. C.-F. Chang, J.-W. Chen, (2006), The experimental investigation of concrete carbonation depth. *Cement and Concrete Research*. 36, 1760-1767.
262. J. E. McDonald, J. N. I. Houghton, D. J. Rooks, H. E. Allison, A. J. McCarthy, (2012), The microbial ecology of anaerobic cellulose degradation in municipal waste landfill sites: evidence of a role for fibrobacters. *Environmental Microbiology*. 14, 1077-1087.
263. J. R. Andreesen, G. Gottschalk, H. G. Schlegel, (1970), Clostridium formicoaceticum nov. spec. isolation, description and distinction from C. aceticum and C. thermoaceticum. *Archiv für Mikrobiologie*. 72, 154-174.

264. E. Fisher *et al.*, (2008), Transformation of Inorganic and Organic Arsenic by *Alkaliphilus oremlandii* sp. nov. Strain OhILAs. *Annals of the New York Academy of Sciences*. 1125, 230-241.
265. E. V. Pikuta, T. Itoh, P. Krader, J. Tang, W. B. Whitman, R. B. Hoover, (2006), *Anaerovirgula multivorans* gen. nov., sp. nov., a novel spore-forming, alkaliphilic anaerobe isolated from Owens Lake, California, USA. *International journal of systematic and evolutionary microbiology*. 56, 2623-2629.
266. S. Kotelnikova, A. J. L. Macario, K. Pedersen, (1998), *Methanobacterium subterraneum* sp. nov., a new alkaliphilic, eurythermic and halotolerant methanogen isolated from deep granitic groundwater. *International journal of systematic and evolutionary microbiology*. 48, 357-367.
267. W. M. Wu, M. K. Jain, E. C. De Macario, J. H. Thiele, J. G. Zeikus, (1992), Microbial composition and characterization of prevalent methanogens and acetogens isolated from syntrophic methanogenic granules. *Applied microbiology and biotechnology*. 38, 282-290.
268. B. Dridi, M.-L. Fardeau, B. Ollivier, D. Raoult, M. Drancourt, (2012), *Methanomassiliicoccus luminyensis* gen. nov., sp. nov., a methanogenic archaeon isolated from human faeces. *International journal of systematic and evolutionary microbiology*. 62, 1902-1907.
269. G. M. Maestrojuan, J. E. Boone, R. A. Mah, J. A. G. F. Menaia, M. S. Sachs, D. R. Boone, (1992), Taxonomy and halotolerance of mesophilic *Methanosarcina* strains, assignment of strains to species, and synonymy of *Methanosarcina mazei* and *Methanosarcina frisia*. *International journal of systematic and evolutionary microbiology*. 42, 561-567.
270. D. Rai, L. Rao, Y. Xia, (1998), Solubility of crystalline calcium isosaccharinate. *Journal of solution chemistry*. 27, 1109-1122.
271. J. Jung, J. Chun, W. Park, (2012), Genome sequence of extracellular-protease-producing *Alishewanella jeotgali* isolated from traditional Korean fermented seafood. *Journal of bacteriology*. 194, 2097-2097.
272. M.-S. Kim, S. K. Jo, S. W. Roh, J.-W. Bae, (2010), *Alishewanella agri* sp. nov., isolated from landfill soil. *International journal of systematic and evolutionary microbiology*. 60, 2199-2203.
273. I. Yumoto, A. Nakamura, H. Iwata, K. Kojima, K. Kusumoto, Y. Nodasaka, H. Matsuyama, (2002), *Dietzia psychralcaliphila* sp. nov., a novel, facultatively psychrophilic alkaliphile that grows on hydrocarbons. *International journal of systematic and evolutionary microbiology*. 52, 85-90.
274. R. J. Koerner, M. Goodfellow, A. L. Jones, (2009), The genus *Dietzia*: a new home for some known and emerging opportunist pathogens. *FEMS Immunology & Medical Microbiology*. 55, 296-305.
275. E. A. Grice *et al.*, (2009), Topographical and temporal diversity of the human skin microbiome. *Science*. 324, 1190-1192.
276. R. Niederdorfer, H. Peter, T. J. Battin, (2016), Attached biofilms and suspended aggregates are distinct microbial lifestyles emanating from differing hydraulics. *Nature Microbiology*. 1, 16178.
277. D. M. Dominiak, J. L. Nielsen, P. H. Nielsen, (2011), Extracellular DNA is abundant and important for microcolony strength in mixed microbial biofilms. *Environmental Microbiology*. 13, 710-721.
278. E. S. Gloag *et al.*, (2013), Self-organization of bacterial biofilms is facilitated by extracellular DNA. *Proceedings of the National Academy of Sciences*. 110, 11541-11546.

279. A. Dell'Anno, R. Danovaro, (2005), Extracellular DNA plays a key role in deep-sea ecosystem functioning. *Science*. 309, 2179-2179.
280. A. Jahn, P. H. Nielsen, (1998), Cell biomass and exopolymer composition in sewer biofilms. *water science and technology*. 37, 17-24.
281. L. Castro, R. Zhang, J. A. Muñoz, F. González, M. L. Blázquez, W. Sand, A. Ballester, (2014), Characterization of exopolymeric substances (EPS) produced by *Aeromonas hydrophila* under reducing conditions. *Biofouling*. 30, 501-511.
282. V. K. Plakunov, M. V. Zhurina, S. S. Beliaev, (2008), [Resistance of the petroleum-oxidizing microorganism *Dietzia* sp. to hyperosmotic shock in reconstituted biofilms]. *Mikrobiologiya*. 77, 581-589.
283. K. Tazaki, (2005), Microbial formation of a halloysite-like mineral. *Clays and Clay Minerals*. 53, 224-233.
284. X. b. Hu, K. Xu, Z. Wang, L. l. Ding, H. q. Ren, (2013), Characteristics of biofilm attaching to carriers in moving bed biofilm reactor used to treat vitamin C wastewater. *Scanning*. 35, 283-291.
285. M. Moscoso, E. García, R. López, (2006), Biofilm formation by *Streptococcus pneumoniae*: role of choline, extracellular DNA, and capsular polysaccharide in microbial accretion. *Journal of bacteriology*. 188, 7785-7795.
286. Z. Filip, S. Hermann, (2001), An attempt to differentiate *Pseudomonas* spp. and other soil bacteria by FT-IR spectroscopy. *European journal of soil biology*. 37, 137-143.
287. V. R. Phoenix, R. E. Martinez, K. O. Konhauser, F. G. Ferris, (2002), Characterization and implications of the cell surface reactivity of *Calothrix* sp. strain KC97. *Applied and environmental microbiology*. 68, 4827-4834.
288. D. C. Sobeck, M. J. Higgins, (2002), Examination of three theories for mechanisms of cation-induced bioflocculation. *Water Research*. 36, 527-538.
289. O. Braissant, A. W. Decho, K. M. Przekop, K. L. Gallagher, C. Glunk, C. Dupraz, P. T. Visscher, (2009), Characteristics and turnover of exopolymeric substances in a hypersaline microbial mat. *FEMS Microbiology Ecology*. 67, 293-307.
290. J. P. de Boer, C. C. H. Cronenberg, D. de Beer, J. C. van den Heuvel, M. J. T. de Mattos, O. M. Neijssel, (1993), pH and glucose profiles in aggregates of *Bacillus laevolacticus*. *Applied and environmental microbiology*. 59, 2474-2478.
291. P. N. L. Lens, D. De Beer, C. C. H. Cronenberg, F. P. Houwen, S. P. P. Ottengraf, W. H. Verstraete, (1993), Heterogeneous distribution of microbial activity in methanogenic aggregates: pH and glucose microprofiles. *Applied and environmental microbiology*. 59, 3803-3815.
292. R. C. Hunter, T. J. Beveridge, (2005), Application of a pH-sensitive fluoroprobe (C-SNARF-4) for pH microenvironment analysis in *Pseudomonas aeruginosa* biofilms. *Applied and environmental microbiology*. 71, 2501-2510.
293. J. T. Babauta, H. D. Nguyen, T. D. Harrington, R. Renslow, H. Beyenal, (2012), pH, redox potential and local biofilm potential microenvironments within *Geobacter sulfurreducens* biofilms and their roles in electron transfer. *Biotechnology and bioengineering*. 109, 2651-2662.
294. V. J. M. Allan, L. E. Macaskie, M. E. Callow, (1999), Development of a pH gradient within a biofilm is dependent upon the limiting nutrient. *Biotechnology letters*. 21, 407-413.
295. A. K. Vangsgaard, M. Mauricio-Iglesias, B. Valverde-Pérez, K. V. Gernaey, G. Sin, (2013), pH variation and influence in an autotrophic nitrogen removing biofilm system using an efficient numerical solution strategy. *water science and technology*. 67, 2608-2615.

296. K. A. Mattos, C. Jones, N. Heise, J. O. Previato, L. Mendonca-Previato, (2001), Structure of an acidic exopolysaccharide produced by the diazotrophic endophytic bacterium *Burkholderia brasiliensis*. *Eur J Biochem.* 268, 3174-3179.
297. T. D. t. Perry *et al.*, (2005), Binding of harvested bacterial exopolymers to the surface of calcite. *Environ Sci Technol.* 39, 8770-8775.
298. T. K. Nam, M. B. Timmons, C. D. Montemagno, S. M. Tsukuda, (2000), Biofilm characteristics as affected by sand size and location in fluidized bed vessels. *Aquacultural Engineering.* 22, 213-224.
299. I. W. Marjaka, K. Miyanaga, K. Hori, Y. Tanji, H. Unno, (2003), Augmentation of self-purification capacity of sewer pipe by immobilizing microbes on the pipe surface. *Biochemical engineering journal.* 15, 69-75.
300. T. Zhu, M. Dittrich, (2016), Carbonate Precipitation through Microbial Activities in Natural Environment, and Their Potential in Biotechnology: A Review. *Frontiers in Bioengineering and Biotechnology.* 4, 4.
301. G. Arp, A. Reimer, J. Reitner, (1999), Calcification in cyanobacterial biofilms of alkaline salt lakes. *European Journal of Phycology.* 34, 393-403.
302. F. Hammes, W. Verstraete, (2002), Key roles of pH and calcium metabolism in microbial carbonate precipitation. *Reviews in environmental science and biotechnology.* 1, 3-7.
303. T. Zhang, I. Klapper, (2010), Mathematical model of biofilm induced calcite precipitation. *water science and technology.* 61, 2957-2964.
304. L. A. Warren, P. A. Maurice, N. Parmar, F. G. Ferris, (2001), Microbially mediated calcium carbonate precipitation: implications for interpreting calcite precipitation and for solid-phase capture of inorganic contaminants. *Geomicrobiology Journal.* 18, 93-115.
305. Y. Jiao *et al.*, (2010), Characterization of extracellular polymeric substances from acidophilic microbial biofilms. *Applied and environmental microbiology.* 76, 2916-2922.
306. I. Tiago, A. P. Chung, A. Veríssimo, (2004), Bacterial diversity in a nonsaline alkaline environment: heterotrophic aerobic populations. *Applied and environmental microbiology.* 70, 7378-7387.
307. S. G. Prowe, G. Antranikian, (2001), Anaerobranca gottschalkii sp. nov., a novel thermoalkaliphilic bacterium that grows anaerobically at high pH and temperature. *Int J Syst Evol Microbiol.* 51, 457-465.
308. V. Gorlenko *et al.*, (2004), Anaerobranca californiensis sp. nov., an anaerobic, alkalithermophilic, fermentative bacterium isolated from a hot spring on Mono Lake. *Int J Syst Evol Microbiol.* 54, 739-743.
309. V. Kevbrin, Y. Boltyanskaya, E. Garnova, J. Wiegel, (2008), Anaerobranca zavarzinii sp. nov., an anaerobic, alkalithermophilic bacterium isolated from Kamchatka thermal fields. *Int J Syst Evol Microbiol.* 58, 1486-1491.
310. M. Engle, Y. Li, C. Woese, J. Wiegel, (1995), Isolation and characterization of a novel alkalitolerant thermophile, Anaerobranca horikoshii gen. nov., sp. nov. *Int J Syst Bacteriol.* 45, 454-461.
311. P. Kampfer *et al.*, (2010), Fontibacter flavus gen. nov., sp. nov., a member of the family 'Cyclobacteriaceae', isolated from a hot spring. *Int J Syst Evol Microbiol.* 60, 2066-2070.
312. J. Zhang, G. Yang, S. Zhou, Y. Wang, Y. Yuan, L. Zhuang, (2013), Fontibacter ferrireducens sp. nov., an Fe(III)-reducing bacterium isolated from a microbial fuel cell. *Int J Syst Evol Microbiol.* 63, 925-929.

313. J. K. Akhwale, M. Goker, M. Rohde, P. Schumann, H. P. Klenk, H. I. Boga, (2015), Belliella kenyensis sp. nov., isolated from an alkaline lake. *Int J Syst Evol Microbiol.* 65, 457-462.
314. B. Janto *et al.*, (2011), The genome of alkaliphilic Bacillus pseudofirmus OF4 reveals adaptations that support the ability to grow in an external pH range from 7.5 to 11.4. *Environmental Microbiology.* 13, 3289-3309.
315. S. D'Hondt *et al.*, (2004), Distributions of microbial activities in deep seafloor sediments. *Science.* 306, 2216-2221.
316. N.N.L., (2015), Demonstration of Carbonation of the NRVB, NNL(14)13296. National Nuclear Labs, Harwell, Oxford.
317. B.G.S., (2014), Results of laboratory carbonation experiments on NRVB cement: Minerals and Waste Programme, OR/14/048. Energy science programme. British Geological Survey, Keyworth, Nottingham.
318. M. Felipe-Sotelo, J. Hinchliff, N. Evans, P. Warwick, D. Read, (2012), Sorption of radionuclides to a cementitious backfill material under near-field conditions. *Mineralogical Magazine.* 76, 3401-3410.
319. G. Purser, A. E. Milodowski, J. F. Harrington, C. A. Rochelle, A. Butcher, D. Wagner, (2013), Modification to the flow properties of repository cement as a result of carbonation. *Procedia Earth and Planetary Science.* 7, 701-704.
320. S. Wei, Z. Jiang, H. Liu, D. Zhou, M. Sanchez-Silva, (2013), Microbiologically induced deterioration of concrete - A Review. *Brazilian Journal of Microbiology.* 44, 1001-1007.
321. L. R. Van Loon, M. A. Glaus, S. Stallone, A. Laube, (1997), Sorption of isosaccharinic acid, a cellulose degradation product, on cement. *Environ Sci Technol.* 31, 1243-1245.
322. C.-T. Wang, (2014), Technology and Application of Microbial Fuel Cells.
323. J. Tourney, B. T. Ngwenya, (2008), Bacterial EPS as a mediator of calcium carbonate morphology and polymorphism. *Mineralogical Magazine.* 72, 291-291.
324. M. D. Curry, P. J. Boston, M. N. Spilde, J. F. Baichtal, A. R. Campbell, (2009), Cottonballs, a unique subaqueous moonmilk, and abundant subaerial moonmilk in Cataract Cave, Tongass National Forest, Alaska. *International Journal of Speleology.* 38, 3.
325. S. E. Jones, J. T. Lennon, (2010), Dormancy contributes to the maintenance of microbial diversity. *Proceedings of the National Academy of Sciences.* 107, 5881-5886.
326. C. C. Dawson, C. Intapa, M. A. Jabra-Rizk, (2011), "Persisters": survival at the cellular level. *PLoS Pathog.* 7, e1002121.
327. A. K. Epstein, B. Pokroy, A. Seminara, J. Aizenberg, (2011), Bacterial biofilm shows persistent resistance to liquid wetting and gas penetration. *Proceedings of the National Academy of Sciences.* 108, 995-1000.
328. M. Liu, Y. Yuan, L.-x. Zhang, L. Zhuang, S.-g. Zhou, J.-r. Ni, (2010), Bioelectricity generation by a Gram-positive Corynebacterium sp. strain MFC03 under alkaline condition in microbial fuel cells. *Bioresource Technology.* 101, 1807-1811.
329. C.-Y. Wu, L. Zhuang, S.-G. Zhou, F.-B. Li, J. He, (2011), Corynebacterium humireducens sp. nov., an alkaliphilic, humic acid-reducing bacterium isolated from a microbial fuel cell. *International journal of systematic and evolutionary microbiology.* 61, 882-887.
330. C. Rückert, J. Kalinowski, (2008), Sulfur metabolism in Corynebacterium glutamicum. *Corynebacteria-Genomics and Molecular Biology Edited.* 217-240.

331. C. J. Bolten, J. Dickschat, C. Wittmann, (2010), Towards methionine overproduction in *Corynebacterium glutamicum*—methanethiol and dimethyldisulfide as reduced sulfur sources. *J Microbiol Biotechnol.* 20, 1196-1203.
332. T. S. Jadhav, N. J. Faldu, P. Patel, S. N. Narolkar, A. S. Nerurkar, (2005), *Alcaligenes faecalis* kw-a biofilm for denitrification of nitrate-rich effluent. *Indian J Exp Biol.* 43, 542-547.
333. T. Aüllo, A. Ranchou-Peyruse, B. Ollivier, M. Magot, (2013), *Desulfotomaculum* spp. and related gram-positive sulfate-reducing bacteria in deep subsurface environments. *Frontiers in microbiology.* 4, 362.
334. R. Villemur, M. Lanthier, R. Beaudet, F. Lepine, (2006), The *Desulfitobacterium* genus. *FEMS Microbiol Rev.* 30, 706-733.
335. G. R. Gibson, J. H. Cummings, G. T. Macfarlane, (1988), Competition for hydrogen between sulphate-reducing bacteria and methanogenic bacteria from the human large intestine. *Journal of applied bacteriology.* 65, 241-247.
336. P. Schönheit, J. K. Kristjansson, R. K. Thauer, (1982), Kinetic mechanism for the ability of sulfate reducers to out-compete methanogens for acetate. *Archives of Microbiology.* 132, 285-288.
337. A. W. Glossner, L. K. Gallagher, L. Landkamer, L. Figueroa, J. Munakata-Marr, K. W. Mandernack, (2016), Factors controlling the co-occurrence of microbial sulfate reduction and methanogenesis in coal bed reservoirs. *International Journal of Coal Geology.* 165, 121-132.
338. D. Ozuolmez, H. Na, M. A. Lever, K. U. Kjeldsen, B. B. Jørgensen, C. M. Plugge, (2015), Methanogenic archaea and sulfate reducing bacteria co-cultured on acetate: teamwork or coexistence? *Frontiers in microbiology.* 6, 492.
339. C. L. Thorpe, G. T. W. Law, C. Boothman, J. R. Lloyd, I. T. Burke, K. Morris, (2012), The synergistic effects of high nitrate concentrations on sediment bioreduction. *Geomicrobiology Journal.* 29, 484-493.
340. B. U. Foesel, H. L. Drake, A. Schramm, (2011), *Defluviimonas denitrificans* gen. nov., sp. nov., and *Pararhodobacter aggregans* gen. nov., sp. nov., non-phototrophic Rhodobacteraceae from the biofilter of a marine aquaculture. *Syst Appl Microbiol.* 34, 498-502.
341. X. Xia *et al.*, (2016), Draft genomic sequence of a chromate- and sulfate-reducing *Alishewanella* strain with the ability to bioremediate Cr and Cd contamination. *Standards in Genomic Sciences.* 11, 48.
342. X. Li *et al.*, (2016), Complete genome sequence of a deeply branched marine Bacteroidia bacterium *Draconibacterium orientale* type strain FH5T. *Marine Genomics.* 26, 13-16.
343. S. C. Marques, J. d. G. O. S. Rezende, L. A. d. F. Alves, B. C. Silva, E. Alves, L. R. d. Abreu, R. H. Piccoli, (2007), Formation of biofilms by *Staphylococcus aureus* on stainless steel and glass surfaces and its resistance to some selected chemical sanitizers. *Brazilian Journal of Microbiology.* 38, 538-543.
344. P. Rajala, L. Carpén, M. Vepsäläinen, M. Raulio, E. Sohlberg, M. Bomberg, (2015), Microbially induced corrosion of carbon steel in deep groundwater environment. *Frontiers in microbiology.* 6, 647.
345. V. Gomis-Yagües, N. Boluda-Botella, F. Ruiz-Beviá, (2000), Gypsum precipitation/dissolution as an explanation of the decrease of sulphate concentration during seawater intrusion. *Journal of Hydrology.* 228, 48-55.
346. F. M. AlAbbas, C. Williamson, S. M. Bhola, J. R. Spear, D. L. Olson, B. Mishra, A. E. Kakpovbia, (2013), Influence of sulfate reducing bacterial biofilm on corrosion

- behavior of low-alloy, high-strength steel (API-5L X80). *International Biodeterioration & Biodegradation*. 78, 34-42.
347. M. M. Fan, H. F. Liu, Z. H. Dong, (2013), Microbiologically influenced corrosion of X60 carbon steel in CO<sub>2</sub>-saturated oilfield flooding water. *Materials and Corrosion*. 64, 242-246.
348. F. King, P. Humphreys, R. Metcalfe, (2011), A Review of the Information Available to Assess the Risk of Microbiologically Influenced Corrosion in Waste Packages, QRS-1384L-1. Nuclear Decommissioning Authority (Radioactive Waste Management Directorate), Harwell, Didcot, Oxfordshire, UK.
349. E. A. Magee, C. J. Richardson, R. Hughes, J. H. Cummings, (2000), Contribution of dietary protein to sulfide production in the large intestine: an in vitro and a controlled feeding study in humans. *Am J Clin Nutr*. 72, 1488-1494.
350. A. Conrad, M. Kontro, M. M. Keinänen, A. Cadoret, P. Faure, L. Mansuy-Huault, J.-C. Block, (2003), Fatty acids of lipid fractions in extracellular polymeric substances of activated sludge flocs. *Lipids*. 38, 1093-1105.
351. L. F. Cruz, P. A. Cobine, L. De La Fuente, (2012), Calcium increases Xylella fastidiosa surface attachment, biofilm formation, and twitching motility. *Applied and environmental microbiology*. 78, 1321-1331.
352. M. Lanthier, P. Juteau, F. Lepine, R. Beaudet, R. Villemur, (2005), Desulfitobacterium hafniense is present in a high proportion within the biofilms of a high-performance pentachlorophenol-degrading, methanogenic fixed-film reactor. *Applied and environmental microbiology*. 71, 1058-1065.
353. S. A. Dar, R. Kleerebezem, A. J. M. Stams, J. G. Kuenen, G. Muyzer, (2008), Competition and coexistence of sulfate-reducing bacteria, acetogens and methanogens in a lab-scale anaerobic bioreactor as affected by changing substrate to sulfate ratio. *Applied microbiology and biotechnology*. 78, 1045-1055.
354. H. Shiratori *et al.*, (2009), Clostridium clariflavum sp. nov. and Clostridium caenicola sp. nov., moderately thermophilic, cellulose-/cellobiose-digesting bacteria isolated from methanogenic sludge. *International journal of systematic and evolutionary microbiology*. 59, 1764-1770.
355. M. Von Jan *et al.*, (2011), Kroppenstedtia eburnea gen. nov., sp. nov., a thermoactinomycete isolated by environmental screening, and emended description of the family Thermoactinomycetaceae Matsuo *et al.* 2006 emend. Yassin *et al.* 2009. *International journal of systematic and evolutionary microbiology*. 61, 2304-2310.
356. E. Petitdemange, F. Caillet, J. Giallo, C. Gaudin, (1984), Clostridium cellulolyticum sp. nov., a cellulolytic, mesophilic: species from decayed grass. *International journal of systematic and evolutionary microbiology*. 34, 155-159.
357. Y. Liu, J.-T. Qiao, X.-Z. Yuan, R.-B. Guo, Y.-L. Qiu, (2014), Hydrogenispora ethanolica gen. nov., sp. nov., an anaerobic carbohydrate-fermenting bacterium from anaerobic sludge. *International journal of systematic and evolutionary microbiology*. 64, 1756-1762.
358. H. Takami, T. A. Krulwich, (2000), Reidentification of facultatively alkaliphilic Bacillus firmus OF4 as Bacillus pseudofirmus OF4. *Extremophiles*. 4, 19-22.
359. J.-S. Lee, K. C. Lee, Y.-H. Chang, S. G. Hong, H. W. Oh, Y.-R. Pyun, K. S. Bae, (2002), Paenibacillus daejeonensis sp. nov., a novel alkaliphilic bacterium from soil. *International journal of systematic and evolutionary microbiology*. 52, 2107-2111.
360. G.-H. Lee, M.-S. Rhee, D.-H. Chang, K. K. Kwon, K. S. Bae, S.-H. Yang, B.-C. Kim, (2014), Bacillus solimangrovi sp. nov., isolated from mangrove soil. *International journal of systematic and evolutionary microbiology*. 64, 1622-1628.

361. D. Y. Sorokin, T. P. Tourova, M. Mußmann, G. Muyzer, (2008), Dethiobacter alkaliphilus gen. nov. sp. nov., and Desulfurivibrio alkaliphilus gen. nov. sp. nov.: two novel representatives of reductive sulfur cycle from soda lakes. *Extremophiles*. 12, 431-439.
362. C. Crespo, T. Pozzo, E. N. Karlsson, M. T. Alvarez, B. Mattiasson, (2012), Caloramator boliviensis sp. nov., a thermophilic, ethanol-producing bacterium isolated from a hot spring. *International journal of systematic and evolutionary microbiology*. 62, 1679-1686.
363. A. Willems *et al.*, (1989), Hydrogenophaga, a new genus of hydrogen-oxidizing bacteria that includes Hydrogenophaga flava comb. nov. (formerly Pseudomonas flava), Hydrogenophaga palleronii (formerly Pseudomonas palleronii), Hydrogenophaga pseudoflava (formerly Pseudomonas pseudoflava and “Pseudomonas carboxydoflava”), and Hydrogenophaga taeniospiralis (formerly Pseudomonas taeniospiralis). *International journal of systematic and evolutionary microbiology*. 39, 319-333.
364. T. N. Zhilina, D. G. Zavarzina, G. A. Osipov, N. A. Kostrikina, T. P. Tourova, (2009), Natronincola ferrireducens sp. nov., and Natronincola peptidovorans sp. nov., new anaerobic alkaliphilic peptolytic iron-reducing bacteria isolated from soda lakes. *Microbiology*. 78, 455-467.
365. X.-Y. Wu, K.-L. Shi, X.-W. Xu, M. Wu, A. Oren, X.-F. Zhu, (2010), Alkaliphilus halophilus sp. nov., a strictly anaerobic and halophilic bacterium isolated from a saline lake, and emended description of the genus Alkaliphilus. *International journal of systematic and evolutionary microbiology*. 60, 2898-2902.
366. I. Brettar, R. Christen, M. G. Höfle, (2004), Aquiflexum balticum gen. nov., sp. nov., a novel marine bacterium of the Cytophaga–Flavobacterium–Bacteroides group isolated from surface water of the central Baltic Sea. *International journal of systematic and evolutionary microbiology*. 54, 2335-2341.
367. Y. Yashiro, S. Sakai, M. Ehara, M. Miyazaki, T. Yamaguchi, H. Imachi, (2011), Methanoregula formicica sp. nov., a methane-producing archaeon isolated from methanogenic sludge. *International journal of systematic and evolutionary microbiology*. 61, 53-59.
368. S. R. Vartoukian, R. M. Palmer, W. G. Wade, (2010), Strategies for culture of ‘unculturable’ bacteria. *FEMS microbiology letters*. 309, 1-7.

# Associated data

## Data associated with Chapter 6.

pH 11 microcosm Eubacterial clones			
Clone	Accession number	Closest matching organisms	Sequence similarity (%)
A01	KP728118	<i>Alishewanella jeotgali</i> strain MS1	99
A02	KP728119	<i>Alishewanella jeotgali</i> strain MS1	96
A03	KP728120	<i>Alishewanella jeotgali</i> strain MS1	99
A05	KP728121	<i>Alishewanella jeotgali</i> strain MS1	95
A06	KP728122	<i>Alishewanella jeotgali</i> strain MS1	99
A07	KP728123	<i>Alishewanella jeotgali</i> strain MS1	98
A08	KP728124	<i>Alishewanella jeotgali</i> strain MS1	99
A09	KP728125	<i>Alishewanella jeotgali</i> strain MS1	97
A11	KP728126	<i>Alishewanella jeotgali</i> strain MS1	98
A12	KP728127	<i>Alishewanella jeotgali</i> strain MS1	98
B01	KP728128	<i>Alishewanella jeotgali</i> strain MS1	99
B02	KP728129	<i>Alishewanella jeotgali</i> strain MS1	98
B03	KP728130	<i>Alishewanella jeotgali</i> strain MS1	98
B04	KP728131	<i>Alishewanella jeotgali</i> strain MS1	99
B09	KP728132	<i>Alishewanella jeotgali</i> strain MS1	96
B12	KP728133	<i>Alishewanella jeotgali</i> strain MS1	97
C01	KP728134	<i>Alishewanella jeotgali</i> strain MS1	98
C05	KP728135	<i>Alishewanella jeotgali</i> strain MS1	98
C07	KP728136	<i>Alishewanella jeotgali</i> strain MS1	99
C08	KP728137	<i>Alishewanella jeotgali</i> strain MS1	99
C09	KP728138	<i>Alishewanella jeotgali</i> strain MS1	99
C12	KP728139	<i>Alishewanella jeotgali</i> strain MS1	98
D01	KP728140	<i>Alishewanella jeotgali</i> strain MS1	99
D03	KP728141	<i>Alishewanella jeotgali</i> strain MS1	98
D05	KP728142	<i>Alishewanella jeotgali</i> strain MS1	98
D06	KP728143	<i>Alishewanella jeotgali</i> strain MS1	99
D07	KP728144	<i>Alishewanella jeotgali</i> strain MS1	98
D08	KP728145	<i>Alishewanella jeotgali</i> strain MS1	97
D09	KP728146	<i>Alishewanella jeotgali</i> strain MS1	99
D11	KP728147	<i>Alishewanella jeotgali</i> strain MS1	98
E01	KP728148	<i>Alishewanella jeotgali</i> strain MS1	97
E02	KP728149	<i>Alishewanella jeotgali</i> strain MS1	96
E04	KP728150	<i>Bacillus pseudofirmus</i> OF4 strain OF4	98
E06	KP728151	<i>Alishewanella jeotgali</i> strain MS1	93
E07	KP728152	<i>Alishewanella jeotgali</i> strain MS1	98
E08	KP728153	<i>Alishewanella jeotgali</i> strain MS1	95
E12	KP728154	<i>Alkaliphilus crotonatoxidans</i> strain B11-2	98
F01	KP728155	<i>Alishewanella jeotgali</i> strain MS1	96
F02	KP728156	<i>Alishewanella jeotgali</i> strain MS1	97

F03	KP728157	Alishewanella jeotgali strain MS1	98
F05	KP728158	Alishewanella jeotgali strain MS1	97
F06	KP728159	Alishewanella jeotgali strain MS1	99
F07	KP728160	Alishewanella jeotgali strain MS1	98
F09	KP728161	Alishewanella jeotgali strain MS1	99
F10	KP728162	Alishewanella jeotgali strain MS1	95
F12	KP728163	Alishewanella jeotgali strain MS1	99
G01	KP728164	Alishewanella jeotgali strain MS1	96
G05	KP728165	Alishewanella jeotgali strain MS1	98
G06	KP728166	Alishewanella jeotgali strain MS1	97
G07	KP728167	Bacillus pseudofirmus OF4 strain OF4	99
G08	KP728168	Alishewanella jeotgali strain MS1	97
G09	KP728169	Alishewanella jeotgali strain MS1	98
G10	KP728170	Alishewanella jeotgali strain MS1	98
G11	KP728171	Alishewanella jeotgali strain MS1	99
H01	KP728172	Alishewanella jeotgali strain MS1	96
H04	KP728173	Alishewanella jeotgali strain MS1	95
H05	KP728174	Alishewanella jeotgali strain MS1	98
H10	KP728175	Alishewanella jeotgali strain MS1	98
H12	KP728176	Alishewanella jeotgali strain MS1	99

Table S6.1: Closest matching organisms and sequence similarities to the Eubacterial colonised cotton clone library.

Cotton Archaeal clones			
Clone	Accession number	Closest matching organisms	Sequence similarity (%)
ct68	KP264044	Methanobacterium alcaliphilum strain NBRC 105226	99
ct69	KP264045	Methanobacterium alcaliphilum strain NBRC 105226	99
ct70	KP264046	Methanobacterium alcaliphilum strain NBRC 105226	99
ct71	KP264047	Methanosarcina mazei Go1	99
ct72	KP264048	Methanobacterium alcaliphilum strain NBRC 105226	99
ct73	KP264049	Methanobacterium alcaliphilum strain NBRC 105226	99
ct74	KP264050	Methanobacterium alcaliphilum strain NBRC 105226	99
ct75	KP264051	Methanobacterium alcaliphilum strain NBRC 105226	99
ct76	KP264052	Methanomassiliococcus luminyensis strain B10	83
ct77	KP264053	Methanobacterium alcaliphilum strain NBRC 105226	99
ct78	KP264054	Methanobacterium alcaliphilum strain NBRC 105226	99
ct79	KP264055	Methanobacterium alcaliphilum strain NBRC 105226	99
ct80	KP264056	Methanomassiliococcus luminyensis strain B10	89
ct81	KP264057	Methanobacterium alcaliphilum strain NBRC 105226	99
ct82	KP264058	Methanobacterium alcaliphilum strain NBRC 105226	99
ct83	KP264059	Methanobacterium alcaliphilum strain NBRC 105226	99
ct84	KP264060	Methanobacterium alcaliphilum strain NBRC 105226	99
ct85	KP264061	Methanobacterium alcaliphilum strain NBRC 105226	99
ct86	KP264062	Methanomassiliococcus luminyensis strain B10	89
ct87	KP264063	Methanobacterium alcaliphilum strain NBRC 105226	99

ct88	KP264064	Methanobacterium alcaliphilum strain NBRC 105226	99
ct89	KP264065	Methanobacterium alcaliphilum strain NBRC 105226	99
ct90	KP264066	Methanobacterium alcaliphilum strain NBRC 105226	99
ct91	KP264067	Methanobacterium alcaliphilum strain NBRC 105226	99
ct92	KP264068	Methanomassiliicoccus luminyensis strain B10	89
ct93	KP264069	Methanobacterium alcaliphilum strain NBRC 105226	99
ct94	KP264070	Methanobacterium alcaliphilum strain NBRC 105226	99
ct95	KP264071	Methanobacterium alcaliphilum strain NBRC 105226	99
ct96	KP264072	Methanobacterium alcaliphilum strain NBRC 105226	99
ct97	KP264073	Methanobacterium alcaliphilum strain NBRC 105226	99
ct98	KP264074	Methanobacterium alcaliphilum strain NBRC 105226	99
ct99	KP264075	Methanobacterium alcaliphilum strain NBRC 105226	99
ct100	KP264076	Methanobacterium alcaliphilum strain NBRC 105226	99
ct101	KP264077	Methanobacterium alcaliphilum strain NBRC 105226	99
ct102	KP264078	Methanobacterium alcaliphilum strain NBRC 105226	99
ct103	KP264079	Methanobacterium alcaliphilum strain NBRC 105226	99
ct104	KP264080	Methanobacterium alcaliphilum strain NBRC 105226	99
ct105	KP264081	Methanobacterium alcaliphilum strain NBRC 105226	99
ct106	KP264082	Methanobacterium alcaliphilum strain NBRC 105226	99
ct107	KP264083	Methanobacterium alcaliphilum strain NBRC 105226	99
ct108	KP264084	Methanobacterium alcaliphilum strain NBRC 105226	99
ct109	KP264085	Methanobacterium alcaliphilum strain NBRC 105226	99
ct110	KP264086	Methanobacterium alcaliphilum strain NBRC 105226	99
ct111	KP264087	Methanobacterium alcaliphilum strain NBRC 105226	99
ct112	KP264088	Methanobacterium alcaliphilum strain NBRC 105226	99
ct113	KP264089	Methanobacterium alcaliphilum strain NBRC 105226	99
ct114	KP264090	Methanobacterium alcaliphilum strain NBRC 105226	99
ct115	KP264091	Methanobacterium alcaliphilum strain NBRC 105226	99
ct116	KP264092	Methanobacterium alcaliphilum strain NBRC 105226	99
ct117	KP264093	Methanobacterium alcaliphilum strain NBRC 105226	99
ct118	KP264094	Methanobacterium alcaliphilum strain NBRC 105226	99
ct119	KP264095	Methanobacterium alcaliphilum strain NBRC 105226	99
ct120	KP264096	Methanobacterium alcaliphilum strain NBRC 105226	99
ct121	KP264097	Methanobacterium alcaliphilum strain NBRC 105226	99
ct122	KP264098	Methanobacterium alcaliphilum strain NBRC 105226	99
ct123	KP264099	Methanobacterium alcaliphilum strain NBRC 105226	99
ct124	KP264100	Methanobacterium alcaliphilum strain NBRC 105226	99
ct125	KP264101	Methanobacterium alcaliphilum strain NBRC 105226	99
ct126	KP264102	Methanobacterium alcaliphilum strain NBRC 105226	99
ct127	KP264103	Methanobacterium alcaliphilum strain NBRC 105226	99
ct128	KP264104	Methanobacterium alcaliphilum strain NBRC 105226	99
ct129	KP264105	Methanobacterium alcaliphilum strain NBRC 105226	99
ct130	KP264106	Methanobacterium alcaliphilum strain NBRC 105226	99
ct131	KP264107	Methanobacterium alcaliphilum strain NBRC 105226	99
ct132	KP264108	Methanobacterium alcaliphilum strain NBRC 105226	99
ct133	KP264109	Methanobacterium alcaliphilum strain NBRC 105226	99

ct134	KP264110	Methanobacterium alcaliphilum strain NBRC 105226	99
ct135	KP264111	Methanobacterium alcaliphilum strain NBRC 105226	99

Table S6.2: Closest matching organisms and sequence similarities to the Archaeal colonised cotton clone library.

pH 11 microcosm Eubacterial clones			
Clone	Accession number	Closest matching organisms	Sequence similarity (%)
A01	KP728118	Alishewanella jeotgali strain MS1	99
A02	KP728119	Alishewanella jeotgali strain MS1	96
A03	KP728120	Alishewanella jeotgali strain MS1	99
A05	KP728121	Alishewanella jeotgali strain MS1	95
A06	KP728122	Alishewanella jeotgali strain MS1	99
A07	KP728123	Alishewanella jeotgali strain MS1	98
A08	KP728124	Alishewanella jeotgali strain MS1	99
A09	KP728125	Alishewanella jeotgali strain MS1	97
A11	KP728126	Alishewanella jeotgali strain MS1	98
A12	KP728127	Alishewanella jeotgali strain MS1	98
B01	KP728128	Alishewanella jeotgali strain MS1	99
B02	KP728129	Alishewanella jeotgali strain MS1	98
B03	KP728130	Alishewanella jeotgali strain MS1	98
B04	KP728131	Alishewanella jeotgali strain MS1	99
B09	KP728132	Alishewanella jeotgali strain MS1	96
B12	KP728133	Alishewanella jeotgali strain MS1	97
C01	KP728134	Alishewanella jeotgali strain MS1	98
C05	KP728135	Alishewanella jeotgali strain MS1	98
C07	KP728136	Alishewanella jeotgali strain MS1	99
C08	KP728137	Alishewanella jeotgali strain MS1	99
C09	KP728138	Alishewanella jeotgali strain MS1	99
C12	KP728139	Alishewanella jeotgali strain MS1	98
D01	KP728140	Alishewanella jeotgali strain MS1	99
D03	KP728141	Alishewanella jeotgali strain MS1	98
D05	KP728142	Alishewanella jeotgali strain MS1	98
D06	KP728143	Alishewanella jeotgali strain MS1	99
D07	KP728144	Alishewanella jeotgali strain MS1	98
D08	KP728145	Alishewanella jeotgali strain MS1	97
D09	KP728146	Alishewanella jeotgali strain MS1	99
D11	KP728147	Alishewanella jeotgali strain MS1	98
E01	KP728148	Alishewanella jeotgali strain MS1	97
E02	KP728149	Alishewanella jeotgali strain MS1	96
E04	KP728150	Bacillus pseudofirmus OF4 strain OF4	98
E06	KP728151	Alishewanella jeotgali strain MS1	93
E07	KP728152	Alishewanella jeotgali strain MS1	98
E08	KP728153	Alishewanella jeotgali strain MS1	95
E12	KP728154	Alkaliphilus crotonatoxidans strain B11-2	98
F01	KP728155	Alishewanella jeotgali strain MS1	96

F02	KP728156	Alishewanella jeotgali strain MS1	97
F03	KP728157	Alishewanella jeotgali strain MS1	98
F05	KP728158	Alishewanella jeotgali strain MS1	97
F06	KP728159	Alishewanella jeotgali strain MS1	99
F07	KP728160	Alishewanella jeotgali strain MS1	98
F09	KP728161	Alishewanella jeotgali strain MS1	99
F10	KP728162	Alishewanella jeotgali strain MS1	95
F12	KP728163	Alishewanella jeotgali strain MS1	99
G01	KP728164	Alishewanella jeotgali strain MS1	96
G05	KP728165	Alishewanella jeotgali strain MS1	98
G06	KP728166	Alishewanella jeotgali strain MS1	97
G07	KP728167	Bacillus pseudofirmus OF4 strain OF4	99
G08	KP728168	Alishewanella jeotgali strain MS1	97
G09	KP728169	Alishewanella jeotgali strain MS1	98
G10	KP728170	Alishewanella jeotgali strain MS1	98
G11	KP728171	Alishewanella jeotgali strain MS1	99
H01	KP728172	Alishewanella jeotgali strain MS1	96
H04	KP728173	Alishewanella jeotgali strain MS1	95
H05	KP728174	Alishewanella jeotgali strain MS1	98
H10	KP728175	Alishewanella jeotgali strain MS1	98
H12	KP728176	Alishewanella jeotgali strain MS1	99

Table S6.3: Closest matching organisms and sequence similarities to the Eubacterial pH 11 microcosm clone library.

Day	(mg L <sup>-1</sup> )					
	$\alpha$ -ISA	SE	$\beta$ -ISA	SE	XISA	SE
0	1227.20	32.92	256.59	7.33	266.57	48.22
2	1142.68	54.36	245.75	6.23	220.39	14.30
4	1056.13	52.42	213.43	1.45	214.33	27.63
6	966.74	57.79	156.60	4.80	156.31	41.17
8	825.20	147.17	86.40	17.54	142.81	58.63
10	832.31	183.52	71.68	27.82	132.88	36.37
12	796.78	149.76	73.71	19.81	134.64	39.51
14	794.65	197.97	73.08	23.67	159.14	31.20

Table S6.4: ISA concentration curves for pH 11 methanogenic floc based reactor.

Day	(mg L <sup>-1</sup> )					
	$\alpha$ -ISA control	SE	$\beta$ -ISA control	SE	XISA control	SE
0	455.94	12.42	360.61	14.99	237.57	18.85
2	478.36	1.74	380.24	3.51	262.12	2.37
4	524.57	48.30	416.65	31.02	257.46	16.09
6	556.62	88.58	444.48	66.53	263.94	10.30
8	473.52	38.56	378.85	24.48	261.69	17.98
10	496.87	33.91	397.03	22.89	258.99	2.94
12	441.52	1.58	346.18	0.04	239.52	28.10
14	475.22	21.19	380.56	9.83	267.37	11.29

Table S6.5: Control ISA concentration curves for pH 11 methanogenic floc based reactor.

Day	(mg L <sup>-1</sup> )				(mmoles)*	
	Microcosm acetate	SE	Control acetate	SE	Hydrogen gas	SE
0	286.66	26.74	27.81	0.47	0.00	0.00
2	329.42	17.52	26.30	0.54	0.32	0.15
4	449.97	41.54	25.71	1.56	0.53	0.05
6	384.50	113.05	25.53	0.23	0.84	0.10
8	466.13	68.55	17.41	11.09	1.07	0.00
10	445.89	81.37	24.33	3.73	0.87	0.01
12	489.21	52.89	24.57	1.86	1.08	0.05
14	499.85	49.68	23.58	2.53	1.00	0.04

\*Pressure remained at approximately 1 atm due to low volume of gas produced. No gas was detected within control systems.

Table S6.6: pH 11 microcosm acetate concentration and hydrogen headspace composition. pH 11 control acetate concentration. No hydrogen gas was detected.

Day	Microcosm (mg L <sup>-1</sup> )				Control (mg L <sup>-1</sup> )			
	TOC	SE	IC	SE	TOC	SE	IC	SE
0	365	17	11.705	1.555	392	1	4.5	0.3
2	354.5	18.5	11.91	0.66	388	7	4.6	0.3
4	298.3	28.7	13.435	1.435	387	3	4.7	0.4
6	281.9	37.1	12.715	2.515	390	2	4.4	0.2
8	325.6	0.6	15.47	1.47	382.5	2.5	4.5	0.5
10	302.85	12.15	17.875	1.075	380	5	4.2	0.3
12	285.75	1.75	18.995	0.545	394.5	2.5	4.9	0.2
14	309.75	15.75	20.64	0.66	388.5	4.5	4.7	0.3

Table S6.7: TOC and IC measurements for pH 11 methanogenic microcosm and control.

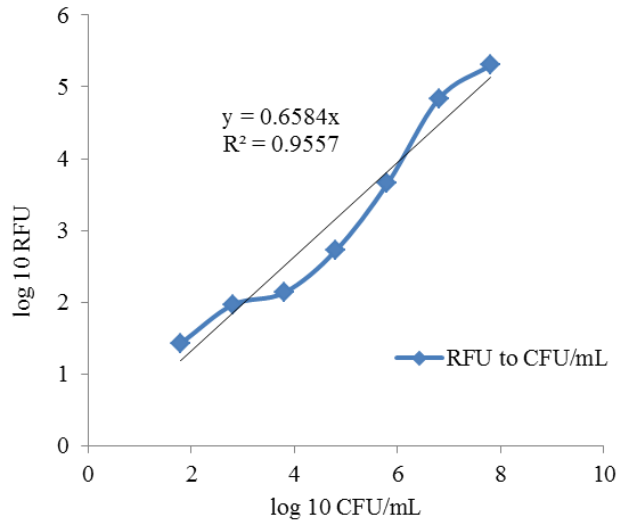


Figure S6.1: *E. coli* standard curve showing relationship between relative fluorescence units of ATP testing to CFU mL<sup>-1</sup>.

Day	Microcosm (RFU)		Control (RFU)	
	Average	SE	Average	SE
0	39215	3350	21	1
7	49540.5	766.5	19	1
14	52063	1555	21	1

Table S6.8: RFU measurements from 3M Clean-Trace biomass detection kit and luminometer.

Class level	(%)	Reads	Family level	(%)	Reads
Gammaproteobacteria	33.5	6310	Alishewanella_f	32.2	6074
Actinobacteria_c	32.9	6209	Dietziaceae	27.3	5154
Clostridia	12.6	2374	Bacillaceae	7.5	1421
Bacilli	11.1	2084	Anaerovirgula_f	4.8	903
Betaproteobacteria	4.7	890	Microbacteriaceae	4.8	901
Cytophagia	2.3	425	Anaerobranca_f	4.6	859
Alphaproteobacteria	1.2	219	Comamonadaceae	4.3	815
AB476673_c	1.1	209	Enterococcaceae	3.1	588
ETC < 1	0.7	132	Tissierella_f	2.7	510
			Cyclobacteriaceae	2.2	424
			AB476673_f	1.1	208
			Xanthomonadaceae	1.1	205
			ETC <1	4.2	790

Table S6.9: Class and family distribution of MiSeq data from pH 11 microcosm.

Size (µm)	Volume in %										
0.010	0.00	0.105	0.00	1.096	0.82	11.482	3.27	120.226	2.10	1258.925	0.00
0.011	0.00	0.120	0.00	1.259	0.90	13.183	2.81	138.038	1.90	1445.440	0.00
0.013	0.00	0.138	0.00	1.445	1.03	15.136	2.38	158.486	0.96	1659.587	0.00
0.015	0.00	0.158	0.00	1.660	1.21	17.378	2.00	181.970	0.42	1905.461	0.00
0.017	0.00	0.182	0.00	1.905	1.45	19.953	1.71	208.930	0.02	2187.762	0.00
0.020	0.00	0.209	0.00	2.198	1.78	22.909	1.53	239.883	0.00	2511.886	0.00
0.023	0.00	0.240	0.03	2.512	2.18	26.303	1.49	275.423	0.00	2884.032	0.00
0.026	0.00	0.275	0.03	2.884	2.63	30.200	1.57	316.228	0.00	3311.311	0.00
0.030	0.00	0.316	0.14	3.311	3.12	34.674	1.79	363.078	0.00	3801.894	0.00
0.035	0.00	0.363	0.26	3.802	3.59	39.811	2.11	418.868	0.00	4365.158	0.00
0.040	0.00	0.417	0.35	4.365	4.01	45.709	2.49	478.630	0.00	5011.872	0.00
0.046	0.00	0.479	0.45	5.012	4.32	52.481	2.87	548.541	0.00	5754.396	0.00
0.052	0.00	0.550	0.53	5.754	4.99	60.256	3.18	630.957	0.00	6606.934	0.00
0.060	0.00	0.631	0.60	6.607	4.51	69.183	3.34	724.436	0.00	7585.776	0.00
0.069	0.00	0.724	0.69	7.586	4.37	79.403	3.31	831.784	0.00	8709.636	0.00
0.079	0.00	0.832	0.73	8.710	4.09	91.201	3.07	954.663	0.00	10000.000	0.00
0.091	0.00	0.955	0.77	10.000	3.71	104.713	2.65	1096.478	0.00		
0.105	0.00	1.096		11.482		120.226		1258.925			

Table S6.10: Size distribution of the pH 11 flocs.

EPS component	(mg g VS <sup>-1</sup> )			
	Sonication + ethanol	SE	EDTA	SE
Carbohydrate	3.21	0.62	38.15	3.10
Protein	0.45	0.10	4.17	0.08
Lipid	8.43	1.29	0.95	0.07
eDNA	0.45	0.10	4.17	0.08

	(RFU)	
	Average	SE
Before extraction	50280	21
Sonication and ethanol	50338	20
EDTA	50493	32
Blank	53	1

Table S6.11: Composition of extracted polymicrobial floc EPS and ATP testing of cell pellet to check for cell lysis.

Calcium added (mg mg EPS <sup>-1</sup> )	Calcium bound (mg Ca mg EPS <sup>-1</sup> )
0.00	0.00
0.10	0.05
0.25	0.08
0.50	0.13
1.00	0.17

Table S6.12: Polymicrobial floc EPS calcium binding curve.

(Log CFU mL <sup>-1</sup> )								
Week	pH 11	SE	pH 11.5	SE	pH 12	SE	pH 13	SE
0	4.40	0.83	4.39	0.60	3.89	0.27	3.21	0.46
1	6.21	0.46	4.49	0.72	3.35	0.27	2.59	0.72
2	6.22	0.91	4.64	0.46	2.61	0.60	0.99	0.60
3	6.25	0.83	4.68	0.60	2.63	0.60	0.00	0.00

(Average RFU)								
Week	pH 11	SE	pH 11.5	SE	pH 12	SE	pH 13	SE
0	24960	7	24527	4	7744	2	1625	3
1	1613002	3	30846	5	2259	2	392	5
2	1678194	8	43947	3	410	4	10	4
3	1768306	7	48201	4	422	4	0	0

(Average RFU)								
pH	Week 0	SE	Week 1	SE	Week 2	SE	Week 3	SE
11.0	28	3	34	3	28	1	26	4
11.5	36	6	42	9	33	3	36	5
12.0	49	6	44	7	39	0	42	5
13.0	17	10	14	4	17	4	14	6

Table S6.13: ATP readings for floc communities and controls during subculture survival work.

pH 11.0 Floc profile		pH 11.5 floc profile		pH 12.0 floc profile	
pH	Distance (um)	pH	Distance (um)	pH	Distance (um)
11.10	0	11.56	0	12.05	0
11.13	5	11.47	5	11.99	5
11.09	10	11.35	10	11.94	10
11.10	15	11.31	15	11.98	15
11.05	20	11.21	20	11.98	20
11.02	25	10.77	25	11.88	25
10.98	30	10.69	30	11.85	30
10.95	35	10.88	35	11.82	35
10.87	40	11.06	40	11.79	40
10.85	45	11.12	45	11.76	45
10.77	50	11.13	50	11.63	50
10.80	55	11.24	55	11.70	55
10.62	60	11.30	60	11.68	60
10.45	65	11.32	65	11.86	65
10.41	70	11.41	70	11.99	70
10.54	75			12.04	75
10.73	80			12.07	80
10.83	85			12.05	85
10.86	90			12.02	90
11.00	95				
11.03	100				
11.05	105				
11.06	110				

Table S6.14: Micro-electrode profiles through flocs at different external pH values.

Distance (um)	pH		
	11	11.5	12
0	11.01	11.57	12.15
5	11	11.56	12.16
10	11.01	11.57	12.17
15	11.01	11.57	12.16
20	11	11.57	12.16
25	11	11.57	12.16
30	11.02	11.55	12.16
35	11.03	11.55	12.16
40	11.02	11.55	12.16
45	11.03	11.55	12.16
50	11.03	11.55	12.16
55	11.03	11.55	12.16
60	11.01	11.55	12.15
65	11	11.55	12.15
70	11	11.57	12.15
75	11	11.57	12.15
80	11	11.56	12.15
85	11.02	11.57	12.15
90	11.02	11.58	12.15
95	11.02	11.56	12.15
100	11.02	11.56	12.15

Table S6.15: Control micro-electrode profiles through agar at different external pH values.

pH	Average Zeta potential (mV)	SE
7	-24.26	3.03
8	-21.52	0.96
9	-22.82	1.44
10	2.65	0.36
11	-22.84	1.24
12	-27.76	0.93

Table S6.16: Zeta potential measurements of flocs at different pH values.

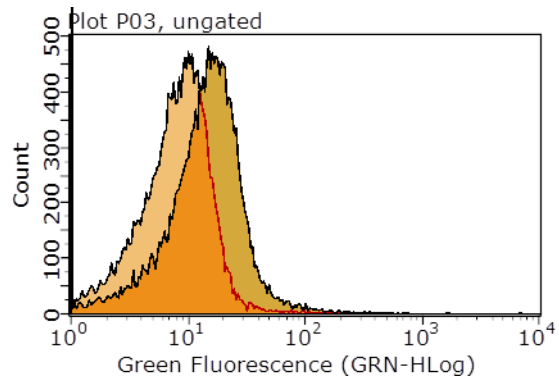


Figure S6.2: Flowcytometry plot of FITC staining and unstained control of flocs.

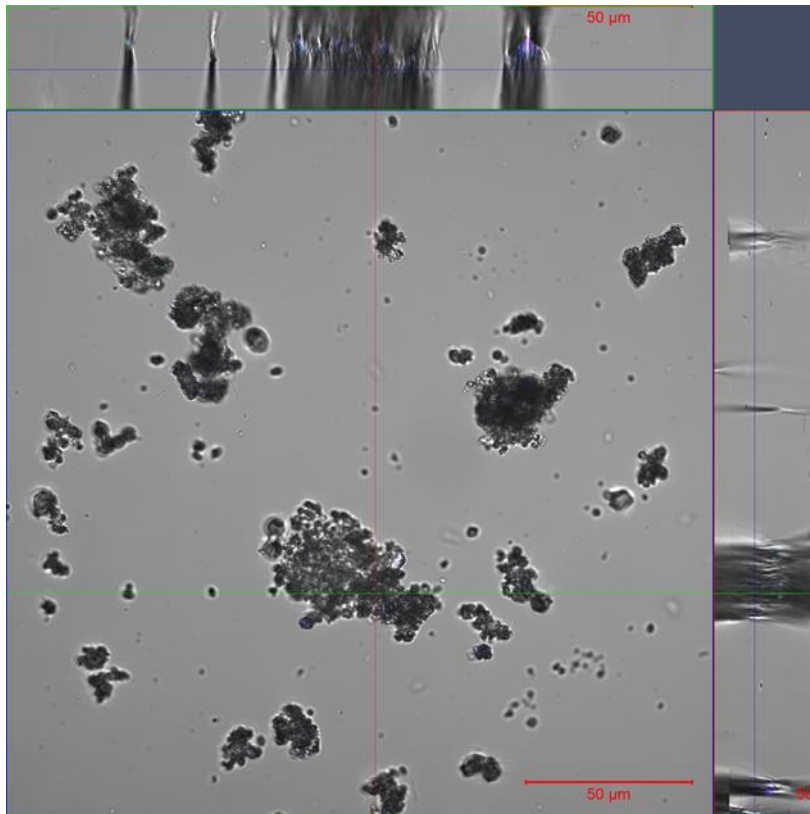


Figure S6.3: Autofluorescence control for FISH imaging of flocs.

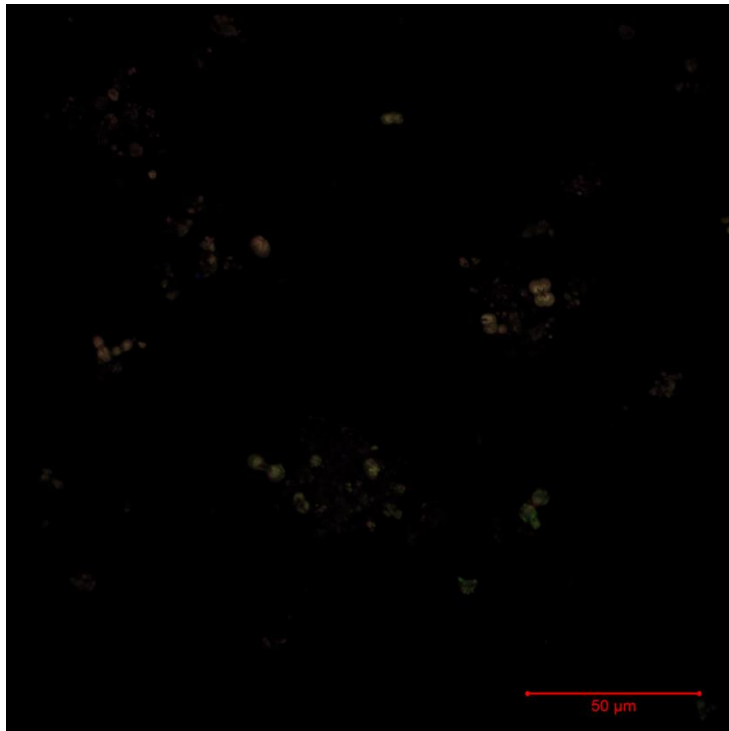


Figure S6.4: Autofluorescence control for 5 colour channel CLSM of flocs (also applicable to fluorescence microscopy imagery).

**Data associated with Chapter 7**

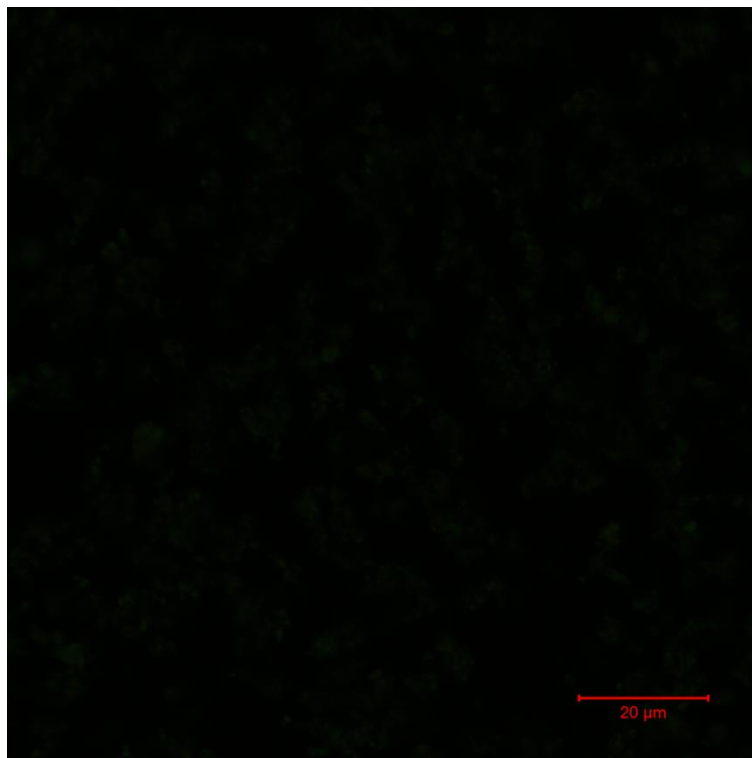


Figure S7.1: CLSM autofluorescence 5 colour channel control of sand biofilm (5 colour).

	$\alpha$ -ISA	$\beta$ -ISA	XISA	Total ISA	CH <sub>4</sub>	(%) CH <sub>4</sub>
mg C	37.4	28.9	3.2	69.5	2.8	4.1

Table S7.1: ISA carbon degraded and CH<sub>4</sub> carbon produced within recirculation system at pH 11.

Day	Microcosm (mg L <sup>-1</sup> )						Control (mg L <sup>-1</sup> )					
	$\alpha$ -ISA	SE	$\beta$ -ISA	SE	XISA	SE	$\alpha$ -ISA	SE	$\beta$ -ISA	SE	XISA	SE
0	186.9	25.1	144.6	21.1	16.0	1.8	706.3	22.3	728.8	34.9	401.2	48.7
2	162.3	0.4	123.3	8.0	7.6	5.9	841.4	1.2	931.4	2.1	526.4	47.1
4	175.4	21.1	159.6	42.8	12.2	5.1	837.0	24.4	899.5	14.3	520.7	111.6
6	114.2	3.9	140.7	27.7	4.9	3.2	875.2	60.7	943.0	46.3	526.7	151.6
8	65.5	45.3	122.4	29.0	2.3	1.4	877.3	74.9	940.5	63.9	534.3	168.0
10	26.9	9.0	79.7	17.6	0.0	0.0	803.1	42.7	886.3	59.6	454.5	66.1
12	5.7	8.1	44.7	6.5	0.0	0.0	684.3	86.8	749.3	104.3	369.9	47.2
14	0.0	0.0	0.0	0.0	0.0	0.0	730.6	72.7	795.9	100.0	429.9	61.5

Table S7.2: ISA concentrations within pH 11 biofilm and control recirculation systems.

TOC/IC	Microcosm (mg L <sup>-1</sup> )				Control (mg L <sup>-1</sup> )			
	TOC	SE	IC	SE	TOC	SE	IC	SE
0	2450.3	235.3	452.7	0.5	1980.5	31.0	26.8	1.6
2	1926.3	218.3	552.2	68.8	1989.7	15.7	27.3	0.9
4	2026.3	164.6	720.1	43.4	1989.2	16.5	26.8	0.1
6	1948.8	220.8	776.7	25.7	1968.3	24.6	26.7	1.0
8	1536.5	15.2	851.9	39.5	2000.8	2.1	26.8	1.7
10	1290.0	8.5	814.8	45.8	1988.5	1.6	27.0	1.2
12	1494.0	13.4	923.0	21.9	2000.0	0.6	28.0	1.3
14	1366.3	205.6	825.8	128.9	1987.9	17.3	29.0	1.4

Table S7.3: TOC and IC concentrations within pH 11 biofilm and control recirculation systems.

	Average acetate (mg L <sup>-1</sup> )	SE
0	39.0	3.2
2	50.8	6.3
4	43.8	1.4
6	46.6	1.9
8	47.0	8.9
10	44.5	7.1
12	41.6	2.7
14	38.5	4.4

Table S7.4: Average acetate concentration in abiotic recirculation control system.

Time	% headspace composition						Time	Volume (L)					Time	mmoles*				
	CO <sub>2</sub>	SE	CH <sub>4</sub>	SE	H <sub>2</sub>	SE		CH <sub>4</sub>	SE	H <sub>2</sub>	SE	CH <sub>4</sub>		SE	H <sub>2</sub>	SE		
0	0.00	0.00	0.00	0.00	0.00	0.02	0	0.0000	0.0000	0.0000	0.0001	0	0.00	0.00	0.00	0.00	0.00	
2	0.00	0.00	0.23	0.05	0.04	0.02	2	0.0012	0.0002	0.0002	0.0001	2	0.05	0.01	0.01	0.01	0.00	
4	0.00	0.00	0.47	0.10	0.16	0.14	4	0.0024	0.0005	0.0008	0.0007	4	0.10	0.02	0.03	0.03	0.03	
6	0.00	0.00	0.69	0.14	0.24	0.21	6	0.0034	0.0007	0.0012	0.0011	6	0.14	0.03	0.05	0.04	0.04	
8	0.00	0.00	0.98	0.22	0.16	0.14	8	0.0049	0.0011	0.0008	0.0007	8	0.20	0.05	0.03	0.03	0.03	
10	0.00	0.00	0.82	0.19	0.10	0.08	10	0.0041	0.0009	0.0005	0.0004	10	0.17	0.04	0.02	0.02	0.02	
12	0.00	0.00	1.15	0.14	0.06	0.07	12	0.0058	0.0007	0.0003	0.0004	12	0.24	0.03	0.01	0.01	0.01	
14	0.00	0.00	1.13	0.11	0.07	0.05	14	0.0057	0.0005	0.0004	0.0003	14	0.23	0.02	0.01	0.01	0.01	

\* Pressure remained at approximately 1 atm due to low volume of gas produced.

Table S7.5: Gas headspace composition of pH 11 biofilm recirculation system. No gas was detected within control systems.

Volume passed through column (mL)	% headspace composition						Volume (L)						mmoles*					
	CH <sub>4</sub>	SE	H <sub>2</sub>	SE	CO <sub>2</sub>	SE	CH <sub>4</sub>	SE	H <sub>2</sub>	SE	CO <sub>2</sub>	SE	CH <sub>4</sub>	SE	H <sub>2</sub>	SE	CO <sub>2</sub>	SE
0	0.00	0.00	0.00	0.00	0	0	0.0000	0.0000	0.0000	0.0000	0	0	0.000	0.000	0.000	0.000	0	0
100	0.05	0.01	0.05	0.02	0	0	0.0003	0.0001	0.0003	0.0001	0	0	0.010	0.002	0.010	0.004	0	0
200	0.07	0.00	0.08	0.04	0	0	0.0003	0.0000	0.0004	0.0002	0	0	0.014	0.001	0.016	0.007	0	0
300	0.09	0.01	0.09	0.02	0	0	0.0004	0.0000	0.0005	0.0001	0	0	0.018	0.001	0.019	0.004	0	0
400	0.09	0.01	0.10	0.05	0	0	0.0005	0.0000	0.0005	0.0003	0	0	0.019	0.002	0.021	0.010	0	0
500	0.09	0.03	0.14	0.05	0	0	0.0005	0.0002	0.0007	0.0003	0	0	0.019	0.006	0.029	0.010	0	0

\* Pressure remained at approximately 1 atm due to low volume of gas produced.

Table S7.6: Gas headspace composition of pH 11 single pass biofilm system.

Day	(% headspace composition)				Volume (L)				mmoles*			
	H <sub>2</sub>	SE	CH <sub>4</sub>	SE	H <sub>2</sub>	SE	CH <sub>4</sub>	SE	H <sub>2</sub>	SE	CH <sub>4</sub>	SE
0	0.00	0.00	0.00	0.00	0.0000	0.0000	0.0000	0.0000	0.0000	0.0000	0.0000	0.0000
2	0.03	0.01	0.02	0.00	0.0002	0.0000	0.0001	0.0000	0.0062	0.0013	0.0031	0.0005
4	0.02	0.00	0.02	0.00	0.0001	0.0000	0.0001	0.0000	0.0042	0.0008	0.0042	0.0000
6	0.06	0.01	0.03	0.01	0.0003	0.0000	0.0002	0.0000	0.0125	0.0012	0.0062	0.0015
8	0.07	0.02	0.04	0.00	0.0004	0.0001	0.0002	0.0000	0.0146	0.0048	0.0083	0.0000
10	0.09	0.01	0.05	0.00	0.0005	0.0001	0.0002	0.0000	0.0187	0.0029	0.0094	0.0009
12	0.09	0.05	0.05	0.00	0.0004	0.0002	0.0002	0.0000	0.0177	0.0100	0.0094	0.0009
14	0.11	0.03	0.06	0.00	0.0006	0.0002	0.0003	0.0000	0.0229	0.0065	0.0114	0.0010

\* Pressure remained at approximately 1 atm due to low volume of gas produced.

Table S7.7: Gas headspace composition of pH 11 liquid only component.

Volume passed (mL)	Concentrations (mg L <sup>-1</sup> )						Decrease (mg L <sup>-1</sup> )			% Decrease		
	$\alpha$ -ISA	SE	$\beta$ -ISA	SE	XISA	SE	$\alpha$ -ISA	$\beta$ -ISA	XISA	$\alpha$ -ISA	$\beta$ -ISA	XISA
0	310.4	12.0	270.4	12.5	30.9	3.1	0.0	0.0	0.0	0.0	0.0	0.0
100	209.0	3.5	163.3	13.5	13.5	4.1	101.4	107.0	17.4	32.7	39.6	56.3
200	193.7	19.4	145.3	14.6	12.4	0.2	116.7	125.1	18.5	37.6	46.3	60.0
300	214.9	18.3	165.1	9.4	17.4	2.2	95.5	105.3	13.5	30.8	39.0	43.6
400	214.7	16.5	160.5	13.0	13.7	0.6	95.7	109.9	17.2	30.8	40.7	55.6
500	218.9	6.3	168.3	4.6	16.9	2.3	91.5	102.1	14.1	29.5	37.8	45.5
Average							100.2	109.9	16.1	32.3	40.6	52.2
SE							4.4	4.0	1.0	1.4	1.5	3.2

Table S7.8: ISA concentrations and associated reductions through single pass biofilm system at pH 11.

Volume passed (mL)	Average acetate (mg L <sup>-1</sup> )	SE
0	0.0	0.0
100	34.1	9.1
200	29.2	5.9
300	37.0	3.4
400	34.2	4.4
500	39.8	4.2

Table S7.9: Acetate production within single pass biofilm system at pH 11.

Day	(mg L <sup>-1</sup> )					
	$\alpha$ -ISA	SE	$\beta$ -ISA	SE	XISA	SE
0	270.7	24.9	253.8	23.7	19.6	1.7
2	220.9	28.2	199.2	29.3	14.9	1.8
4	201.0	17.6	168.8	13.5	12.8	0.3
6	253.0	5.1	193.3	1.6	14.6	1.1
8	257.8	13.4	152.0	6.8	14.6	0.2
10	211.9	11.7	116.9	4.8	12.1	0.3
12	209.1	26.1	84.5	8.1	10.1	1.2
14	231.8	10.7	114.7	0.3	12.6	1.2

Table S7.10: ISA concentration levels within liquid only component of pH 11 sand biofilm circulation system.

	Total ISA degraded in biofilm (mg)*					
	Sample					
	$\alpha$ -ISA	SE	$\beta$ -ISA	SE	XISA	SE
pH 11	38.8	3.7	45.5	4.1	19.0	0.8
pH 12	30.8	6.6	51.3	3.8	35.0	2.4
pH 13	1.8	0.6	8.1	5.8	3.6	2.5

\*Calculated taking into account ISA removed via control system.

Table S7.11: ISA degraded by biofilm units over 14 day testing period at different pH values.

Volume passed through system (mL)	pH 11 sand column biofilm outlet ISA concentration (mg L <sup>-1</sup> )											
	Sample		Control		Sample		Control		Sample		Control	
	$\alpha$ -ISA	SE	$\alpha$ -ISA	SE	$\beta$ -ISA	SE	$\beta$ -ISA	SE	XISA	SE	XISA	SE
0	98.7	3.4	98.7	3.4	92.0	3.2	92.0	3.2	56.7	3.1	56.7	3.1
100	56.1	17.0	95.9	3.3	50.7	15.4	95.6	4.5	41.8	12.3	45.3	2.7
200	47.8	4.1	117.9	5.0	24.9	1.9	122.8	7.3	25.4	2.4	46.4	9.3
300	21.2	1.2	66.8	0.7	12.8	0.7	60.2	7.2	15.0	0.8	36.1	4.9
400	28.4	1.9	102.7	4.2	15.8	1.0	90.3	21.5	15.1	1.0	24.4	13.0
500	27.4	2.8	88.3	0.6	16.5	1.5	74.6	2.0	18.1	1.6	47.2	7.6
600	38.3	1.5	75.9	0.2	25.9	0.6	70.8	6.3	19.1	0.4	47.3	3.0
700	57.1	0.8	76.0	6.3	39.4	2.3	64.0	6.1	31.4	1.3	45.3	6.1
800	43.2	0.4	99.9	7.5	29.7	1.3	84.0	7.8	25.2	1.0	63.0	11.0
900	52.7	2.8	98.5	7.9	32.4	1.5	83.2	7.6	29.5	1.4	61.2	8.6
1000	57.1	2.6	100.5	8.7	35.3	1.4	84.6	8.4	32.0	1.3	62.3	9.3

Table S7.12 : Concentrations of ISA after taken after the passage of each 100 mL over 14 day period within both biotic and abiotic systems at pH 11.

Volume passed through system (mL)	pH 12 sand column biofilm outlet ISA concentration (mg L <sup>-1</sup> )											
	Sample		Control		Sample		Control		Sample		Control	
	$\alpha$ -ISA	SE	$\alpha$ -ISA	SE	$\beta$ -ISA	SE	$\beta$ -ISA	SE	XISA	SE	XISA	SE
0.0	109.5	0.2	109.5	0.2	114.7	1.0	114.7	1.0	88.5	0.6	88.5	0.6
100.0	93.7	6.6	140.0	2.4	73.7	7.9	153.9	0.9	62.9	0.3	100.5	0.0
200.0	71.1	12.5	137.6	0.1	58.4	10.6	151.4	3.1	45.1	9.2	91.1	2.5
300.0	69.2	22.0	121.3	0.9	57.3	19.2	130.5	2.4	40.2	11.0	85.6	1.6
400.0	66.8	4.2	129.9	2.0	35.3	3.4	144.1	5.8	48.5	0.0	81.1	6.0
500.0	80.7	14.6	123.1	0.5	67.5	14.2	134.2	6.8	42.2	0.4	77.8	11.1
600.0	58.1	17.6	96.6	2.6	50.0	16.6	103.5	6.7	37.1	4.4	68.5	5.1
700.0	74.5	4.2	107.9	0.0	64.8	5.8	113.0	4.7	55.0	13.6	77.9	6.7
800.0	68.6	18.8	100.3	1.0	54.4	17.0	119.0	2.7	44.7	6.7	62.4	5.7
900.0	83.2	4.6	108.9	2.1	23.8	1.3	126.7	3.7	47.0	4.8	70.7	4.1
1000.0	59.0	9.4	107.4	2.9	42.6	8.3	110.3	6.5	43.6	0.1	86.8	4.9

Table S7.13 : Concentrations of ISA after taken after the passage of each 100 mL over 14 day period within both biotic and abiotic systems at pH 12.

Volume passed through system (mL)	pH 13 sand column biofilm outlet ISA concentration (mg L <sup>-1</sup> )											
	Sample		Control		Sample		Control		Sample		Control	
	$\alpha$ -ISA	SE	$\alpha$ -ISA	SE	$\beta$ -ISA	SE	$\beta$ -ISA	SE	XISA	SE	XISA	SE
0	99.8	0.6	99.8	0.6	106.8	2.3	106.8	2.3	103.3	4.6	103.3	4.6
100	101.7	20.7	113.6	9.0	106.7	25.1	112.5	3.9	96.6	19.8	111.5	2.8
200	132.3	29.2	97.6	1.2	152.8	40.9	103.2	0.1	127.2	28.4	99.0	1.9
300	160.0	32.3	126.2	3.3	153.6	35.2	140.7	1.3	119.7	20.3	116.0	0.3
400	125.3	19.2	115.3	2.3	91.8	16.4	121.9	0.8	102.4	13.8	113.2	2.0
500	150.1	25.4	125.5	3.6	151.2	29.5	135.4	1.4	123.1	19.7	108.1	2.8
600	117.4	20.8	105.2	2.7	124.1	24.8	110.8	1.5	110.4	19.6	98.1	0.9
700	116.4	23.6	108.0	3.8	150.9	34.9	114.3	2.1	123.2	25.2	101.2	1.1
800	121.8	17.1	114.8	6.7	127.6	19.9	119.5	12.3	107.8	19.5	129.1	3.0
900	64.9	11.6	134.2	6.8	65.5	13.1	143.8	4.8	63.1	11.0	120.6	5.4
1000	81.5	18.4	113.7	6.4	83.6	20.1	121.5	5.0	82.4	20.3	113.5	1.8

Table S7.14 : Concentrations of ISA taken after the passage of each 100 mL over 14 day period within both biotic and abiotic systems at pH 13.

Volume passed (mL)	Average acetate (mg L <sup>-1</sup> )	SE
0	0.00	0.00
100	0.00	0.00
200	0.31	0.01
300	0.62	0.03
400	0.42	0.00
500	0.42	0.01
600	0.51	0.08
700	0.46	0.00
800	0.44	0.01
900	0.43	0.05
1000	0.40	0.01

Table S7.15: Average acetate produced within pH 11 flow through system. No acetate was detected with the pH 12 or pH 13 biotic flow through systems and no acetate was detected within the abiotic control systems at all pH values tested.

pH 11												
Volume passed (mL)	% Headspace composition				Volume (L)				mmoles			
	CH <sub>4</sub>	SE	H <sub>2</sub>	SE	CH <sub>4</sub>	SE	H <sub>2</sub>	SE	CH <sub>4</sub>	SE	H <sub>2</sub>	SE
0	1.0E-02	0.0E+00	0.0E+00	0.0E+00	0.0E+00	0.0E+00	0.0E+00	0.0E+00	0.0E+00	0.0E+00	0.0E+00	0.0E+00
100	-1.0E-02	1.0E-02	1.0E-01	0.0E+00	0.0E+00	0.0E+00	6.5E-04	0.0E+00	0.0E+00	0.0E+00	0.0E+00	2.7E-05
200	1.0E-02	0.0E+00	1.5E-01	5.0E-03	0.0E+00	0.0E+00	9.4E-04	3.2E-05	0.0E+00	0.0E+00	0.0E+00	3.9E-05
300	2.0E-02	0.0E+00	1.7E-01	5.0E-03	6.5E-05	0.0E+00	1.1E-03	3.3E-05	2.7E-06	0.0E+00	0.0E+00	4.5E-05
400	5.5E-02	5.0E-03	2.2E-01	4.0E-02	2.9E-04	2.7E-05	1.4E-03	2.6E-04	1.2E-05	5.5E-08	6.0E-05	2.8E-06
500	9.5E-02	1.5E-02	2.4E-01	3.5E-02	5.5E-04	8.7E-05	1.5E-03	2.3E-04	2.3E-05	4.0E-07	6.4E-05	2.6E-06
600	9.5E-02	5.0E-03	2.6E-01	3.0E-02	5.5E-04	2.9E-05	1.7E-03	2.0E-04	2.3E-05	1.2E-07	7.0E-05	2.4E-06
700	1.0E-01	0.0E+00	2.6E-01	1.5E-02	5.9E-04	0.0E+00	1.7E-03	9.8E-05	2.4E-05	0.0E+00	6.9E-05	1.1E-06
800	9.0E-02	3.0E-02	2.7E-01	5.0E-03	5.2E-04	1.7E-04	1.7E-03	3.3E-05	2.2E-05	4.3E-07	7.2E-05	3.6E-07
900	1.1E-01	1.0E-02	2.9E-01	5.0E-03	6.5E-04	5.9E-05	1.9E-03	3.2E-05	2.7E-05	2.5E-07	7.7E-05	3.9E-07
1000	1.7E-01	4.2E-02	3.1E-01	5.0E-03	1.0E-03	2.5E-04	2.0E-03	3.3E-05	4.4E-05	1.4E-06	8.3E-05	4.1E-07
pH 12												
0	0.0E+00	0.0E+00	0.0E+00	0.0E+00	0.0E+00	0.0E+00	0.0E+00	0.0E+00	0.0E+00	0.0E+00	0.0E+00	0.0E+00
100	0.0E+00	0.0E+00	0.0E+00	0.0E+00	0.0E+00	0.0E+00	0.0E+00	0.0E+00	0.0E+00	0.0E+00	0.0E+00	0.0E+00
200	0.0E+00	0.0E+00	0.0E+00	0.0E+00	0.0E+00	0.0E+00	0.0E+00	0.0E+00	0.0E+00	0.0E+00	0.0E+00	0.0E+00
300	0.0E+00	0.0E+00	1.0E-02	4.4E-18	0.0E+00	0.0E+00	6.5E-05	2.9E-20	0.0E+00	0.0E+00	2.7E-06	1.2E-21
400	1.0E-02	1.0E-02	3.0E-02	2.0E-02	6.5E-05	6.5E-05	2.0E-04	1.3E-04	2.7E-06	2.7E-06	8.1E-06	5.4E-06
500	5.0E-03	5.0E-03	4.0E-02	2.0E-02	3.3E-05	3.3E-05	2.6E-04	1.3E-04	1.4E-06	1.4E-06	1.1E-05	5.4E-06
600	2.0E-02	8.8E-18	3.5E-02	1.5E-02	1.3E-04	5.7E-20	2.3E-04	9.7E-05	5.4E-06	2.4E-21	9.5E-06	4.1E-06
700	3.0E-02	1.0E-02	3.0E-02	1.4E-17	2.0E-04	6.5E-05	2.0E-04	9.0E-20	8.1E-06	2.7E-06	8.1E-06	3.8E-21
800	3.5E-02	5.0E-03	2.5E-02	5.0E-03	2.3E-04	3.3E-05	1.6E-04	3.3E-05	9.5E-06	1.4E-06	6.8E-06	1.4E-06
900	6.0E-02	1.0E-02	5.5E-02	1.5E-02	3.9E-04	6.5E-05	3.6E-04	9.7E-05	1.6E-05	2.7E-06	1.5E-05	4.1E-06
1000	8.5E-02	5.0E-03	4.0E-02	1.1E-17	5.5E-04	3.3E-05	2.6E-04	7.1E-20	2.3E-05	1.4E-06	1.1E-05	3.0E-21

Table S7.16: Average gas headspace compositions of pH 11 and pH 12 biofilm systems. No gas was detected within the pH 13 biofilm systems and all abiotic control systems.

Volume passed (mL)	pH 11 control				pH 11				pH 12 control				pH 12				pH 13 control				pH 13			
	Sand column outlet	SE	NRVB column outlet	SE	Sand column outlet	SE	NRVB column outlet	SE	Sand column outlet	SE	NRVB column outlet	SE	Sand column outlet	SE	NRVB column outlet	SE	Sand column outlet	SE	NRVB column outlet	SE	Sand column outlet	SE	NRVB column outlet	SE
0	11.1	0.0			11.0	0.0			12.0	0.0			12.0	0.0			13.0	0.0	>14.00	0.0	13.0	0.0	>14.00	0
100	11.1	0.0	12.5	0.0	10.0	0.0	12.8	0.0	12.0	0.0	12.8	0.0	11.3	0.0	13.8	0.0	13.0	0.0	>14.00	0.0	12.6	0.0	>14.00	0
200	11.1	0.0	12.8	0.0	9.9	0.0	12.9	0.0	12.0	0.0	12.9	0.0	11.5	0.0	13.7	0.0	13.0	0.0	>14.00	0.0	12.5	0.0	>14.00	0
300	11.1	0.0	13.0	0.0	10.0	0.0	13.1	0.0	12.0	0.0	13.0	0.0	11.4	0.0	13.5	0.0	13.0	0.0	>14.00	0.0	12.5	0.0	>14.00	0
400	11.1	0.0	13.0	0.0	10.0	0.0	13.1	0.0	12.0	0.0	13.1	0.0	11.4	0.0	13.5	0.0	13.0	0.0	>14.00	0.0	12.5	0.0	>14.00	0
500	11.1	0.0	13.0	0.0	10.0	0.0	13.0	0.0	12.0	0.0	13.1	0.0	11.4	0.0	13.4	0.0	13.0	0.0	>14.00	0.0	12.5	0.1	>14.00	0
600	11.1	0.0	13.1	0.0	10.0	0.0	12.8	0.0	12.0	0.0	13.2	0.0	11.5	0.0	13.4	0.0	13.0	0.0	>14.00	0.0	12.5	0.0	>14.00	0
700	11.1	0.0	13.1	0.0	10.1	0.0	12.8	0.0	12.0	0.0	13.2	0.0	11.4	0.0	13.4	0.0	13.0	0.0	>14.00	0.0	12.7	0.1	>14.00	0
800	11.1	0.0	13.2	0.0	10.0	0.0	12.8	0.0	12.0	0.0	13.2	0.0	11.4	0.0	13.4	0.0	13.0	0.0	>14.00	0.0	12.4	0.1	>14.00	0
900	11.1	0.0	13.2	0.0	10.0	0.0	12.6	0.0	12.0	0.0	13.4	0.2	11.3	0.0	13.3	0.0	13.0	0.0	>14.00	0.0	12.5	0.0	>14.00	0
1000	11.1	0.0	13.2	0.0	10.1	0.0	12.6	0.0	12.0	0.0	13.4	0.0	11.4	0.0	13.2	0.0	13.0	0.0	>14.00	0.0	12.6	0.0	>14.00	0

Table S7.17: pH values of media at sand biofilm outlet and NRVB column outlet taken after the passage of each 100 mL over 14 day period within both biotic and abiotic systems.

pH 11		pH 12		pH 13		Control pH			
Distance (µm)	pH	Distance (µm)	pH	Distance (µm)	pH	Distance (µm)	11	12	13
0	11.1	0	11.8	0	13.0	0	11.0	12.0	13.0
20	11.1	10	11.8	10	12.8	100	11.0	12.0	13.0
30	10.8	20	11.6	20	12.7	200	11.0	12.0	13.0
40	10.3	30	11.1	30	12.2	300	11.0	12.0	13.0
60	10.2	40	10.8	40	12.2	400	11.0	12.0	13.0
80	9.9	50	10.5	50	12.2	500	11.0	12.0	13.0
100	9.5	60	10.4	60	12.2				
120	9.6	70	10.1	70	12.2				
140	9.6	80	10.2	80	12.2				
160	9.6	90	10.3	90	12.2				
180	9.7	100	10.4	100	12.2				
200	9.7	110	10.4	110	12.2				
220	9.5	120	10.4	120	12.2				
240	9.5	130	10.4	130	12.2				
260	9.5	140	10.4	140	12.2				
		150	10.4	150	12.2				
		160	10.4	160	12.2				
		170	10.4	170	12.2				
		180	10.5	180	12.2				
		190	10.5	190	12.2				
		200	10.4	200	12.0				

Table S7.18: Micro-electrode pH profiles through biofilm and related agar controls.

	Average ATP concentration (RFU)					
	pH 11	SE	pH 12	SE	pH 13	SE
Before extraction	1.22E+05	4.48E+03	8.11E+04	2.12E+03	9.26E+03	2.40E+02
After extraction	1.26E+05	6.75E+02	8.10E+04	1.22E+02	9.66E+03	4.80E+01

Table S7.19: ATP concentrations of biofilm materials before and after EPS extraction procedures.

Class	No. of reads			% Distribution		
	pH 11	pH 12	pH 13	pH 11	pH 12	pH 13
Methanobacteria	47	303	243	0.3	1.4	2.1
Corynebacteriales	2905	5989	4691	16.6	28.2	40.3
Bacteroidia	407	12	0	2.3	0.1	0.0
Cytophagia	2478	101	523	14.2	0.5	4.5
Bacilli	3890	3815	2588	22.3	17.9	22.2
Clostridia	1978	7114	3080	11.3	33.4	26.4
Erysipelotrichi	248	1319	33	1.4	6.2	0.3
Alphaproteobacteria	2835	1324	197	16.2	6.2	1.7
Betaproteobacteria	5	1	6	0.0	0.0	0.1
Gammaproteobacteria	2677	1296	284	15.3	6.1	2.4

Table S7.20: Class level distribution of 16S rRNA gene community analysis of biofilms at different pH values.

Family	No. of reads			% distribution		
	pH 11	pH 12	pH 13	pH 11	pH 12	pH 13
Methanobacteriaceae	47	303	243	0.3	1.4	2.1
Dietzia	2767	5903	4661	15.8	27.7	40.0
ML635J-40_aquatic_group	407	11	0	2.3	0.1	0.0
Cyclobacteriaceae	2478	101	523	14.2	0.5	4.5
Bacillaceae	3890	3814	2588	22.3	17.9	22.2
Clostridiaceae	244	694	561	1.4	3.3	4.8
Family_XIV_Incertae_Sedis	404	2374	2384	2.3	11.2	20.5
Family_XI_Incertae_Sedis	1324	4046	135	7.6	19.0	1.2
Erysipelotrichaceae	248	1319	33	1.4	6.2	0.3
Brucellaceae	50	317	45	0.3	1.5	0.4
Phyllobacteriaceae	649	766	28	3.7	3.6	0.2
Rhodobacteraceae	2134	241	124	12.2	1.1	1.1
Alteromonadaceae	2667	1296	284	15.3	6.1	2.4
Below 1%	161	89	36	0.9	0.4	0.3

Table S7.21: Family level distribution of 16S rRNA gene community analysis of biofilms at different pH values.

	Biotic						Abiotic control			
	Biofilm	SE	Sand biofilm outlet	SE	NRVB outlet	SE	Sand outlet	SE	NRVB outlet	SE
pH 11	9259.5	239.5	2197.0	73.0	57.0	4.0	47.5	0.5	39.0	2.0
pH 12	81065.5	2115.5	1830.0	2.0	24.0	1.5	31.5	0.5	27.5	0.5
pH 13	121921.0	4483.0	465.2	2.7	51.0	3.0	27.0	1.0	21.0	1.0

Table S7.22: ATP readings for biofilm, liquid outlets of sand biofilm cell and NRVB cell and associated abiotic controls.

pH 11		pH 12		pH 13	
Distance ( $\mu\text{m}$ )	mV	Distance ( $\mu\text{m}$ )	mV	Distance ( $\mu\text{m}$ )	mV
0	-96.1	0	-3.4	0	-23.9
10	-185.9	10	-66.0	20	-29.9
20	-281.7	20	-37.6	40	-34.7
40	-313.0	30	-104.5	60	-39.1
60	-323.0	40	-113.8	80	-47.2
80	-326.9	50	-120.6	100	-100.4
100	-332.3	60	-122.6	120	-112.7
120	-337.5	70	-131.5	140	-108.0
140	-345.8	80	-151.4	160	-112.0
160	-342.8	90	-154.6	180	-153.9
180	-340.9	100	-160.4	200	-170.8
200	-353.5	120	-175.7	220	-178.6
		140	-182.1	240	-183.5
		160	-188.5		
		180	-196.0		
		200	-192.6		

Table S7.23: Micro-electrode redox profiling through biofilm. Probes were tested using pH 4 and pH 7 buffer saturated with quinhydrone in accordance with manufacturer's instructions.

Sample (mg)						Control (mg)					
$\alpha$ -ISA	SE	$\beta$ -ISA	SE	XISA	SE	$\alpha$ -ISA	SE	$\beta$ -ISA	SE	XISA	SE
39.7	3.3	27.9	2.7	21.4	2.1	52.2	3.4	49.6	5.8	18.5	4.1
9.7	5.2	11.2	6.4	16.2	12.2	98.2	6.7	96.5	10.3	65.3	10.1
96.4	22.2	98.6	25.8	76.6	19.1	84.5	10.0	93.2	7.6	65.3	4.8

Table S7.24: Total ISA bound by NRVB under both biotic and abiotic conditions at different pH values.

Volume passed through system (mL)	pH 11 NRVB column biofilm outlet ( $\text{mg L}^{-1}$ )											
	Sample		Control		Sample		Control		Sample		Control	
	$\alpha$ -ISA	SE	$\alpha$ -ISA	SE	$\beta$ -ISA	SE	$\beta$ -ISA	SE	XISA	SE	XISA	SE
100	4.9	0.4	41.2	0.4	17.7	2.7	32.3	1.0	1.1	0.0	33.8	2.3
200	6.0	0.1	25.6	1.9	0.7	0.1	20.7	0.8	0.6	0.4	27.1	2.9
300	1.8	0.2	26.2	1.5	0.8	0.0	21.2	0.6	0.4	0.0	26.4	2.2
400	0.8	0.1	25.5	1.0	0.1	0.0	21.0	0.5	0.4	0.2	27.4	2.2
500	0.9	0.1	13.3	0.5	0.1	0.0	10.8	0.4	0.4	0.1	13.5	0.7
600	4.6	0.4	19.0	1.2	0.2	0.0	15.5	1.4	13.2	1.2	19.6	1.3
700	3.6	0.2	34.3	0.1	0.7	0.1	27.1	0.6	8.4	0.6	29.4	1.3
800	2.5	0.2	31.8	0.3	0.6	0.0	25.7	0.5	1.7	0.1	29.0	1.4
900	3.7	0.4	37.7	4.0	0.1	0.0	31.6	3.4	6.2	0.8	26.8	3.7
1000	3.6	0.5	41.1	0.5	0.5	0.1	36.0	0.4	6.0	1.1	33.9	0.1

Table S7.28: Concentrations of ISA taken after the passage of each 100 mL over 14 day period through NRVB column under both biotic and abiotic systems at pH 11.

pH 12 NRVB column biofilm outlet (mg L <sup>-1</sup> )												
Volume passed through system (mL)	Sample		Control		Sample		Control		Sample		Control	
	$\alpha$ -ISA	SE	$\alpha$ -ISA	SE	$\beta$ -ISA	SE	$\beta$ -ISA	SE	XISA	SE	XISA	SE
100	48.7	6.6	6.9	1.8	112.1	6.3	8.4	2.1	23.7	14.3	10.4	2.2
200	77.5	12.5	27.7	7.1	31.2	0.4	31.6	7.5	34.9	20.6	40.4	8.2
300	69.4	22.0	17.8	4.7	59.1	1.1	23.4	5.7	31.3	17.4	32.6	7.3
400	63.0	4.2	14.3	4.0	52.4	0.7	18.8	4.8	28.6	16.2	25.9	6.4
500	64.1	14.6	8.8	2.5	47.2	1.0	9.7	2.5	27.1	16.1	11.2	2.9
600	62.6	17.6	3.5	0.9	43.2	3.4	2.6	1.4	26.9	15.9	9.0	2.6
700	73.9	4.2	5.3	2.0	45.1	5.4	4.6	2.4	29.3	16.4	13.9	1.0
800	83.0	18.8	11.6	3.4	55.6	5.4	13.9	3.6	32.0	10.7	23.4	6.7
900	100.7	4.6	10.8	2.8	62.1	9.9	12.6	2.8	38.2	8.6	15.7	3.8
1000	113.5	9.4	15.7	3.8	74.4	17.0	19.6	4.1	42.4	8.9	28.4	5.9

Table S7.29: Concentrations of ISA taken after the passage of each 100 mL over 14 day period through NRVB column under both biotic and abiotic systems at pH 12.

pH 13 NRVB column biofilm outlet (mg L <sup>-1</sup> )												
Volume passed through system (mL)	Sample		Control		Sample		Control		Sample		Control	
	$\alpha$ -ISA	SE	$\alpha$ -ISA	SE	$\beta$ -ISA	SE	$\beta$ -ISA	SE	XISA	SE	XISA	SE
100	40.2	1.1	6.8	0.4	136.7	32.6	8.3	0.6	50.0	0.7	15.0	0.7
200	63.9	0.0	5.0	0.4	40.4	0.4	5.9	0.4	77.0	3.2	9.1	0.5
300	11.8	0.2	3.2	0.3	66.2	1.6	3.6	0.3	18.5	0.5	5.1	0.3
400	50.5	1.8	10.6	0.8	12.9	0.1	13.4	1.1	60.2	0.6	20.7	1.1
500	7.1	0.3	12.8	1.2	52.5	0.5	15.4	1.6	13.1	0.2	21.1	1.4
600	10.3	0.3	11.5	0.8	8.3	0.2	14.0	1.0	17.8	0.1	18.9	0.7
700	7.6	0.2	25.7	2.1	11.9	0.1	33.1	2.7	14.1	0.2	44.5	2.5
800	7.5	0.2	48.1	4.4	9.0	0.0	60.1	5.8	15.8	0.0	86.7	4.5
900	3.0	0.2	54.8	3.8	9.3	0.2	72.2	6.5	7.1	0.4	112.4	2.6
1000	5.3	0.5	36.8	2.3	3.7	0.2	49.8	4.0	16.2	2.5	76.7	1.4

Table S7.30: Concentrations of ISA taken after the passage of each 100 mL over 14 day period through NRVB column under both biotic and abiotic systems at pH 13.

Volume passed (mL)	pH 11 (mg L <sup>-1</sup> )				pH 11 control (mg L <sup>-1</sup> )				pH 12 (mg L <sup>-1</sup> )				pH 12 control (mg L <sup>-1</sup> )				pH 13 (mg L <sup>-1</sup> )				pH 13 control (mg L <sup>-1</sup> )			
	TOC	SE	IC	SE	TOC	SE	IC	SE	TOC	SE	IC	SE	TOC	SE	IC	SE	TOC	SE	IC	SE	TOC	SE	IC	SE
0	576.5	26.0	0.0	0.0	434.8	5.6	0.0	0.0	479.0	6.8	0.0	0.0	470.7	0.5	0.0	0.0	359.2	2.0	0.0	0.0	412.7	0.5	0.0	0.0
100	505.9	5.7	72.1	72.1	267.7	3.8	33.2	0.1	209.9	5.7	59.3	0.9	88.7	11.4	0.0	0.0	297.1	3.1	0.0	0.0	149.5	11.4	0.0	0.0
200	344.2	32.4	106.8	106.8	285.1	3.0	33.2	0.6	280.0	0.1	69.0	0.0	164.6	4.9	0.0	0.0	315.9	1.5	0.0	0.0	135.1	4.9	0.0	0.0
300	366.5	3.6	79.6	79.6	183.3	26.2	34.0	0.8	288.3	1.4	72.7	1.7	153.4	2.9	0.0	0.0	222.2	24.3	0.0	0.0	141.9	2.9	0.0	0.0
400	372.5	6.9	63.2	63.2	219.2	3.5	32.2	0.2	273.1	2.1	70.0	0.1	166.7	2.2	0.0	0.0	271.1	0.8	0.0	0.0	171.4	2.2	0.0	0.0
500	237.6	16.9	74.0	74.0	259.7	8.1	32.9	0.9	230.3	0.3	64.3	1.1	128.9	0.7	0.0	0.0	165.4	1.1	0.0	0.0	215.7	0.7	0.0	0.0
600	226.6	8.1	44.3	44.3	143.1	17.9	29.3	5.0	272.7	1.5	85.2	0.1	97.0	3.5	0.0	0.0	108.5	8.5	0.0	0.0	225.7	3.5	0.0	0.0
700	373.8	3.1	49.7	49.7	179.8	5.5	40.1	1.9	292.4	1.8	100.3	0.3	118.0	17.6	0.0	0.0	168.4	1.6	0.0	0.0	269.2	17.6	0.0	0.0
800	382.7	1.7	77.6	77.6	293.6	10.2	41.6	1.5	247.3	7.0	78.1	2.1	291.7	159.4	0.0	0.0	202.3	0.8	0.0	0.0	263.4	159.4	0.0	0.0
900	382.9	1.5	87.6	87.6	293.2	11.4	36.5	1.3	317.6	21.2	80.6	0.4	443.7	4.2	0.0	0.0	104.6	0.1	0.0	0.0	248.3	4.2	0.0	0.0
1000	425.9	2.4	85.9	85.9	318.7	15.1	45.0	2.8	281.9	6.9	102.6	0.2	206.8	0.7	0.0	0.0	67.6	8.0	0.0	0.0	91.4	0.7	0.0	0.0

Table S7.31: TOC and IC measurements of single pass biofilm systems at different pH values.

	Total TOC removed (mg)	SE	Total IC increase (mg)	SE
pH 11	214.7	8.2	74.1	1.9
pH 11 control	190.5	10.5	35.8	1.5
pH 12	209.6	4.8	78.2	0.7
pH 12 control	284.8	20.7	0.0	0.0
pH 13	166.9	5.0	0.0	0.0
pH 13 control	221.5	3.0	0.0	0.0

Table S7.32 Total TOC removed and IC increase within single pass biofilm systems at different pH values.

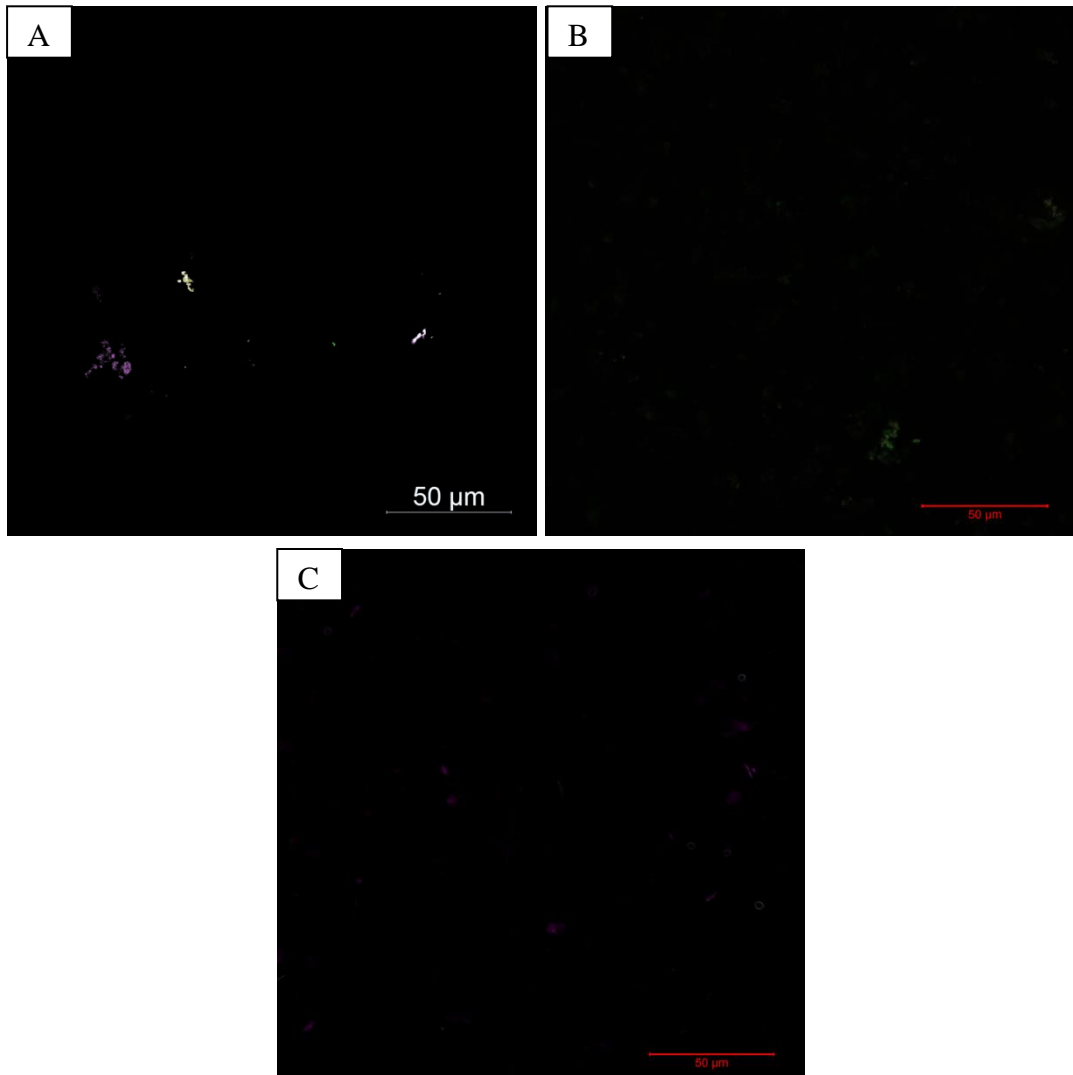


Figure S7.2: CLSM autofluorescence 5 colour channel controls of NRVB [A], graphite [B] and steel surfaces colonised with biofilm [C].

## Data associated with Chapter 8

Day	Microcosm (mg L <sup>-1</sup> )						Control (mg L <sup>-1</sup> )					
	$\alpha$ -ISA	SE	$\beta$ -ISA	SE	XISA	SE	$\alpha$ -ISA	SE	$\beta$ -ISA	SE	XISA	SE
0	671.5	35.7	529.1	16.1	229.2	0.5	272.8	50.4	214.9	43.4	64.5	0.4
2	672.0	35.0	497.4	19.7	231.1	25.9	338.6	2.3	267.1	3.8	63.2	2.9
4	633.6	11.1	489.4	48.1	195.8	33.0	343.9	6.7	270.5	7.4	65.9	2.5
6	558.9	63.2	439.6	20.9	171.4	40.3	302.4	44.3	238.2	33.6	64.7	3.8
8	586.7	53.3	440.9	10.0	184.9	43.8	345.0	44.8	278.6	43.1	67.0	3.0
10	541.4	57.6	418.1	11.5	159.8	29.8	332.2	51.6	267.6	50.5	59.2	6.3
12	562.4	33.0	423.3	21.3	167.0	25.9	319.7	14.3	255.9	4.2	68.3	1.4
14	499.1	68.7	382.0	28.8	152.4	38.8	319.0	9.2	255.6	0.1	76.9	12.9

Table S8.1: ISA concentrations within pH 11 sulphate reducing liquid microcosm and associated controls.

Day	Acetate (mg L <sup>-1</sup> )	SE	Control acetate (mg L <sup>-1</sup> )	SE	Hydrogen gas (mmoles)*	SE
0	90.8	8.4	19.5	0.1	0.0	0.0
2	123.1	0.5	18.9	0.4	0.2	0.1
4	100.0	13.9	18.5	0.9	0.3	0.2
6	115.0	1.1	20.0	0.4	0.6	0.2
8	108.7	24.7	18.9	0.0	0.7	0.2
10	117.6	17.4	19.0	0.2	0.5	0.0
12	123.2	0.2	18.2	1.4	0.7	0.1
14	129.4	2.5	19.5	0.6	0.7	0.0

\*Pressure remained at approximately 1 atm due to low volume of gas produced.

Table S8.2: Acetate concentrations within pH 11 sulphate reducing liquid microcosm and associated controls. Hydrogen headspace amount within pH 11 sulphate reducing microcosm. Controls showed no gas generation.

Day	Microcosm (mg L <sup>-1</sup> )				Control (mg L <sup>-1</sup> )			
	TOC	SE	IC	SE	TOC	SE	IC	SE
0	339.5	121.8	11.6	4.1	392.0	1.0	4.5	0.3
2	337.0	118.8	11.9	3.5	388.0	7.0	4.6	0.3
4	318.5	111.6	12.3	3.0	387.0	3.0	4.7	0.4
6	312.9	109.5	13.0	2.5	390.0	2.0	4.4	0.2
8	305.5	106.1	13.6	2.1	382.5	2.5	4.5	0.5
10	301.5	104.1	15.3	1.9	380.0	5.0	4.2	0.3
12	287.5	98.7	15.4	1.3	394.5	2.5	4.9	0.2
14	277.0	94.1	16.0	0.8	388.5	4.5	4.7	0.3

Table S8.3: TOC and IC concentrations within pH 11 sulphate reducing liquid microcosm and associated controls.

pH 11 SRB Floc		Control	
Distance ( $\mu\text{m}$ )	pH	Distance ( $\mu\text{m}$ )	pH
0	11.17	0	11.22
5	11.17	5	11.22
10	11.17	10	11.22
15	11.17	15	11.22
20	11.13	20	11.22
25	11.03	25	11.22
30	10.99	30	11.22
35	10.93	35	11.23
40	10.84	40	11.20
45	10.53	45	11.21
50	10.94	50	11.22
55	11.11	55	11.21
60	11.17	60	11.21
65	11.20	65	11.22
70	11.22	70	11.22
75	11.22	75	11.22
		80	11.22
		85	11.22
		90	11.22
		95	11.22
		100	11.22

Table S8.4: Micro-electrode pH profile through floc under pH 11 sulphate reducing conditions and control agar profile.

EPS component	(mg g VS <sup>-1</sup> )			
	Sonication + ethanol	SE	EDTA	SE
Carbohydrate	20.8	3.0	13.1	0.2
eDNA	0.0	0.0	9.1	0.2
Protein	1.8	0.4	5.7	1.5
Lipid	10.4	2.5	2.9	0.3

	(RFU)	
	Average	SE
Before extraction	3472	352
Sonication and ethanol	3654	334
EDTA	3710	266
Blank	46	4

Table S8.5: Results of EPS extraction procedure of pH 11 sulphate reducing flocs and the associated before and after ATP check of cell pellets.

Day	Sulphate reducing subculture (mg L <sup>-1</sup> )						Mo treated subcultures (mg L <sup>-1</sup> )						Chloramphenicol treated subcultures (mg L <sup>-1</sup> )					
	$\alpha$ -ISA	SE	$\beta$ -ISA	SE	XISA	SE	$\alpha$ -ISA	SE	$\beta$ -ISA	SE	XISA	SE	$\alpha$ -ISA	SE	$\beta$ -ISA	SE	XISA	SE
0	436.5	18.7	327.3	42.4	164.9	0.2	491.9	51.6	319.4	14.7	148.8	8.4	601.2	95.6	576.5	78.0	59.8	14.0
2	395.9	35.9	272.7	5.7	153.6	0.1	456.1	42.3	324.2	23.5	150.2	3.6	582.5	85.9	559.2	58.7	55.4	5.0
4	378.8	9.3	300.9	33.7	145.4	0.1	422.1	31.0	303.6	27.8	136.2	1.4	572.8	42.9	566.1	25.4	75.1	10.6
6	302.0	76.1	231.2	56.5	105.8	0.2	416.1	29.1	305.4	25.4	139.1	7.2	626.9	129.6	500.2	112.9	58.0	16.7
8	278.5	25.0	221.0	19.5	103.9	0.1	405.2	21.4	292.5	11.8	133.2	3.0	713.2	149.3	560.2	138.8	69.8	17.5
10	294.4	23.4	225.9	26.8	119.3	0.1	389.2	29.2	267.6	15.1	120.5	0.6	720.4	130.2	566.3	104.1	58.0	7.1
12	286.1	20.4	214.5	10.7	101.0	0.1	381.5	24.3	275.1	12.8	124.0	4.2	387.0	124.0	347.1	125.8	33.5	10.8
14	315.3	23.8	242.7	18.4	130.1	0.1	346.5	25.9	253.7	14.8	111.2	5.2	371.7	168.2	284.4	122.4	32.4	13.8
16	267.5	23.2	214.8	23.8	94.9	0.1	338.2	22.7	246.4	16.3	114.2	4.2	543.0	105.1	480.7	102.6	71.4	14.4
18	118.5	75.0	69.8	48.7	31.7	0.2	328.7	19.2	239.7	10.6	102.3	7.1	601.6	158.7	454.3	105.0	73.0	23.0
20	42.1	27.6	22.0	11.0	0.0	0.0	305.9	11.9	219.4	6.1	95.9	7.4	496.8	96.2	439.3	89.6	65.2	13.8
22	0.5	0.5	0.0	0.0	0.0	0.0	241.5	27.5	181.8	21.6	84.9	9.9	753.5	130.5	566.4	101.1	79.2	14.9
24	0.0	0.0	0.0	0.0	0.0	0.0	231.2	37.6	176.1	32.9	90.9	18.3	751.6	138.9	590.1	116.8	78.2	18.0
26	0.0	0.0	0.0	0.0	0.0	0.0	172.9	52.8	164.9	33.5	78.7	9.7	645.6	119.8	549.6	91.2	75.3	13.8

Table S8.6: ISA concentrations of different free drift subcultures.

pH values	Sulphate reducing		Mo treated		chloramphenicol treated	
	Day	pH	SE	pH	SE	pH
0	11.0	0.0	11.0	0.0	10.8	0.1
2	10.7	0.0	10.5	0.1	10.7	0.0
4	10.6	0.0	10.6	0.1	10.6	0.0
6	10.1	0.0	10.3	0.0	10.6	0.0
8	9.8	0.0	10.0	0.2	10.4	0.0
10	9.5	0.0	9.9	0.3	10.5	0.0
12	9.0	0.1	9.6	0.2	10.6	0.0
14	8.8	0.1	9.5	0.2	10.5	0.0
16	8.5	0.1	9.6	0.3	10.6	0.0
18	8.1	0.1	9.4	0.3	10.6	0.0
20	7.3	0.1	9.3	0.2	10.5	0.0
22	7.7	0.1	9.2	0.2	10.5	0.0
24	7.8	0.2	9.2	0.2	10.5	0.0
26	7.9	0.2	9.1	0.2	10.6	0.0

Table S8.7: pH values of different free drift subcultures.

Day	(mg L <sup>-1</sup> )					
	Sulphate reducing	SE	Mo treated	SE	chloramphenicol treated	SE
0	36.8	18.4	43.2	1.2	35.9	2.4
2	0.0	0.0	46.8	1.3	37.5	2.9
4	54.5	3.0	61.6	4.0	40.1	2.2
6	19.4	19.4	55.8	1.5	42.8	7.3
8	16.6	16.6	73.7	1.5	42.2	6.4
10	21.9	21.9	100.2	0.5	41.2	3.3
12	0.0	0.0	101.2	2.9	40.9	5.0
14	17.7	17.7	104.2	4.7	40.7	4.3
16	0.0	0.0	124.9	4.2	36.6	2.4
18	99.7	21.0	135.7	17.3	40.9	2.8
20	148.0	28.1	177.0	0.9	38.6	2.7
22	194.0	23.7	185.4	0.8	45.3	4.1
24	170.8	45.2	195.7	1.2	46.8	1.5
26	0.0	0.0	190.0	3.6	40.1	3.2

Table S8.8: Acetate concentrations of different free drift subcultures.

Day	(mg L <sup>-1</sup> )					
	Sulphate reducing	SE	Mo treated	SE	chloramphenicol treated	SE
0	282.4	9.8	275.5	8.7	267.9	0.8
2	243.5	14.6	261.3	4.4	268.8	2.3
4	241.3	10.5	255.7	3.9	267.7	2.2
6	212.5	20.1	253.8	4.2	269.7	0.9
8	223.9	27.0	251.7	1.4	269.0	1.9
10	206.6	5.5	238.9	6.8	265.1	1.4
12	209.7	13.8	231.7	13.3	267.7	0.9
14	211.0	6.4	234.5	8.0	266.9	1.2
16	203.2	12.3	232.7	5.3	269.6	1.9
18	209.1	6.1	237.5	7.9	265.3	0.9
20	209.9	16.9	235.4	8.4	265.8	1.4
22	204.3	13.8	237.4	5.9	265.0	1.0
24	157.2	3.8	235.9	5.6	265.0	2.1
26	96.6	7.9	236.0	4.7	264.1	0.8

Table S8.9: Sulphate concentrations of different free drift subcultures.

Day	(mg L <sup>-1</sup> )	
	Aqueous sulphide	SE
0	0.0	0.0
4	0.0	0.0
6	5.2	3.1
10	87.4	4.6
12	104.8	7.4
16	134.7	12.7
18	121.0	9.0
20	96.8	1.5
26	106.0	0.6

Table S8.9: Sulphide concentrations of different free drift subcultures.

Day	Sulphate reducing (mg L <sup>-1</sup> )				Mo treated (mg L <sup>-1</sup> )				chloramphenicol treated (mg L <sup>-1</sup> )			
	TOC	SE	IC	SE	TOC	SE	IC	SE	TOC	SE	IC	SE
0	1037.8	166.2	68.4	5.6	1157.1	160.1	49.8	12.5	1012.8	16.3	70.3	4.1
2	757.6	218.4	55.5	10.2	1090.2	77.9	60.6	5.2	1005.0	53.5	67.4	8.6
4	823.2	281.8	54.0	11.0	1248.7	74.8	48.4	5.8	1076.4	159.4	80.6	8.6
6	639.7	169.5	48.9	6.6	1214.5	119.8	64.1	19.8	1118.6	120.5	87.3	6.2
8	651.4	267.0	49.7	10.8	1050.0	95.3	75.0	4.8	896.9	140.3	66.9	8.0
10	929.7	278.6	69.6	9.6	1213.0	70.3	73.1	12.3	1079.4	135.8	77.9	4.7
12	889.0	169.8	53.1	7.3	1051.0	163.3	71.3	3.5	1080.1	113.8	85.0	9.7
14	964.6	171.6	70.2	5.7	1184.7	81.8	89.3	7.0	1080.5	80.8	86.3	7.7
16	858.9	193.8	73.2	2.8	1187.0	32.6	92.9	3.0	1104.2	71.3	83.0	5.7
18	739.7	142.2	64.8	4.9	1282.0	137.5	109.2	16.9	1013.7	75.4	69.7	0.8
20	823.1	193.4	69.3	2.3	1209.3	79.0	87.4	8.5	1016.4	61.8	79.6	2.5
22	785.1	202.6	62.6	4.2	1174.3	73.7	98.5	7.7	1093.3	118.8	84.5	7.4
24	784.7	188.3	68.6	4.5	1140.7	77.4	95.4	15.2	1006.0	77.5	72.8	6.8
26	769.0	156.7	67.9	4.0	1117.7	75.3	106.2	10.7	1049.0	58.3	71.2	5.1

Table S8.10: TOC and IC measurements of different free drift subcultures.

<i>D.Multivorans</i> standard curve		
Sample (ng DNA)	Ct	Log gene copy
100	11.3	7.29
10	16.9	6.29
1	19.62	5.29
0.1	23.38	4.29
0.01	28.4	3.29
0.001	30.29	2.29

pH	DNA (log gene copy $\mu$ L template <sup>-1</sup> )		mRNA (log gene copy $\mu$ L template <sup>-1</sup> )		mRNA/DNA gene ratio	
	Average	SE	Average	SE	average	SE
11	5.10	0.11	3.36	0.12	0.66	0.03
10.5	4.46	0.31	3.52	0.27	0.79	0.08
10	4.68	0.27	3.60	0.14	0.77	0.06
9.5	4.87	0.33	3.82	0.17	0.79	0.02
9	4.60	0.16	4.03	0.09	0.88	0.04
8.5	5.14	0.17	4.79	0.07	0.93	0.04
8	5.47	0.14	4.97	0.06	0.91	0.02
7.5	5.81	0.10	6.39	0.35	1.10	0.04

Table S8.11: qPCR results of *D.Multivorans* standard curve and *drsA* gene and transcript measurements at different pH values.

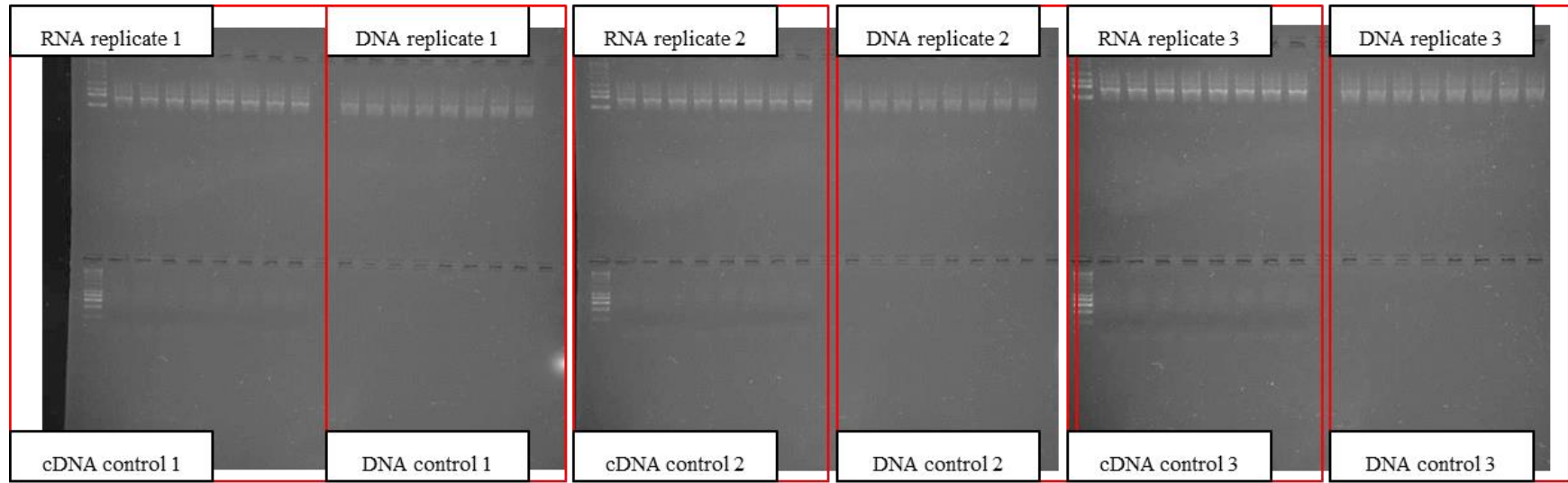


Figure S8.1: Agarose gel electrophoresis images of *dsrA* qPCR work and associated controls.

Day	(mmoles)										
	$\alpha$ -ISA	$\beta$ -ISA	XISA	ISA total	Theoretical ISA acetate	Cumulative Theoretical ISA acetate	Acetate removed by sulphate reduction	Final theoretical acetate	Measured acetate	Theoretical sulphide from measured sulphate removal	Measured sulphide
0	0.00	0.00	0.00	0.00	0.00	0.00	0.00	0.00	0.16	0.00	0.00
2	0.06	0.08	0.02	0.15	0.30	0.30	0.10	0.20	0.00	0.00	0.00
4	0.02	0.00	0.01	0.04	0.07	0.38	0.11	0.27	0.23	0.00	0.00
6	0.11	0.10	0.07	0.27	0.54	0.92	0.18	0.73	0.08	0.02	0.04
8	0.03	0.01	0.00	0.05	0.10	1.02	0.18	0.83	0.07	-	-
10	0.00	0.00	0.00	0.00	0.00	1.02	0.23	0.79	0.09	0.33	0.66
12	0.01	0.02	0.03	0.06	0.12	1.13	0.23	0.90	0.00	0.40	0.79
14	0.00	0.00	0.00	0.00	0.00	1.13	0.23	0.90	0.08	=	-
16	0.07	0.04	0.06	0.16	0.33	1.46	0.25	1.21	0.00	0.51	1.02
18	0.21	0.20	0.11	0.51	1.03	2.49	0.25	2.24	0.42	0.37	0.91
20	0.11	0.07	0.05	0.23	0.45	2.94	0.25	2.69	0.63	-	0.73
22	0.06	0.03	0.00	0.09	0.18	3.11	0.26	2.85	0.82	-	-
24	0.00	0.00	0.00	0.00	0.00	3.11	0.38	2.73	0.72	-	-
26	0.00	0.00	0.00	0.00	0.00	3.11	0.54	2.57	0.00	0.40	0.80

Table S8.12: Theoretical calculations for sulphate reducing subculture system.

Class	Read number distribution				% Distribution			
	pH 11	pH 9.5	pH 7	Mo treated	pH 11	pH 9.5	pH 7	Mo treated
Clostridia	1766	5773	6364	3916	25.0	55.9	54.7	32.4
Actinobacteria	3723	2448	956	3123	52.8	23.7	8.2	25.9
Alphaproteobacteria	171	1760	1244	1155	2.4	17.0	10.7	9.6
Betaproteobacteria	643	11	17	2612	9.1	0.1	0.1	21.6
Gammaproteobacteria	384	43	881	398	5.4	0.4	7.6	3.3
Bacteroidia	45	55	1350	245	0.6	0.5	11.6	2.0
Erysipelotrichi	74	15	683	372	1.0	0.1	5.9	3.1
Bacilli	241	91	40	71	3.4	0.9	0.3	0.6
Unknown Bacteria	0	74	63	119	0.0	0.7	0.5	1.0
ETC <1	8	61	45	61	0.1	0.6	0.4	0.5

Family	Read number				(%)			
	pH 11	pH 9.5	pH 7	Mo treated	pH 11	pH 9.5	pH 7	Mo treated
Corynebacteriaceae	3364	2243	783	2960	47.7	21.7	6.7	24.5
Tissierella_f	545	1851	1127	1955	7.7	17.9	9.7	16.2
Ruminococcaceae	6	858	2870	584	0.1	8.3	24.7	4.8
Brucellaceae	49	1701	1207	1090	0.7	16.5	10.4	9.0
Alcaligenaceae	643	1	0	2507	9.1	0.0	0.0	20.8
Anaerovirgula_f	881	1220	273	143	12.5	11.8	2.3	1.2
Anaerobranca_f	266	842	92	674	3.8	8.2	0.8	5.6
Draconibacterium_f	4	32	1313	47	0.1	0.3	11.3	0.4
Pseudomonadaceae	0	4	835	325	0.0	0.0	7.2	2.7
Erysipelotrichaceae	74	15	669	360	1.0	0.1	5.7	3.0
Dietziaceae	303	110	112	42	4.3	1.1	1.0	0.3
Clostridiales_uc	0	100	220	147	0.0	1.0	1.9	1.2
Eubacteriaceae	7	242	75	79	0.1	2.3	0.6	0.7
Alishewanella_f	382	0	2	3	5.4	0.0	0.0	0.0
Sedimentibacter_f	3	156	170	48	0.0	1.5	1.5	0.4
Thermohalobacter_f	1	37	269	15	0.0	0.4	2.3	0.1
Desulfotomaculum_f	15	5	266	35	0.2	0.0	2.3	0.3
Clostridium_g7_f	3	136	173	2	0.0	1.3	1.5	0.0
Bacillaceae	153	70	13	46	2.2	0.7	0.1	0.4
Uknown Bacteria	0	74	63	119	0.0	0.7	0.5	1.0
Desulfitobacterium_f	1	5	245	4	0.0	0.0	2.1	0.0
EU845084_f	0	1	0	174	0.0	0.0	0.0	1.4
Christensenellaceae	7	10	110	47	0.1	0.1	0.9	0.4
Caulobacteraceae	89	10	0	12	1.3	0.1	0.0	0.1
Enterococcaceae	87	7	4	7	1.2	0.1	0.0	0.1
ETC < 1	172	601	752	647	2.4	5.8	6.5	5.4

Table S8.13: Class and family distribution of sulphate reducing and Mo treated subculture systems.

Day	Microcosm (mg L <sup>-1</sup> )						Control (mg L <sup>-1</sup> )					
	$\alpha$ -ISA	SE	$\beta$ -ISA	SE	XISA	SE	$\alpha$ -ISA	SE	$\beta$ -ISA	SE	XISA	SE
0	302.0	19.9	309.9	25.0	182.5	48.2	301.5	11.0	302.6	32.2	90.1	42.2
2	247.7	0.7	270.5	3.4	141.6	7.4	310.7	16.9	316.5	0.3	87.0	42.8
4	201.9	49.5	219.8	59.1	108.8	41.4	295.5	20.1	305.3	12.5	88.9	43.9
6	209.0	22.4	224.6	27.4	92.2	12.7	306.7	1.0	310.1	12.9	107.1	49.8
8	232.1	0.9	237.7	13.4	88.6	8.7	364.8	45.2	368.5	74.1	156.3	80.4
10	200.6	9.3	197.3	5.3	53.4	32.5	353.3	42.0	354.4	73.5	157.0	79.3
12	208.1	6.9	204.3	5.1	52.3	34.5	382.5	76.4	351.4	99.5	193.9	115.9
14	162.3	33.6	164.2	26.9	17.8	17.8	427.3	29.2	387.7	52.8	218.7	106.1

Table S8.14: ISA concentrations of sulphate reducing and control steel disc microcosms at pH 11.

Day	(mg L <sup>-1</sup> )		(mmoles)*			
	Acetate	SE	CH <sub>4</sub>	SE	H <sub>2</sub>	SE
0	234.0	92.1	0.00	0.00	0.00	0.00
2	202.1	8.0	0.18	0.02	0.13	0.04
4	228.3	52.0	0.20	0.01	0.15	0.01
6	237.9	29.6	0.16	0.03	0.45	0.00
8	357.8	50.8	0.15	0.00	0.55	0.02
10	244.8	40.3	0.21	0.00	0.50	0.00
12	569.2	62.2	0.26	0.02	0.47	0.01
14	546.6	30.7	0.30	0.01	0.33	0.00

\*Pressure remained at approximately 1 atm due to low volume of gas produced.

Table S8.15: Acetate concentrations of sulphate reducing microcosm and associated hydrogen and methane gas headspace amounts at pH 11. No acetate or gas was detected within control system.

Day	Microcosm (mg L <sup>-1</sup> )				Control (mg L <sup>-1</sup> )			
	TOC	SE	IC	SE	TOC	SE	IC	SE
0	640.5	12.5	139.0	3.4	540.1	56.9	42.5	4.9
2	825.5	101.5	144.4	5.0	538.2	79.7	40.3	4.3
4	1230.5	365.5	131.5	14.2	448.5	70.2	33.4	4.0
6	918.0	11.0	152.4	2.2	539.7	67.9	39.0	2.4
8	1095.5	149.5	135.9	21.6	506.4	8.2	35.2	2.0
10	608.8	237.8	159.8	3.7	502.5	26.8	33.7	4.3
12	680.5	71.5	153.4	3.0	559.3	60.3	43.7	3.1
14	696.5	19.5	162.7	2.5	540.2	40.4	43.2	3.9

Table S8.16: TOC and IC concentrations of sulphate reducing and control steel disc microcosms at pH 11.

Day	Microcosm		Control	
	Sulphate	SE	Sulphate	SE
0	352.3	5.9	369.7	0.2
2	339.2	14.3	370.7	1.9
4	283.7	10.9	369.1	0.9
6	298.0	23.5	367.9	0.4
8	337.0	29.7	366.2	2.0
10	265.5	24.9	364.8	4.2
12	329.3	38.8	368.3	0.1
14	324.8	1.8	372.8	1.8

Table S8.17: Sulphate concentrations of sulphate reducing and control steel disc microcosms at pH 11.

Class	Reads distribution		% Distribution		
	316	304	316	304	Average
Clostridia	5173	5504	34.4	34.2	34.3
Alphaproteobacteria	3662	3797	24.3	23.6	24.0
Gammaproteobacteria	1948	2162	12.9	13.4	13.2
Actinobacteria_c	1771	1952	11.8	12.1	11.9
Bacteroidia	1283	1282	8.5	8.0	8.2
Bacilli	544	645	3.6	4.0	3.8
Erysipelotrichi	244	275	1.6	1.7	1.7
ETC <1	426	489	2.8	3.0	2.9

Family	Reads distribution		% Distribution		
	316	304	316	304	Average
Anaerobranca_f	2836	2969	18.8	18.4	18.6
Brucellaceae	2418	2422	16.1	15.0	15.6
Anaerovirgula_f	2070	2257	13.8	14.0	13.9
Alishewanella_f	1779	1979	11.8	12.3	12.1
Rhodobacteraceae	1086	1199	7.2	7.4	7.3
Corynebacteriaceae	1123	1143	7.5	7.1	7.3
Draconibacterium_f	1130	1097	7.5	6.8	7.2
Dietziaceae	570	718	3.8	4.5	4.1
Bacillaceae	525	624	3.5	3.9	3.7
Erysipelotrichaceae	242	275	1.6	1.7	1.7
Pseudomonadaceae	164	180	1.1	1.1	1.1
DQ206420_f	146	182	1.0	1.1	1.1
ETC < 1	962	1061	6.4	6.6	6.5

Table S8.18: Class and family level distribution of 16S rRNA gene microbial community of biofilms extracted from grade 304 and 316 steel discs.

## Data associated with Chapter 9

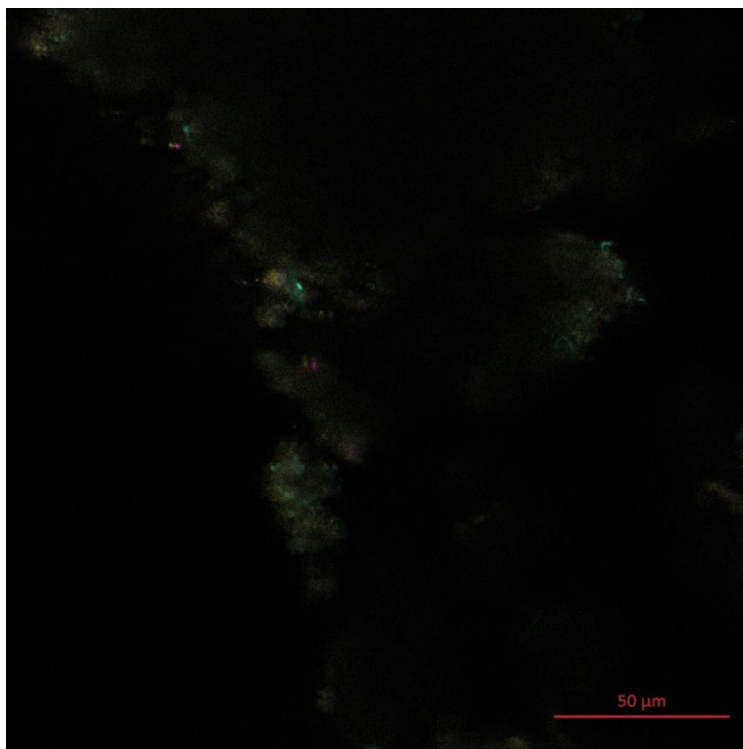


Figure S9.1: Autofluorescence 5 colour channel CLSM control of colonised cotton.

Class	Read Distribution			% Distribution		
	Site B	Site H	Site T	Site B	Site H	Site T
Methanomicrobia	21	10	197	95.5	47.6	69.9
Methanobacteria	1	11	5	4.5	52.4	1.8
Thermoplasmata	0	0	12	0.0	0.0	4.3
MBGB_c	0	0	68	0.0	0.0	24.1
Total	22	21	282	100.0	100.0	100.0

Family	Read Distribution			% Distribution		
	Site B	Site H	Site T	Site B	Site H	Site T
Methanoregula_f	16	9	164	72.7	42.9	58.2
AY835409_f	0	0	68	0.0	0.0	24.1
Methanosarcinaceae	0	1	19	0.0	4.8	6.7
Methanospirillaceae	5	0	13	22.7	0.0	4.6
Methanobacteriaceae	1	11	5	4.5	52.4	1.8
Methanomassiliicoccus_f	0	0	12	0.0	0.0	4.3
Methanosaetaceae	0	0	1	0.0	0.0	0.4
Total	22	21	282	100.0	100.0	100.0

Table S9.1: Archaea class and family level distribution of 16S rRNA cotton biofilm communities at different potential analogue sites.

Class	Read Distribution			% Distribution		
	Site B	Site H	Site T	Site B	Site H	Site T
Clostridia	7050	1993	5067	37.0	10.5	26.3
Betaproteobacteria	4163	2381	1833	21.8	12.5	9.5
Actinobacteria_c	1616	6303	98	8.5	33.1	0.5
Bacilli	3028	4061	383	15.9	21.3	2.0
DQ513087_c	373	364	5578	2.0	1.9	29.0
AB476673_c	1136	653	577	6.0	3.4	3.0
Cytophagia	258	1135	944	1.4	6.0	4.9
Alphaproteobacteria	562	219	706	2.9	1.1	3.7
Gammaproteobacteria	175	754	272	0.9	4.0	1.4
Bacteroidia	108	157	776	0.6	0.8	4.0
Deltaproteobacteria	94	204	357	0.5	1.1	1.9
Fibrobacteria	48	18	502	0.3	0.1	2.6
Planctomycetacia	205	86	61	1.1	0.5	0.3
Phycisphaerae	10	5	314	0.1	0.0	1.6
Synergistia	14	292	6	0.1	1.5	0.0
Below 1%	213	437	1775	1.1	2.3	9.2
Total	19053	19062	19249	100.0	100.0	100.0

Family	Read Distribution			% Distribution		
	Site B	Site H	Site T	Site B	Site H	Site T
Dietziaceae	1449	6186	68	7.6	32.5	0.4
Comamonadaceae	3418	1423	1228	17.9	7.5	6.4
Bacillaceae	1986	3305	240	10.4	17.3	1.2
DQ513087_f	151	261	4872	0.8	1.4	25.3
Veillonellaceae	1306	387	2481	6.9	2.0	12.9
Desulfitobacterium_f	3281	412	44	17.2	2.2	0.2
Cyclobacteriaceae	258	1132	943	1.4	5.9	4.9
AB476673_f	1130	648	492	5.9	3.4	2.6
Ruminococcaceae	408	275	1093	2.1	1.4	5.7
Christensenellaceae	1015	65	598	5.3	0.3	3.1
Vulcanibacillus_f	580	591	13	3.0	3.1	0.1
DQ513087_o_uc	222	103	706	1.2	0.5	3.7
Acetobacteraceae	354	26	441	1.9	0.1	2.3
Hydrogenispora_f	611	193	3	3.2	1.0	0.0
Desulfotomaculum_f	117	164	386	0.6	0.9	2.0
Fibrobacteraceae	47	17	501	0.2	0.1	2.6
Bacteroidaceae	60	86	417	0.3	0.5	2.2
Rhodocyclaceae	173	364	21	0.9	1.9	0.1
Sphaerotilus_f	489	45	22	2.6	0.2	0.1
Alishewanella_f	10	508	4	0.1	2.7	0.0
Zoogloea_f	14	184	234	0.1	1.0	1.2
Alcaligenaceae	46	353	28	0.2	1.9	0.1

Xanthomonadaceae	156	234	7	0.8	1.2	0.0
Planctomycetaceae	205	86	61	1.1	0.5	0.3
Paenibacillaceae	291	10	0	1.5	0.1	0.0
Aminobacterium_f	10	287	3	0.1	1.5	0.0
Methylophilaceae	2	3	282	0.0	0.0	1.5
HQ697838_f	0	1	233	0.0	0.0	1.2
Enterobacteriaceae	0	2	213	0.0	0.0	1.1
Anaerovirgula_f	3	203	1	0.0	1.1	0.0
Below 1%	1261	1508	3614	6.6	7.9	18.8
Total	19053	19062	19249	100.0	100.0	100.0

Table S9.1: Bacteria class and family level distribution of 16S rRNA cotton biofilm communities at different potential analogue sites.

Group	OTU 95%	%
All shared	111	5.8
BLT	73	3.8
BH	140	7.3
HT	65	3.4
H	595	31.1
T	398	20.8
B	533	27.8
Total	1915	100.0

	Read Distribution				% Distribution			
	Site B	Site H	Site T	Total	Site B	Site H	Site T	Total
All shared	13464	11707	4809	29980	21.9	19.1	7.8	48.8
BT	1462	0	3393	4855	2.4	0.0	5.5	7.9
BH	7164	8174	0	15338	11.7	13.3	0.0	25.0
HT	578	0	3368	3946	0.9	0.0	5.5	6.4
H	2158	0	0	2158	3.5	0.0	0.0	3.5
T	0	0	2988	2988	0.0	0.0	4.9	4.9
B	2185	0	0	2185	3.6	0.0	0.0	3.6
Total	27011	19881	14558	61450	44.0	32.4	23.7	100.0

Table S9.2: Distribution of reads and OTU's shared between biofilms from the different potential analogue sites.

Taxonomy	Site-B	Site-H	Site-T
AQSL_f_uc	1	4	49
AY214182_g	2	2	5
EU246070_f_uc	9	1	3
AB511016_g	2	23	8
EU245367_f_uc	3	4	6
FJ889275_g	40	62	125
AM997775_g	3	108	1
AY548942_g	1	2	105
Silanimonas	106	52	4
Fibrobacteraceae_uc	44	17	457
GQ458248_g	5	1	22
JN697815_g	13	28	42
Clostridiales_uc	172	234	47
AB239481_g	233	6	110
Christensenellaceae_uc	38	35	5668
AB234270_g	6	54	1
Desulfotomaculum	5	35	2
GQ356941_g	2	68	1
Desulfitobacterium	2328	4	36
Saccharofermentans	99	54	280
Anaerosporobacter	25	37	93
EF603968_g	1	7	1
FN436105_g	463	21	1
Proteiniclasticum	2	5	4
Ercella	10	35	3
EU009800_f_uc	1	25	39
Bacillus	97	2	2
Bacillaceae_uc	4	4	7
Vulcanibacillus_f_uc	448	2	6
Bacillus_g23	158	49	3
AB476673_g	357	54	301
Aminivibrio	9	285	1
EU266864_g	2	2	10
Methanoregula	16	9	147
Methanobacterium	1	6	2
Opiritaceae_uc	5	47	88
Leucobacter	1	90	1
Dietzia	1173	534	66
DQ513087_o_uc	221	407	399
EU881314_o_uc	4	22	42
Methylobacterium	11	16	122
Mesorhizobium	80	18	3
Defluviimonas	5	39	1
Sediminicoccus	45	3	20

Parabacteroides	5	6	49
Bacteroides	58	77	341
AB240501_f_uc	3	10	102
GQ451200_g	1	6	1
Malikia	1777	6	6
Hydrogenophaga	314	109	976
Aquabacterium	384	13	35
Azovibrio	41	2	21
Alcaligenes	38	342	26
Uliginosibacterium	3	3	13
Aquiflexum	213	838	906
Trichococcus	82	42	122
Bacillus_g6	1452	532	231
GQ406188_g	32	38	1550
AJ009486_g	649	11	6
HQ660796_g	293	93	1
AB513436_g	7	4	217
Veillonellaceae_uc	1	2	9
HQ904156_g	100	155	517

Table S9.3: Shared read distribution at genus level between biofilms at different potential analogue sites.